



University of HUDDERSFIELD

University of Huddersfield Repository

Hejjaji, Ezzeddin M. A.

Tuneable Chitosan Particles with Potential Forensic and Pharmaceutical Applications

Original Citation

Hejjaji, Ezzeddin M. A. (2018) Tuneable Chitosan Particles with Potential Forensic and Pharmaceutical Applications. Doctoral thesis, University of Huddersfield.

This version is available at <http://eprints.hud.ac.uk/id/eprint/34843/>

The University Repository is a digital collection of the research output of the University, available on Open Access. Copyright and Moral Rights for the items on this site are retained by the individual author and/or other copyright owners. Users may access full items free of charge; copies of full text items generally can be reproduced, displayed or performed and given to third parties in any format or medium for personal research or study, educational or not-for-profit purposes without prior permission or charge, provided:

- The authors, title and full bibliographic details is credited in any copy;
- A hyperlink and/or URL is included for the original metadata page; and
- The content is not changed in any way.

For more information, including our policy and submission procedure, please contact the Repository Team at: E.mailbox@hud.ac.uk.

<http://eprints.hud.ac.uk/>

Tuneable Chitosan Particles with Potential Forensic and Pharmaceutical Applications

Ezzeddin M. A. Hejjaji

**B.Sc. (Chemistry); M.Sc. (Forensic Science, Drugs &
Chemical Analysis)**



University of
HUDDERSFIELD

**Thesis submitted in partial fulfilment of the
requirements for the Degree of Doctor of Philosophy**

October 2018

ABSTRACT

Chitosan (CS), a natural cationic polymer obtained by the partial N-deacetylation of chitin, has been investigated widely for its potential in the development of food and drug delivery systems and pharmaceutical applications, however it has not generally been considered in forensic applications for example fingerprints (fingermarks). The purpose of this study was to prepare chitosan micro/nanoparticles through cross-linking with tripolyphosphate (TPP) utilising the ionotropic interaction between positively charged amino groups (CS) and negatively charged counter ions (TPP). The investigation into the potential of these particles was divided into two parts: forensic and pharmaceutical applications. Firstly, these formulations were characterized (relative viscosity, zeta potential, particle size, FT-IR, XRD, SEM) and evaluated for forensic applications (fingerprint visualisation). This can be controlled by the charge density of CS and TPP, which depends on the pH and ionic strength of the solution. Secondly, the combined effects of three independent variables (pH, ionic strength and CS: TPP ratio) on three important physico-chemical properties (viscosity, zeta potential and particle size) during the preparation of microparticles were investigated. CS: TPP microparticles (CSMPs) were prepared using experimental design and equations were generated and used to predict relative viscosity, zeta potential and particle size under different conditions. This gives us the ability to design tuneable CS: TPP microparticles with desired size for specific pharmaceutical or forensic applications *e.g.* latent fingerprint visualisation. Fingerprints are a very common form of physical evidence. The most commonly used procedure for revealing the ridge pattern is powder dusting, which relies on the mechanical adherence of fingerprint formulation to the fatty components of the skin deposit that are secreted by sweat pores that exist on friction ridges. The development of latent fingermarks using

CSMPs was analysed by using a 2^3 factorial design, which considered simultaneously three main factors: pH, ionic strength and CS: TPP (v/v) ratio. CS: TPP ratio has the strongest effect on fingerprint quality. The best conditions for fingerprint visualisation were microparticles prepared using a buffer of pH 4.8, 0.2 M ionic strength at a CS: TPP of 2:1. Although we have demonstrated that CSMPs can be used to develop latent fingerprints there are limitations in that they are only applicable as a powder and are only sensitive up to the third depletion level for a fingerprint aged for one day.

In the final sections of this thesis, chitosan nanoparticles were prepared and characterized for potential applications in drug delivery (using ibuprofen as a model drug) and in terms of their interactions with mucin (mucoadhesion). It has been demonstrated that chitosan nanoparticles can incorporate appreciable quantities of ibuprofen into nanoparticles (CS-IBU-TPP), although the order addition of the individual components is important. The carboxylate ions of the ibuprofen (negative charge) and could bind strongly to the ammonium group (positive charge) of chitosan, thereby allowing greater drug-loading capacity in the chitosan nanoparticles. In addition, the interaction between different ratios chitosan nanoparticles (CS: TPP) and mucin were evaluated based on relative viscosity, zeta potential and particle size. It has been suggested that chitosan nanoparticle-mucin interactions are driven by electrostatic forces. The results conclude that interactions between CS: TPP nanoparticles and mucin occur, with a CS: TPP ratio of 4:1 displaying the strongest interaction with mucin. This is observed through differences in relative viscosity, zeta potential and particle size.

ACKNOWLEDGEMENTS

I would like to express my thanks to God who is the source and origin of all knowledge. I feel highly privileged to express my heartiest gratitude to the worthy and kind supervisor, Prof. Gordon Morris, for his dynamic supervision, encouragement, guidance, support, and freedom in the development of this project. His wide knowledge and logical way of thinking has been of great value for me. As well as, his intensive and creative comments have helped me step by step throughout this project. Special thanks also go to Dr. Alan Smith and Dr. Adeola Adebisi for their help, contributions and valuable advice. I also wish to thank Mr. James Rooney for his invaluable help with SEM.

I would also like to thank Dr. Kofi Asare-Addo, Ms. Hayley Markham and Mr. Ibrahim George and all the technical staff of the School of Applied Sciences for their laboratory assistance. I will also like to thank my colleague Dr. Atiga Abodinar for all her support, companionship and creating a friendly working environment. I would like to express my gratitude to my wonderful parents, wife, sisters and brothers for their long distance cheering, encouragement and support. Finally, I would like to thank the Libyan government for their funding of my PhD.

This thesis is dedicated to

My Parents,

My wife,

My Sisters,

My Brother Adel,

I will always Love you

LIST OF ABBREVIATIONS

AB	Acetate buffers
Abs	Absorbance
ACE-V	Analysis, comparison, evaluation and verification
AFIS	Automated Fingerprint Identification System
ALG	Alginate
ANOVA	Analysis of variance
BCS	Biopharmaceutical classification system
BSA	Bovine serum albumin
BSE	Backscattered electron
CS	Chitosan
CSMPs	Chitosan microparticles
DA	Deacetylation
DC	Drug content
DD	Degree of deacetylation
DDS	Drug delivery system
DEE	Drug entrapment efficiency
DFO	Diazafluorenone
DLS	Dynamic Light Scattering
DM	Demineralization
DOE	Design of experiments
DP	Deproteinization
E-T	Everhart-Thornley
FITC	Fluorescein isothiocyanate

FTIR	Fourier transform infrared spectroscopy
GA	Glutaraldehyde
GAGs	Glycosaminoglycans
GI	Gastrointestinal
IB-MSNs	Ibuprofen-mesoporous silica nanoparticles
IBU	Ibuprofen
IS	Ionic strength
LD	Laser diffraction
LMW	Low molecular weight
LOD	Limit of detection
LOQ	Limit of quantification
MMD	Multi-metal deposition
MMT	Montmorillonite
MMW	Medium molecular weight
MW	Molecular weight
NMC	Nickel Manganese Cobalt
PBS	Phosphate buffer saline
PD	Physical developer
PDI	Polydispersity index
p-DNA	Plasmid deoxyribonucleic acid
PEG	Polyethylene Glycol
QDs	Quantum dots
RP	Ruhemann's purple
RSD	Relative standard deviation
SE	Standard error

SEM	Scanning electron microscopy
siRNA	Small interfering Ribonucleic acid
SPR	Small-particle reagent
TEM	Transmission electron microscopy
TPP	Tripolyphosphate
TR	Tandem repeats
UV-VIS	Ultraviolet-Visible
VMD	Vacuum metal deposition
WPS	white powder suspensions
XRD	X-Ray Diffraction
ZP	Zeta potential
η_{rel}	Relative viscosity

TABLE OF CONTENTS

ABSTRACT.....	I
LIST OF ABBREVIATIONS.....	V
TABLE OF CONTENTS.....	VIII
LIST OF FIGURES.....	XV
LIST OF TABLES.....	XXV
1 General Introduction.....	2
1.1 Carbohydrates.....	2
1.1.1 Polysaccharides.....	5
1.1.1.1 Homopolysaccharides.....	5
1.1.1.2 Heteropolysaccharides.....	6
1.2 Chitosan	7
1.2.1 Production of chitin and chitosan.....	8
1.2.1.1 Deproteinization	10
1.2.1.2 Demineralization.....	11
1.2.1.3 Decolouration	12
1.2.1.4 Deacetylation	12
1.2.2 Applications for Chitosan.....	14
1.2.3 Structural and physicochemical characteristics of chitosan.....	19
1.2.3.1 Solubility.....	20
1.2.3.2 Biodegradability, biocompatibility and toxicity	21
1.3 Mucin	22
1.3.1 Mucoadhesive properties	27
1.3.2 Factors Influencing Mucoadhesive Properties.....	32
1.3.2.1 Molecular Weight of polymer	32
1.3.2.2 Concentration of polymer.....	32
1.3.2.3 Flexibility, length of polymer chains and cross-linking density	33
1.3.2.4 Functional group contribution	34
1.3.2.5 pH and polymer charge.....	34
1.3.2.6 Initial contact time	35
1.3.2.7 Degree of hydration	35

1.3.3	Advantages of mucoadhesive delivery systems	36
1.4	Drug delivery system.....	36
1.5	Nanotechnology.....	37
1.5.1	Advantages of nanoscale drug delivery system.....	37
1.5.2	Polysaccharide nano/microparticles.....	38
1.5.2.1	Methods of preparation of chitosan micro/nanoparticles (cross-linking of chitosan) 40	
1.5.2.1.1	Ionotropic gelation	43
1.6	Fingerprints	45
1.6.1	History of Fingerprints	47
1.6.2	Classification of Fingerprints.....	49
1.6.3	Fingermark composition	53
1.6.3.1	Eccrine glands	54
1.6.3.2	Apocrine glands.....	54
1.6.3.3	Sebaceous glands.....	55
1.6.4	Types of fingerprints/fingermarks	57
1.6.4.1	Visible (patent) fingermarks.....	57
1.6.4.2	A plastic marks (alternatively called an impression or indented).....	58
1.6.4.3	Latent fingermarks	58
1.6.5	Surface characteristics	59
1.6.5.1	Porous surfaces	59
1.6.5.2	Semi porous surfaces	61
1.6.5.3	Nonporous surfaces	61
1.6.6	Detection of fingerprints.....	62
1.6.6.1	Physical methods	62
1.6.6.2	Chemical methods	63
1.6.6.3	Physical/chemical methods	63
1.6.6.3.1	Multi-metal deposition (MMD)	64
1.6.6.3.2	Iodine fuming method	64
1.6.6.3.3	Cyanoacrylate fuming (Super-glue method).....	65
1.6.6.3.4	The combination of optical methods.....	65
1.7	Research aims and objectives.....	74
1.8	Publications and Presentations.....	76
2	Instrumental techniques (background theory).....	79

2.1	Zeta potential.....	79
2.2	Particle size analysis.....	82
2.3	Rheometry (Rheology).....	83
2.3.1	Viscosity.....	85
2.4	Powder X-Ray Diffraction (p-XRD).....	86
2.5	Fourier Transform Infrared – Attenuated Total Reflectance (FTIR-ATR) Spectroscopy.....	88
2.6	Ultraviolet—Visible Spectrometry (UV-Vis).....	89
2.7	Scanning electron microscopy (SEM).....	91
2.8	Summary.....	96
3	Factors Affecting the Physico-Chemical Properties of Chitosan-Tripolyphosphate Microparticles Formed by Ionotropic Gelation.....	99
3.1	Introduction.....	99
3.2	Design of experiments (Factorial Design).....	99
3.3	Materials.....	101
3.4	Experimental.....	101
3.4.1	Sample preparation.....	101
3.4.1.1	Preparation of chitosan and TPP samples with different ionic strengths and pH value (Acetate buffers AB-1 to AB-9).....	102
3.4.1.2	Preparation of CS: TPP microparticles.....	103
3.4.1.3	Model validation (prediction method).....	104
3.4.2	Characterisation of chitosan microparticles.....	105
3.4.2.1	Fourier transform infrared (FTIR).....	105
3.4.2.2	Powder X-ray diffraction (p-XRD).....	105
3.4.2.3	Determination of relative viscosities.....	106
3.4.2.4	Determination of zeta potential.....	106
3.4.2.5	Determination of particle size.....	107
3.4.2.6	Scanning electron microscopy (SEM).....	108
3.4.3	Effect of cross-linker TPP concentration and chitosan molecular weight using acetic acid at different conditions to formulate CS: TPP nanoparticles.....	109
3.5	Results and discussion.....	112
3.5.1	FTIR analysis.....	112
3.5.2	Crystallographic characterisation.....	114
3.5.3	Relative viscosity and zeta potential for varying chitosan solutions.....	117

3.5.4	Analysis of different ratios of CS: TPP microparticles using scanning electron microscope (SEM)	122
3.5.5	Model validation of relative viscosity, zeta potential and particle size	132
3.6	Effect of chitosan molecular weight and TPP concentration in acetic acid to formulate CS: TPP nanoparticles	138
3.7	Summary	143
4	The potential of chitosan-tripolyphosphate microparticles in the visualisation of latent fingerprints	145
4.1	Introduction	145
4.2	Materials	151
4.3	Factorial design experiment	151
4.4	Experimental	153
4.4.1	Microparticle preparation (CS: TPP)	153
4.4.2	Samples preparation and fingerprints development	153
4.4.2.1	First technique (spray)	155
4.4.2.2	Second technique (microparticles in solution)	155
4.4.2.3	Third method (microparticles as powder).....	156
4.4.2.3.1	Split print depletion series	157
4.4.3	Photography of Samples	159
4.4.4	Scanning electron microscopy (SEM).....	159
4.5	Results and discussion	161
4.5.1	Proposed mechanism for interaction	163
4.5.2	Scanning electron microscopy (SEM).....	193
4.5.3	Ageing study of latent fingerprints.....	210
4.5.4	Method limitation (Split fingerprints depletion series).....	213
4.6	Summary	224
5	Formulation, characterization and <i>in vitro</i> evaluation of ibuprofen loaded chitosan-TPP nanoparticles as a model pharmaceutical application	227
5.1	Introduction	227
5.2	Methods and materials.....	230
5.2.1	Chemicals	230
5.2.2	Sample preparation	230
5.2.2.1	Viscosity analysis of chitosan	230
5.2.2.2	Fourier transform infrared (FTIR).....	232
5.2.2.3	Preparation of chitosan and TPP samples	233

5.2.2.4	Preparation of ibuprofen samples	233
5.2.3	Ibuprofen assay.....	233
5.2.3.1	Wavelength of maximum absorbance	234
5.2.3.2	Standard curve	234
5.2.3.3	Validation of Analytical Method	234
5.2.3.4	UV light absorbance by chitosan and TPP.....	235
5.2.4	Preparation of blank chitosan-TPP nanoparticles.....	235
5.2.5	Preparation of drug loading/incorporation into chitosan nanoparticles (CS-IBU-TPP) 236	
5.2.5.1	Internal entrapment of ibuprofen into chitosan matrix (ibuprofen first mixed with chitosan), referred to as (IBU+CS)/TPP	236
5.2.5.2	Internal entrapment of ibuprofen into chitosan matrix (ibuprofen first mixed with TPP), referred to as CS/(TPP+IBU).....	237
5.2.6	Effects of CS: TPP ratio on CS-IBU-TPP nanoparticles.....	238
5.2.7	Effects of ibuprofen concentration on CS-IBU-TPP nanoparticle	239
5.2.8	Characterization of chitosan nanoparticles	239
5.2.9	Drug entrapment efficiency (DEE) of ibuprofen in CS-IBU-TPP nanoparticles 240	
5.2.10	<i>In vitro</i> release of ibuprofen from CS-IBU-TPP nanoparticles.....	241
5.2.11	Statistical analysis	242
5.3	Results and discussion	243
5.3.1	Ibuprofen assay.....	243
5.3.1.1	Wavelength of maximum absorbance	243
5.3.1.2	UV light absorbance by chitosan and TPP.....	244
5.3.1.3	Standard curve and validation for ibuprofen.....	246
5.3.1.3.1	Nanoparticle formation observations.....	249
5.3.1.4	Fourier transform infrared (FT-IR) studied	250
5.3.2	Ibuprofen entrapment results using two methods UV-spectrophotometry .252	
5.3.3	Characterization of chitosan nanoparticles and effects of CS-TPP ratio on CS-IBU-TPP nanoparticles	257
5.3.3.1	Dynamic light scattering (DLS)	257
5.3.4	Effects of CS: TPP ratio on CS-IBU-TPP nanoparticles.....	261
5.3.5	Effects of ibuprofen concentration on CS-IBU-TPP nanoparticles.....	262
5.3.6	<i>In vitro</i> release of ibuprofen (IBU) from CS-IBU-TPP nanoparticles.....	265
5.3.6.1	Comparison of Drug Release Profiles: f_2 Analysis	270

5.4	Summary	272
6	Evaluation of mucoadhesive properties of chitosan nanoparticles prepared using different chitosan to tripolyphosphate (CS: TPP) ratios	275
6.1	Introduction	275
6.2	Methods and materials	277
6.2.1	Chemicals	277
6.3	Experimental	277
6.3.1	Preparation of chitosan-TPP nanoparticles	277
6.3.2	Mucin sample preparation.....	277
6.3.3	Evaluation of the mucoadhesive properties of chitosan-TPP nanoparticles .	278
6.3.3.1	Adsorption of mucin on to chitosan-TPP nanoparticles (CS: TPP).....	278
6.3.3.1.1	Viscosity analysis of chitosan nanoparticles-mucin mixtures.....	279
6.3.3.1.2	Zeta potential of chitosan nanoparticles-mucin mixtures.....	279
6.3.3.1.3	Particle Size analysis of chitosan nanoparticles-mucin mixtures	280
6.3.4	Mucin adsorption assay	281
6.3.4.1	Calibration curve of mucin using PAS/Schiff colorimetric assay.....	281
6.4	Statistical analysis	282
6.5	Results and discussion	283
6.5.1	Mucoadhesion Studies.....	286
6.5.1.1	First preparation incubation with mucin	286
6.5.1.1.1	Assessment of chitosan nanoparticle-mucin interactions by relative viscosity	286
6.5.1.1.2	Zeta potential of chitosan nanoparticles-mucin mixtures.....	289
6.5.1.1.3	Particle size of chitosan nanoparticle-mucin mixtures.....	291
6.5.1.1.4	Mucin binding test (adsorption) as indicator of mucoadhesiveness... 294	
6.5.1.2	Second preparation incubation with mucin	297
6.5.1.2.1	Assessment of chitosan nanoparticles-mucin interactions by relative viscosity, zeta potential and particle size	297
6.6	Summary	301
7	General Conclusions and Future Recommendations.....	303
8	References	308
9	Appendices.....	343
9.1	Appendix A:.....	343
9.2	Appendix B:	345
9.3	Appendix C:	345

9.4	Appendix D:.....	346
9.5	Appendix E:	350
9.6	Appendix F:	352
9.7	Appendix G:.....	355
9.8	Appendix H:.....	359
9.9	Appendix I:	360

LIST OF FIGURES

Figure 1.1: D- and L- form of glucose compared with D- and L- glyceraldehyde	3
Figure 1.2: Mode of conversion of α and β glucose from Haworth projections.	4
Figure 1.3: Structure of D-Glucosamine.	4
Figure 1.4: Structure of cellulose (The repeating unit 'n' may be several thousands).....	6
Figure 1.5: Structure of chitosan (The repeating unit 'n' may be several thousands)	7
Figure 1.6: Production of chitin and chitosan from raw material..	9
Figure 1.7: Chemical structure of chitin.	10
Figure 1.8: Preparation of chitosan (B) by the deacetylation of chitin (A).....	13
Figure 1.9: Protonated chitosan in acid solution.....	20
Figure 1.10: Representative structures of (a) Fucose, (b) Sialic acid (c) N-Acetyl-Galactosamine, (d) Galactose, and (e) Mannose.....	23
Figure 1.11: Representative structure of mucin glycoproteins and interaction sites where mucoadhesion may take place.	24
Figure 1.12: A secretory mucin glycoprotein representing a MUC protein backbone and its O-glycans. A MUC protein backbone usually consists of an NH ₂ group domain (blue), one or more central domain with a high number of tandem repeat (TR) domains (yellow), and a COOH group domain (green).	26
Figure 1.13: Mucus membrane structure.....	28
Figure 1.14: The contact and consolidation stages of mucoadhesion	29
Figure 1.15: Schematic diagram showing wetting theory of mucoadhesion	31
Figure 1.16: Diffusion theory of mucoadhesion.	31
Figure 1.17: Fracture theory of mucoadhesion.	32
Figure 1.18: An example of (a) TEM of a carbon black nanoparticle showing particle diameters ranging from 30 to 100 nm (b) SEM of NMC microparticles showing an average particle size of 10 μ m (Morelly et al., 2017), (c) SEM image of black granular fingerprint powder, the elemental carbon has a particle size of 5-10 μ m	39
Figure 1.19: Scheme of the preparation of chitosan particles by ionotropic gelation.....	44
Figure 1.20: Schematic of chitosan: TPP particle formation process of by ionotropic gelation process.	45
Figure 1.21: Different types of fingerprint patterns (a) Arch (b) Loop (c) Whorl	51
Figure 1.22: Each type of level 1 pattern (Figure 1.21) can be subdivided in to eight fingerprint sub-pattern types (Level 1 features): (a) plain arch, (b) tented arch, (c) right	

slanted loop (ulnar), (d) left slanted loop (radial), (e) plain whorl, (f) central pocked loop whorl, (g) double-loop whorl and (h) accidental whorl.....	51
Figure 1.23: An examples of level 2 and level 3 fingerprint ridge pattern features details used for the classification and individualisation of fingerprints.	52
Figure 1.24: Friction ridge skin diagram of longitudinal section	54
Figure 1.25: Molecular structure of fatty acids identified in fingermark residues: (a) Dodecanoic acid, 12: 0; (b) Myristoleic acid, 14: 1 (Tetradecenoic acid); (c) Palmitic acid, 16:0 (Hexadecanoic acid); (d) Oleic acid, 18: 1 (Octadecenoic acid).	55
Figure 1.26: Molecular structure of a wax ester (myristyl palmitoleate).....	56
Figure 1.27: Cholesterol molecular structure.....	56
Figure 1.28: Triglyceride molecular structure.	56
Figure 1.29: Types of fingermarks (a) visible fingermarks, (b) plastic marks and (c) latent fingermarks.	57
Figure 1.30: Aging of latent fingermark on a porous substrate.	60
Figure 1.31: Aging of latent fingermark on a non-porous substrate (a) cross section of latent deposit immediately after deposition (b) numerous weeks/months after deposition.....	61
Figure 2.1: Schematic representation of zeta potential: ionic concentration and potential differences as a function of distance from the charged surface of a particle suspended in a medium.....	79
Figure 2.2: Evaluation of dispersion stability by zeta potential/particle size.....	80
Figure 2.3: Particle size distribution of chitosan nanoparticle CS-TPP at (4:1) ratio, 216.0 ± 1.9 nm.	82
Figure 2.4: Models for determination of particle size distribution	83
Figure 2.5: Classifications of materials in sample shear. Where γ represents strain rate, η represents viscosity, σ represents stress, μ , expressed as the coefficient of viscosity and G represents the constant of proportionality or elastic modulus.....	84
Figure 2.6: Flow curves (shear stress vs shear rate) for Newtonian and non-Newtonian flow behaviour with yield stress region shown	86
Figure 2.7: X-ray diffraction, lattice planes (1, 2 and 3 are incident X-rays; $1'$, $2'$, and $3'$ are reflected x-rays).	87
Figure 2.8: Schematic of infrared- Attenuated Total Reflection Spectroscopy (IR-ATR).....	89
Figure 2.9: The larger arrow on the incident beam indicates a higher radiant power P_0 than that transmitted by the solution P . The path length of the absorbing solution is b and the concentration is c	90
Figure 2.10: The visible absorption spectrum respond to wavelengths from about 390 to 700 nm. The visible spectrum is the part of electromagnetic spectrum which is visible to the human eye.	91

Figure 2.11: Shows SEM setup's schematic representation as well as features within the two main areas: the specimen chamber and the electron column.....	92
Figure 2.12: Schematic diagram of the positioning of the two SEM detectors.....	94
Figure 3.1: Procedure of chitosan microparticle formation, where V represents the appropriate volumes of TPP and chitosan respectively.....	104
Figure 3.2: FTIR spectrum of (a) TPP, (b) CS, (c) CS: TPP (6:1), (d) CS: TPP (4:1), (e) CS: TPP (2:1), (f) CS: TPP (1:1), (g) CS: TPP (1:2), (h) CS: TPP (1:4), (i) CS: TPP (1:6) in buffer AB-1....	113
Figure 3.3: X-ray diffraction pattern of TPP, chitosan and of CS: TPP microparticles of seven different ratios in buffer (a) AB-10 (b) AB-11 (c) AB-12 and (d) AB-13.....	116
Figure 3.4: Relative viscosities of nine different chitosan solutions (using AB-1 to AB-9) at varying ionic strength and pH values at 25.0 ± 0.1 °C.....	118
Figure 3.5: Schematic representation of chitosan in (a) low ionic strength and (b) high ionic strength solution.....	119
Figure 3.6: Zeta potentials of nine different chitosan solutions (using AB-1 to AB-9) at varying ionic strength and pH values.	121
Figure 3.7: Example of SEM images of chitosan microparticles CS: TPP using AB-12 (a) 6:1, (b) 4:1, (c) 2:1, (d) 1:1, (e) 1:2, (f) 1:4 and (g) 1:6. Where the scale bar is 100 µm and the estimated total surface areas (based on the measurement of the sizes and areas of the particles using Image J, version 1.52a (National Institute of Health, Bethesda, USA)) of the particles are approximately ~31000, 14000, 25000, 24000, 10000, 11000 and 12000 µm ² , respectively.	123
Figure 3.8: Relative viscosities of chitosan (green columns) and CS: TPP microparticles (blue columns) solutions (using AB-1 to AB-9) at varying ionic strength and pH values.....	126
Figure 3.9: Zeta potentials of chitosan (green columns), TPP (red columns) and CS: TPP microparticles chitosan (blue columns) solutions (using AB-1 to AB-9) at varying ionic strength and pH values.	128
Figure 3.10: Particle size (D _[4,3]) of CS: TPP microparticles solutions (using AB-1 to AB-9) at varying ionic strength and pH values.....	130
Figure 3.11: Linear correlation plot (scattergram) between the experimental and predicted of relative viscosity (a), zeta potential (b) and practical size (c) for validation data.	133
Figure 4.1: Latent fingerprint development using green magnetic powder consisting of iron (I,II) oxide as a control. (a) Donor 1, (b) donor 2, (c) donor 3, (d) donor 4 and (e) donor 5..	153
Figure 4.2: Schematic representation depletion method (first approach)	154
Figure 4.3: An example of CS: TPP particles at ratio of 2:1 using buffer AB-12.	156
Figure 4.4: Schematic representation of the deposition of a fingerprints the split depletion series (second approach) for four different acetate buffers (AB-10, AB-11, AB-12 and AB-13) at CS:TPP ratios of 2:1 and 1:1 (two techniques per four formulations).....	158

Figure 4.5: An examples of latent fingerprint (donor 1) on glasses slides with different development method utilised, (a) first technique (spraying method), (b) second technique (particles in solution method) and (c) third technique (powder method)	162
Figure 4.6: An example of development of latent fingermark (donor 1) on paper using third technique (powder method).....	163
Figure 4.7: Schematic representation of third technique (A) chitosan carbon chains with ionic ends and TPP anions (B) chitosan polycations attraction with TPP polyanions making them lipophilic (C) the hydrophobic (lipophilic) ends of long carbon chains from chitosan microparticles burying themselves into the lipid residues of the latent fingerprint.....	165
Figure 4.8: Development of first depletion latent fingermarks of CS: TPP at 1:1 ratio as a powder on glass microscope slides (Naked eye) for five donors, using (a) AB-10 (b) AB-11 (c) AB-12 and (d) AB-13. All are poor quality (grade 1)	168
Figure 4.9: Development of first depletion latent fingermarks of CS: TPP at 2:1 ratio as a powder on glasses microscope slides (Naked eye) for five donors, using buffers (a) AB-10 (grade 2) (b) AB-11 (grade 3) (c) AB-12 (grade 4) and (d) AB-13 (grade 1).....	169
Figure 4.10: Development fingermarks depletion series (donor 1). Stage 1 using CS:TPP at 2:1 (a) in buffer AB-12 (left column), (b) in buffer AB-11 (right column). Stage 2 repeated but development reversed (c) in buffer AB-11 (left column), (d) in buffer AB-12 (right column).	170
Figure 4.11: Development fingermarks depletion series (donor 2). Stage 1 using CS:TPP at 2:1 (a) in buffer AB-12 (left column), (b) in buffer AB-11 (right column). Stage 2 repeated but development reversed (c) in buffer AB-11 (left column), (d) in buffer AB-12 (right column).	171
Figure 4.12: development fingermarks depletion series (donor 3). Stage 1 using CS:TPP at 2:1 (a) in buffer AB-12 (left column), (b) in buffer AB-11 (right column). Stage 2 repeated but development reversed (c) in buffer AB-11 (left column), (d) in buffer AB-12 (right column).	171
Figure 4.13: development fingermarks depletion series (donor 4). Stage 1 using CS:TPP at 2:1 (a) in buffer AB-12 (left column), (b) in buffer AB-11 (right column). Stage 2 repeated but development reversed (c) in buffer AB-11 (left column), (d) in buffer AB-12 (right column).	172
Figure 4.14: Development fingermarks depletion series (donor 5). Stage 1 using CS:TPP at 2:1 (a) in buffer AB-12 (left column), (b) in buffer AB-11 (right column). Stage 2 repeated but development reversed (c) in buffer AB-11 (left column), (d) in buffer AB-12 (right column).	172
Figure 4.15: (a) The main effect plots for quality fingerprint (Y4): pH; I.S and CS: TPP ratio. The reference line (1.75) is shown as dotted line and the steeper the slope the greater the effect of a particular parameter. (b) The interactions plot for quality finger. To visualize these effects, the Y-axis scale is always the same for each combination of factors. This graph shows that the pH*IS interaction effect is the largest.....	178

Figure 4.16: (a) A developed latent fingerprint (donor 1) on glass slide using chitosan microparticle as a powder at CS: TPP of 2:1 in buffer AB-12 (Naked eye), (b) chitosan microparticle adsorbed on fingerprint ridges under low power optical microscope, magnification 20x (grade 4).	179
Figure 4.17: (a) A developed latent fingerprint (donor 2) on glass slide using chitosan microparticle as a powder at CS: TPP of 2:1 in buffer AB-12 (Naked eye), (b) chitosan microparticle adsorbed on fingerprint ridges under low power optical microscope, magnification 20x (grade 4).	180
Figure 4.18: (a) A developed latent fingerprint (donor 3) on glass slide using chitosan microparticle as a powder at CS: TPP of 2:1 in buffer AB-12 (Naked eye), (b) chitosan microparticle adsorbed on fingerprint ridges under low power optical microscope, magnification 20x (grade 4).	180
Figure 4.19: (a) A developed latent fingerprint (donor 4) on glass slide using chitosan microparticle as a powder at CS: TPP of 2:1 in buffer AB-12 (Naked eye), (b) chitosan microparticle adsorbed on fingerprint ridges under low power optical microscope, magnification 20x (grade 4).	181
Figure 4.20: (a) A developed latent fingerprint (donor 5) on glass slide using chitosan microparticle as a powder at CS: TPP of 2:1 in buffer AB-12 (Naked eye), (b) chitosan microparticle adsorbed on fingerprint ridges under low power optical microscope, magnification 20x (grade 4).	181
Figure 4.21: Comparison of latent fingermarks development on microscope glass slides between chitosan particles at CS:TPP of 2:1 in buffer AB-12 (left halves) and green magnetic powder as a control (right halves), (a) donor 1, (b) donor 2, (c) donor 3, (d) donor 4 and (e) donor 5.	182
Figure 4.22: Representative examples of the three levels of features on latent fingermarks developed on glass slides under low power optical microscope (donor 1) using chitosan microparticles at 2:1 in buffer AB-12. Magnification (a) 8x, (b and c) 35x.	184
Figure 4.23: Representative examples of the three levels of features on latent fingermarks developed on glass slides under low power optical microscope (donor 2) using chitosan microparticles at 2:1 in buffer AB-12. Magnification: (a) 8x, (b and c) 35x.	185
Figure 4.24: Representative examples of the three levels of features on latent fingermarks developed on glass slides under low power optical microscope (donor 3) using chitosan microparticles at 2:1 in buffer AB-12. Magnification: (a) 8x, (b and c) 35x.	186
Figure 4.25: Representative examples of the three levels of features on latent fingermarks developed on glass slides under low power optical microscope (donor 4) using chitosan microparticles at 2:1 in buffer AB-12. Magnification: (a) 8x, (b and c) 35x.	187
Figure 4.26: Representative examples of the three levels of features on latent fingermarks developed on glass slides under low power optical microscope (donor 5) using chitosan microparticles at 2:1 in buffer AB-12. Magnification: (a) 8x, (b and c) 35x.	188
Figure 4.27: (a-c) High power optical microscope magnified images of latent fingermarks (donor 1) on glass microscope slide, (a) before development, magnification 4x, (b) after	

development chitosan microparticles at CS: TPP of 2:1 in buffer AB-12, magnification 4x (c) a close up view of ridges, magnification 10x shows particles adsorbed on fingermarks ridges	189
Figure 4.28: High power optical microscope images of latent fingermarks (donor 2) on glass slide; (a) development by chitosan microparticles at CS: TPP of 2:1 in buffer AB-12, magnification 4x; (b) a close up view of ridges, magnification 10x shows particles adsorbed on fingermarks ridges.	190
Figure 4.29: High power optical microscope images of latent fingermarks (donor 3) on glass slide; (a) development by chitosan microparticles at CS: TPP of 2:1 in buffer AB-12, magnification 4x; (b) a close up view of ridges, magnification 10x shows particles adsorbed on fingermarks ridges.	191
Figure 4.30: High power optical microscope images of latent fingermarks (donor 4) on glass slide; (a) development by chitosan microparticles at CS: TPP of 2:1 in buffer AB-12, magnification 4x; (b) a close up view of ridges, magnification 10x shows particles adsorbed on fingermarks ridges.	191
Figure 4.31: High power optical microscope images of latent fingermarks (donor 5) on glass slide; (a) development by chitosan microparticles at CS: TPP of 2:1 in buffer AB-12, magnification 4x; (b) a close up view of ridges, magnification 10x shows particles adsorbed on fingermarks ridges.	192
Figure 4.32: High power optical microscope images of latent fingermarks to donor 1, 3 and 5 on glass slides, (a) development by chitosan microparticles at CS: TPP of 1:1 in buffer AB-12, magnification 4x; (b) a close up view of ridges, magnification 10x.	193
Figure 4.33: SEM images (donor 1) of fingerprint development on a glass microscope slide with chitosan microparticles at 2:1 ratio in buffer AB-12; (a) magnification 22x, general overview with digital camera (inset). (b-d) Magnification 50x, 100x and 200x respectively.	195
Figure 4.34: SEM images (donor 1) of fingerprint development on glass slide with chitosan microparticles at 2:1 ratio in buffer AB-13; (a) magnification 22x, general overview with digital camera (inset). (b-d) Magnification 50x, 100x and 200x respectively.	197
Figure 4.35: SEM images (donor 2) of fingerprint development on glass microscope slide with chitosan microparticles at 2:1 ratio in buffer AB-12; (a) magnification 22x, general overview with digital camera (inset). (b-d) Magnification 50x, 100x and 200x respectively. Representative particles adhered on ridges.	198
Figure 4.36: SEM images (donor 2) of fingerprint development on glass microscope slide with chitosan microparticles at 2:1 ratio in buffer AB-13; (a) magnification 22x, general overview with digital camera (inset). (b-d) Magnification 50x, 100x and 200x respectively.	199
Figure 4.37: SEM images (donor 3) of fingerprint development on glass microscope slide with chitosan microparticles at 2:1 ratio in buffer AB-12; (a) magnification 22x, general overview with digital camera (inset). (b-d) Magnification 50x, 100x and 200x respectively. Representative particles adhered on ridges.	200

Figure 4.38: SEM images (donor 3) of fingerprint development on glass microscope slide with chitosan microparticles at 2:1 ratio in buffer AB-13; (a) magnification 22x, general overview with digital camera (inset). (b-d) Magnification 50x, 100x and 200x respectively. 201

Figure 4.39: SEM images (donor 4) of fingerprint development on glass microscope slide with chitosan microparticles at 2:1 ratio in buffer AB-12; (a) magnification 22x, general overview with digital camera (inset). (b-d) Magnification 50x, 100x and 200x respectively. Representative particles adhered on ridges. 202

Figure 4.40: SEM images (donor 4) of fingerprint development on glass microscope slide with chitosan microparticles at 2:1 ratio in buffer AB-13; (a) magnification 22x, general overview with digital camera (inset). (b-d) Magnification 50x, 100x and 200x respectively. 203

Figure 4.41: SEM images (donor 5) of fingerprint development on glass microscope slide with chitosan microparticles at 2:1 ratio in buffer AB-12; (a) magnification 22x, general overview with digital camera (inset). (b-d) Magnification 50x, 100x and 200x respectively. Representative particles adhered on ridges. 204

Figure 4.42: SEM images (donor 5) of fingerprint development on glass microscope slide with chitosan microparticles at 2:1 ratio in buffer AB-13; (a) magnification 22x, general overview with digital camera (inset). (b-d) Magnification 50x, 100x and 200x respectively. 205

Figure 4.43: SEM images (donor 1) latent fingerprint developed of CS:TPP microparticles in buffer AB-12 on glass slides (Magnification 22x) at ratio (a) 2:1 and (b) 1:6. 206

Figure 4.44: SEM images of the surface of CS: TPP microparticles using buffer AB-12 at CS:TPP ratio of (a) 2:1 and (b) 1:6. The insert of each SEM images display high magnified images (the scale bar was 10 μ m). 207

Figure 4.45: (a) SEM image low magnification (donor 1) of fingerprint development by CS:TPP particles in buffer AB-12 at ratio 1:6 on glass slide from **Figure 4.43b**. (b) Increased magnification SEM image from the centre of (a). (c, d) Two more increased in magnification. 208

Figure 4.46: Split depletion of dusted fingerprints aged on glass slides for 7 days (left halves) and 14 days (right halves) using CS:TPP at 2:1 in buffer AB-12, (a) donor 1, (b) donor 2, (c) donor 3, (d) donor 4, (e) donor 5; where index finger (left column), middle finger (medium column) and ring finger (right column). 211

Figure 4.47: Latent fingerprints deposited on glass slides and developed using chitosan microparticle as a powder at CS: TPP (2:1) in buffer AB-12 for five donors. Those pictures have been observed and taken: (a) after the 24 h post-development (upper row) and (b) after two months post-development (lower row). 213

Figure 4.48: Depletion series (donor 5 index finger), with split halves developed by chitosan microparticle CS:TPP ratio at (a) 2:1 (left) vs 1:1 (right) using AB-12; (b) 2:1 (left) vs 1:1 (right) using AB-11; (c) 2:1 (left) vs 1:1 (right) using AB-10; and (d) 2:1(left) vs 1:1 (right) using AB-13 216

Figure 4.49: Depletion series (donor 5 middle finger), with split halves developed by chitosan microparticle CS:TPP ratio at (a) 2:1 (left) vs 1:1 (right) using AB-12; (b) 2:1 (left) vs 1:1 (right)

using AB-11; (c) 2:1 (left) vs 1:1 (right) using AB-10; and (d) 2:1(left) vs 1:1 (right) using AB-13	217
Figure 4.50: Depletion series (donor 5 ring finger), with split halves developed by chitosan microparticle CS:TPP ratio at (a) 2:1 (left) vs 1:1 (right) using AB-12; (b) 2:1 (left) vs 1:1 (right) using AB-11; (c) 2:1 (left) vs 1:1 (right) using AB-10; and (d) 2:1 (left) vs 1:1 (right) using AB- 13	217
Figure 4.51: Depletion series (donor 4 index finger), with split halves developed by chitosan microparticle CS:TPP ratio at (a) 2:1 (left) vs 1:1 (right) using AB-12; (b) 2:1 (left) vs 1:1 (right) using AB-11; (c) 2:1 (left) vs 1:1 (right) using AB-10; and (d) 2:1 (left) vs 1:1 (right) using AB- 13	218
Figure 4.52: Depletion series (donor 4 middle finger), with split halves developed by chitosan microparticle CS:TPP ratio at (a) 2:1 (left) vs 1:1 (right) using AB-12; (b) 2:1 (left) vs 1:1 (right) using AB-11; (c) 2:1 (left) vs 1:1 (right) using AB-10; and (d) 2:1 (left) vs 1:1 (right) using AB- 13	218
Figure 4.53: Depletion series (donor 4 ring finger), with split halves developed by chitosan microparticle CS:TPP ratio at (a) 2:1 (left) vs 1:1 (right) using AB-12; (b) 2:1 (left) vs 1:1 (right) using AB-11; (c) 2:1 (left) vs 1:1 (right) using AB-10; and (d) 2:1 (left) vs 1:1 (right) using AB- 13	219
Figure 4.54: Depletion series (donor 3 index finger), with split halves developed by chitosan microparticle CS:TPP ratio at (a) 2:1 (left) vs 1:1 (right) using AB-12; (b) 2:1 (left) vs 1:1 (right) using AB-11; (c) 2:1 (left) vs 1:1 (right) using AB-10; and (d) 2:1 (left) vs 1:1 (right) using AB- 13	219
Figure 4.55: Depletion series (donor 3 middle finger), with split halves developed by chitosan microparticle CS:TPP ratio at (a) 2:1 (left) vs 1:1 (right) using AB-12; (b) 2:1 (left) vs 1:1 (right) using AB-11; (c) 2:1 (left) vs 1:1 (right) using AB-10; and (d) 2:1 (left) vs 1:1 (right) using AB- 13	220
Figure 4.56: Depletion series (donor 3 ring finger), with split halves developed by chitosan microparticle CS:TPP ratio at (a) 2:1 (left) vs 1:1 (right) using AB-12; (b) 2:1 (left) vs 1:1 (right) using AB-11; (c) 2:1 (left) vs 1:1 (right) using AB-10; and (d) 2:1 (left) vs 1:1 (right) using AB- 13	220
Figure 4.57: Depletion series (donor 2 Index finger), with split halves developed by chitosan microparticle CS:TPP ratio at (a) 2:1 (left) vs 1:1 (right) using AB-12; (b) 2:1 (left) vs 1:1 (right) using AB-11; (c) 2:1 (left) vs 1:1 (right) using AB-10; and (d) 2:1(left) vs 1:1 (right) using AB-13	221
Figure 4.58: Depletion series (donor 2 Middle finger), with split halves developed by chitosan microparticle CS:TPP ratio at (a) 2:1 (left) vs 1:1 (right) using AB-12; (b) 2:1 (left) vs 1:1 (right) using AB-11; (c) 2:1 (left) vs 1:1 (right) using AB-10; and (d) 2:1 (left) vs 1:1 (right) using AB- 13	221
Figure 4.59: Depletion series (donor 2 ring finger), with split halves developed by chitosan microparticle CS:TPP ratio at (a) 2:1 (left) vs 1:1 (right) using AB-12; (b) 2:1 (left) vs 1:1 (right)	

using AB-11; (c) 2:1 (left) vs 1:1 (right) using AB-10; and (d) 2:1 (left) vs 1:1 (right) using AB-13.	222
Figure 4.60: Depletion series (donor 1 index finger), with split halves developed by chitosan microparticle CS:TPP ratio at (a) 2:1 (left) vs 1:1 (right) using AB-12; (b) 2:1 (left) vs 1:1 (right) using AB-11; (c) 2:1 (left) vs 1:1 (right) using AB-10; and (d) 2:1(left) vs 1:1 (right) using AB-13	222
Figure 4.61: Depletion series (donor 1 middle finger), with split halves developed by chitosan microparticle CS:TPP ratio at (a) 2:1 (left) vs 1:1 (right) using AB-12; (b) 2:1 (left) vs 1:1 (right) using AB-11; (c) 2:1 (left) vs 1:1 (right) using AB-10; and (d) 2:1(left) vs 1:1 (right) using AB-13	223
Figure 4.62: Depletion series (donor 1 ring finger), with split halves developed by chitosan microparticle CS:TPP ratio at (a) 2:1 (left) vs 1:1 (right) using AB-12; (b) 2:1 (left) vs 1:1 (right) using AB-11; (c) 2:1 (left) vs 1:1 (right) using AB-10; and (d) 2:1 (left) vs 1:1 (right) using AB-13	223
Figure 5.1: Ibuprofen dissociation	229
Figure 5.2: First method an internal entrapment of ibuprofen into chitosan nanoparticles, ibuprofen first mixed with chitosan: (IBU+CS)/TPP.	237
Figure 5.3: Second method an internal entrapment of ibuprofen into chitosan nanoparticles, ibuprofen first mixed with TPP: CS/(TPP+IBU).....	238
Figure 5.4: Method summary for drug release experiment.	242
Figure 5.5: UV- absorption spectrum of chitosan (red) and ibuprofen (green).	243
Figure 5.6: UV- absorption spectrum of ibuprofen in PBS (pH 7.4); the maximum absorbance wavelength (λ_{max}) of ibuprofen in PBS was found to be value at 263.9 nm.....	244
Figure 5.7: UV- absorbance scan for chitosan.	245
Figure 5.8: UV- absorbance scan for TPP.....	245
Figure 5.9: Mean calibration curve for ibuprofen preparation in PBS (pH 7.4)..	246
Figure 5.10: Scheme illustration ibuprofen loading/incorporation into chitosan nanoparticles (CS-IBU-TPP).....	250
Figure 5.11: FT-IR spectra of (a) Pure ibuprofen, (b) blank CS-TPP nanoparticles (c) ibuprofen loaded chitosan nanoparticles (CS-IBU-TPP).	251
Figure 5.12: First method an internal entrapment of ibuprofen into chitosan nanoparticles, ibuprofen first mixed with chitosan: (IBU+CS)/TPP. The entrapment efficiency of ibuprofen generally increased with CS:TPP ratio for the CS+IBU/TPP design.	254
Figure 5.13: Second method an internal entrapment of ibuprofen into chitosan nanoparticles, ibuprofen first mixed with TPP: CS/(TPP+IBU).The entrapment efficiency of ibuprofen differed greatly and appeared to be independent of CS:TPP ratio in the CS/(TPP+IBU) design.	254

Figure 5.14: The effect of (CS: TPP) ratio on the (a) particle size and (b) polydispersity index (PDI), ibuprofen free nanoparticles (blue columns); ibuprofen loaded nanoparticle (brown columns).....	259
Figure 5.15: The effect of (CS:TPP) ratio on zeta potential, ibuprofen free nanoparticles (blue columns); ibuprofen loaded nanoparticle (brown columns).	261
Figure 5.16: <i>In vitro</i> release profiles of ibuprofen from CS-IBU-TPP nanoparticles with respect to different concentration of ibuprofen, carried out in phosphate buffer at pH 7.4 maintained at 37 °C.	266
Figure 6.1: Periodate oxidation of sialic acid to aldehyde.....	281
Figure 6.2: Relative viscosity of mucin (red column), chitosan (green column), a native chitosan nanoparticles (blue columns) and chitosan nanoparticle-mucin mixtures-mucin (white columns) at 37 °C.	287
Figure 6.3: Zeta potential values obtained for mucin (red column), chitosan (green column), native chitosan nanoparticles (blue columns) and chitosan nanoparticle-mucin mixtures (white columns) at 37 °C.....	290
Figure 6.4: Particle size of mucin (red column), a native chitosan nanoparticles (blue columns) and chitosan nanoparticle–mucin mixtures (white columns) at 37 °C..	292
Figure 6.5: PDI of mucin (red column), a native chitosan nanoparticles (blue columns) and chitosan nanoparticles–mucin mixtures (white columns) at 37 °C.	293
Figure 6.6: Calibration curve of mucin..	295
Figure 6.7: Mucin binding efficiency (adsorption) of different chitosan nanoparticles of different CS:TPP ratios..	296
Figure 6.8: Diagrammatic representation of adsorption of mucin on CS:TPP nanoparticles and aggregation of nanoparticles in the presence of an excess of mucin.	300

LIST OF TABLES

Table 1.1: Examples of chitosan-based biomedical devices and drug delivery systems.....	15
Table 1.2: Classification of mucins classification of mucins.....	25
Table 1.3: Theories of mucoadhesion.	30
Table 1.4: Different methods of preparation of micro/nanoparticles of chitosan.	42
Table 1.5: An examples of chemical compounds used to detect of fingerprint.	72
Table 3.1: Acetate buffers of varying ionic strength and pH. Buffers AB-1 to AB-9 were used to create generate model equations and buffers AB-10 to AB-13 were used in model validation (pKa of acetic acid is 4.75).....	102
Table 3.2: Summaries the different concentrations required to make CS: TPP particles	109
Table 3.3: Observed (Exp.) responses and predicted (Pred.) values and percent error (bias ^a %) for relative viscosity (Y1), zeta potential (Y2) and particle size (Y3).....	136
Table 3.4: Change in particle size and zeta potential as concentrations of TPP and molecular weight of chitosan are changed.....	142
Table 4.1: Various chemicals or powders used for development of latent fingerprints.....	147
Table 4.2: Parameters used in the factorial design.	151
Table 4.3: Characteristics of the chitosan microparticles obtained by the factorial design 2 ³ for different formulation F1 to F8. Fingerprint quality was assessed using chitosan microparticles on glass microscope slides.....	174
Table 5.1: UV-Spectrophotometric method validation for ibuprofen assay.....	248
Table 5.2: The particle size, zeta potential, drug content (DC) and DEE of CS-IBU-TPP nanoparticles at variable CS: TPP ratios.	262
Table 5.3: The particle size, zeta potential, drug content (DC) and DEE of CS-IBU-TPP nanoparticles at variable concentrations of ibuprofen (IBU).	264
Table 6.1: Second stage measurements of relative viscosity, zeta potential and particle size of different CS: TPP nanoparticles before and after incubation with mucin.....	298

Chapter 1

General Introduction

1 General Introduction

1.1 Carbohydrates

Carbohydrates are also known as saccharides (Greek: sakcharon – sugar) and they are the most broadly distributed molecules in both plant and animal tissues. In addition, carbohydrates are necessary for all living organisms, as skeletal structures in plants (cellulose), exoskeleton of some insects and crustaceans (chitin). In fact, plant and animal tissues differ widely in the relative abundance of the many major classes of organic compounds such as carbohydrates, proteins and lipids. Animals have 1 % of carbohydrates, whereas plants have 30 %. Some carbohydrates such as glycoproteins and glycolipids are present in the cell membrane and are important in cellular functions such as cell growth. Carbohydrates may be defined as polyhydroxy aldehydes or ketones or compounds which produce them on hydrolysis (Pigman and Goepf, 1945).

Carbohydrates can be classified into three major types: monosaccharides, oligosaccharides and polysaccharides. This classification is based on the number of sugar units. Monosaccharides are the simplest type of carbohydrates which cannot be hydrolysed to smaller units. In addition, they contain three to seven carbons with a functional a free aldehyde ($R-CHO$) or ketone ($R_2=CO$) group and two or more hydroxyl ($R-OH$) groups (Hedley, 2001).

The most abundant monosaccharides in nature are the 6-carbon sugars such as glucose (aldohexoses) and fructose (ketohexose). Monosaccharides are crystalline, colourless and readily soluble in water. Due to the presence of an asymmetric carbon atom, monosaccharides are optically active. The structures of D-glucose and L-glucose (**Figure 1.1**), are examples for optical isomers, based on the reference monosaccharide, D- and L-glyceraldehyde (David and Michael, 2013).

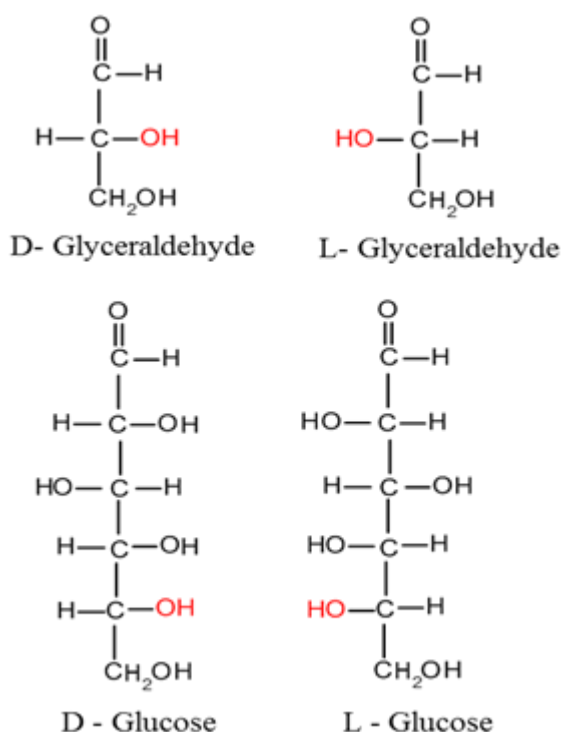


Figure 1.1: D- and L- form of glucose compared with D- and L- glyceraldehyde (David and Michael, 2013)

There are two different forms of D-glucose known as α -form and β -form. The 6-membered rings from sugars are derived from pyran. So, this results in the formation of a stable 6-membered ring oxygen heterocycle (pyranose form) (**Figure 1.2**).

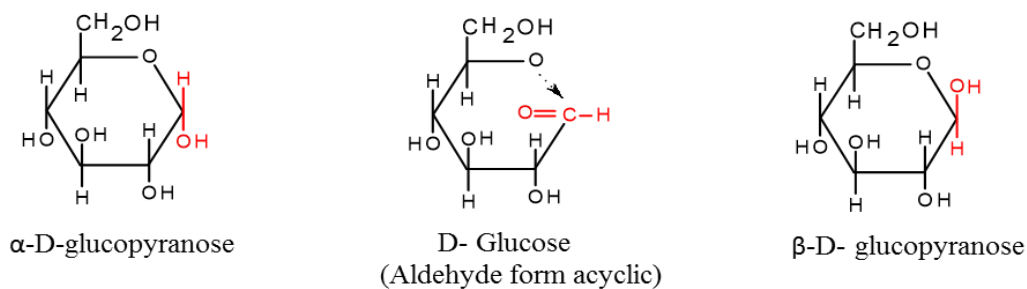


Figure 1.2: Mode of conversion of α and β glucose from Haworth projections.

There are several derivatives of monosaccharides, some of which are physiologically important such as amino sugars which are widely distributed naturally. Amino sugars have an amine group (NH_2) has been replaced the hydroxyl group (OH) group usually at carbon 2 (C2) in the parent hexose *e.g.* D-glucosamine, D-galactosamine and N-Acetylneuraminic acid (sialic acid) (**Figure 1.3**) (Pigman and Goepp, 1945, Satyanarayana and Chakrapani, 2013).

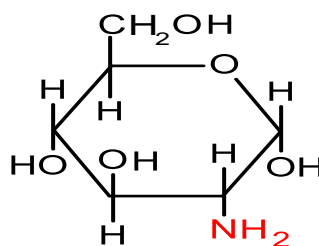


Figure 1.3: Structure of D-Glucosamine.

Oligosaccharides (disaccharides) are crystalline, water-soluble and sweet to taste. They consist of two (or more) monosaccharide units joined together by glycosidic bonds. Oligosaccharides consist of 2 to 10 monosaccharide molecules on hydrolysis.

Maltose, sucrose and lactose for example are all disaccharides (Jain et al., 2005). Oligosaccharides are most commonly found in plants.

1.1.1 Polysaccharides

Polysaccharides are formed of repeating units of monosaccharides or their derivatives. These units are joined together by glycosidic bonds, therefore polysaccharides can have high molecular weight. Moreover, they can be either linear or branched polymers, depending upon the arrangement of the monosaccharide units in the chain. Polysaccharides have a large number of reactive functional groups such as amino, hydroxyl and carboxyl groups which could form bonds with other compounds. In addition, polysaccharides can be changed chemically and biochemically resulting in many types of polysaccharide derivatives, due to the presence of reactive functional groups on molecular chains (Liu et al., 2008b). There are abundant source of polysaccharides in nature such as, plant based (*e.g.* pectin), animal based (*e.g.* chitosan) and microbial origin (*e.g.* xanthan gum). Chemically, polysaccharides may be classified into two types: homopolysaccharides and heteropolysaccharides (Pigman and Goepf, 1945).

1.1.1.1 Homopolysaccharides

When all the monosaccharides in a polysaccharide are of the same type, the polysaccharide is called a homopolysaccharide. Cellulose (**Figures 1.4**) and amylose for example are both linear homopolysaccharides which consist of glucose repeating units (Pigman and Goepf, 1945). In addition, homopolysaccharides may also be branched, such as amylopectin and glycogen.

As glycosidic linkage can be formed at any one of the hydroxyl groups of a monosaccharide therefore lead to the occurrence of branches in polysaccharides.

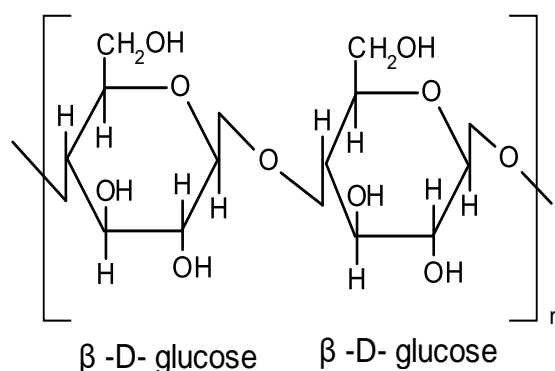


Figure 1.4: Structure of cellulose (The repeating unit 'n' may be several thousands).

1.1.1.2 Heteropolysaccharides

When the polysaccharide contains different monosaccharides or their derivatives, they are referred to as heteropolysaccharides, which can also be linear or branched polysaccharides. Mucopolysaccharides are heteropolysaccharides composed of repeating units of sugar derivatives, namely amino sugars and uronic acids. These are more commonly known as glycosaminoglycans (GAGs). Hyaluronic acid, chondroitin sulfate, and heparin are important examples for mucopolysaccharides. Polysaccharides have come under increasing attention due to their industrially useful physical, chemical and biological properties amongst these polysaccharides it is chitosan (**Figure 1.5**) and its derivatives, which have generated particular interest (Rampino et al., 2013).

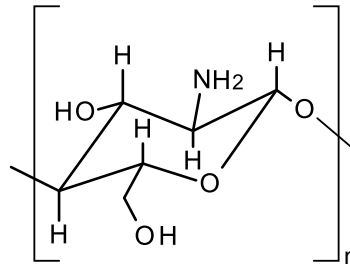


Figure 1.5: Structure of chitosan (The repeating unit 'n' may be several thousands)
(Nyström et al., 1999).

1.2 Chitosan

The term chitosan (CS) is generally understood to be the generic name for a family of strongly polycationic polysaccharide derivatives, and chitosan is classified as heteropolymer that consists of glucosamine and N-acetyl glucosamine residues linked together by $\beta(1\rightarrow4)$ glycosidic bonds. Chitosan is a biomaterial derived from deacetylation of chitin (poly-N-acetyl-D-glucosamine), which is second most abundant naturally occurring polysaccharide on earth after cellulose (Roberts, 1992). Moreover, chitosan is potentially more useful than chitin, due to its solubility in some solvents.

In addition, chitosan refers to a family of copolymers with different fractions of acetylated units, and consists of two types of monomers which are chitin-monomers and chitosan-monomers (Roberts, 1992). Chitosan is a semi-crystalline polymer which appears in the form of colourless and odourless flakes. The advantage of chitosan over other polysaccharides is that its chemical structure allows specific modifications at the C-2 position without too many difficulties (Nyström et al., 1999).

1.2.1 Production of chitin and chitosan

Many polysaccharides such as pectin, alginate and carrageenan are acidic/ negatively charged in nature (polyanions), on the other hand chitin and chitosan are the only examples of naturally occurring positively polysaccharides which are polycations, as mucin for example is negatively charged this may prove useful in mucoadhesive applications.

Chitin is a linear polysaccharide consisting of (1→4)-linked 2-acetamido-2-deoxy-β-D-glucose (N-acetyl-D-glucosamine), while chitosan is a linear polysaccharide consisting of β (1→4)-linked 2-amino-2-deoxy-D-glucopyranose (D-glucosamine) and 2-acetamido-2-deoxy-D-glucose (N-acetyl-D-glucosamine) units. Commercial chitin and chitosan both consist of types of monomers. Chitin is found in the cell walls of microorganisms such as fungi and yeasts, in the exoskeletons of crustaceans such as crab and shrimp, and insects, as well as in various other specialized organs, such as the beaks of cephalopods (Roberts, 1992). Moreover, commercial chitosan can be obtained by hydrolysis of the amino acetyl group of chitin (Giri et al., 2012). There are three different types of structures in which chitin occurs in nature: alpha, beta and gamma chitin. The exoskeletons of crustaceans contain approximately 30 – 40 % protein, 30 – 50 % calcium carbonate, and 20 – 30 % chitin on a dry basis, chitosan can be extracted from crustacean shells (Aranaz et al., 2009) and the isolation of chitosan involves four stages including: demineralization (DM), deproteinization (DP), decolorization, and deacetylation (DA) (**Figure 1.6**).

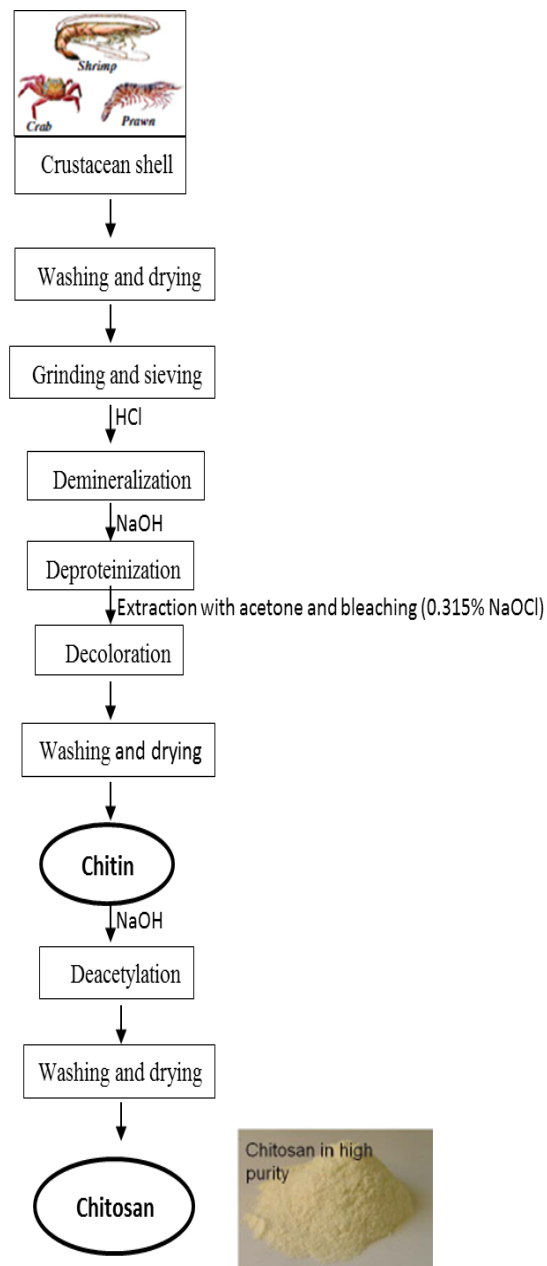


Figure 1.6: Production of chitin and chitosan from raw material (Aranaz et al., 2009).

Nevertheless, the isolation of chitin (**Figure 1.7**) specifically consists of only two stages: demineralization (DM) and deproteinization (DP). The structure of α -chitin has been studied more widely than that of either the β - or γ -forms, because it is the most common polymorphic form (Saito et al., 1997). In addition, β -chitin is degraded

more easily than α -chitin (Kurita, 1998) due their crystalline and amorphous structures. In α -chitin, β -chitin and γ -chitin, the chitosan chains are ordered into sheets. In the α -form, adjacent sheets are oriented in opposite directions, with strong inter- and intra-sheet hydrogen bonds, leading to a strong crystal form which solvents have difficulty to penetrate. In the β -form, sheets are oriented in the same direction allowing only weak intra-sheet hydrogen bonds which result in higher reactivity to reactions such as acetylation, acetolysis, tritylation, tosylation, *etc.* and affinity for solvents than α -chitin (Buschmann et al., 2013, Kurita, 1998). In γ -chitin every third sheet has the opposite direction to the two previous sheets (**Figure 1.7**) (Aranaz et al., 2009).

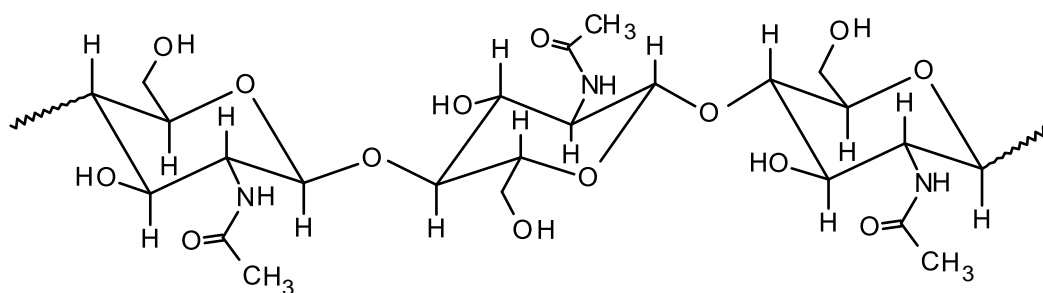


Figure 1.7: Chemical structure of chitin.

1.2.1.1 Deproteinization

Crustacean shells are commonly ground then treated with dilute sodium hydroxide solution NaOH (1-10 %) at high temperature (65 - 100 °C) for 0.5 to 12 hours to dissolve the proteins and other sugars present. Then samples are filtered under vacuum, after which the filtrate is washed with water and oven dried. Reports suggest that the optimum conditions for deproteinization step is treatment of the crawfish

shells with 3.5 % (w/w) NaOH solution for 2 hours at 65 °C with constant stirring and the optimum ratio of a solid to solvent is 1:10 (w/v) (No and Meyers, 1989).

1.2.1.2 Demineralization

Demineralization process is carried out on the deproteinised shells with dilute hydrochloric acid (HCl) at room temperature overnight with constant stirring to dissolve calcium carbonate as calcium chloride. This requires a solid to liquid ratio of approximately 1:15 - 1:20 (w/v) prior to filtration under vacuum. The filtrate is washed with water and oven dried (Oduor-Odeto et al., 2005, Mathur and Narang, 1990).



Previous research has shown that optimum demineralization is accomplished by constant stirring of the dried ground crawfish shell with 1M HCl for 30 - 60 min at room temperature and the solid to solvent ratio is 1:15 – 1:20 (w/v). During the demineralization process undesirable foams are produced due to the CO₂ formed. To reduce these foams, it is often necessary to use a commercial antifoam which consists of a 10 % solution of active silicone polymer without an emulsifier (No and Meyers, 1989, Puvvada et al., 2012).

1.2.1.3 Decolouration

The pigments in the crustacean shells produce complex compounds with chitin. Moreover, the deproteinization and demineralization processes produce a coloured chitin product from crustacean sources, therefore a decolouration step is added to remove pigments and obtain a white chitin powder (Rinaudo, 2006). A number of studies have used reagents to remove pigments from crustacean exoskeleton usually crab. One study has reported decolourised chitin for overnight with a 1:1 mixture of acetone/ethanol at a solid: liquid ratio of 1:10 (Oduor-Odeto et al., 2005). In another study, it has been suggested that to produce a near white coloured product requires extraction with acetone and to be dried for 2 hours at room temperature after that bleaching with sodium hypochlorite solution NaOCl 0.315% (v/v) for 5 min. Also, a solid to solvent ratio is 1:10 (w/v), based on dry shell after that samples are washed with water and dried using vacuum for 2-3 hours until the powder is crispy (No and Meyers, 1989).

1.2.1.4 Deacetylation

Deacetylation can be defined as a process which to convert acetamide groups (NHCOCH_3) of chitin to amino groups (NH_2) of chitosan (Huang et al., 2004) (**Figure 1.8**). It is usually achieved by treatment of decolourised chitin with concentrated sodium or potassium hydroxide solution (40 - 50 % w/v) usually at 100 °C for 30 – 60 min or longer to remove some or all of the acetyl groups from the chitin (Oduor-Odeto et al., 2005). Afterwards the samples are cooled for 30 min at room temperature then are washed continuously with the 50 % NaOH and filtered in order to retain the solid substance, which is the chitosan polymer. Finally, in order to

dry chitosan, the samples were left in oven at 110 °C for 6 hours (Mathur and Narang, 1990).

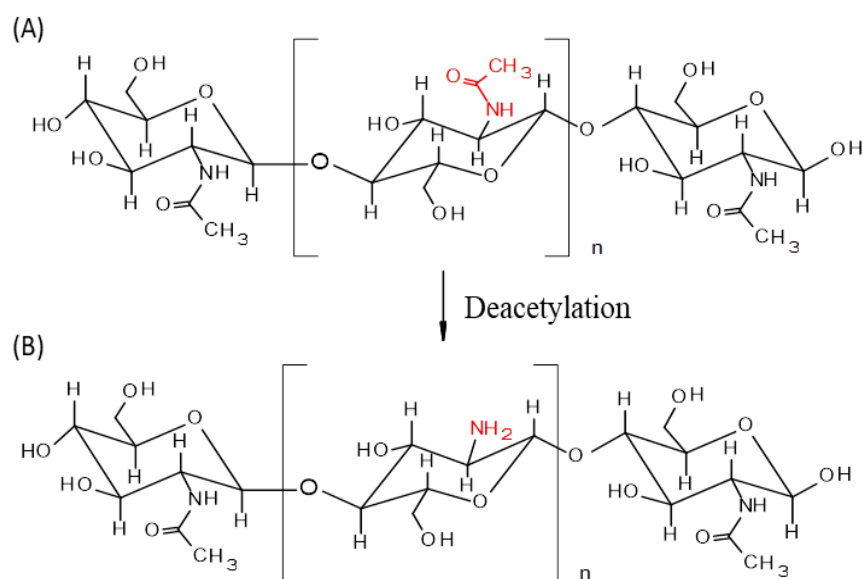


Figure 1.8: Preparation of chitosan (B) by the deacetylation of chitin (A)
(Pillai et al., 2009).

The term used to describe the percentage of primary amino group in the polymer backbone is degree of deacetylation (DD). The majority of commercial grades of chitosan are obtained by alkaline deacetylation of chitin, which leads to material containing 70-100 % glucosamine and 0-30 % N-acetyl glucosamine units. Therefore, grades of chitosan vary in their degree of deacetylation (DD), as well as molecular weight (MW) (Hamdine et al., 2005, Sinha et al., 2004). Moreover, the DD of commercial chitosan is approximately 66 - 95 %, and the molecular weight (MW) approximately 10,000 – 1,000,000 g/mol (Kas, 1997, Mathur and Narang, 1990). According to chitin and chitosan chemical structures, the difference between chitin

and chitosan is the acetyl group content of the polymers, therefore as the chitosan chain has a free amino group it is the most useful derivative of chitin (**Figure 1.8**).

The extracted chitosan has to be purified to make it suitable for the pharmaceutical usage. Therefore a further three processes are carried out including: filtration to remove of insoluble particles, precipitation of chitosan with 1N NaOH to neutralise the NH_3^+ groups to NH_2 and finally, demetallisation of retrieved chitosan (Puvvada et al., 2012).

1.2.2 Applications for Chitosan

Chitosan has some industrially useful characteristics such as gel-forming ability at low pH, and has therefore been widely studied for a number of pharmaceutical and biomedical applications (Kumar et al., 2004). Some applications of chitosan in both the polymeric and particle form over the last ten years in the pharmaceutical and medical fields are summarized in **Table 1.1**.

Table 1.1: Examples of chitosan-based biomedical devices and drug delivery systems

Type of system	Active Substance (drug)	Application	Reference
Chitosan:TiO ₂	Ibuprofen	Drug-delivery system	(Kamari and Ghiaci, 2016)
Chitosan nanoparticles	Docetaxel	Drug delivery system for cancer Chemotherapy	(Jain et al., 2016)
Chitosan nanoparticles	Timolol	(Eye) drug-delivery system	(Siafaka et al., 2015)
Chitosan nanoparticles	Alendronate sodium	Drug-delivery system	(Miladi et al., 2015)
Chitosan polymer	Catechol	Mucoadhesion	(Kim et al., 2015)
Chitosan: TPP nanospheres	Capecitabine	Anticancer therapy	(Katakam et al., 2015)
Chitosan: TPP nanospheres	Albendazole	Drug-delivery system	(Kang et al., 2015)
Chitosan-glutaraldehyde microspheres	Puerarin	Mucoadhesive drug-delivery carriers	(Hu et al., 2015)
CS-MMT/TPP	Betaxolol hydrochloride	Ocular drug delivery	(Hou et al., 2015)

Chitosan Film	Ibuprofen	Oral mucosal drug Delivery	(Tang et al., 2014)
Chitosan– (PEG) nanoparticles	Ibuprofen	Drug delivery systems	(Najafabadi et al., 2014)
Chitosan	Porcine gastric mucin	Mucoadhesive buccal drug delivery systems	(Meng-Lund et al., 2014)
Chitosan	Mucin from porcine stomach	Mucoadhesion	(Menchicchi et al., 2014)
CS-TPP nanoparticles	Thiocolchicoside	Potential oral drug delivery system	(Nanda et al., 2012)
CS-TPP nanoparticles	Mesobuthus eupeus venom	An antigen delivery system	(Mohammadpour Dounighi et al., 2012)
Chitosan: TPP microparticles	Heparin	Controlled release of drug	(Martins et al., 2012)
Chitosan: TPP nanoparticles	BSA	Protein drug delivery	(Kafshgari et al., 2011)
Chitosan: TPP nanoparticles	Methotrexate and calcium folinate	Drug delivery	(Jingou et al., 2011)
Chitosan: TPP nanoparticles	(BSA), Ribonuclease A, Fibrinogen, α -Lactalbumin and Transferrin	Drug delivery	(Jarudilokkul et al., 2011)
Chitosan: TPP nanoparticles	p-DNA	Gene delivery application	(Gaspar et al., 2011)

TCS: TPP nanoparticles	Cytocompatibility	Biomedical applications	(Anitha et al., 2011)
CS: TPP nanoparticles	Silver	Biomedical applications	(Ali et al., 2011)
CS: TPP nanoparticles	Ascorbyl palmitate	Drug delivery	(Yoksan et al., 2010)
CS: TPP nanoparticles	Snake venom	Protein delivery system	(Mohammadpourounighi et al., 2010)
CS: TPP nanoparticles	Hyaluronic acid	Drug delivery applications	(Nasti et al., 2009)
CS: TPP nanoparticles	Ciprofloxacin	Drug delivery systems	(Liu and Gao, 2009)
CS: TPP microparticles	Cyclosporin A	Drug delivery systems	(Cheon and Chung, 2009)
CS: TPP nanoparticles	Estradiol	Drug delivery systems	(Wang et al., 2008a)
CS: TPP nanoparticles	Dorzolamide and pramipexole	Drug delivery systems	(Papadimitriou et al., 2008)
CS: ALG	Gatifloxacin	Drug carriers for ocular delivery	(Motwani et al., 2008)

nanoparticles			
CS: TPP	Albumin and gelatin	Drug delivery Systems	(Jain and Banerjee, 2008)
nanoparticles			
CS: TPP	Tea catechins	Drug delivery Systems	(Hu et al., 2008)
nanoparticles			
CS: GA microspheres glutaraldehyde	Ibuprofen	Drug delivery	(Kulkarni et al., 2007)
nanoparticles			
CS: TPP	BSA	Protein delivery	(Gan and Wang, 2007)
nanoparticles			
CS: TPP	FITC	Applications in biological staining	(Zhao and Wu, 2006)
nanoparticles			
CS: TPP	siRNA	Delivery system for siRNA	(Katas and Alpar, 2006)
nanoparticles			
CS: GA microspheres glutaraldehyde	Centchroman	Drug delivery	(Gupta and Jabrail, 2006)
nanoparticles			
Chitosan Microspheres	Carbamazepine	Drug delivery	(Gavini et al., 2006)
nanoparticles			
CS: TPP microspheres	Ampicillin	Drug delivery	(Anal et al., 2006)

1.2.3 Structural and physicochemical characteristics of chitosan

The structural units of chitosan have one reactive primary amino group (NH_2) on the C-2 position of each D-glucosamine unit, and two reactive free hydroxyl groups (OH) for each C-6 and C-3 position building unit (glucosamine and N-acetyl-D-glucosamine). These groups (both amino and hydroxyl) can be modified to obtain different chitosan derivatives, and provide opportunities for chemical modification to impart useful physicochemical properties and distinctive biological functions (Giri et al., 2012, Chen et al., 2011, Nyström et al., 1999).

In addition, the amino and hydroxyl groups are responsible for the formation of hydrogen bonds (H-bonds) between molecules of the polymer. The chitosan molecules form a large inter-chain structural network due to these hydrogen bonds, which affect several properties such as viscosity, solubility and absorbability.

The pKa, which means the logarithmic scale of the acid dissociation constant, of the glucosamine unit in chitosan is approximately 6.3, therefore it is ionised in acidic medium (Yalpani and Hall, 1984). Moreover, some properties of chitosan can be modified, such as the pKa and solubility, by changing the degree of deacetylation and formulating conditions such as the ionic strength and pH (Dyer et al., 2002). The free amine groups NH_2 on chitosan molecules can be easily protonated to NH_3^+ in acidic aqueous solutions, therefore the net charge/ zeta potential on the chitosan is influenced by pH.



Therefore, chitosan is present in solutions in a cationic polyelectrolyte form, which opens the possibility for interactions with negatively charged substances (anions and polyanions) including for example mucin (Qaqish and Amiji, 1999).

1.2.3.1 Solubility

Chitosan is a weak base and it is insoluble at neutral and alkaline pH, as well as in water and some organic solvents such as ethanol (Hu et al., 2008, Kotze et al., 1999, Sudha, 2017), due to the formation of intermolecular hydrogen bonds (He et al., 1998). However, chitosan is soluble in a dilute aqueous acidic environment (pH < 6.0). The solubility of chitosan depends on the distribution of free amino and N-acetyl groups. In dilute acids (pH < 6.0), the free amino groups on glucosamine units take up hydrogen ions (H^+) which lead to protonated R-NH_3^+ , and consequently the chitosan molecule becomes a polycationic electrolyte and is then soluble (**Figure 1.9**) (Kwang-hee, 1983).

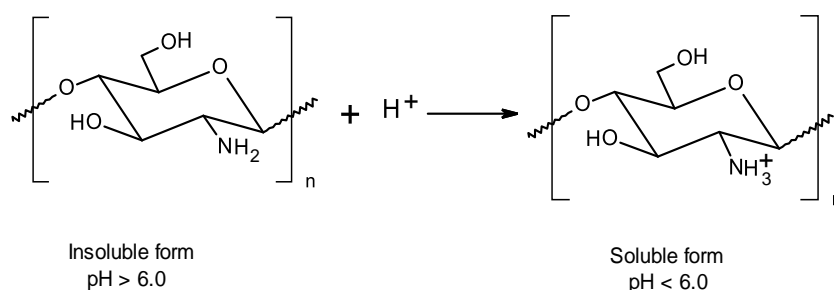


Figure 1.9: Protonated chitosan in acid solution (Kumirska et al., 2011).

Therefore, chitosan is capable of reacting with organic and inorganic acids, such as hydrochloric acid and acetic acid, under acidic conditions (Rinaudc et al., 1999, Kim et al., 2006). On the other hand, in alkaline solutions or with polyanions, chitosan tends to lose its charge on the NH_3^+ group, and therefore may precipitate from solution due to deprotonation of the amino groups (Nyström et al., 1999). There are factors which affect the solubility of chitosan. The solubility increases with increases in the degree of deacetylation, temperature and stirring rate, whereas it decreases with increasing molecular weight (Wu et al., 2005).

1.2.3.2 Biodegradability, biocompatibility and toxicity

In the recent decades, chitosan has been one of the major interesting research subjects due to its significant biological, physical and chemical properties, such as biocompatibility, biodegradability, hydrophilicity, nontoxicity, adsorptive properties, film-forming ability and antimicrobial activity (Lee et al., 1995, He et al., 1998). Chitosan is a biodegradable polysaccharide. Biodegradation is the breakdown of polymer chains into oligomers and monomers assisted via a biological compounds after responding to the physio-chemical conditions (Chellat et al., 2000). The most significant advantage of biodegradable substances is the ease of disappearance of these substances from the body as a result of their biodegradation after implantation in human body (Yang et al., 2007). Using chitosan as drug delivery system depends on its biodegradation and metabolic fate in the body (Kean and Thanou, 2010). There are two biodegradation mechanisms: chemical and enzymatic. An acid catalysed degradation *i.e.* in the stomach for example is a chemical degradation. Moreover, lysozymes in the body example is an enzyme degradation of chitosan into glucosamine and N-acetyl-glucosamine (Dash et al., 2011). The biodegradation of

chitosan depends on its degree of deacetylation, molecular weight and strength of cross-linking (for example with TPP as an ionic cross-linker). Therefore, the higher degree of deacetylation, molecular weight and strength of cross-linking of chitosan results in the slower biodegradation (Yamamoto and Amaike, 1997, Zhang and Neau, 2001, Kean and Thanou, 2010). Moreover, chitosan is degraded slowly by the chitanase enzyme to monomers of amino sugars, which are harmless and can be completely absorbed by the human body (Aiba, 1992, Chellat et al., 2000).

1.3 Mucin

Mucus is a thick complex material that lines the luminal surface of the gastrointestinal, urogenital, respiratory and eye tissues, also, the peritoneal surface of intra-abdominal organs in humans and most animals (Lai et al., 2009). The function of mucus is as a protective barrier against pathogens and toxins, as well as providing the innate defensive system in mucosal immunology. Moreover, mucus is continuously secreted, recycled, digested and discarded (Rose and Voynow, 2006). In addition, mucus is the first boundary with which nutrients and enteric drug must interact with then diffuse through, in order to be absorbed and obtain access to the circulatory system and their target end organs (Bansil and Turner, 2006, Lai et al., 2009). Mucus is composed mostly of water (~95 %). However, it contains inorganic salts, lipids, enzymes such as lysozyme, immunoglobulins, growth factors and trefoil factors. Nevertheless, the main components of mucus which are responsible for the viscous and elastic gel-like properties are mucins (Bansil and Turner, 2006). Mucins are a family of complex high molecular weight ($5 - 20 \times 10^5$ g/mol) glycoproteins secreted by the epithelia of the intestinal, respiratory and urogenital tracts, consisting of linear or branched oligosaccharides attached to the protein core. These glycoproteins consist

mostly of carbohydrates, which can account for 60-80 % of their weight. The carbohydrate fraction consists of five sugars are N-acetyl-galactosamine, N-acetyl-galactosamine, galactose, and fucose and sialic acid (N-acetyl-neuraminic), as well as traces of mannose and ester sulfate (**Figure 1.10**) (Thornton and Sheehan, 2004, Abodinar et al., 2016). The rigidity of the structure of mucin is mostly due to the high sialic acid and sulfate ester contents which leads to a negative charge on mucin which is the main reason for its gelling and mucoadhesive properties (Harding et al., 1999).

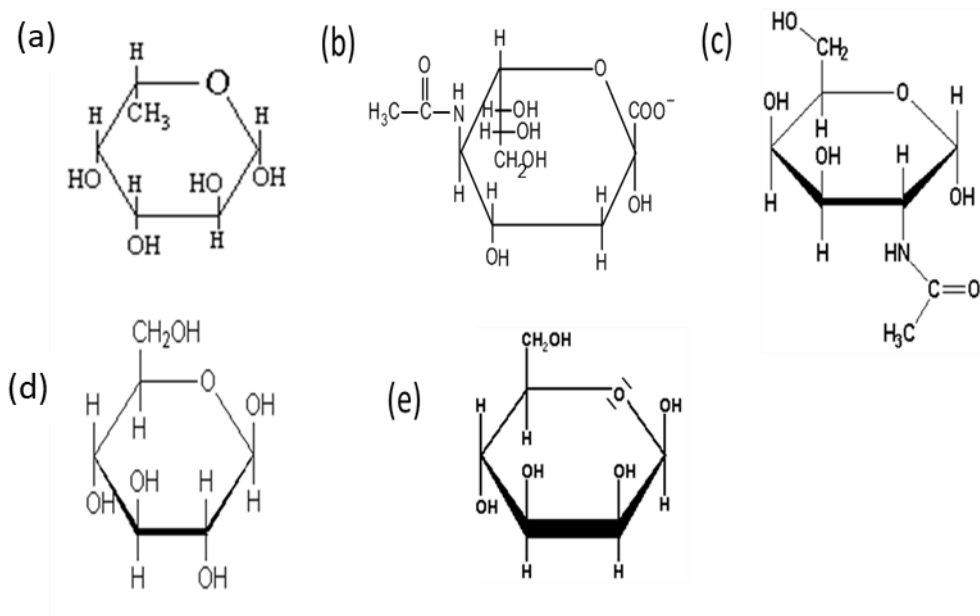


Figure 1.10: Representative structures of (a) Fucose, (b) Sialic acid (c) N-Acetyl-Galactosamine, (d) Galactose, and (e) Mannose.

Sialic acid, which is distributed throughout human tissues, is present in several fluids, including, cerebrospinal fluid, serum, urine, amniotic fluid saliva, and breast milk. In addition it is found in high levels in some organs such as the heart, adrenal glands, and brain (Matsuno and Suzuki, 2008). The glycosylated proteins have a defining

feature of a repeating sequence of amino acids, namely serine and threonine. The oligosaccharides chains consist of about 5–15 units indicating moderate branching and are attached to the protein by O-glycosidic linkages to the hydroxyl (OH) side chains of serine and threonines then arranged in a bottle brush shape about the protein core (**Figure 1.11**) (Bansil and Turner, 2006).

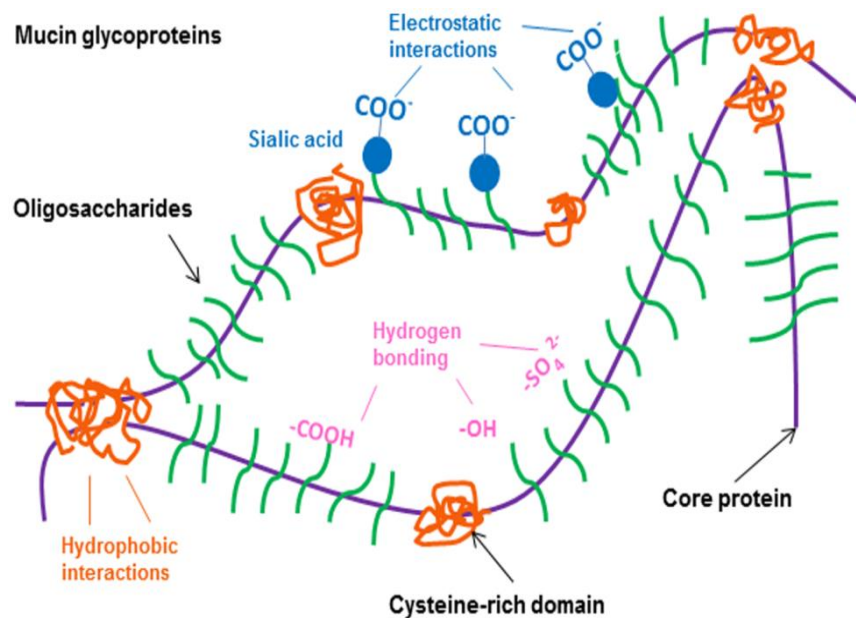


Figure 1.11: Representative structure of mucin glycoproteins and interaction sites where mucoadhesion may take place (Yang et al., 2012).

Mucins can be classified by their MUC protein backbone into three groups and are summarized in **Table 1.2**.

Table 1.2: Classification of mucins classification of mucins (Niv and Boltin, 2012).

Classification	Mucins	Presence
Secreted, gel-forming mucins	MUC2, MUC5AC, MUC5B, MUC6, MUC19	Eyes, middle ear epithelia, small intestines, colon, respiratory tract, stomach, cervix, salivary glands, gallbladder, seminal fluid, duodenum, pancreas and submandibular gland
Secreted, non-gel-forming mucins	MUC7, MUC8	In salivary glands, respiratory tract and middle ear epithelium (Linden et al., 2008)
Membrane bound (structural) members	MUC1, MUC3A, MUC3B, MUC4, MUC12, MUC13, MUC15, MUC16, MUC17, MUC20 and MUC21	On the apical membrane of epithelial cells (Linden et al., 2008)

All mucins have one or more mucin-like domain which hold the usual mucin O-glycosylation. In addition, the domain is made of different tandem repeats (TR) rich in threonine, serine and proline residues in the protein backbone (Rose and Voynow, 2006).

The glycoprotein core is arranged into different regions. Firstly, a central glycosylated region involved of a large number of tandem repeats which are rich in serine, threonine and proline (STR) repeats that may make up more than 60 % of the amino acids. Secondly, located on the amino and carboxyl groups, and occasionally interspersed between the STR-repeats, are regions with an amino acid conformation more representative of proteins, relatively few O-glycosylation and a few N-glycosylation sites **Figure 1.12** (Bansil and Turner, 2006).

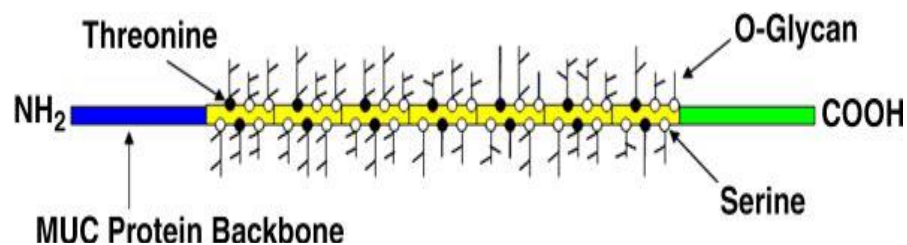


Figure 1.12: A secretory mucin glycoprotein representing a MUC protein backbone and its O-glycans. A MUC protein backbone usually consists of an NH₂ group domain (blue), one or more central domain with a high number of tandem repeat (TR) domains (yellow), and a COOH group domain (green) (Rose and Voynow, 2006).

Mucoadhesive drug delivery systems are advantageous in several ways. Other than prolonged contact time resulting in high drug flux at the intended tissue site, they are able to target and localise a dose form at a specific site, for example, oral cavity, eye

conjunctiva, vagina, nasal cavity and gastrointestinal tract (GIT). Due to preventing the washing away of the active agent by oral secretions, the delivery systems are usually coated with a drug and water impermeable film (Remuñán-López et al., 1998).

There are several possibilities for mucoadhesive drug delivery systems. Mucoadhesive tablets can adhere to any mucosal tissue including those found in stomach, as a result offering the possibilities of localised and systemic controlled release of drugs. The application of mucoadhesives in a semisolid dosage form, such as gels and ointments, provide an extended retention time in the oral cavity, suitable drug penetration and high efficacy and patient acceptability (Boddupalli et al., 2010).

1.3.1 Mucoadhesive properties

Mucoadhesion is often defined as the adherence of a bioadhesive polymer to biological surfaces (either secreted mucus or a mucosal surface) (Meng-Lund et al., 2014, Madsen et al., 1998). Mucosal membranes in the human organism are relatively porous surfaces and allow fast drug absorption. Mucus is a complex biological substance that lubricates and protects epithelial surfaces in the human body including lungs, gastrointestinal (GI) tract, vagina, eyes, and other moist mucosal surfaces. Furthermore, the mucus contains 5 % mucin glycoproteins, lipids, inorganic salts and 95 % water, DNA, cellular debris, secretory IgA, lactoferrin, lysozyme, uric acid, ascorbic acid, reduced glutathione and prostaglandins (Lai et al., 2009, Caramella et al., 2015, Hoang et al., 2010) (**Figure 1.13**).

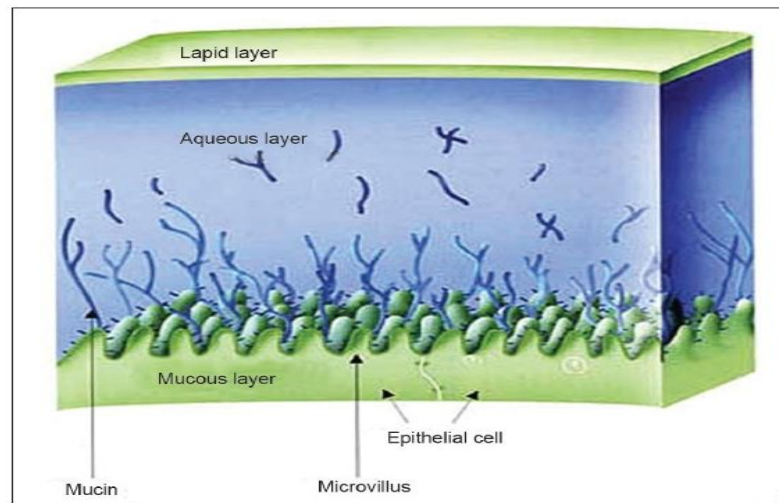


Figure 1.13: Mucus membrane structure (Boddupalli et al., 2010).

Chitosan is very highly regarded in the medicinal world because it demonstrates mucoadhesive behaviour, however the interactions of chitosan with mucus are complicated. Depending on the physiological conditions and physiochemical properties such as pH and the presence of other materials, it is generally understood that electrostatic interactions can occur between chitosan's positively charged amino groups and the negatively charged sialic acid residue on mucin, as well as hydrophobic, hydrophilic interactions and hydrogen bonding are also very important (Illum et al., 1994, Deacon et al., 1999). Mucoadhesion is divided into stages based on the interaction between mucoadhesive materials and a mucous membrane. Firstly, the contact stage also known as the wetting stage, which is contact between the mucoadhesive material and the mucous membrane. Secondly, the consolidation stage it is at this stage adhesive interactions are formed (Smart, 2005) (**Figure 1.14**).

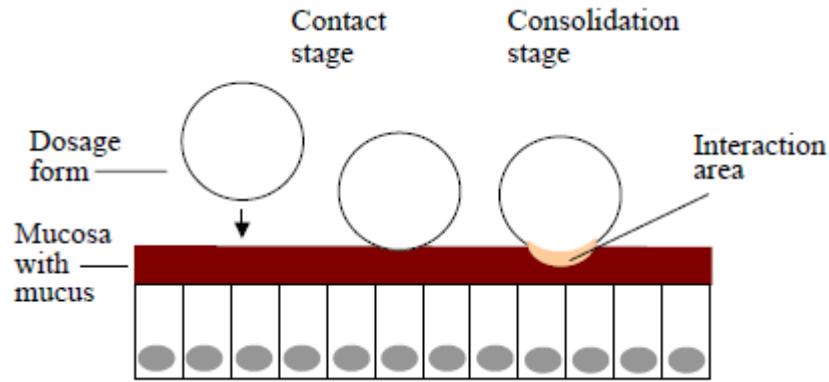


Figure 1.14: The contact and consolidation stages of mucoadhesion (Smart, 2005).

During the consolidation stage, if mucoadhesive materials are activated by the presence of moisture, it leads to a strong adherence between mucoadhesive materials and dry solid surfaces. The presence of moisture is very important that will effectively plasticize the system, allowing mucoadhesive materials to break free and interact via weaker van der Waal forces and hydrogen bonding or electrostatic interactions. Therefore, there are electrostatic interactions between cationic chitosan and negatively charged groups, for example, carboxylate ions or sulphate ions on cell or the mucous surfaces (Artursson et al., 1994, Illum et al., 1994). There are five different theories of mucoadhesion which are summarized in **Table 1.3** (Vasir et al., 2003).

Table 1.3: Theories of mucoadhesion.

Theory	Mechanism of adhesion	Comments
Electronic	Based on the electrostatic forces (opposing electrical charges) between the mucoadhesive material and biological materials	When both materials combine together, the electrons transfer, as a result a double electronic layer is formed at the surface
Adsorption	Based on a chemical bonds due to a surfaces forces	The mucoadhesive material adheres to the biological material (mucus) by formation of van der Waals forces, hydrogen bonds, electrostatic attraction or hydrophobic interactions
Wetting (Figure 1.15) Carvalho et al., 2010	Based on the ability of bioadhesive polymers to spread onto mucus membranes	Applies to fluid systems which present affinity to the surface in order to spread over it. Contact angle between mucoadhesive polymer and cells must be near to zero
Diffusion (Figure 1.16) Carvalho et al., 2010	Physical entanglement of mucin strands and the flexible polymer chains	The interpenetration of both polymer and mucin chains to a enough depth to create a semi-permanent adhesive bond. Therefore, the adhesion force rises with the degree of penetration of the polymer chains
Fracture (Figure 1.17) Carvalho et al., 2010	Analyses the maximum tensile stress developed during detachment of the bioadhesive drug delivery system from mucosal surfaces	Does not require physical entanglement of bioadhesive polymer chains and mucin strands, therefore suitable to study the bioadhesion of hard polymers which lack flexible

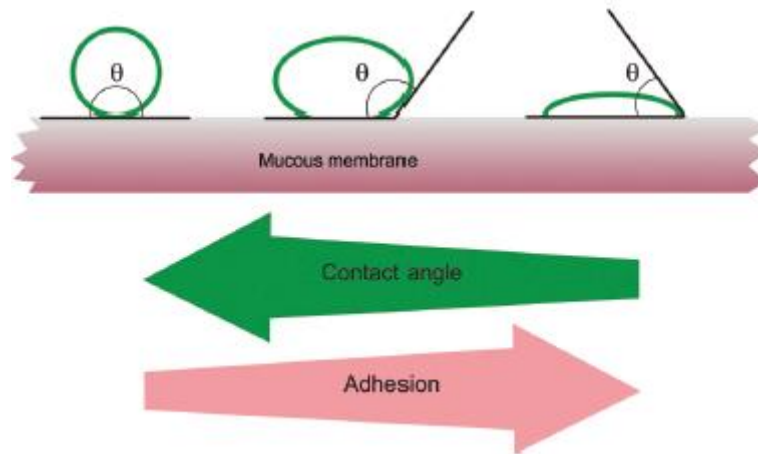


Figure 1.15: Schematic diagram showing wetting theory of mucoadhesion (Carvalho et al., 2010).

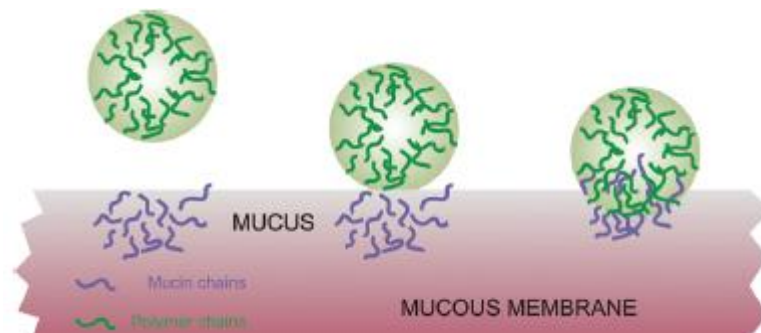


Figure 1.16: Diffusion theory of mucoadhesion (Carvalho et al., 2010).

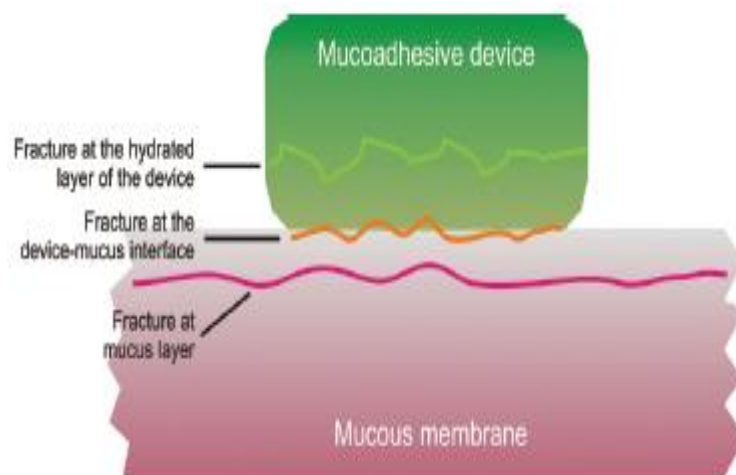


Figure 1.17: Fracture theory of mucoadhesion (Carvalho et al., 2010).

1.3.2 Factors Influencing Mucoadhesive Properties

1.3.2.1 Molecular Weight of polymer

There is positive correlation between the mucoadhesive strength of a linear polymers and their molecular weights above 100,000 g/mol, because linear polymers enable better interpenetration and entanglement which is significant for bioadhesiveness. On the other hand, the same relationship does not hold for non-linear polymers. Moreover, lower molecular weight polymers can readily dissolve then form weak gels, whereas, large molecular weight polymers do not hydrate readily to allow binding groups on polymers to interact with mucus layer. (Lee et al., 2000, Boddupalli et al., 2010, Smart, 2005).

1.3.2.2 Concentration of polymer

A very low concentration polymer would result a weak adhesive bond with the mucus, due to the number of penetrating polymer chains per unit volume of the mucus

being small and lead to the interaction between polymer and mucus being unstable. However, the a concentrated polymer system would result in a strong adhesive bond with the mucus, due to more polymer chains being available to penetrate into the mucus layer and better adhesion. On the other hand, there is a critical concentration for each polymer. For a highly concentrated formulation (higher than the a critical concentration level), the adhesive strength decreases due to the coiled molecules separating from the medium, therefore the chains available for interpenetration become limited (Lee et al., 2000).

1.3.2.3 Flexibility, length of polymer chains and cross-linking density

Chain flexibility is very important to combine the interpenetration between formulation and mucus. If a polymer is a higher flexibility, this leads to more diffusion into the mucus network. Cross-linked hydrophilic polymers swell in the presence of water allowing them to keep their structure. The swelling process allows more control of drug release and increases the surface area for polymer/mucus interpenetration (Andrews et al., 2009). Therefore, as the cross-linking of water-soluble polymer increases, the mobility and flexibility of the polymer chains decrease, and consequently the effective length of the chain which can penetrate into the mucus membrane decreases, which reduces bioadhesive strength (Lee et al., 2000, Boddupalli et al., 2010).

1.3.2.4 Functional group contribution

Mucoadhesive polymers commonly have a several hydrophilic polar functional groups such as, carboxyl (COOH), hydroxyl (OH) and amine groups (NH₂). The bonding of bioadhesive polymers to the mucus layer occurs essentially through interpenetration followed by secondary bonding between mucus layers. Moreover, the secondary bonding mainly increases due to hydrogen bond formation (Andrews et al., 2009). Typically, hydrogen bonds contribute to the formation of a strengthened network; therefore polymers that demonstration a large density of available hydrogen bonding groups would be able to interact more strongly with mucus membrane (Madsen et al., 1998).

1.3.2.5 pH and polymer charge

The pH can affect the formation of ionisable groups in bioadhesive polymers and the formation of charges on the mucus surface. Bioadhesive polymer charges are affected by the pH of the physiological environment due to the dissociation of functional groups. In addition, mucus possesses a different charge density depending on pH due to differences in dissociation of functional groups on substances such as the carbohydrate and the amino acids of the polypeptide backbone (Lee et al., 2000). Mucoadhesive polymers can be divided into three main types in terms of overall charge, *i.e.*, anionic, cationic and non-ionic systems. Non-ionic polymers exhibit a smaller degree of adhesion compared to anionic polymers. Strong anionic and cationic polymers are one of the required characteristics for mucoadhesion (Andrews et al., 2009, Boddupalli et al., 2010). In general, carboxylated polymers, at pH values below its pK_a value would be favourable (Riley et al., 2001). For example, mucoadhesion of polyacrylic acid is favoured when the most of the carboxylate groups (COOH) are in

the non-ionised form, which occurs at pH below the pKa. However, at higher pH values, there is electrostatic repulsion of the carboxylate anions (COO⁻) between mucin and polyacrylic acid (Smart, 2005, Lee et al., 2000). On the other hand, in systems with a high density of ionisable groups, such as chitosan which could form polyelectrolyte complexes (at pH < 6) with negatively charged mucins and consequently stronger mucoadhesion (Andrews et al., 2009).

1.3.2.6 Initial contact time

Another important factor affecting the mucoadhesive strength of polymeric components is initial contact time. It has conclusively been shown that mucoadhesive strength increases with the longer initial contact time between the bioadhesive polymer and mucus layer. Contact time between bioadhesive polymer and mucus layer determines the degree of chain interpenetration (Lee et al., 2000, Carvalho et al., 2010).

1.3.2.7 Degree of hydration

Hydration is important for the relaxation and interpenetration of bioadhesive polymer chains. However, super hydration of system would lead to decreased mucoadhesion due to the formation of moist slippery mucilage. In addition, it has been suggested that cross-linked polymers permit a certain degree of hydration which would provide a prolonged mucoadhesive effect (Andrews et al., 2009).

1.3.3 Advantages of mucoadhesive delivery systems

If bioadhesive molecules can bind with the active drug pharmaceutical formulation, the formulation will remain longer on the biological surface. Then the drug will be released close to the absorptive membrane, resulting in an improved bioavailability of the drug. Moreover, when using specific bioadhesive molecules such as chitosan, it will allow the possible targeting of a tissue or particular site for example the gastrointestinal tract. In addition, mucoadhesion is very important in the reduction of drug degradation during the first-pass metabolism (Andrews et al., 2009).

1.4 Drug delivery system

A drug delivery system (DDS) is a formulation or a device that enables the introduction of a therapeutic material to the body. Drug delivery systems are used to maintain a drug which has been administered using the therapeutic product for a determined period of time and the release of the active ingredients by the product across the biological membranes to the site of action. The concentration of drug must remain between the minimum and maximum blood values. This means, at high level, drugs could cause side effects and at lower levels the drug no longer provides a therapeutic effect (Winstanley et al., 2007). Due to chitosan's efficiency in the entrapment of specific drugs and its ability to control drug release, it is one of the most widely used polymers in drug delivery systems (**Table 1.1**). Chitosan demonstrates promising properties as support agent in drug delivery. Chitosan is the only naturally occurring positively charged biopolymer rendering it unique among all other biodegradable polymers. This cationic character based on its primary amino groups is responsible for several properties and consequently for its use in drug delivery systems. Chitosan is generally used in the several forms including tablets,

powder, film, micro/nanocapsules and micro/nanospheres in drug delivery applications (Banerjee et al., 2002, Boonsongrit et al., 2006, Tang et al., 2003, Calvo et al., 1997b, Liu et al., 1997, Meshali and Gabr, 1993, Patel Jayvadan et al., 2009, Bhardwaj et al., 2010).

1.5 Nanotechnology

In 1974, Prof. Taniguchi first used the word “nanotechnology”. In addition, in 2000 National Nanotechnology Initiative (NNI) was initiated by US President Bill Clinton (Agarwal et al., 2015). Nanotechnology can be defined as the design, which focuses on the characterisation and production of organic or inorganic compounds, structures, fabrication, manipulation, devices and systems by controlling their size and shape within the scale of sub-micron dimensions. Therefore, it refers to structures that are up to several hundred nanometres in size (Farokhzad and Langer, 2009). In 1959 the physicist Richard Feynman discovered that the possibility of manipulating substances at the nanoscale and also stated a process through which scientists might be able to manipulate the individual atoms or molecules as a more powerful tool of scientific chemistry than those used at that time. Therefore nanotechnology has applied in a variety of fields such as the electronics physical, material science and manufacturing at molecular or submicron level (Agarwal et al., 2015).

1.5.1 Advantages of nanoscale drug delivery system

Drug delivery is defined as the method of releasing a bioactive agent at a specific site and at a specific rate. The most important advantages of nanotechnology offers is

targeted drug delivery to the site of disease (Torchilin, 2000). The many advantages of nanoparticles include (Parveen et al., 2012):

- Easier to penetrate cells and tissue to arrive at target organ(s) (Yih and Al-Fandi, 2006, Monsky et al., 1999)
- Protects the drug from degradation (Danhier et al., 2010)
- Increases the aqueous solubility of the drug (Van Eerdenbrugh et al., 2010)
- Prolonged release of the drug (zur Mühlen et al., 1998)
- Improved utility of the drug (Brown et al., 2010)
- Reduction undesired side effects of the drug (Mitra et al., 2001)
- Rapid-formulation development (de la Escosura-Muñiz et al., 2009)
- Offers suitable forms for all routes of administration (Parveen et al., 2012)
- Improves the bioavailability of the drug (Wang and Zhang, 2012)

1.5.2 Polysaccharide nano/microparticles

Nanoparticles are defined as solid colloidal particles that are frequently composed of insoluble polymers and have a minimum of one dimension that is ranging from 10 – 1000 nm in diameter. Nano size also, refers to one thousand millionth (one billionth) of a metre (Sahoo et al., 2007). On the other hand, microparticles, called microspheres or microcapsule, are defined as spherical microscopic particles that range from 1-1000 μm in diameter (**Figure 1.18**).

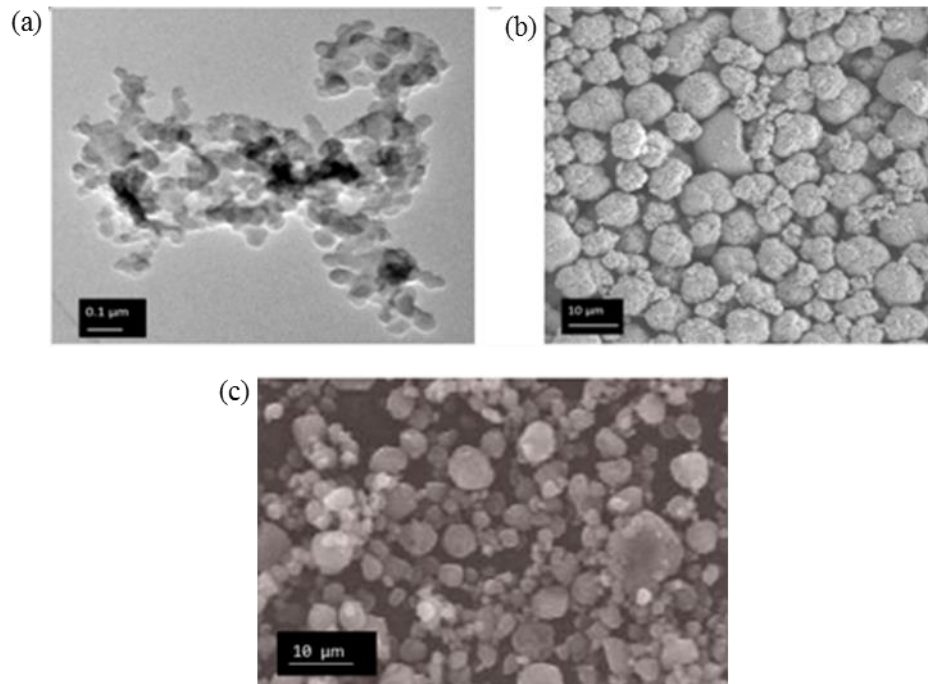


Figure 1.18: An example of (a) TEM of a carbon black nanoparticle showing particle diameters ranging from 30 to 100 nm (b) SEM of NMC microparticles showing an average particle size of 10 μm (Morelly et al., 2017), (c) SEM image of black granular fingerprint powder, the elemental carbon has a particle size of 5-10 mm (Bandey and Gibson, 2006).

Nanotechnology is one of the most interesting areas of biopolymer research which finds exciting applications in drug delivery systems and food technology. Biopolymer particles can be formed by self-association or aggregation of single biopolymers or by inducing phase separation in mixed biopolymer systems. Nanoparticles have a small size and are therefore used in or have been evaluated for use in, many fields and applications.

Chitosan, alginate and glucomannan are examples of polysaccharides which have been used to produce nanoparticles for different applications in the pharmaceutical, medical, food and cosmetic industries (Zhang and Kosaraju, 2007, Alonso-Sande et

al., 2006, Janes et al., 2001, Liu et al., 2008b). The properties of substances may change when formulated into nanoparticles, hence the surface chemistry of a nanoparticle is unusually different from that of the original substances (Christian et al., 2008). Microparticles, for example, have a lower surface area to volume ratio than nanoparticles. The higher surface area of nanoparticles allows them to be more reactive to certain other molecules. As a consequence, nanoparticles have a high carrier capacity to allow numerous drug molecules to be combined in the particle matrix, this includes the ease of combination of both hydrophilic and hydrophobic molecules. In addition, the advantage of their small size allows nanoparticles to be more readily taken up by the human body, to cross biological membranes then enter cells, tissue and finally organ, whereas the larger size particles such as microparticles cannot (Panyam et al., 2003, Desai et al., 1997, Desai et al., 1996).

1.5.2.1 Methods of preparation of chitosan micro/nanoparticles (cross-linking of chitosan)

Cross-linking is the development of primary bonds that form between polymer molecules, and it occurs when a chemical substance, known as a cross-linking agent, cross-links between polysaccharide macromolecules or introduces intermolecular bridges (Sinha et al., 2004, Shweta and Sonia, 2013). Moreover, cross-linking of chitosan is based on the addition of a cross-linker. The amino and hydroxyl groups which exist on chitosan are active sites that lead to the formation of a number of linkages, including amide and ester bonding as well as Schiff base formation. Chitosan can be physically cross-linked with polyanoins (Berger et al., 2004, Jonassen et al., 2012). In addition, this cross-linking may be achieved at different pH values: acidic, neutral or basic pH, depending on the method applied. Therefore, cross-linked

chitosan is very important in many applications, particularly in the pharmaceutical field for the formulation of several novel drug delivery systems such as microspheres, nanospheres, hydrogels and films/membranes. Some methods using chemical crosslinking agents such as glutaraldehyde, ethylene glycol diglycidyl ether and sodium hydroxide have been used to prepare particles. These chemical crosslinking agents may cause of undesirable effects. Glutaraldehyde for example, can cause irritation to mucosal membranes due to its toxicity (Mi et al., 2001, Mi et al., 1999, Chandy and Sharma, 1996, Ko et al., 2002). On the other hand, sodium tripolyphosphate (TPP) is a multivalent polyanion which is non-toxic and available at low cost (Sezer and Akbuğa, 1995, Bodmeier et al., 1989, Mathur and Narang, 1990) and it is an inorganic compound of the sodium salt of the polyphosphate penta-anion. Sodium tripolyphosphate (molecular formula $\text{Na}_5\text{P}_3\text{O}_{10}$) is the conjugate base of triphosphoric acid (molecular formula $\text{H}_5\text{P}_3\text{O}_{10}$).

Various techniques have been developed to prepare chitosan micro/nanoparticles, including emulsion crosslinking, coacervation/precipitation, spray drying, emulsion droplet coalescence method, ionic gelation, reverse micellar method and sieving method. Selection of any of the methods depends on factors such as particle size requirement, chemical stability of the active agent, reproducibility of the release kinetic profiles, stability of the final product, the nature of the active molecule and the type of the delivery device (Agnihotri et al., 2004). Different methods of preparation of micro/nanoparticles of chitosan are summarised in **Table 1.4**. These methods are based on dropwise addition of chitosan under constant stirring to the cross-linking agent.

Table 1.4: Different methods of preparation of micro/nanoparticles of chitosan (Agnihotri et al., 2004).

Method	Process	Crosslinking agent	Reference
Emulsion cross-linking	Emulsion of chitosan aqueous solution in the phase water (w/o)	Glutaraldehyde	(Kotadiya et al., 2009)
Coacervation/precipitation	Sodium sulfate solution is added to an aqueous acidic chitosan solution	Glutaraldehyde	(Berthold et al., 1996)
Spray drying	Drug is dispersed in an chitosan acidic aqueous solution	Vitamin D	(Shi and Tan, 2002)
Emulsion droplet coalescence method	Both emulsion cross-linking and precipitation. emulsifying chitosan aqueous solution in an oil phase with	Emulsifying chitosan aqueous solution in NaOH	(Tokumitsu et al., 1999)
Iontropic gelation	The complexation between oppositely charged (polycation chitosan acidic solution)	TPP, sodium Alginate	(Kleine-Brueggeney et al., 2015, Severino et al., 2016)
Reverse micellar method	Surfactant dissolved in organic solvent then mixed with an aqueous solution of chitosan and drug	Glutaraldehyde	(Mitra et al., 2001)
Sieving method	An aqueous acidic chitosan solution. Microparticle obtained passed through sieve	Glutaraldehyde	(Agnihotri and Aminabhavi, 2004)

1.5.2.1.1 Ionotropic gelation

Among the methods above, the ionic gelation method (also known as ionotropic gelation) is the most widely used approach to ionic physical cross-linking. This method has been applied using a variety of polymers, including chitosan, alginates, gellan gums, and carboxymethyl cellulose, to form micro- and nanoparticles for encapsulation and controlled release of therapeutic agents (Patil et al., 2010, Liu et al., 1997, Kawashima et al., 1985a, Calvo et al., 1997b, Sezer and Akbuğa, 1995, Shu and Zhu, 2000). Moreover, this technique provides several advantages, such as its simple and mild method of preparation without the use of organic solvents or high temperatures. As well as decreasing the possible toxicity effect of reagents products which come with chemical cross-linking (Tiyaboonchai, 2003, Agnihotri et al., 2004). Electrostatic interactions can occur inside the network via interactions between the negative charges of the cross-linker TPP and the positively charged amino groups of chitosan molecules (Kawashima et al., 1985a, Kawashima et al., 1985b). For this process, as depicted in **Figure 1.19**, chitosan is dissolved in acidic solution such as dilute acetic acid. Then it is added dropwise to TPP solution, where chitosan undergoes ionic gelation and precipitation to form particles due to the presence of an oppositely charged species (Aydin and Akbuğa, 1996, López-León et al., 2005).

..

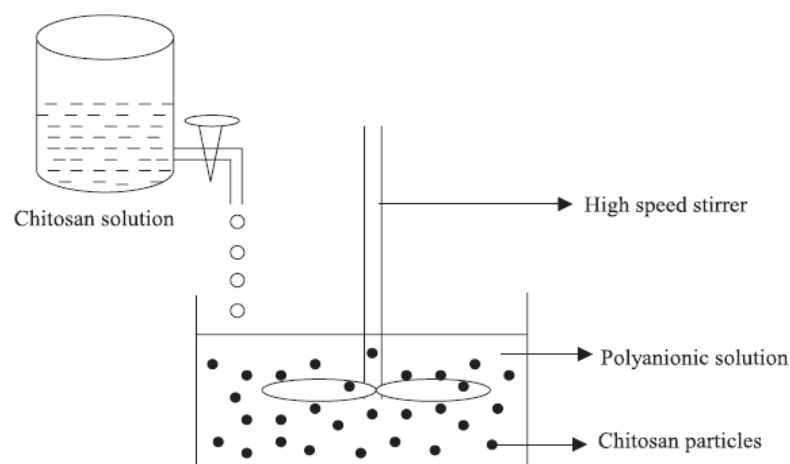


Figure 1.19: Scheme of the preparation of chitosan particles by ionotropic gelation (Agnihotri et al., 2004).

Calvo and co-workers (1997) first stated use of ionic gelation method to form of hydrophilic chitosan-polyethylene oxide nanoparticles. It was observed that the particles had a great entrapment capacity and allowed for continued release of bovine serum albumin for up to seven days. The size of nanoparticles ranged from 200 – 1000 nm and the zeta potential ranged from +20 mV and +60 mV depending upon the concentration polyethylene oxide, TPP and chitosan; as well as chitosan molecular weight and degree of deacetylation of the chitosan (Calvo et al., 1997a). Finally, ionotropic gelation was selected as the method of micro/nanoparticle production for this thesis because of the process's mild effective conditions, simplicity, previous encapsulation results with other therapeutic agents and CS: TPP particles may also interact with fingermarks (Il Dueik and Morris, 2013) **Figure 1.20.**

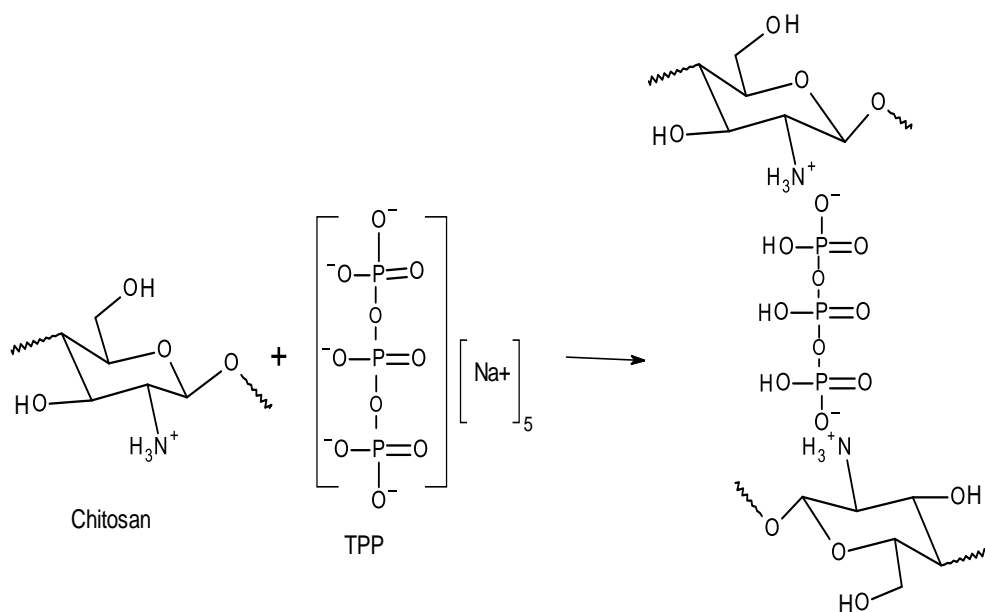


Figure 1.20: Schematic of chitosan: TPP particle formation process of by ionotropic gelation process (Ponnuraj et al., 2015).

1.6 Fingerprints

Fingerprints are made up of groups of various whirling lines including hills and valleys. These lines are made by features that are called ridges (hills), while the narrow spaces between them are called furrows (valleys), also ridges and furrows together form the unique character of a fingerprint (Wilshire, 1996). Fingerprints or fingermarks are left behind when fingers come into contact with a surface. The functions of the friction ridge skin is to assist the sense of touch, act as friction ridges in gripping, and raise the openings of the sweat glands to the surface for the discharge of sweat and to assist in temperature regulation (Junqueira and Carneiro, 2003). In forensic science, the revealing of traces on crime scenes or related substances represents a continuous challenge for scientists working on the enhancement or the

development of new detection techniques (Becue et al., 2008). Fingermarks are recovered from a crime scene, while, fingerprints are taken from suspect under controlled conditions such as inked elimination prints. Therefore, the identification of each fingermarks located at crime scenes is one of the most important of forensic examination (Knowles, 1978). In 1892 Galton reported that friction ridge was unique to each person and persistent (Galton, 1892). Hence, fingermark recognition is very important in any forensic investigation, because there are no two humans possess identical fingerprints, also it is characterized by stability from birth to death (uniqueness and persistent) (Faulds, 1880). In addition, different fingerprints will be found even in identical twins (White, 2010, Sun et al., 2010). As DNA is the same in both individuals in a pair of identical twins, in the case fingerprints are stronger for identification purposes (Kong et al., 2005, Kong et al., 2006). In a previous study (Jain et al., 2002) collected ninety four pairs of identical twins and reported that the fingerprint recognition system is able to discriminate them as different individuals based on fingerprint features (ridge details). The friction ridge skin (fingerprint) remains the same throughout an individual's life, and it has not been found to have changed from birth until death (Lee and Gaensslen, 2001). Therefore, fingerprints are one of the best methods of identification which can be used during the life of person, and even remains useful for a period after death prior to decomposition. However, if there was some serious damage to the skin, such as a severe burn, a deep scar or cut which reaches the dermis layer this may alter the fingerprint's features (Lee and Gaensslen, 2001).

1.6.1 History of Fingerprints

Evidence exists on the use of fingerprints in ancient culture as a means of personal identification (Ashbaugh, 1999, Berry and Stoney, 2001). Herschel (Herschel, 1916), Henry (Henry, 1905), Galton (Galton, 1892), and Faulds (Faulds, 1880) pioneered work succeeded in establishing ways by which the recognition of humans on the basis of their fingerprints is possible. Sir William Herschel and Dr Henry Faulds were the first two individuals, who, in nineteenth century, systematically explored the use of friction ridge skin as a method of making personal identification (Faulds, 1880). Dr Henry Faulds also undertook a study in friction ridges and also succeeded in realising their value as a method in making identification. Faulds (1880) also came to understand the persistency of the friction ridge arrangements. The realisation that the perpetrator of crimes could be identified through the fingerprints they left at the crime scene is credited to Faulds (Faulds, 1880). It was Faulds who also succeeded in recognising that fingerprint patterns make it possible for identification. Years later, Sir Edward Henry (1905) succeeded in developing a classification system for fingerprints storage and retrieval (Henry, 1905). Moreover, Sir Francis Galton earned the distinction of being known as the father of fingerprints as a result of the seminal text "Finger prints" which he wrote in 1892 (Galton, 1892). Galton explained that this was achieved through friction ridge systematic study detail, building upon Faulds work. Nonetheless, Herschel, the first individual to discover fingerprint's lifelong consistency, conceded in 1917 that the idea of using fingerprints as a way of implicating people in crime and equally exonerating innocent parties was first conceived by Faulds (Lee and Gaensslen, 2001). It was only during the latter part of the 19th century that the discovery of the fingerprints permanence was made and the unique idea was given a sound practical basis (Maltoni et al., 2009). In fact, Herschel

and Faulds had both devised classification methods (Berry and Stoney, 2001). Sir Francis Galton, one other British contemporary, developed an identical system to that of Henry and was thus, the first to provide definitions to precise specific minutiae details (Galton's Points), thereby giving recognition in terms of their role for individualisation (Polson, 1950). Starting from the first known case in central police department in Argentina in 1893 where acceptance as evidence of the fingerprints discovered at the crime scene was used in convicting a suspect (Hawthorne, 2008), friction ridge analysis has turned out to become one of the most important methods in worldwide crime scene investigations.

Artefacts recovered from archaeological excavations of ancient civilisations indicate that fingerprint and handprint patterns used as means of personal identification thousands of years ago. Early potters may have used them to sign their work, and records indicate the use of fingerprints and handprints as marks of validity in China at least 2000 years ago (Xiang-Xin and Chun-Ge, 1988). In addition, fingerprint detection has been used as identification evidence for more than 100 years (Henry, 1905). Fingerprint detects subjects through their unique natural characteristics comprising the pattern of ridges on fingers (Lee and Gaensslen, 2001). It is suggested that fingermark development techniques were in use even prior to the seminal works of Galton (1882) and Faulds (1890) where iodine was used to enhance latent marks in the 1860s, and in the following 150 years many different techniques have been proposed for fingermark enhancement (Quinche and Margot, 2010).

1.6.2 Classification of Fingerprints

The skin is the largest organ of the body. The friction ridge skin forms various patterns on the fingers and toes (and to an extent on the palms and soles of the feet). There are levels used to describe features visible in the fingerprint. The Henry system uses three basic fingerprint patterns (**Figure 1.21**), with several subdivisions (**Figures 1.22-1.23**) (Rao and Balck, 1980). First: an arch is a type of fingerprint in which ridges across the fingerprint and rise in the middle then flows out on the other side; including plain arch and tented arch. Arch patterns contain no delta and account for about 5 % of all fingerprint patterns. Secondly a loop is pattern in which one or more of the ridges exit and enter on same side of the impression, and it has a stronger curve than arches these include: radial loop where the ridges slant towards right in case of left hand fingers or towards left in right hand fingers; and the ulnar loop, where the ridges about the core slant towards left in the case of left hand fingers or right in right hand fingers (Rao and Balck, 1980). Thirdly a whorl is any pattern which has two deltas and usually makes a spiral pattern around a centre of point and includes the plain whorl, which involves one or more ridges that make a complete circuit and comprises two deltas; the central pocket loop whorl, which comprises at least one ridge that recurves an obstruction at a right angle to the line of flow, and contains two deltas; the double loop whorl, which contains two separate loop patterns which encompass two distinct and separate sets of shoulders and deltas; and the accidental whorl, is comprised two or more deltas (Rao and Balck, 1980). Additionally there is another fingerprint type called the composite pattern which is a combination two or more patterns types within one fingerprint (Sam et al., 2015, Knowles, 1978). Characteristic fingerprint features are mostly categorized in three different levels: Level 1 (patterns), which are useful for classification and exclusion. Level 2 (minutia)

and level 3 (features), in order to classify fingerprint records into primary groups, so simplifying any consequent ridge detail (minutiae) comparisons. These features (three levels) are used to compare between the fingermarks recovered from a crime scene, and fingerprints taken from suspect to decide whether they are or are not from the same source. Due to the flexibility of skin, level 1 features may be wholly distorted (Ashbaugh, 1999) and appear relatively different in a print than in the comparable mark, therefore level 1 features is not unique and refer to the macro details of the fingerprint such as pattern and ridge flow (Jain et al., 2007). Level 2 refer to ridge characteristics or minutiae of the fingerprint, such as ridge bifurcations which may be split into two ridges; and endings where some of this ridge terminates at a point; and the ridges may be a short in length called dot (Jain et al., 2007). In addition, it may be form an island by two bifurcations facing one another. Level 2 are the most commonly used for identification purposes because they provide specific rides and more detailed information of fingerprint such as the ridge interruptions, endings and bifurcations Therefore they have sufficient discriminating power to establish the individuality of fingerprints (Pankanti et al., 2002, Stosz and Alyea, 1994). When the Level 1 and Level 2 features present in the fingerprints are not adequate to make a decision of fingerprint matching, level 3 features are claimed to contain suitable details to compare fingerprints, and it can provide discriminatory information for human identification of individuality of fingerprints based on attributes of the ridge such as sweat pores and shapes, ridge path deviation, width, pores, edge contour, scars, incipient ridges, breaks, *etc.* (Ashbaugh, 1999, Jain et al., 2007).

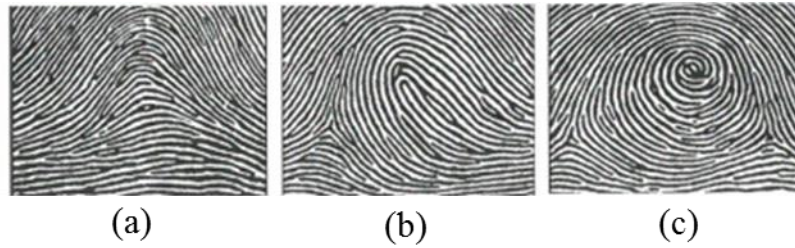


Figure 1.21: Different types of fingerprint patterns (a) Arch (b) Loop (c) Whorl (Knowles, 1978).

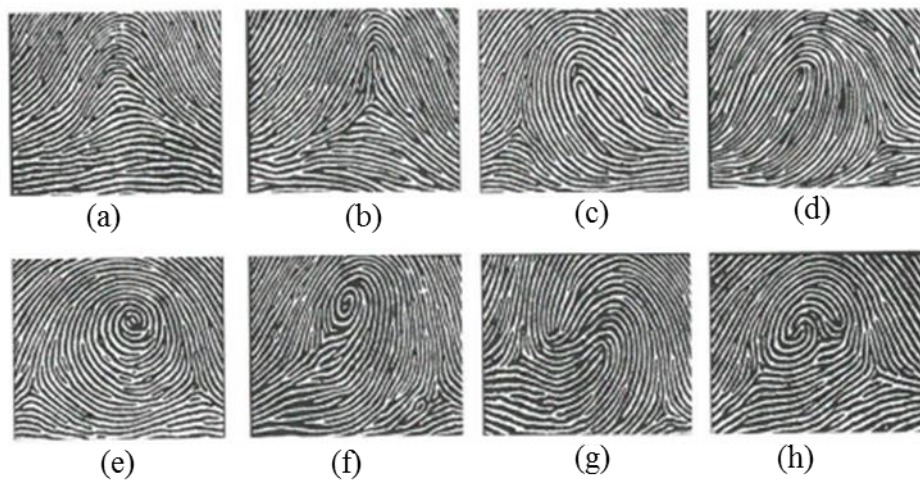


Figure 1.22: Each type of level 1 pattern (**Figure 1.21**) can be subdivided in to eight fingerprint sub-pattern types (Level 1 features): (a) plain arch, (b) tented arch, (c) right slanted loop (ulnar), (d) left slanted loop (radial), (e) plain whorl, (f) central pocked loop whorl, (g) double-loop whorl and (h) accidental whorl (Jain et al., 2007).

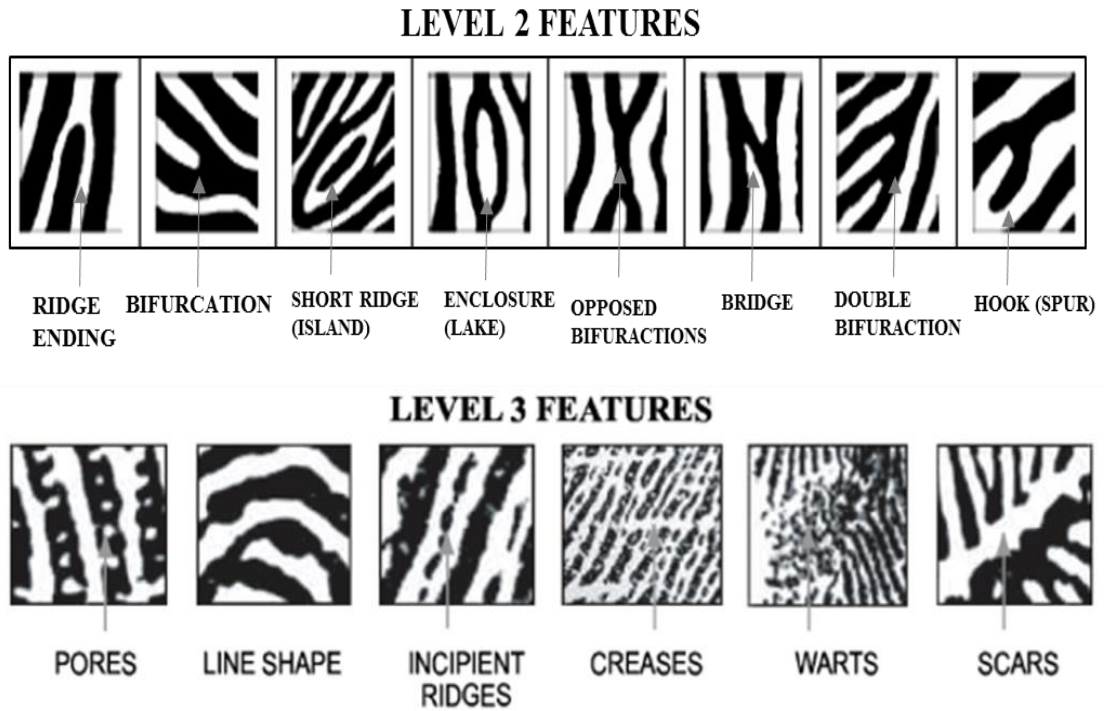


Figure 1.23: An examples of level 2 and level 3 fingerprint ridge pattern features details used for the classification and individualisation of fingerprints (Jain et al., 2007, Champod et al., 2004).

The basics of the discovery of Edward Henry together with more modern systems depending on ridge flow features still work in the current international computerised fingerprint identification systems (AFIS) (Jain and Feng, 2011). Those systems are used to perform two major types of forensic search known as latent search and ten print search. The ten print search includes a plain or rolled impression prints from every one of the ten fingers of individuals being searched against a database of identified persons. For the reason that plain and rolled impression prints are controllably collected, they are invariably of appropriate quality to give the entire information needed for a match (Komarinski, 2005). This is a four-step method referred to as ACE-V or analysis, comparison, evaluation and verification in the UK and several other countries (Jain and Feng, 2011). Analysing is the first stage of

assessing if the latent has adequate ridge detail and is of appropriate quality for identification, if the required characteristics are noted (Ashbaugh, 1999). The second step includes comparing the three levels of characteristics with paired print so as to measure their similarity level. Evaluation is the arrangement of latent paired fingermark and fingerprint as personal match or identification, non-match/exclusion or not conclusive depending the previous comparisons (Vanderkolk, 2001). Lastly the verification step is fundamentally a repetition of the first 3 steps and includes independent re-examination of latent print by one or two extra fingerprint experts (Druce and Bristow, 2010, Jain and Feng, 2011). At least sixteen of the fingerprint characteristics are required by the courts in the United Kingdom to describe the uniqueness of a fingerprint, consequently, the fingermark found at a crime scene is useful as proof identification and only if it is able to distinguish sixteen features of comparison with a fingerprints taken from a suspect (Knowles, 1978, Evett and Williams, 2015).

1.6.3 Fingermark composition

Many chemical compounds found in fingermarks can have three different sources (Champod et al., 2004). These compounds are a complex mixture of natural secretions of the body, and external contaminations from the environment (Champod et al., 2004). The dermis, which is the bottom layer of the skin, contains three types of secretory glands including eccrine, apocrine and sebaceous glands (Thomas, 1978), whose secretions reach the skin surface through epidermal pores (**Figure 1.24**).

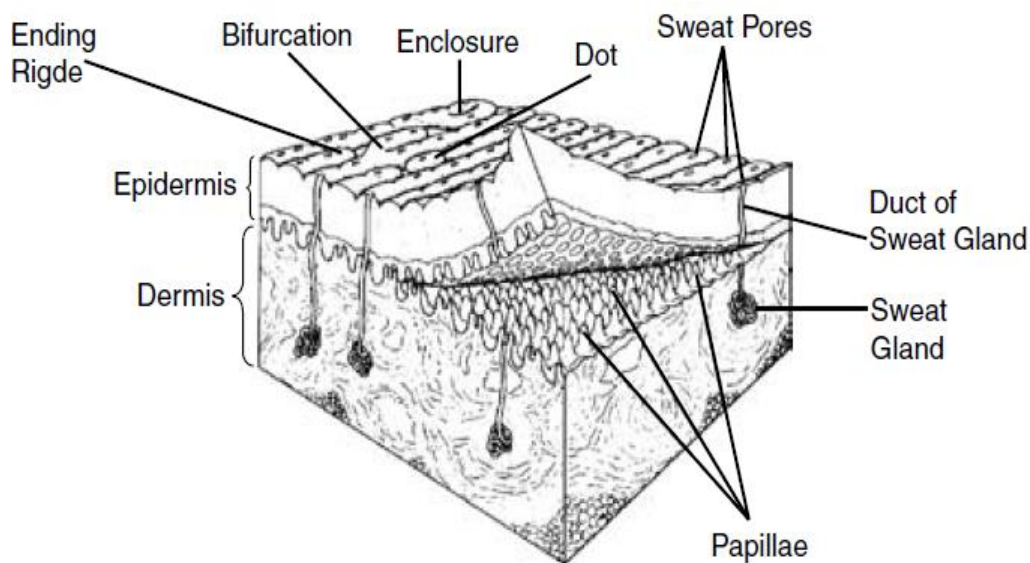


Figure 1.24: Friction ridge skin diagram of longitudinal section
(James and Nordby, 2003).

1.6.3.1 Eccrine glands

Eccrine secretions, which are located on the hands, play an important role in fingerprint composition (Light and Cooley, 2004). Eccrine glands produce the main compound of their secretions is water (99 %), while several other inorganic compounds such as sodium chloride and organic compounds such as amino acids, lactic acid, urea and sugar can be secreted (Scruton et al., 1975, Wargacki et al., 2007).

1.6.3.2 Apocrine glands

Apocrine glands are found in the breast, genital, inguinal and axillary regions. Apocrine secretions are found less in latent fingerprints (Choi et al., 2008). Apocrine

secretions include organic compound such as carbohydrates and proteins (Knowles, 1978).

1.6.3.3 Sebaceous glands

Sebaceous glands are found all over the body except on soles of the feet and the palms of the hands. The major compound, which sebaceous glands secrete, is oil (the sebum) and often found in latent fingermarks. Organic compound (fat soluble) such as fatty acids, wax esters, cholesterol and glycerides are found in the secretions from sebaceous glands (**Figures 1.25 - 1.28**) (Bramble, 1995, Thomas and Reynoldson, 1975). Sebum is transferred onto fingertips after contact with other parts of the body such as face and hair (Weyermann et al., 2011, Lewis et al., 2001).

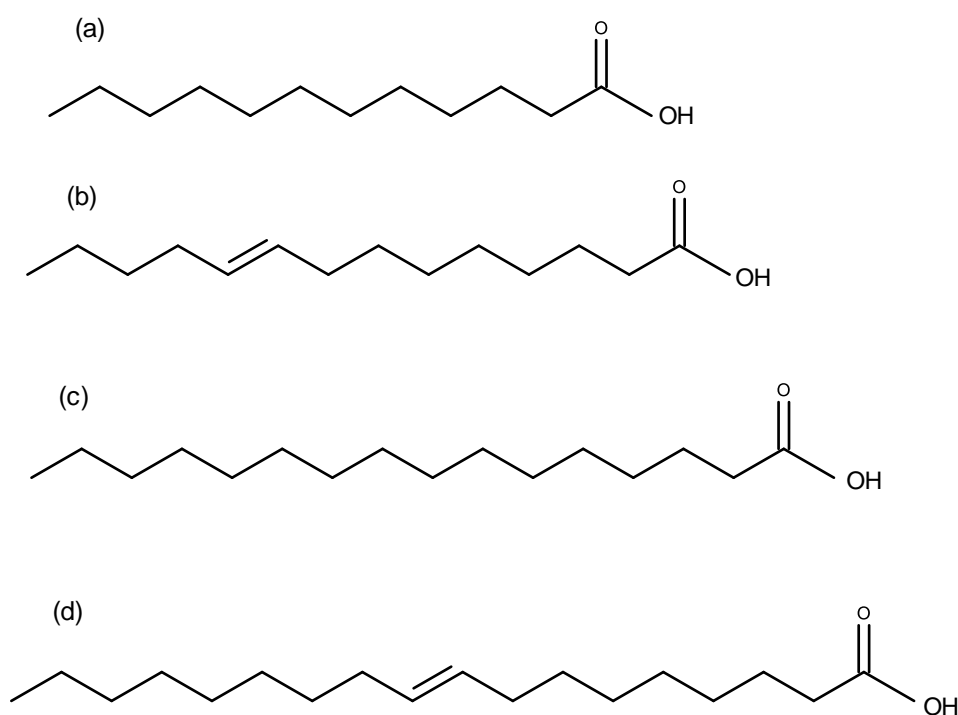


Figure 1.25: Molecular structure of fatty acids identified in fingerprint residues: (a) Dodecanoic acid, 12: 0; (b) Myristoleic acid, 14: 1 (Tetradecenoic acid); (c) Palmitic acid, 16:0 (Hexadecanoic acid); (d) Oleic acid, 18: 1 (Octadecenoic acid) (Girod et al., 2012).

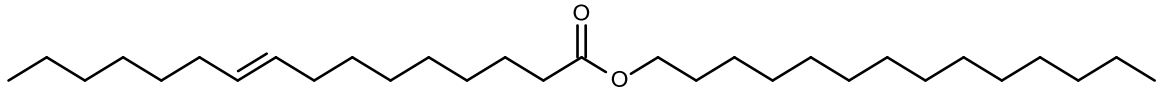


Figure 1.26: Molecular structure of a wax ester (myristyl palmitoleate) (Girod et al., 2012).

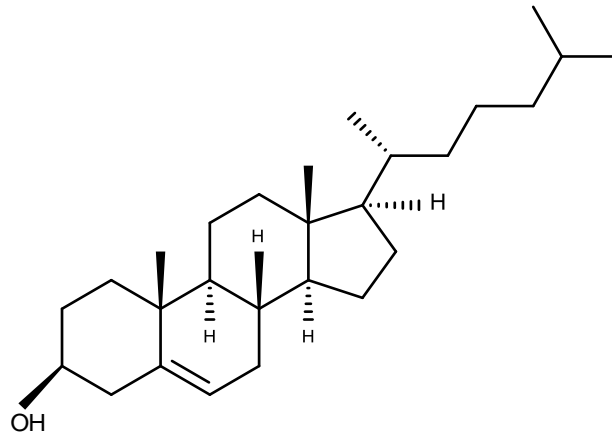


Figure 1.27: Cholesterol molecular structure (Wydro et al., 2007).

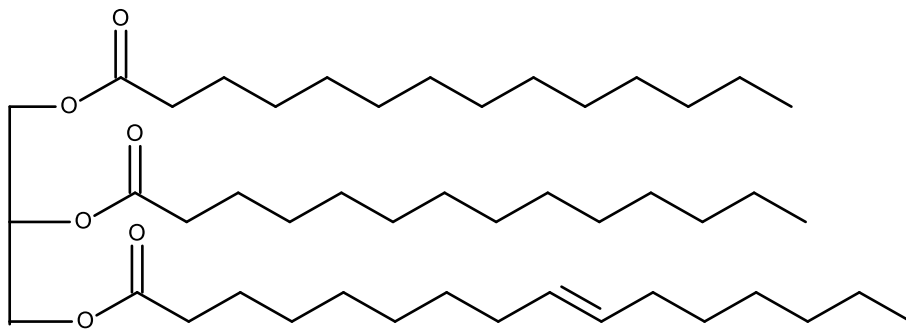


Figure 1.28: Triglyceride molecular structure (Girod et al., 2012).

1.6.4 Types of fingerprints/fingermarks

There are three general categories to describe the fingerprint evidence which may be found at a crime scene or on an item of evidence to a criminal matter: visible fingerprints, impression fingerprints and latent fingerprints (Knowles, 1978) (Figure 1.29) .

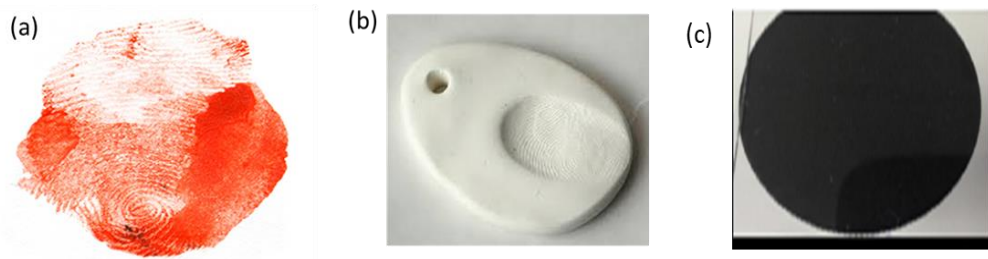


Figure 1.29: Types of fingerprints (a) visible fingerprints, (b) plastic marks and (c) latent fingerprints.

1.6.4.1 Visible (patent) fingerprints

Visible fingerprints (**Figure 1.29a**) are often more readily visible without processing any treatment to be clearly recognizable as a fingerprint. Such marks may be formed by fingers contaminated with blood, dark oil, grease and dirt (positive image) or when some substances such as dust removed from the surface by contact (negative image) (Bobev, 1995, Champod et al., 2004).

1.6.4.2 A plastic marks (alternatively called an impression or indented)

It may be detectable and left in a soft surface or malleable substances, such as wet paint, candle wax, butter, and silly putty (**Figure 1.29b**). These fingermarks should be immediately recognizable, and often needs no further processing (Thomas, 1978).

1.6.4.3 Latent fingermarks

Latent fingerprint is mark which left when a person touches a surface or an item with unprotected hands (Thomas, 1978). The latent fingermark (**Figure 1.29c**) is not readily visible (it is “latent”) and it is commonly found at crime scenes (Wilshire, 1996). The latent fingermark is the usual form of fingerprint evidence and is invisible, so it requires the use of detection techniques such as physical (*e.g.*, powdering), or chemical (*e.g.*, ninhydrin), or optical (*e.g.*, ultraviolet imaging) to develop (enhance) in order for a readily visible fingermark to be recovered that can be used for comparison purposes (Almog et al., 2000, Lee and Gaensslen, 2001, Sodhi and Kaur, 2001). Selection of the technique for fingermark development/visualisation is dependent on the composition of latent print residue (Choi et al., 2008).

In latent fingerprint visualisation it is now accepted that particles adhere to fingermarks due to the mechanical attraction with the fingerprint residues (Wilshire, 1996). The factors with influence this interaction are particle size, particle charge, particle shape and relative surface area (James et al., 1991b, Yamashita and French, 2011) all of which could be controlled by processing parameters such as chitosan

concentration, pH and ionic strength of the dissolution media, temperature of cross-linking, stirring rate, *etc* (Wang et al., 2011).

1.6.5 Surface characteristics

Fingerprints can be left at a crime scene, when the fingers touch a solid surface. The various glands in the skin produced mixture of natural secretions, and these are set down by the ridges details on the surface of the skin. These secretions are transferred, depending on a number of factors including temperature of the surface, surface structure, electrostatic forces of the receptor surface, and humidity. These factors play significant roles in the visualisation or development latent fingermarks (Baniuk, 1990). A sebaceous compound adheres better to a surface that is cooler than the human body. Moreover, a rough surface will have more adhesion forces (Champod et al., 2004).

Many different techniques have been used for developing a latent print, the method of choice depends on the surface. There are three types of surfaces are considered to choice suitable detection methods, because they influence the composition of fingerprints (Champod et al., 2004).

1.6.5.1 Porous surfaces

Porous surfaces tend to absorb the latent fingerprint deposit very quickly (normally within seconds) such as paper, cardboard, cloth, and wood (Champod et al., 2004). The water-soluble compounds are quickly absorbed on the surface. During absorption,

water will be evaporated, and then leaving a mixture of residues behind on the surface. The residues include amino acids, urea, and sodium chloride (NaCl). As the fingerprint ages, the amino acids will remain relatively stable provided that the surface of the substrate is stored under normal environmental conditions (relative humidity < 80%). On the other hand, other components such as urea and sodium chloride will tend to migrate continuously, depending on the environmental conditions. The higher the relative humidity, the faster is the movement. Thus, older marks will tend to alter in appearance significant due to diffusion of urea and sodium chloride (Champod et al., 2004). The fat-soluble compounds (non-water-soluble) remain longer period on the surface (Champod et al., 2004) (**Figure 1.30**).

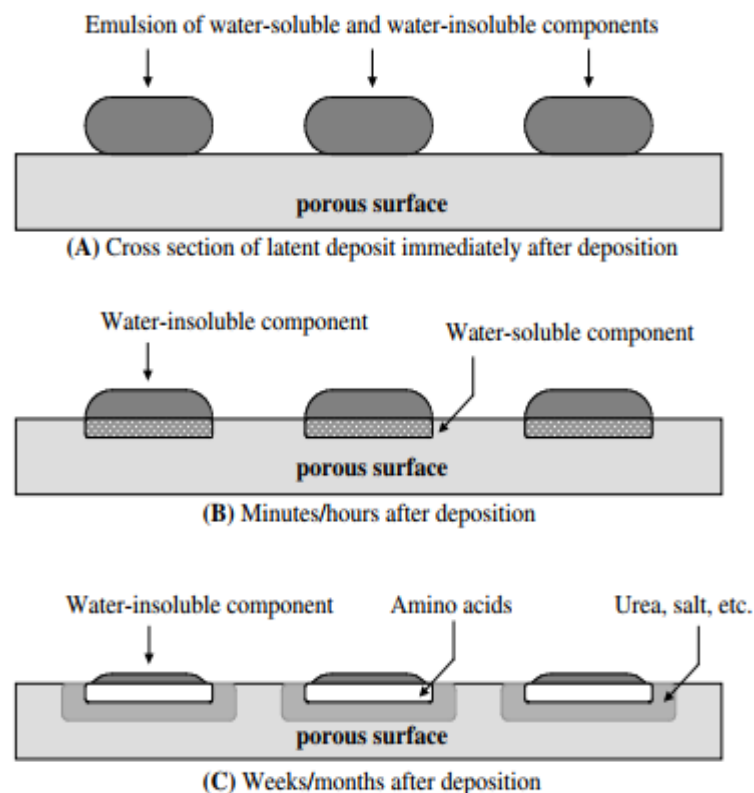


Figure 1.30: Aging of latent fingerprint on a porous substrate (Champod et al., 2004).

1.6.5.2 Semi porous surfaces

The surface absorbs the water-soluble compounds, but more slowly than for porous surfaces (from minutes to hour), whereas, the fat soluble compounds (non-water-soluble) stay much longer (from one day to several days) than it does on porous surfaces. A small amount of the fat soluble compounds may stay on the surface for a significant period. Semi-porous surfaces include metal, paints, and plastics (Champod et al., 2004).

1.6.5.3 Nonporous surfaces

This surface does not absorb any compounds deposited with the latent fingerprints (water-soluble and non-water-soluble compounds), and they will therefore remain on the surface (several weeks/months) unless they are removed, or are degraded. Usual examples of nonporous surfaces are plastics, glass, and shiny metal surfaces, mirrors, tiles, and glossy paints (**Figure 1.31**) (Weyermann et al., 2011).

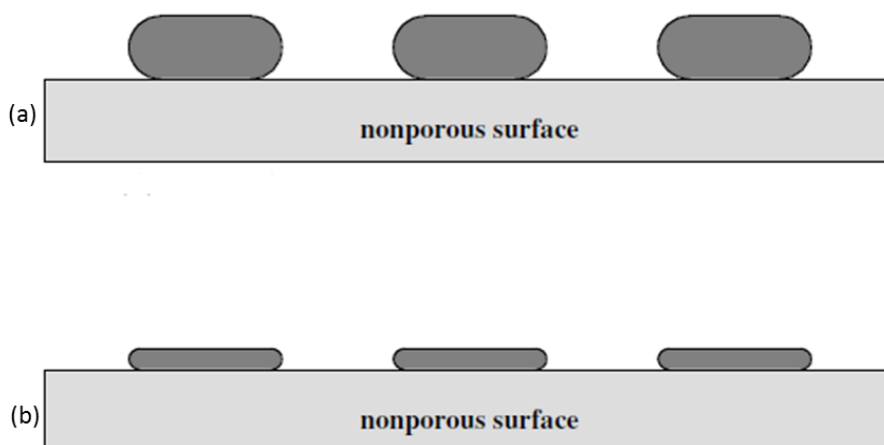


Figure 1.31: Aging of latent fingerprint on a non-porous substrate (a) cross section of latent deposit immediately after deposition (b) numerous weeks/months after deposition (Champod et al., 2004).

1.6.6 Detection of fingerprints

The detection of fingermarks represents an important interest in forensics, because it plays a significant role in individual identification (Wang et al., 2009). Several of techniques have been used to develop the visibility of latent fingermarks deposition on various surfaces. These techniques commonly employed may be broadly divided into four groups (Mohamed, 2011).

1.6.6.1 Physical methods

Physical methods, including powdering, small particle reagents (SPR) (Cuce et al., 2004, Haque et al., 1989), and vacuum metal deposition (VMD) (Theys et al., 1968, Kent et al., 1976), but do not involve any chemical reaction (Cantu, 2001, Champod et al., 2004, Schnetz and Margot, 2001). The process of powder dusting is physical one, which the powder particles adhere to the latent residue (humid, sticky, or fatty compounds) in the latent fingerprint deposit. Fingerprint powders are most commonly reserved for crime scene use on objects which cannot be readily transported back to the laboratory. Small-particle reagent is usually applied by spraying or immersion in an aqueous suspension (the most common molybdenum disulfide) followed by rinsing with water. The powder suspension is normally referred to as small-particle reagent. The particles adhere to the lipid components of the residue on the fingerprint deposit. SPR technique is effective on surfaces that have been recovered from adverse conditions such as snow, rain, or high humidity (Haque et al., 1989).

1.6.6.2 Chemical methods

In these methods, various techniques for revealing a latent fingerprint through chemical reactions with the organic and inorganic components will be investigated. These techniques include ninhydrin and its analogues (Odén and Von Hofsten, 1954), metal complexation after ninhydrin treatment, diazafluorenone (DFO) (Pounds et al., 1990), 1,2-indanedione (Hauze et al., 1998), silver nitrate (O'Neill, 1937) and genipin (Champod et al., 2004). Chemical methods of fingerprint development have the potential advantage that the non-moisture components may, under certain conditions, remain unaltered for a period of several days/weeks. Ninhydrin reacts with amino acids to give a dark purple product known as Ruhemann's purple (Ruhemann, 1910). In addition, the ninhydrin reaction is slow unless accelerated by heat in the presence of humidity. As the eccrine component of a latent mark deposit contains amino acids, therefore the small amount of amino acids in sweat (0.3-2.59 mg/L) can be used as a means of developing fingermarks on porous surfaces such as paper and cardboard (Hansen and Joullié, 2005). Ninhydrin is applied by spraying, painting, or dipping. Silver nitrate reacts with the chloride ions (Cl^-) contained in secretion residue of fingermark to produce silver chloride (AgCl). When silver chloride upon exposure to light, it decomposes to produce metallic silver, resulting in a black fingermark.

1.6.6.3 Physical/chemical methods

Classically, the physical/chemical methods are physical developer, multi-metal deposition (MMD), iodine (O'Neill, 1937, Trowell, 1975) and cyanoacrylate (Karlinszky and Harkai, 1990, Menzel et al., 1983). Physical developer (PD) is a fingerprint processing technique for porous surfaces like paper, and it is the most effective to visualise water insoluble components of the latent fingerprint deposit

(Cantu, 2001). PD is a photographic physical developer process based on the deposition of silver (Ag) onto latent fingerprint residue (Phillips et al., 1990) from an aqueous solution (at low pH) containing a ferrous/ferric redox (reduction/oxidation) system, citric acid (as a buffer) and silver salt mixture in solution. The mechanism is that the ferrous ions (Fe^{2+}) in an aqueous solution reduce the silver ions (Ag^+) to silver metal (solid) (Ag). The silver particles (as colloids) deposit along the ridges, giving dark grey/black prints (Cantu, 2001).

1.6.6.3.1 Multi-metal deposition (MMD)

The comprises of two steps: the first is the immersion of the object (porous and non-porous surfaces) in a solution containing gold nanoparticles as the active component; and the second is visualisation of the detected fingermarks using a silver physical developer (AgPD). So the silver deposit onto the surface of the gold nanoparticle (Schnetz and Margot, 2001).

1.6.6.3.2 Iodine fuming method

Iodine crystals are heated to transform into vapour (sublimation) that physically adsorbs onto the greasy substances of a fingermarks to produce brown coloured prints. The iodine fuming method can be used of porous and nonporous surfaces. In contrast, due to its limited sensitivity, the iodine fuming technique works best on fresh marks no more five days old. One disadvantage is that the developed print will disappear with time and so needs to be either fixed or photographed as quickly as possible. (O'Neill, 1937, Trowell, 1975).

1.6.6.3.3 Cyanoacrylate fuming (Super-glue method)

Super-glue is a mixture of 98-99 % of methyl, ethyl, or butyl-2-cyanoacrylate (Kendall and Rehn, 1983). The polymerisation reaction, which makes the glue set, is easily catalysed by basic compounds, including water. The object and super glue are placed in the enclosed cabinet. The residues of moisture, amino acids, fatty acids, and proteins in found on the fingerprints is the reason that the super glue fume can stick latent finger ridge together fast to give a white colour on latent print. Super-glue fuming technique is most effective for a non-porous substrate (Kendall and Rehn, 1983, Wood, 1991, Tissier et al., 1999). Previous research developed this method using cyanoacrylate fuming followed by a thin layer of gold and zinc particles is deposited on fingermarks (VMD) (Jones et al., 2012).

1.6.6.3.4 The combination of optical methods

The combination of optical methods includes absorption, diffuse reflection, luminescence, ultraviolet absorption and reflection (Champod et al., 2004). Luminescent techniques are usually preferred due to their a high sensitivity and their ability to get rid of the pattern or the colour of the support on which the fingerprint lies (Dalrymple et al., 1977, Sears et al., 2012). Moreover, the most common important techniques that were mentioned, there still are numerous methods which can be used to develop or enhance the fingerprints. Each method is used according to number of factors; the cleanliness of surface, if it porous or non-porous, the environment, weather conditions, amount of contaminant, pressure applied, movement during transfer and condition of the friction ridge detail (Dilag et al., 2013).

In recent years, in forensic science research, one of the main achievements is the application of nanoparticles in fingerprint detection. In this period, numerous forensic science research has been done on the advancement in detection methods that depend on the application of nanoparticles in fingermark detection (Choi et al., 2008). One such attempt was undertaken to design new powders that acted as dusting agents with more potential than the classical methods. A previous study suggested the use of gold nanoparticles which had been grafted with aliphatic chains would improve the affinity of the powder towards sebaceous secretions (Choi et al., 2006). The same development was put in use with titanium dioxide nanoparticles, whereby they were grafted with aliphatic chains and a fluorescent dye. These new powders were applied using a brush (Choi et al., 2007). Similarly, two types of molecules; hydrophobic chain and Eosin Y (fluorescent dye) were used to coat aluminium oxide nanoparticles (Sodhi and Kaur, 2006), and in order to ensure latent fingermark detection on different surfaces a fluorescent dye was used in combined with silica nanoparticles (Theaker et al., 2008). Alternative research strategies include an attempt to improve existing physico-chemical methods utilising on nanoparticles. Research from other authors indicate the possibility of using gold nanoparticles, in increasing the silver deposition during the physical development process (Sametband et al., 2007). On the other hand, other researchers have modified classical multi-metal deposition methods through replacing the silver on gold nanoparticles with zinc oxide, to create luminescent fingermarks (Becue et al., 2008). Studies on gold nanoparticles are mainly motivated by the need to improve multi-metal deposition, a technique that depends on the application of colloidal gold in the fingermark detection on various substrates (**Table 1.5**) (Schnetzer and Margot, 2001). In addition, studies have suggested multi metal deposition of luminescent materials where zinc oxide

deposition was used instead of silver coating (Becue et al., 2008). It has also been suggested that the application of a one-step multi metal deposition like process in fingerprint detection which can be operated on a wide pH range and uses glucose capped gold nanoparticles (Gao et al., 2009). Some authors used glutamate-capped gold nanoparticles trapped in polycation chitosan, which implies to develop latent fingerprint after immersion for several hours. The appearance of the fingermarks in this case is because of oil enriched fingerprints (Islam et al., 2007). Over the past decade, the application of fluorescent nanomaterials in detection of latent fingerprints has yielded much interest in forensic science because of their excellence in physical and chemical characteristics such as high intensity in fluorescent and larger surface area (Liu et al., 2008a, Becue et al., 2008, Ma et al., 2011). Currently, the widely investigated fluorescent nanomaterials in fingerprint development are quantum dots (QDs), which are excited by ultraviolet to produce strong visible fluorescence (Jin et al., 2008, Becue et al., 2009, Dilag et al., 2009, Wang et al., 2009, Liu et al., 2010). QDs are one to ten nanometres diameter extreme luminescent nanoparticles that can be solubilized and functionalized in either organic or aqueous solvents. The strong fluorescent emission lowers the background interference and increases contrast in the nanomaterials fingerprints development. Furthermore, over the past years, the uncommon earth fluorescent nanomaterials that have the merit of tiny particles size, high quantum yield, large surface area, good optical stability, narrow emission peak, and high fluorescent intensity (Shen et al., 2008) are the most efficient in fluorescent labels for fingerprint development (Wang et al., 2015a, Wang et al., 2015b). Some studies relied on the application of QDs in the fingerprint detection. In the latent secretion detections there are three methods of integrating QDs that is; as an aqueous solution, as a dry powder, or as embedded as polymer which can

bond covalently with the secretion. For the detection of freshly marked fingerprints on aluminium foil, cadmium sulfide (CdS) encapsulated in a matrix of biopolymeric chitosan functioned as the dusting powder. The later detects luminescent fingermarks; however, using nanoparticles that are cadmium based poses a serious safety and health issues (Dilag et al., 2009). Alternative cadmium selenide (CdSe) quantum dots that are water soluble were synthesized for the detection of fresh fingerprints on adhesive surface tapes including black electrical tape, yellow electrical tape, blue electrical tape and yellow sealing tape; as a result, it was found to be successful (Wang et al., 2009). In the detection of bloody fingerprints on different non porous surfaces for instance, glass transparent polypropylene, black polyethylene, aluminium foil, cadmium telluride (CdTe) quantum dots produced in aqueous solution can be used. Quantum dots have an attraction to blood, due to of the presence of haemoglobin (Becue et al., 2009). A comparison of QDs with acid yellow 7 which is among the best blood reagents used in non-porous substrates showed that they are superior and more effective on aluminium than acid yellow 7. For detection of fingermark on non-porous substrates, it was proposed that samples should be immersed in an aqueous CdTe solution (Cheng et al., 2008, Liu et al., 2010), however, the immersion requires several hours. To improve the contrast of fumed fingerprints on non-porous surfaces, the QDs should be embedded in a polyamidoamine dendrimer (Jin et al., 2008, Wang et al., 2008b). In 2000, cadmium sulphide nanocrystals were used in staining cyanoacrylate though binding them with dendrimers (Menzel et al., 2000). Nonetheless, the immersion times took an entire day, destabilising the working solution; thus it did not offer an alternative method to the cyanoacrylate stains. In a recent improvement of this study, researchers grafted aliphatic chains on the surfaces of QDs in ether in an attempt to stabilise them and

used them in detection of sebaceous fingermarks on paper substrates and silicon wafers. This proved useful for the silicon surface but its high background luminescence makes it unsuitable for paper (Sametband et al., 2007). Moreover, silica nanoparticles refer to a different type of reliable nanocomposites used for fingerprint detection because it offers a great freedom in relation to dye doping and functionalism. According to previous research, there is entrapment of different fluorescent and coloured dyes including thiazole orange, rhodamine 6G, rhodamine B, oxazine perchlorate, methylene blue, fluorescein, basic red 28, and basic yellow 40 within the silica particles (Theaker et al., 2008). The obtained doped nanoparticles were applied in aqueous solution for fingermarks detection as dusting reagents. In both new fingermarks (twenty minutes old) and old fingermarks (forty days old) they produced an accurate definition after development. In addition, another study incorporated europium-based dye within silica nanoparticles and powdered further to acquire nanocomposites for fresh detection of latent fingermarks (six day old) on different substances such as green leaf, coloured paper, rubber glove, and plastic bag (Liu et al., 2008a). Silica nanoparticles enhanced with carbon black also function as fingerprint powder in the fingerprint detection on metal and glass surfaces prior to lifting them using a lifting tape (Benton et al., 2010b, Benton et al., 2010a, Rowell et al., 2009). The powder particles improve adhesion on the fingerprint greatly depending on their shape and size. Large particles have a less adhesion than fine powder particles; hence, the powder is categorised according to sizes ranging from 1 to 10 μm (Theaker et al., 2008). More recently (Dhall and Kapoor, 2016), studies formulations of titanium dioxide, zinc oxide, and zinc carbonate based fluorescent particle reagents and compared and analysed them in the formation of latent fingermarks affected by destructive conditions. Then the three compositions were

developed using fresh latent prints and prints affected by simulated or natural destructive crime scene situations such as burial in soil, explosion, arson, burial in snow and immersion in drainage water. Even after exposure to destructive crime scene simulations, the researchers successfully obtained the latent prints. Furthermore, the fresh prints with better quality prints were recovered from drainage water, soil burial, and arson; but for snow burial and explosion conditions the results were relatively poor. Titanium dioxide, has a 205.8 nm average particle size, circular shape; and the morphology of particles is uniform in size and shape and it forms soft agglomerates. For zinc carbonate, it has a 13.57 μm average particle size, spherical to irregular shape; and the morphology of particles is porous spherical grains with extensive variation in shape and size of particles. For zinc oxide it has a 464.7 nm average particle size, characteristic nanorods shape; and its morphology of particles is typical of nanorods with soft agglomerate formations and clumpings. The study concludes that latent fingerprints exposed to destructive crime scene conditions should not be neglected. Fluorescent SPR compositions based on titanium dioxide or zinc carbonate are suitable reagents for the development of fingermarks exposed to destructive crime scene conditions. Wet powder based suspensions were found suitable for development of fingerprints exposed to destructive conditions and the efficiency of the reagents was found in the order: titanium dioxide > zinc carbonate > zinc oxide (Dhall and Kapoor, 2016). Reynolds' (2008) study concluded that powder particles comprised of titanium dioxide particles of an average size 300 nm in diameter and have a rich coat of silicon or aluminium. This coating is loosely packed in Sirchie powder and in titanium dioxide the coating is 100 nm thick. Conversely, Stan Chem powder has a thinner, denser coating that covers titanium dioxide irregularly with a 20 nm thickness. The composition and existence of a coating that

adheres to titanium dioxide particles may be related to the cause of different powder performance in the development of fingerprint (Reynolds et al., 2008). In terms of background staining and ridge quality numerous studies shown that the commercially available powder suspensions differ in effectiveness. Previous research has made a comparison of Wet Powder™ white, titanium dioxide grade RG-15, Adhesive side Powder light Cat No. ASP50L – Sirchie, and Wetwop™ white #1-0078 (Jones et al., 2010a). Then, the white powder suspensions (WPS) formulations were smeared on a black insulating tape and the outcome was investigated using X-rays photoelectron spectroscopy and electron microscopy. For all 200 – 500 nm particles the distribution of particle size was similar with insignificance influence on effectiveness. However, with respect to WPS formulations chemical composition and morphology, the particle coating is different and is responsible for the variation in the performance of different brands (Reynolds et al., 2008). In a different study, a similar situation applied scanning electron microscopy and atomic force microscopy to study surface smoothness categorized as non-porous which refers to unplasticised polyvinyl chloride, polyethylene, and formica. Afterwards, they attempted to compare the iron oxide powder suspension effectiveness with these analytical measures in the fingerprints detection on those substrates (plastic formica, polyethylene and unplasticised polyvinyl chloride) using 18 hour old sebum. They proved that both topographical feature and average roughness substantially affect the latent finger marks processing (Jones et al., 2010b). In addition, there are more studies which development of fingerprint using different substance and different surfaces (**Table 1.5**).

Table 1.5: An examples of chemical compounds used to detect of fingerprint.

Substance	Method	Surface	Interaction	Reference
Colloidal gold/ silver	MMD	Porous (white paper), Non-porous (white polythene plastic bag)	Gold particles (pH 2.5-2.8) as active component attract to some components of fingermark residue then develop print with PD (silver)	(Schnetz and Margot, 2001)
Polycyanoacrylate/ gold and zink	CA fuming and BY40 dye followed by VMD of gold and zink	Low-density polyethylene	Polymerisation CA around pores in fingermarks, subsequent additional areas (not coated with CA) development by VMD.	(Jones et al., 2012)
Turmeric (<i>Curcuma longa</i>). 1,7-bis-(4-hydroxy-3-methoxy-phenyl)-hepta-1,6-diene-3,5-dione	Powder dusting	Porous and non-porous surfaces including normal paper, bond paper, thermal paper, transparency sheet, aluminium foil, wooden surface (sun mica-glossy), plastic sheet, painted steel and top as well as writing surface of CD.	Formation of hydrogen bonds between the lipid residue (fatty acids) of sebum and the carbonyl and hydroxyl group of the curcumin component of the turmeric powder	(Garg et al., 2011)
Titanium dioxide particles. Acid yellow, acid violet and acid black)	Wet powder suspensions/or small particle reagent (SPR)	Dark coloured, smooth non-porous surfaces	Titanium dioxide primarily interact with the non-bloodied part of the mark, thus producing a contrasting effect with the background and acid dyes	(Au et al., 2011)

Traditionally the most widely used techniques for latent fingerprint development are powder dusting, ninhydrin dipping and iodine fuming and their effectiveness will depend upon the surface on to which the latent fingerprint has been deposited. However, these traditional methods for latent print detection are not always effective and researchers and practitioners are continually trying to improve upon these existing techniques. In recent years, there has been an increasing interest to detect and develop latent fingerprints using modern instrumentation. For example gas chromatography-mass spectrometry (GC/MS) to determine the natural composition of fingerprints such as cholesterol, fatty acids and wax esters for aging (Weyermann et al., 2011, Bailey et al., 2012); X-ray photoelectron spectroscopy (XRP), X-ray fluorescence (XRF), transmission electronmicroscopy (TEM) (Jones et al., 2010a); time-of-flight secondary ion mass spectrometry (ToF-SIMS) (Attard-Montalto et al., 2014, Montalto et al., 2013) and SEM analysis (Bacon et al., 2013, Jones et al., 2010b, Jones et al., 2012, Wei et al., 2017).

1.7 Research aims and objectives

The aim of this research was to prepare chitosan particles at different CS: TPP ratios then investigation the potential of these particles for forensic and pharmaceutical applications. To achieve this aim the following objectives will be followed:

- Study the effect of different variables of three independent variables (pH, ionic strength and CS: TPP ratio) on formulation parameters of chitosan microparticles using the mathematical models obtained to predict the relative viscosity, zeta potential and particle size under different preparation conditions.
- Illustrate the optimisation of different chitosan- TPP microparticles using a 2³ factorial factor design with eight experiments to use in latent fingerprint visualisation. Development of aged latent fingerprints and the evaluation of the effectiveness of CS: TPP microparticles in samples with a decreased amount of fingerprint residue in either individual depositions or in a split depletion series.
- Preparation and optimisation parameters produce chitosan-TPP nanoparticles for the delivery of poorly water soluble drug ibuprofen for potential pharmaceutical applications.
- *in vitro* release studies of the ibuprofen from chitosan-TPP nanoparticles
- Evaluate the mucoadhesion properties of chitosan-TPP nanoparticles and how these nanoparticles may interact with mucin through viscosity, particle size

and zeta potential measurements performed on chitosan nanoparticles alone and their mixture with mucin.

1.8 Publications and Presentations

Publications from this thesis are as follows:

Journal Publications:

- Ezzeddin, M. A. Hejjaji, Alan M. Smith and Gordon A. Morris. (2017). "Designing chitosan-tripolyphosphate microparticles with desired size for specific pharmaceutical or forensic applications." *International Journal of Biological Macromolecules*, 95: 564-573. This publication forms part of chapter 3.
- Ezzeddin, M. A. Hejjaji, Alan M. Smith and Gordon A. Morris. (2017). "The potential of chitosan-tripolyphosphate microparticles in the visualisation of latent fingerprints." *Food Hydrocolloids*, 71: 290-298. This publication forms part of chapter 4.
- Ezzeddin, M. A. Hejjaji, Alan M. Smith and Gordon A. Morris. (2018). "Evaluation of the mucoadhesive properties of chitosan nanoparticles prepared using different chitosan to tripolyphosphate (CS: TPP) ratios." *International Journal of Biological Macromolecules*, 120: 1610–1617. This publication forms part of chapter 6.

Conference Presentations:

The potential of chitosan-tripolyphosphate microparticles for forensic and pharmaceutical applications.

- 13th International Conference on Chitin and Chitosan. Munster - Germany (2015): Poster
- 2nd UK Hydrocolloids Symposium, Birmingham - UK (2015): Flash Oral Presentation
- 19th European Carbohydrate Symposium EUROCARB. Barcelona - Spain (2017): Poster

Chapter 2

Instrumental techniques

(Background theory)

2 Instrumental techniques (background theory)

The main purpose of this chapter is to give a general background to the theory of the techniques which will be applied in this thesis to characterise chitosan particles.

2.1 Zeta potential

Zeta potential is the potential that exists at the boundaries of the outer diffuse layer surrounding charged particles. Under the effect of an electric field, the particles migrate in the direction which has the opposite charge. In colloids, zeta potential is the electrical potential difference across the ionic layer around a charged colloid ion (Hunter, 1981) (**Figure 2.1**).

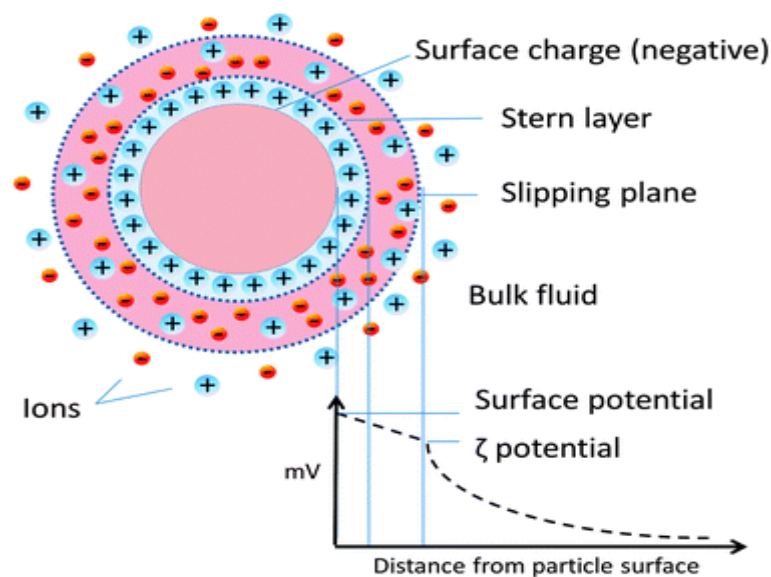


Figure 2.1: Schematic representation of zeta potential: ionic concentration and potential differences as a function of distance from the charged surface of a particle suspended in a medium (Liese and Hilterhaus, 2013).

The zeta potential is important, since it plays a major role in the stability of suspensions. If suspended particles have large negative or positive zeta potential values, they tend to repel each other, minimizing flocculation. When the zeta potential is low the electrical repulsion between the particles does not exceed the attractive van der Waals forces and the dispersion will break and flocculate or precipitate (**Figure 2.2**). However, if the zeta potential is high, this leads to a high value of the electrical double-layer thickness, and the solution will resist aggregation (Avadi et al., 2010).

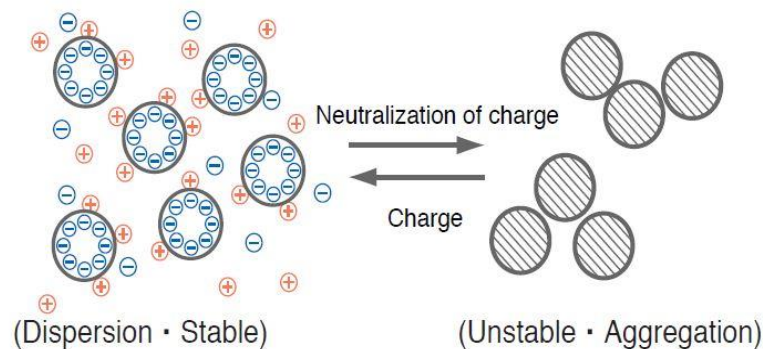


Figure 2.2: Evaluation of dispersion stability by zeta potential/particle size (Liese and Hilterhaus, 2013).

Generally, the higher the zeta potential, the more stable the colloid becomes. Therefore, particles which have zeta potential greater than +30mV or less than -30 mV are considered stable (Müller et al., 2001, Hu et al., 2008).

The Zetasizer instrument can also quantify the size of the particles at nanoscales using a process called Dynamic Light Scattering (DLS) that measures Brownian motion and

relates it to the particles size. Brownian motion is defined as the constant movement of particles in liquid due to the random collision with the molecules of the liquid which surrounds the particle. The relationship between the particle size and its speed (diffusion) due to Brownian motion is related via the Stokes-Einstein equation.

$$R_H = K_B T / (6\pi \eta D) \quad \text{Eq. (2.1)}$$

Where R_H is the hydrodynamic radius, K_B is the Boltzmann's constant (1.381×10^{-23} J/K), T is the temperature (K), D is the diffusion constant and η is the viscosity of the solvent in which the particles are suspended.

The laser is used to provide a light source to illuminate the sample particles. Most of the laser beam passes straight through the sample, however some are scattered by the particles within the sample. A detector measures the intensity of the scattered light. Therefore, when large particles are being measured, the large particles move slowly and the intensity of the pattern will also fluctuate slowly. Whereas, the small particles move more quickly and the intensity of the speckle pattern will also fluctuate quickly. The instrument software uses algorithms for a number of size classes to produce a size distribution. The particle size distribution can be reported as the intensity of the scattered light (y-axis) against the distribution of size classes (x-axis). The particle size distribution graph is characteristic and can be shown in **Figure 2.3**.

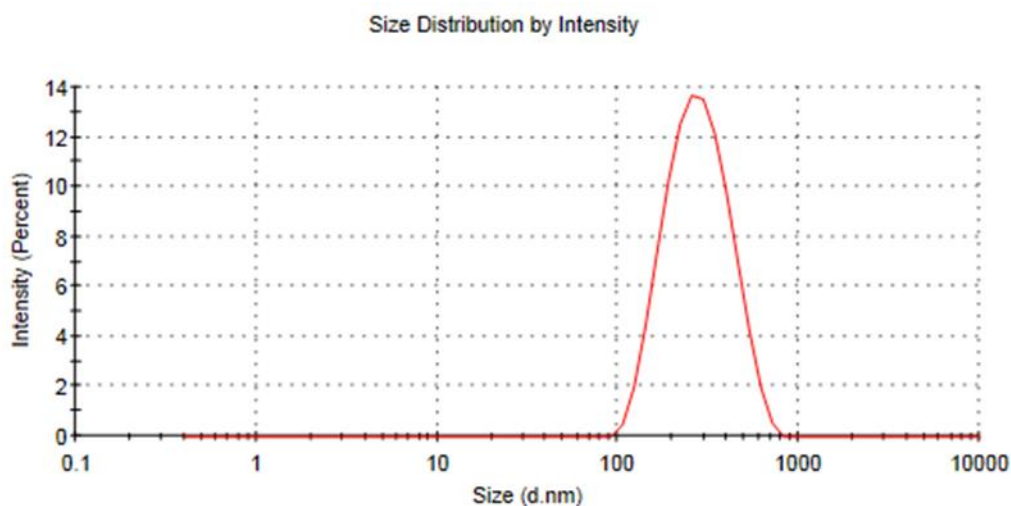


Figure 2.3: Particle size distribution of chitosan nanoparticle CS-TPP at (4:1) ratio, 216.0 ± 1.9 nm.

2.2 Particle size analysis

The Malvern Mastersizer 2000 can be used to determine the particle size distribution at the microscale. Laser diffraction (LD) is the method used for measuring the light scattering which is dependent on particle size. Particle sizes can be measured by laser diffraction analysis from 0.02 to 2000 μm . The LD technique uses the fact that the laser beam is scattered by the particles and this scattered laser light is registered on detectors (**Figure 2.4**). The light sources of the laser beam are helium and neon having two different wavelengths. The blue laser is used for measuring the amount of back scattering from the sample (small particles), whereas the red laser detects the larger particles, for which the diffraction pattern is measured by a series of detectors. The angle at which the beam is scattered is inversely proportional to the particle size. The pattern is characteristic of the particle size and using mathematical analysis the result is transformed into an accurate, repeatable picture of the size distribution (Stojanovic and Markovic, 2012).

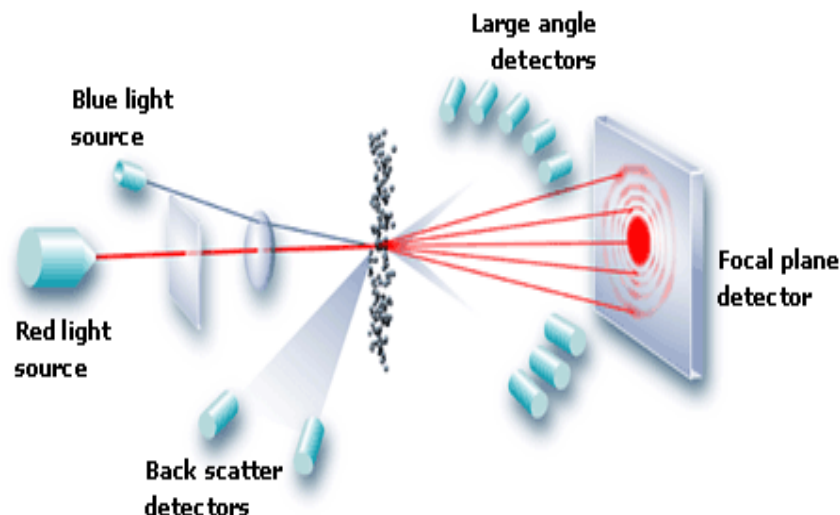


Figure 2.4: Models for determination of particle size distribution
(Stojanovic and Markovic, 2012).

2.3 Rheometry (Rheology)

Rheometry is a technique to determine the rheological data that consists of measuring systems, instruments, test and analysis methods (Mezger, 2006). In addition, rheology is the scientific study of the deformation and flow properties of substance. Therefore, the word ‘rheology’ comes from the Greek words *rheo* (“to flow”) and *logos* (“science”). Rheology can be defined as the relationship between strain and stress within a material as a function of temperature, time, and frequency. Stress and strain are important parameters in studying rheological properties of hydrocolloid systems. The term ‘strain’ refers to the deformation as a result of the applied stress whereas, the term ‘stress’ refers to the force (F) per unit area (A) applied on a system (Picout and Ross-Murphy, 2003). Rheometry gives information about the physical and mechanical properties of a sample, as well as it is important to use rheometry measurements to evaluate the viscoelastic properties of pharmaceutical formulations

as this behaviour can have an effect on all the stages of dosage form development right through to administration. Compounds are classified according to observed physical behaviour *i.e.* liquid (viscous) or solid (elastic) with the two extremes of behaviour corresponding to a perfect (Newtonian) liquid or and a perfect (Hookean) solid. Bipolymers such as polysaccharides have properties that are both viscous and elastic, therefore, are referred to as viscoelastic (**Figure 2.5**) (Mezger, 2006).

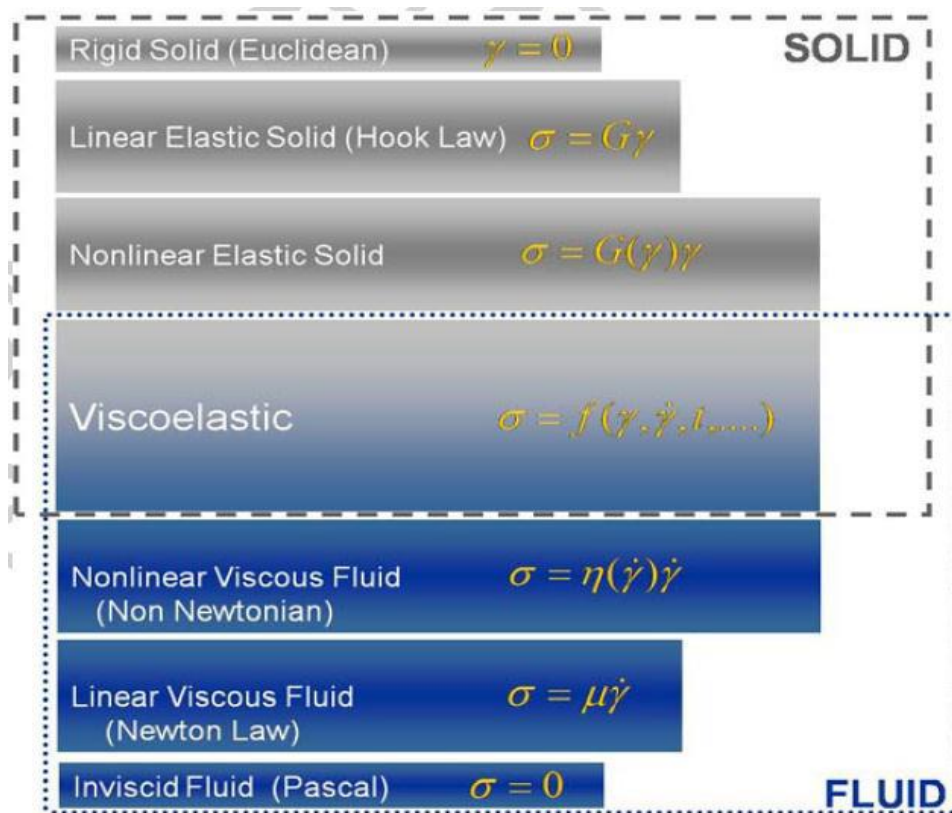


Figure 2.5: Classifications of materials in simple shear. Where γ represents strain rate, η represents viscosity, σ represents stress, μ , expressed as the coefficient of viscosity and G represents the constant of proportionality or elastic modulus (Partal and Franco, 2010).

Another important parameter as the change in strain over the time is known shear rate or strain rate ($\dot{\gamma}$); it is essential parameter and its unit the reciprocal of seconds (1/s) (Mezger, 2006, Rao, 2010).

2.3.1 Viscosity

Viscosity is a measure of a liquid's resistance to flow. The higher the viscosity, the greater a liquid's ability to resist flow (the friction between the internal molecules of a material). All fluids become less viscous as the liquid's temperature increases and more viscous as the fluid gets cooler. The viscosity of a liquid is an important parameter which can be used to predict the behaviour of products, on application and storage, as well as can have an impact of drug release (Lewis, 1990).

The flow of Newtonian liquids is directly proportional to the stress applied which expresses in **Equation 2.2** (Barbosa-Canovas and Ibarz, 2014).

$$\text{Viscosity } (\eta) = \text{Stress } (\sigma) / \text{rate of shear } (\gamma) \quad \text{Eq. (2.2)}$$

If shear is applied in Newtonian liquids system such as water, alcohols and oils, at temperature constant, there is no change in viscosity as a linear relationship between the shear stress and shear rate (Chhabra and Richardson, 2008). On the other hand, if shear is applied to non-Newtonian fluids system, there is change in viscosity as there is a non-linear relationship between the shear stress and shear rate. There are numerous common types of non-Newtonian flow behaviour such as dilatant, pseudo-plastics and Bingham plastic (**Figure 2.6**) which can be estimated by plotting shear stress vs. shear rate.

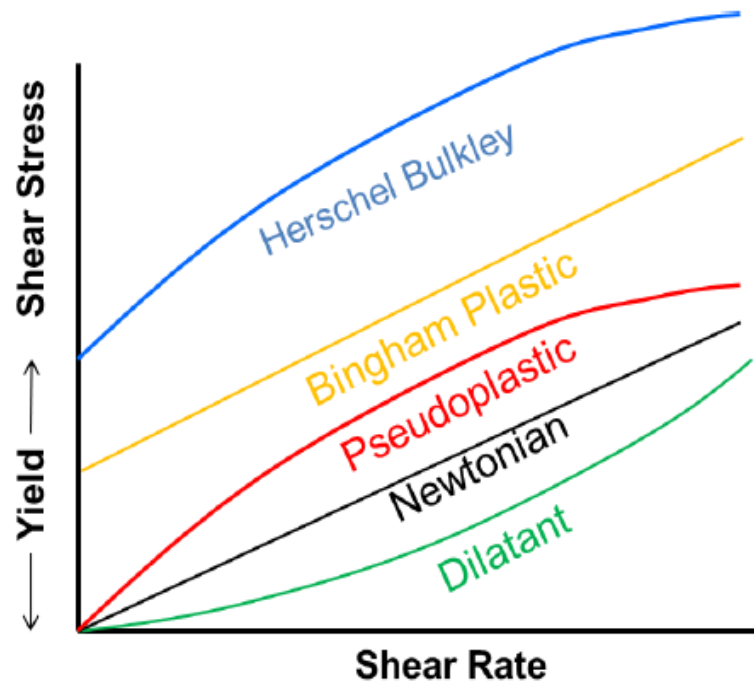


Figure 2.6: Flow curves (shear stress vs shear rate) for Newtonian and non-Newtonian flow behaviour with yield stress region shown (Miri, 2011).

Several factors such as concentration, temperature and pH may effect flow properties (Koliandris et al., 2008). Dissolution of chitosan molecules will increase the viscosity of a solution because it disrupts the streaming of the flow. The polymer conformation and the polymer–solvent interactions depend on the number of positive charges (-NH_3^+) on chitosan (Kasaai et al., 2000).

2.4 Powder X-Ray Diffraction (p-XRD)

X-Ray Diffraction has been used to characterise microparticles. XRD pattern is quite characteristic and usually used to determine crystallographic, molecular structure of material. A monochromatic beam of X-rays may be diffracted by atoms in a crystal. The angle θ that intense reflections are detected is governed by interferences between

X-ray beams reflected by neighbouring planes of atoms in the crystal. These angles θ , the spacing between the several planes of atoms can be determined. The intensity of reflections against 2θ , where θ is both of the incident and reflect angle between the X-ray beam and the planes of the atoms, are called diffraction patterns. The diffraction pattern is recorded for individual crystalline substances and can be interpreted in terms of the crystal structure of substance (**Figure 2.7**).

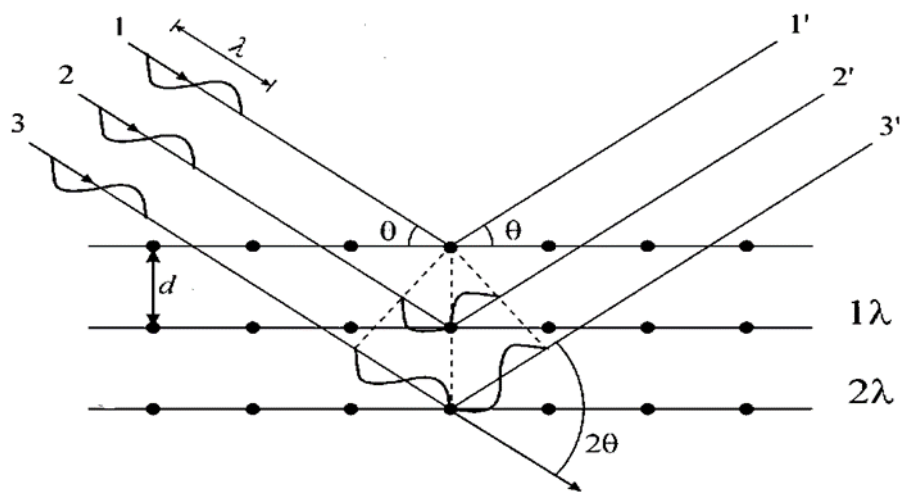


Figure 2.7: X-ray diffraction, lattice planes (1, 2 and 3 are incident X-rays; 1', 2', and 3' are reflected x-rays) (Bahl and Tuli, 2010).

Reflated X-ray from a set of planes interfere constructively when the Bragg condition is met (**Equation 2.3**)

$$n\lambda = 2d \sin \theta \quad \text{Eq. (2.3)}$$

where n is an integer, the order of reflection; λ is wavelength of beam; d is the spacing between the planes; θ is the angle between either incident and reflected beams and

the plane. The Bragg equation is useful to determine the lattice d-spacing of crystals. Each peak in the diffractogram therefore results from the d-spacing in the crystal (Atkins and De Paula, 2011).

2.5 Fourier Transform Infrared – Attenuated Total Reflectance (FTIR-ATR)

Spectroscopy

(FTIR-ATR) Spectroscopy was used in this thesis for qualitative study the spectroscopic behaviour of the particles prepared. It is a surface sensitive technique and it is depending the interaction of electromagnetic radiation with sample within 4000 – 400 cm^{-1} region of the electromagnetic spectrum. This interaction excites the molecules making their covalent bonds vibrate by stretching or bending (deformation). Infrared spectra can be reported as the infrared intensity against the wavenumber of light (cm^{-1}). The advantages to use FTIR-ATR as follows:

- It uses the sample without any further preparation *e.g.* diluting it with an IR transparent salt such as potassium bromide.
- ATR is the very thin sampling path length and depth of penetration of the electromagnetic infrared beam into the sample.

The basic principle of operation in a typical FTIR-ATR technique is described according to **Figure 2.8**.

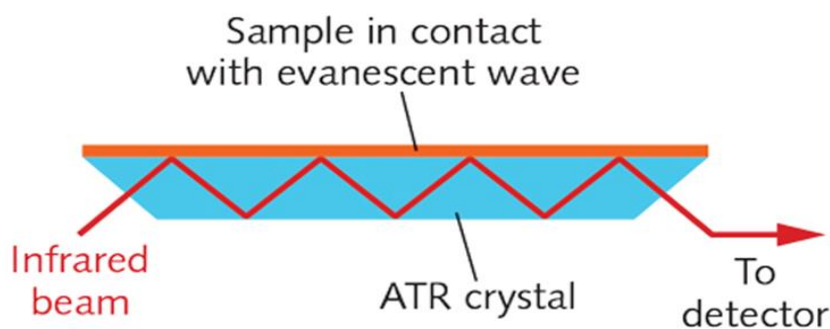


Figure 2.8: Schematic of infrared- Attenuated Total Reflection Spectroscopy (IR-ATR)
(Pavia et al., 2008).

The infrared light passes through a sample which is placed in close contact with a transmitting crystal *e.g.* diamond, zinc selenide (ZnSe) or germanium (Ge) which has a relatively high refractive index. Then this light reflects from the internal surface and penetrates the sample with each reflection along the top surface. This process eventually generates an evanescent wave which produces some energy that gets absorbed by the sample and reflected radiation that attenuates and goes into the detector and converts to infrared spectrum by the Fourier Transform. Different crystals have different refractive indices depending on the material used and are applied to different transmission ranges for example ZnSe for 20,000 - 650 cm^{-1} , Ge for 5,500 - 800 cm^{-1}).

2.6 Ultraviolet—Visible Spectrometry (UV-Vis)

The interaction of radiation with matter is the subject of the science called spectroscopy. Ultraviolet and visible spectrometers have become the most important tool in analytical chemistry. This technique can give both qualitative and quantitative

analysis in many fields such as in chemistry, biology, forensic science, engineering, agriculture, clinical chemistry, and many other fields. Different molecules absorb radiation of different wavelengths and the amount of light absorption can be measured as a function of wavelength. Furthermore, most organic molecules absorb ultraviolet or visible light that is the regions where wavelengths range from 190 nm to 700 nm. The absorbance of a solution increases as the beam increases. On the other hand, the absorbance of a solution increases, the transmittance decreases. The relationship between transmittance and absorbance is shown **Figure 2.9** (Pavia et al., 2008).

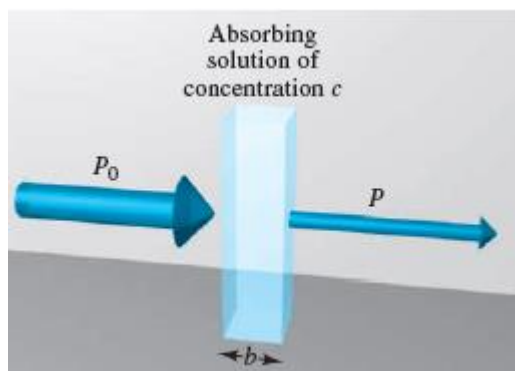


Figure 2.9: The larger arrow on the incident beam indicates a higher radiant power P_0 than that transmitted by the solution P . The path length of the absorbing solution is b and the concentration is c (Skoog et al., 2013).

In spectrometric technique, the sample solution absorbs electromagnetic radiation from a suitable source, and the amount absorbed is related to the concentration of the sample. UV-VIS spectrum is usually recorded as a plot of absorbance against wavelength (**Figure 2.10**) (Christian and O'Reilly, 1988).

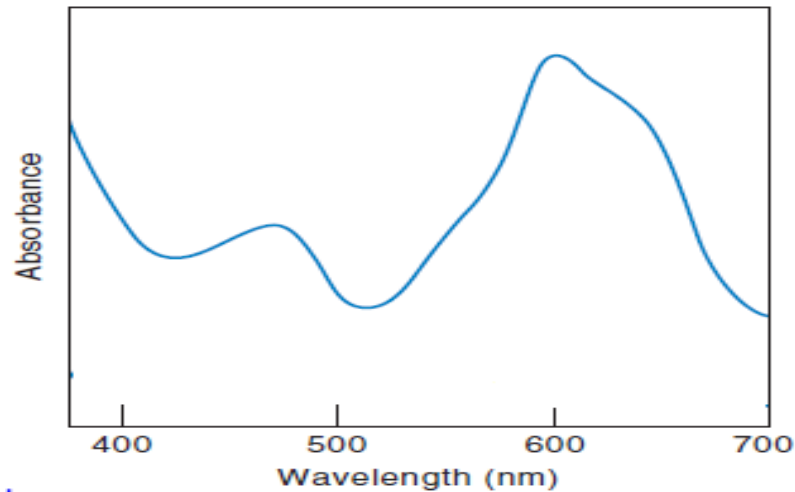


Figure 2.10: The visible absorption spectrum respond to wavelengths from about 390 to 700 nm. The visible spectrum is the part of electromagnetic spectrum which is visible to the human eye (Pavia et al., 2008).

2.7 Scanning electron microscopy (SEM)

Scanning Electron Microscopy (SEM) is indeed one of the most powerful and efficient characterization techniques that scientific inquiries can utilize. SEM utilizes a shorter wavelength high-energy electron beam instead of light photons, as is the case in optical microscopy. SEM has been identified as the most efficient and versatile tool in performing the analysis of chemical composition characterizations and surface morphology. Consequently, the SEM is crucial in looking at the surface topographic details due to its high resolution (Goldstein and Harvey, 1975). Therefore, thorough SEM, high levels of magnification allow the visualization of how the fingermarks, developmental techniques and deposition surfaces interact with each other and also with various external factors.

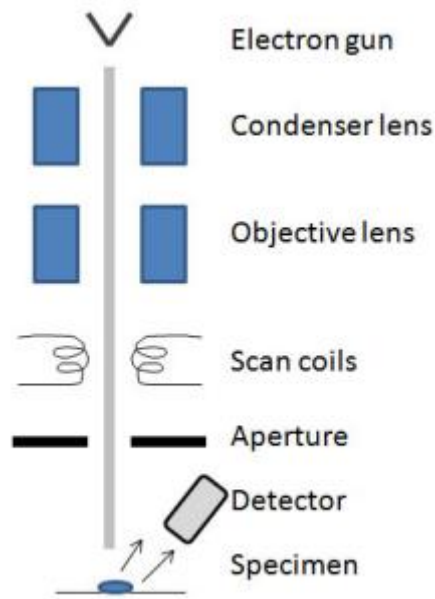


Figure 2.11: Shows SEM setup’s schematic representation as well as features within the two main areas: the specimen chamber and the electron column (Barron et al., 2012).

As indicated by **Figure 2.11**, the typical SEM setup schematic representation has two main areas namely the specimen chamber and the electron column (Barron et al., 2012). The electron gun source is instrumental in forming a stream of electrons that are accelerated, by use of a positive electrical potential, towards the specimen.

At the top of the electron column, the electron gun or electron beam source is located. In the modern Scanning Electron Microscopy, there are two main kinds of guns, described as field emission or thermionic guns (Leng, 2009). The thermionic gun is usually a twisted tungsten, which works through high temperature heating of the cathode filament to provide strong kinetic energy for the escape of electrons. In addition, a brighter beam results from the lanthanum hexaboride as compared to tungsten having the same accelerating power or voltage (kV) (Goldstein and Harvey,

1975). When the beam passes the anodic terminal, two condenser lenses (electromagnetic condenser lenses) forces the beams to converge and thus passing through a focal point. Depending on the changes on the column's magnetic fields, the lenses work by having some beams of electron selectively deflected, thus effectively creating focal points of varied lengths in each lens (this is digitally controlled in the modern SEM software in focusing the beam on the selected sample) (Goldstein and Harvey, 1975). In order to improve resolution, the beam is directed through the aperture, which functions to exclude electrons that are not part of the optical axis.

One the electron beam strikes the sample's surface; there are a number of signals that are emitted due to the interaction with the beam of the sample. In the case of two major imaging modes as well as a number of emissions' characteristics, the emissions include secondary electrons and the primary backscattered electrons (BSE) (Stokes, 2008). Often, the sample's atom nucleus can collide with the electron beam thus bouncing to yield a backscattered electron as indicated in **Figure 2.12**.

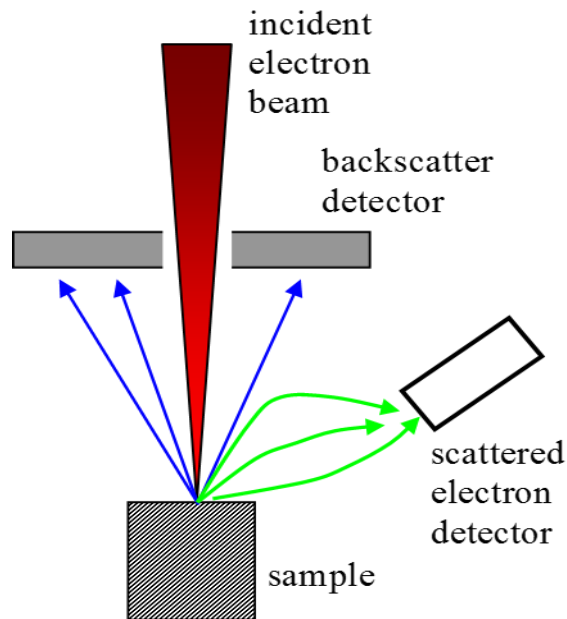


Figure 2.12: Schematic diagram of the positioning of the two SEM detectors.

The image is produced from the backscattered electrons. According to (Scrivener, 2004), the lighter atoms backscatter less electrons than the heavy ones and thus image formed is blurred. Therefore, the heavy atoms, due their ability to backscatter more electrons produces brighter images. In SEM, the image can also be produced through detection of secondary electron. As indicated in **Figure 2.12**, the atom in the sample can collide with the electron beam leading to one being knocked out as a secondary electron, which in turn may also collide with other atoms producing numerous secondary electrons. These secondary electrons are also utilized to produce images. The accelerating voltage utilized has been identified to affect the penetration of the electron beam into the sample and that penetration would be determined by the voltage used (the higher the voltage the higher the penetration). The E-T (Everhart-Thornley) scintillator detector is the most common SEM electron detector, because the electrons emitted from the sample are usually less than 50 eV). The E-T detector easily attracts the SEs due to their low energy. The positive charge on a grid in front

of the detector attracts the electrons and captures them prior to amplifying them through a photo-multiplier and then digitising and sending them to a screen. This gives a signal, which is then transferred to a viewing screen as a beam that is scanned to create an image (Leng, 2009). However, there may be a selective bias on the BSE collection by the E-T detector thus leading to a reduction of voltage's collector grid to a negative voltage (-50V) and thus limiting low energy.

2.8 Summary

This chapter highlighted the main techniques which are applied in this thesis including: Zetasizer, Mastersizer, rheology, viscometry, FTIR, UV-Vis and SEM. Zetasizer identifies zeta potential (surface charge) which is a very important factor in the characterization of chitosan particles. Moreover, zeta potential can provide information on the stability of chitosan particles in suspension. High zeta potential, which is greater than +30 mV or less than -30 mV, indicates high stability of chitosan particles. Measuring of chitosan surface charge can help to obtain an understanding as to how well the particles will interact with fingerprints. Additionally, this could also be used to help understand how well the nanoparticles would interact with the different membranes present in the body and give an indication as to how well these would perform in terms of drug delivery.

Another key parameter providing size are Mastersizer and Zetasizer. It is important to be able to evaluate particle size and polydispersity index (size distributions) as this enables the cell membrane interactions to be better understood and also how well the physiological drug barriers can be penetrated by the drug. As well as, this could potentially enable the fine tuning of chitosan particles size for forensic applications (visualisation of latent fingermarks) and to help understand suitable particle size to attach between ridges in fingermarks. Viscometry (rheology) can provide useful information about mechanical properties of a chitosan which in turn is important in physical characterisation. Evaluation of the relative viscosity is a vital parameter for the testing of polymers in solution. For example, if the viscosity is too low, the chitosan particles will not exhibit prolonged contact time with the mucosal epithelium as it will either be excreted with the clearance of the mucus, or the entire drug

complex will be absorbed. This is because the chitosan particles will flow straight in to the stomach contents rather than interact with the mucin on the stomach walls. An XRD study is a valuable in investigating the crystallinity of chitosan in the cross-linked with TPP and through chemical modification in the arrangement of molecules in the crystal lattice. The FT-IR of chitosan is characteristic of chitosan structure due to determine the molecular changes in the resulted cross-linked chitosan particles. Studies of surface morphology of particles is important using SEM, due to the surface characteristics being dependent on the process parameters such as CS: TPP ratio. Additionally, SEM is useful technique used on to study fingerprint development. Knowledge of viscosity, zeta potential, particle size and shape has an influence on potential applications of CS: TPP particles in drug delivery (Wang et al., 2011) or in forensic applications (Il Dueik and Morris, 2013) and can therefore enable the investigations of the aims outlined in Section 1.7.

Chapter 3

Factors Affecting the Physico- Chemical Properties of Chitosan- Triphosphate Microparticles Formed by Ionotropic Gelation

3 Factors Affecting the Physico-Chemical Properties of Chitosan-Tripolyphosphate Microparticles Formed by Iontropic Gelation

3.1 Introduction

Cross-linking of chitosan is based on the addition of a cross-linker, for example chitosan can be physically cross-linked with polyanions such as TPP. There are numerous of experimental parameters which can be controlled in the preparation of chitosan particles including: type of chitosan (molecular weight, DD and concentration), chitosan to TPP (CS: TPP) ratio, pH, ionic strength, temperature and stirring rate. These will all have an influence on for example, the particle size, particle surface charge, particle shape, relative surface area, colloidal stability, *etc* (Hu et al., 2008, Wang et al., 2011). It is therefore the purpose of the present study to investigate the systematic manipulation of three independent processing parameters (pH, ionic strength and CS: TPP ratio) on three important physicochemical properties (relative viscosity, zeta potential and particle size) during the preparation of CS: TPP microparticles loaded with dye (for visualisation purposes) by the ionotropic gelation method. This will then enable the use of mathematical models obtained to predict the relative viscosity, zeta potential (net surface charge) and particle size under different conditions to obtain predicable and programmable microparticle properties in relation to, for example, latent fingerprint enhancement, drug release kinetics or mucoadhesion.

3.2 Design of experiments (Factorial Design)

In statistics, design of experiments (DOE) is a powerful tool for improving and controlling experiments which all levels of one independent variable (I.V), which are

also sometimes called factors, are combined with all levels of another (Altekar et al., 2007). In a full factorial experiment, the response dependent variables (Y) are measured at all combinations of the independent factor levels. The combinations of independent factor levels represent the conditions at which responses dependent variable (Y) will be measured. A dependent variable is a variable with a value which depend on that of the independent variable. Whereas, independent variable is variable which value do not depend on the value of another variable. Factorial design is used to statistically optimise the formulation parameters. Moreover, factorial design allows the investigator to perform many experiments involving the simultaneous study of the effects of two or several factors on the response dependent variable (Y), also the effects of interactions between factors on the response dependent variable (Y). In other words, design of experiment for predicting response by varying the different factors at a specific level, factorial designs are most efficient for this type of experiment (Shah and Londhe, 2011). Use of experimental design allows for testing a large number of factors simultaneously and precludes the use of a huge number of independent runs. Procedures are then carried out through the selection of an objective function and finding the most important or contributing factors. In the present study, Minitab[®] 17.1.0 software 2³ factorial design was carried out to find optimised conditions for response (Y), and eight experimental runs were constructed. A run is each experimental condition. Linear regression model equations were employed for fitting the response surface in the following form:

$$Y = A_0 + A_1 X_1 + A_2 X_2 + A_3 X_3 + A_4 X_1^2 + A_5 X_1X_2 + A_6 X_1X_3 + A_7 X_2^2 + A_8X_2X_3 + A_9X_3^2 + A_{10} X_1X_2X_3 \quad \text{Eq. (3.1)}$$

Where Y is the measured response with each factor level combination; A_0 is an intercept; A_1 to A_{10} are regression coefficient of the respective independent variable; and X_1 , X_2 and X_3 are the coded levels of independent variables. The terms $X_1 X_2 X_3$ and X_i^2 ($i = 1, 2$ or 3) represent the interaction and quadratic terms, respectively.

3.3 Materials

Chitosan of medium molecular weight (MMW $\sim 295,000$ g/mol) was obtained from Sigma–Aldrich (Gillingham, UK) and reported to have an average degree of deacetylation (DD) of ~ 75 – 85% . In addition, chitosan of low molecular weight (LMW $\sim 50,000$ – $190,000$ g/mol) was purchased from Sigma–Aldrich (Gillingham, UK) and was reported to have an average degree of deacetylation of ~ 75 – 85% . Glacial acetic acid, sodium acetate trihydrate and tripolyphosphate (TPP) sodium salt were obtained from Sigma–Aldrich (Gillingham, UK) and red food colouring was from Silver Spoon (Peterborough, UK). All materials were used without any further purification.

3.4 Experimental

3.4.1 Sample preparation

Nine different acetate buffers (AB) coded AB-1, AB-2, AB-3, AB-4, AB-5, AB-6, AB-7, AB-8, and AB-9 were prepared (**Table 3.1**, further details on their preparation are in Appendix A) in order to investigate the effect of three independent variables: pH value, ionic strength and volumetric ratio of chitosan to TPP on the physicochemical properties of CS: TPP microparticles. According to literature chitosan is soluble in acidic solution ($\text{pH} < 6.0$), so the pH (3.3 – 5.3) were chosen to cover a good range of pHs (Dyer et al., 2002).

Table 3.1: Acetate buffers of varying ionic strength and pH. Buffers AB-1 to AB-9 were used to create generate model equations and buffers AB-10 to AB-13 were used in model validation (pKa of acetic acid is 4.75).

Acetate buffer (AB)	pH	Ionic strength (IS)
AB-1	3.3	0.1 M
AB-2	3.3	0.3 M
AB-3	3.3	0.5 M
AB-4	4.3	0.1 M
AB-5	4.3	0.3 M
AB-6	4.3	0.5 M
AB-7	5.3	0.1 M
AB-8	5.3	0.3 M
AB-9	5.3	0.5 M
AB-10	3.8	0.2 M
AB-11	3.8	0.4 M
AB-12	4.8	0.2 M
AB-13	4.8	0.4 M

3.4.1.1 Preparation of chitosan and TPP samples with different ionic strengths and pH value (Acetate buffers AB-1 to AB-9)

2.0 mg/mL of nine different chitosan medium molecular weight solutions were dissolving in acetate buffers (AB-1 to AB-9). The chitosan solutions were stirred overnight at room temperature using a magnetic stirrer. The solutions were then filtered using Gooch crucible (AG 1 X 3) vacuum filtration to remove residues of insoluble chitosan molecules and the solutions were collected for further analysis. 0.84 mg/mL of nine different TPP solutions were dissolved in the acetate buffers

(AB-1 to AB-9). A previous study observed that the optimal concentrations of chitosan and TPP solutions were 2 mg/ml and 0.84 mg/ml respectively to form chitosan particles (Dyer et al., 2002). In addition, another recent research used chitosan and TPP solutions at concentrations of 2 mg/ml and 0.84 mg/ml respectively, and obtained chitosan microparticles which were successfully applied in fingerprint enhancement (Il Dueik and Morris, 2013), although in a very small-scale preliminary experiment. Therefore, these concentrations were subsequently used for the preparation of particles.

3.4.1.2 Preparation of CS: TPP microparticles

Chitosan microparticles were prepared according to ionotropic gelation procedure (**Figure 3.1**) (Morris et al., 2011, Dyer et al., 2002). To prepare the CS: TPP microparticles, an appropriate volume of the TPP solution was added drop wise to the appropriate volume of the chitosan solution to make seven ratios of CS: TPP microparticles (6:1, 4:1, 2:1, 1:1, 1:2, 1:2, 1:4 and 1:6), and the samples were then stirred at 600 rpm for 60 min at room temperature. The resultant microparticles spontaneously formed due to the ionic crosslinking of chitosan by sodium tripolyphosphate. Then 30 drops (~2 mL) of red dye added to all ratios to make the particles clearly visible and more amenable in latent fingerprint visualisation. The resultant microparticle solutions were left standing overnight at room temperature, prior to centrifugation (Thermo Fisher Scientific Biofuge Primo R, Germany) for 90 minutes at 8500 rpm, the supernatant was discarded, and the microparticles were rinsed with deionized water for further analysis.

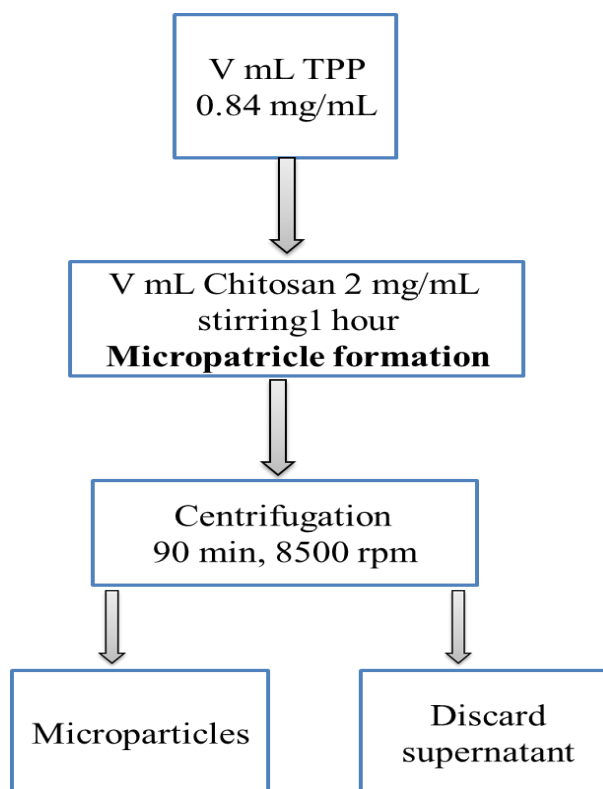


Figure 3.1: Procedure of chitosan microparticle formation, where V represents the appropriate volumes of TPP and chitosan respectively.

3.4.1.3 Model validation (prediction method)

Chitosan medium molecular weight solutions were prepared by dissolving 2 mg/mL of polymer in a further four different acetate buffers (AB-10, AB-11, AB-12 and AB-13) (**Table 3.1**) and TPP solutions were prepared by dissolving TPP at a concentration of 0.84 mg/mL in the same acetate buffers (AB-10, AB-11, AB-12 and AB-13). The resultant solutions were prepared as per Section 3.4.1.2 to give CS: TPP volume ratios (v/v) of 6:1, 4:1, 2:1, 1:1, 1:2, 1:4 and 1:6 respectively.

3.4.2 Characterisation of chitosan microparticles

3.4.2.1 Fourier transform infrared (FTIR)

Spectroscopy FTIR spectra of chitosan, TPP and chitosan microparticles were recorded using a Fourier transform infrared spectrophotometer (Thermo Nicolet 380 FT-IR spectrometer, Thermo Electron Corporation). FTIR depends on the interaction of electromagnetic radiation with sample and it is a surface sensitive technique. The ATR (Attenuated total reflectance) crystal was cleaned with Isopropyl alcohol. A background check was performed before to obtain samples spectra. A powdered small amount of samples were placed on the crystal using micro spatula and force applied by twisting top of the arm of sample stage. The test sample spectra was collected from 4000 to 500 cm^{-1} . Each sample was run in triplicate.

3.4.2.2 Powder X-ray diffraction (p-XRD)

A crystallinity study was carried out by comparing XRD spectrum of microparticles using Bruker AXS diffractometer (D2 PHASER) with Cu $K\alpha$ radiation to characterise chitosan, TPP and CS: TPP microparticles. Powdered sample (chitosan, TPP and CS: TPP microparticles) was placed in a stainless steel holder then the surface of powder was levelled manually to make appropriate a flat surface for analysis. The sample was exposed to X-ray Cu $K\alpha$ radiation with a wavelength of 1.5406 Å. An electron beam is directed across a field of high voltage in a vacuum which is sealed and it hits a solid anode target that is either rotating or stationary, thus X-rays are emitted. Collisions with atoms in the target causes the electrons to decelerate hence X-ray streams are continuously generated. Some elements such as Cr, Co, and Cu are the most common X-ray tube targets that are used and they emit 14 keV X-rays that have a wavelength

of 0.8 Å, and 8 keV X-rays that have a wavelength of 1.54 Å. Peaks in a pattern of an X-ray diffraction are related directly to atomic distances. The data was recorded at 2θ range of 5°–80° at a scanning rate of 4°/min. Each sample was run in triplicate.

3.4.2.3 Determination of relative viscosities

All samples were analysed using a Bohlin Gemini HR Nano Rheometer (Malvern Instruments, Worcestershire, UK). Rheological measurements give information about the viscoelastic properties of a sample. 5 mL of sample (acetate buffer, chitosan solution and CS: TPP particles in suspension) was placed into 55 mm parallel plate geometry using 1mm gap at a constant shear rate of 500 s⁻¹ under precise temperature control (25.0 ± 0.1°C). All measurements were performed in triplicate.

$$\eta_{rel} = \left(\frac{\eta}{\eta_0} \right) \quad \text{Eq. (3.2)}$$

where η is the average ($n = 3$) viscosity of chitosan, the CS: TPP microparticles and, η_0 is the viscosity for the appropriate acetate buffer (Harding, 1997).

3.4.2.4 Determination of zeta potential

Zeta potential was measured for chitosan, TPP and CS: TPP microparticles of different ratios using a Malvern Zetasizer NANO-Z (Malvern Instruments Limited, Malvern, UK). All Measurements were performed in the appropriate buffers using a folded capillary cell and refractive index of the CS: TPP microparticles was set at 1.6–1.8 (Azofeifa et al., 2012) and no significant effect of refractive index was

identified. To determine the zeta potential approximately 1.0 mL of sample was pipetted into a folded capillary cell by using a syringe and measurements were performed at 25 ± 0.1 °C in triplicate to obtain data value an average of ten measurements. Doppler electrophoresis is the phenomenon of taking place during zeta potential measurements. The laser is divided to give a reference and an incident beam. The latter (incident beam) goes through the sample cell centre, then the forward angle is used to spot and observe scattered light. Immediately the measurement of zeta potential commences, the reference beam's intensity is taken. This technique takes into account the speed with which particles can move in liquids after an application of electric field (its velocity). As soon as the applied electrical field and the particle's velocity are known in advance and by use of sample constants; dielectric and viscosity constant, zeta potential now becomes determinable.

3.4.2.5 Determination of particle size

The particle size distributions of the resultant chitosan particles were measured directly by a dynamic light scattering (DLS) using a Malvern Mastersizer 2000 (Malvern Instruments Ltd., Malvern, UK). The microparticles were dispersed in deionized water. Refractive index of particles and dispersion medium (water) was set to 1.8 and 1.330, respectively. Before the analysis was started, apparatus was left to warm-up for not less than one hour after it was turned on. Alignment of the optics was performed after addition of dispersant to the cell sample and subsequently the background measurements were observed and recorded. Particle samples were added to reach an obscuration ranging from 10 to 30%. This process was repeated prior to all sample measurements. The analysis was performed with a constant stirring rate of 1500 rpm. The apparatus was rinsed well between each experiment to get rid of any

contamination. The average particle size was described using the volume-weighted mean diameter $D_{[4,3]}$. The intensity of scattered light was transformed into the diffusion factor, the mean value of ten measurements of the particle size was obtained and each formulation and was repeated three times.

3.4.2.6 Scanning electron microscopy (SEM)

The surface microparticle morphology was characterised using scanning electron microscopy (SEM). The samples of chitosan particle powders were mounted on aluminium stubs using double sided carbon adhesive tape attached to stub. Then the samples were vacuum dried, coated with gold-palladium and observed microscopically (JEOL JSM 6060 LV – Oxford instruments, Abingdon, UK). Scanning electron microscope refers to the surface of the sample examination using a beam of electrons of high energy. Backscattered electrons are produced as a result of interaction between the atoms and the electrons and they carry information about the topography of the surface of the sample. Images were taken by applying an electron beam accelerating voltage of 10 kV. This accelerating voltage was chosen to improve surface sensitivity and obtain high quality images (Bacon et al., 2013). Images were also analysed using Image J software (version 1.42q, National Institute of Health, Bethesda, USA) to estimate the particle surface areas.

3.4.3 Effect of cross-linker TPP concentration and chitosan molecular weight using acetic acid at different conditions to formulate CS: TPP nanoparticles

Chitosan low and medium molecular weight and varying concentrations of TPP solutions were made up as shown below in **Table 3.2**. Chitosan of a suitable weight (LMW and MMW) were then dissolved in dilute acetic acid (0.3 %) and this were left stirring overnight at room temperature on a magnetic hot plate at 800 rpm. The following day this solution was then filtered under vacuum filtration and pH was adjusted to 5.3 using dilute sodium hydroxide (0.1 N). However, the pH of TPP solution was controlled by adding dilute hydrochloric acid (0.1 N) until a final pH of 5.3 was obtained to make sure that $\text{H}_2\text{P}_3\text{O}_{10}^{3-}$ ions exist in solution, this is also beneficial in producing less polydisperse nanoparticles. TPP when dissolved in water numerous anions could be present in solution depending on the pH, which is undesirable as they can competitively react with the protonated ammonium groups of chitosan solution (pH 5.3), the hydroxide ion will also effect of pH of solution. Thus, the pH of TPP was adjusted to 5.3 (Sullivan et al., 2018).

Table 3.2: Summaries the different concentrations required to make CS: TPP particles

Chitosan (mg/mL)	TPP (mg/mL)
3	0.84
3	1.0
3	1.25

A water bath was created using a beaker on a hot plate and the temperature was regulated. An appropriate volume of TPP was added to a sample vial and this was

placed in the water bath for half an hour to allow the temperature to equilibrate at 30 °C. A magnetic stirrer was included and the required volume of chitosan was added to ratio of CS: TPP at (5:1) particles. This ratio was chosen as it gives the smallest particle size and highest zeta potential. Thermometers were also placed in the samples to ensure the correct temperature was reached. This was checked periodically and adjusted if required. The magnetic hot plates were then adjusted to the correct speed at 750 rpm and samples were left stirring for an hour. The resultant (CS: TPP) particles spontaneously formed due to the ionic crosslinking of chitosan by TPP. All samples were sonicated for 5 min (the cycle and amplitude was adjusted to 0.5 and 80 % respectively; Hielscher Ultrasonics GmbH, Teltow, Germany) before being subjected to further analysis.

Measurement of the mean particle diameter, polydispersity and zeta potential of CS-TPP nanoparticles in the suspension were performed using Malvern Zetasizer NANO-Z (Malvern Instruments Limited, Malvern, UK) on the basis of DLS techniques. The dispersion medium (water) and refractive index of particles was set at 1.330 and 1.6 respectively. To determine particle size a glass cuvette was used and an angle scattering of 173° was utilized. Approximately 1.0 mL of sample was pipetted into the cuvette and three readings were taken. The laser is used to provide a light source to illuminate the sample particles. Some of the laser beam scattered by the particles within the sample then the detector measures the intensity of the scattered light. An average of these readings was then recorded. Zeta potential of samples was measured using the same instrument used to determine particle size. Measurements were performed using a folded capillary zeta cell. Approximately 1.0 mL of sample was pipetted into a folded capillary cell by using a syringe and measurements were

performed at 25 ± 0.1 °C in the same method as described earlier. The data value of an average of three measurements of the zeta potential were obtained.

3.5 Results and discussion

3.5.1 FTIR analysis

The FTIR spectrum of pure TPP (**Figure 3.2a**) showed characteristic bands at 1217 cm^{-1} which indicates P=O stretching (Dudhani and Kosaraju, 2010), 1138 cm^{-1} which indicates symmetrical and asymmetric stretching vibration of the PO_2 groups (Gierszewska-Drużyńska and Ostrowska-Czubenko, 2010), 1094 cm^{-1} which indicates symmetric and asymmetric stretching vibration of the PO_3 groups and 892 cm^{-1} (P-O-P) asymmetric stretching (Martins et al., 2012). As can be seen in **Figure 3.2b** the spectrum of CS shows characteristic absorption bands at 3424 cm^{-1} indicates the combined broad non-symmetric band of the N-H and O-H group stretching vibration of functional groups involved in hydrogen bonds, and the peak at 2873 cm^{-1} indicates the -C-H stretching vibration (Ali et al., 2011, Dudhani and Kosaraju, 2010, Pierog et al., 2009). The peak at 1650 cm^{-1} indicates C=O stretching in amide I vibration group (CONH_2), and 1560 cm^{-1} which indicates N-H deformation in amide II group vibration (NH_2) (Wang and Liu, 2014, Gierszewska-Drużyńska and Ostrowska-Czubenko, 2010). Peaks at 1377 cm^{-1} and 1322 cm^{-1} might be attributed to O-H deformation of $\text{-CH}_2\text{-OH}$ and -CH-OH , and absorption bands at 1151 cm^{-1} indicates asymmetric bridge oxygen (C-O-C) stretching (Wang and Liu, 2014).

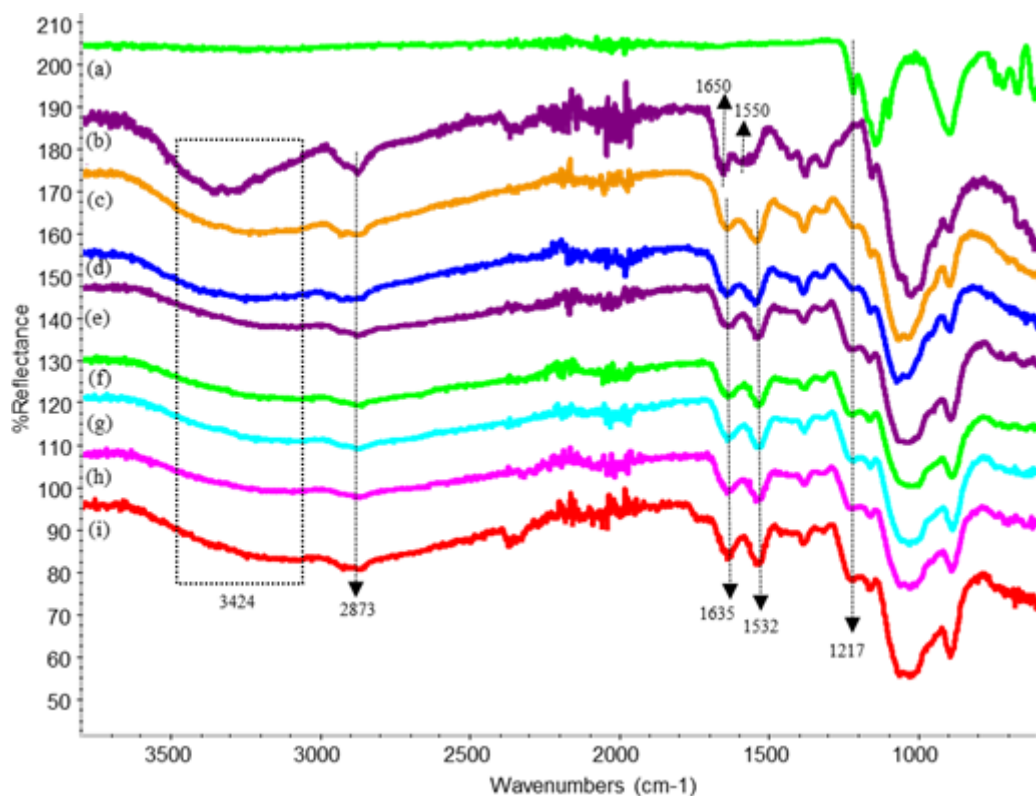


Figure 3.2: FTIR spectrum of (a) TPP, (b) CS, (c) CS: TPP (6:1), (d) CS: TPP (4:1), (e) CS: TPP (2:1), (f) CS: TPP (1:1), (g) CS: TPP (1:2), (h) CS: TPP (1:4), (i) CS: TPP (1:6) in buffer AB-1.

The CS: TPP particles were characterized through FTIR spectroscopy, and the spectra are presented in Figures 3.2c – 3.2i. Crosslinking process in the spectra of all CS:TPP ratios samples the band of 3424 cm^{-1} becomes wider, this indicates that hydrogen bonding is enhanced (Wu et al., 2005). In addition, in microparticles the band of 1650 cm^{-1} disappears and there appears a new band at 1635 cm^{-1} . This band can be assigned to anti-symmetric deformation N-H bond vibrations in NH_3^+ ion. The 1560 cm^{-1} peak in pure chitosan shifts to a new sharp peak at 1532 cm^{-1} (Wu et al., 2005). These two new peaks as mentioned above (1635 cm^{-1} and 1535 cm^{-1}) show that a linkage has been formed between the ammonium ions and phosphate ions (Bhumkar

and Pokharkar, 2006). In other words, the new $\text{NH}_3^+ - \text{PO}^-$ bond is formed due to one hydrogen atom of the amino group in chitosan is substituted by the phosphate group. It further proves that the amino group is the only reactive functional group chitosan. Moreover, the characteristic peaks of the hydroxyl groups at 1377 cm^{-1} and 1322 cm^{-1} mentioned above do not change (Wang and Liu, 2014). The cross-linked microparticles also show a new peak at 1217 cm^{-1} which may be attributed to the $\text{P}=\text{O}$ stretching from TPP (Qi and Xu, 2004). Therefore, clearly indicating that the protonated amino groups of chitosan are linked with negatively charged tripolyphosphate groups of TPP, clearly demonstrating the formation of CS: TPP particles.

3.5.2 Crystallographic characterisation

Crystallographic structures of chitosan powder and chitosan microparticles were determined by X-Ray Diffraction (XRD). The XRD spectra of the chitosan microparticles were characteristic of amorphous structures. As can be seen in **Figure 3.3** there are two strong characteristic peaks in the diffractogram of chitosan powder at $2\theta = 10^\circ$ (amine I “ $-\text{N}-\text{CO}-\text{CH}_3$ ” of chitosan) and $2\theta = 20^\circ$ (amine II “ $-\text{NH}_2$ ” of chitosan), indicating the high degree of crystallinity of chitosan chains (Liu et al., 2012, Moharram et al., 2012). The peak at 10° is due to the integration of water molecules into the hydrated chitosan crystal structure and the latter peak at 20° is assigned to the crystal lattice of the chitosan orthorhombic unit cell (110) (Matet et al., 2013), moreover there is no indication of impurities in the chitosan formulation (Lad et al., 2013). It is known that the width of X-ray diffraction peak is related to the size of crystallite and an increase in the amorphous nature of the material (Rhim et al., 2006). Imperfect crystals usually lead to a broadened peak (Jingou et al., 2011). After

ionic cross-linking with TPP, a shift of peak positions, significant reduction in the intensity of characteristic peaks of chitosan (at $2\theta = 20^\circ$), and broadness of peaks were observed, reflecting the destruction of the native chitosan packing structure, which is in agreement with the results reported by (Wan et al., 2003, Shah et al., 2009). **Figure 3.3** also highlights similarity between the CS: TPP ratios 2:1, 1:1, 1:2, 1:4 and 1:6. Consequently the broad peak of the chitosan microparticles may have been caused by ionic cross-linking interaction between amino groups on chitosan and the TPP, which is known to destroy the crystalline structure of chitosan (Shah et al., 2009).

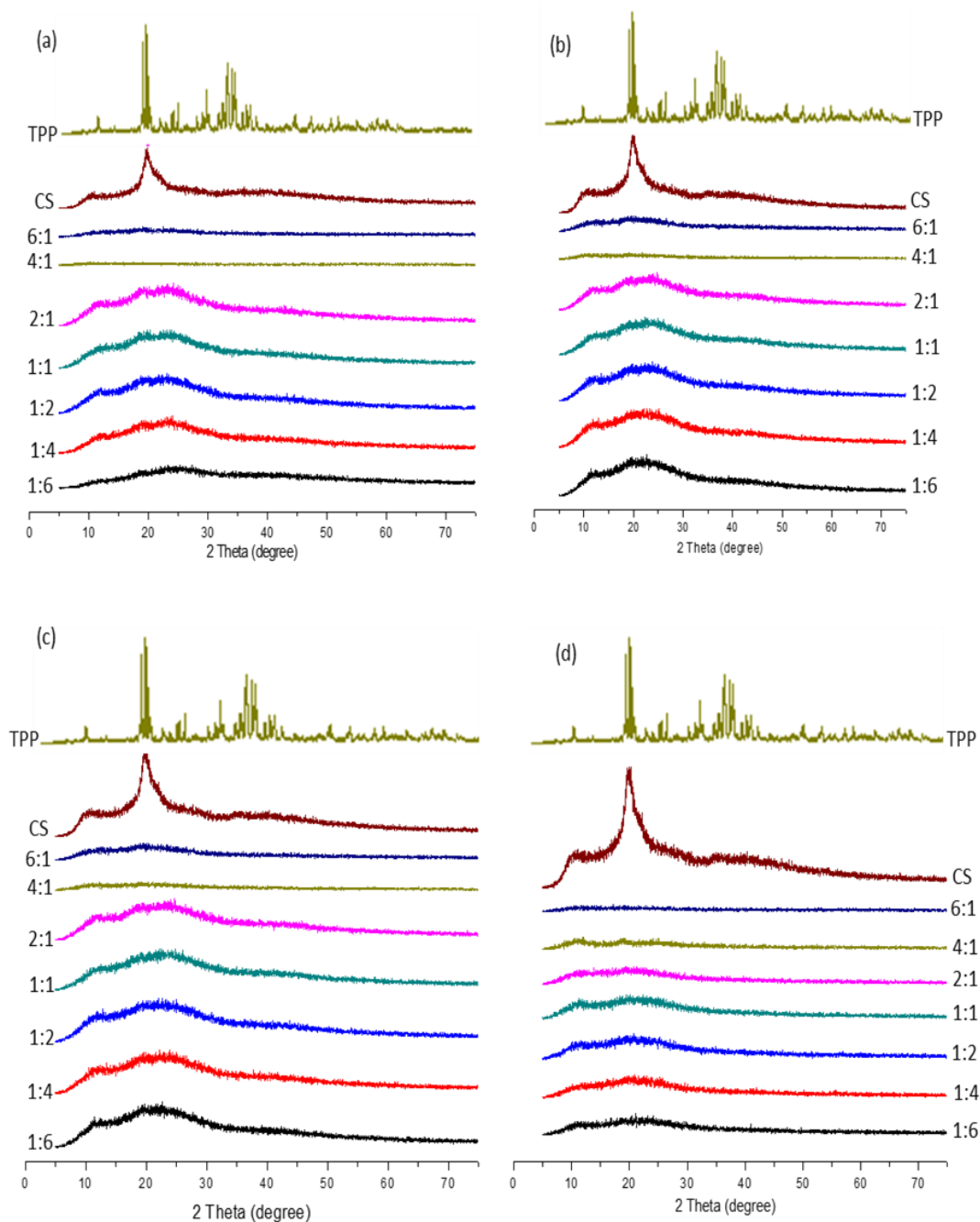


Figure 3.3: X-ray diffraction pattern of TPP, chitosan and of CS: TPP microparticles of seven different ratios in buffer (a) AB-10 (b) AB-11 (c) AB-12 and (d) AB-13.

Integration of the two crystalline peaks ($2\theta = 10^\circ$ and 20°) as a proportion of the total integrated area gives an approximate estimate of the degree of crystallinity in each of the samples. Based on this calculation the degree of crystallinity was calculated from the areas under the two peaks at $2\theta = 10^\circ$ and 20° relative to the total area using the

in-built area under the curve (AUC) function in Origin version 6.1 (OriginLab, Northampton, USA). Therefore, the degree of crystallinity of the native chitosan was ~30 % and the degrees of crystallinity of the TPP-chitosan microparticles are all ~10 %, this is almost entirely due to the decrease in the chitosan orthorhombic unit cell reflection (110) at ~20°. Other than for 6:1 and 4:1 the reflection (020) at ~10° remains unchanged during ionotropic gelation with TPP. Changes in chitosan crystallinity is important in terms of polymer degradation, tensile strength, moisture content, cell responses in *in vivo* applications and contact angles, which are important during hydration. All of these are factors are important to consider when developing novel chitosan-based formulations for forensic or pharmaceutical applications. The cross-linked chitosan with lower concentrations of TPP show less intense and broader crystalline peaks (6:1 and 4:1) which may be due to a greater amorphisation as compared with those of less 2:1, 1:1, 1:2, 1:4 and 1:6 (Moharram et al., 2012, Hosseini et al., 2013). The distinct differences in the diffractogram of chitosan and cross-linked chitosan might be attributed to chemical modification in the arrangement of molecules in the crystal lattice (Bhumkar and Pokharkar, 2006) and this is also in agreement with FT-IR as to the absence of native chitosan. In addition, in chitosan cross-linked with TPP at AB-13 (**Figure 3.3 d**) more suppressed peaks at 10 degree (2θ) and 20 degree (2θ) were observed, which might be due to more amorphization.

3.5.3 Relative viscosity and zeta potential for varying chitosan solutions

Chitosan when in solution is a polycation which is influenced by the presence of electrolytes (Smidsrød and Haug, 1971). Therefore, the effect of ionic strength and pH value on nine different solutions of chitosan was studied. It can be seen from **Figure 3.4** that the relative viscosity of nine chitosan solutions, with fixed pH

including AB-1, AB-2 and AB-3; AB-4, AB-5 and AB-6; AB-7, AB-8 and AB-9 decreased with increasing ionic strength solution.

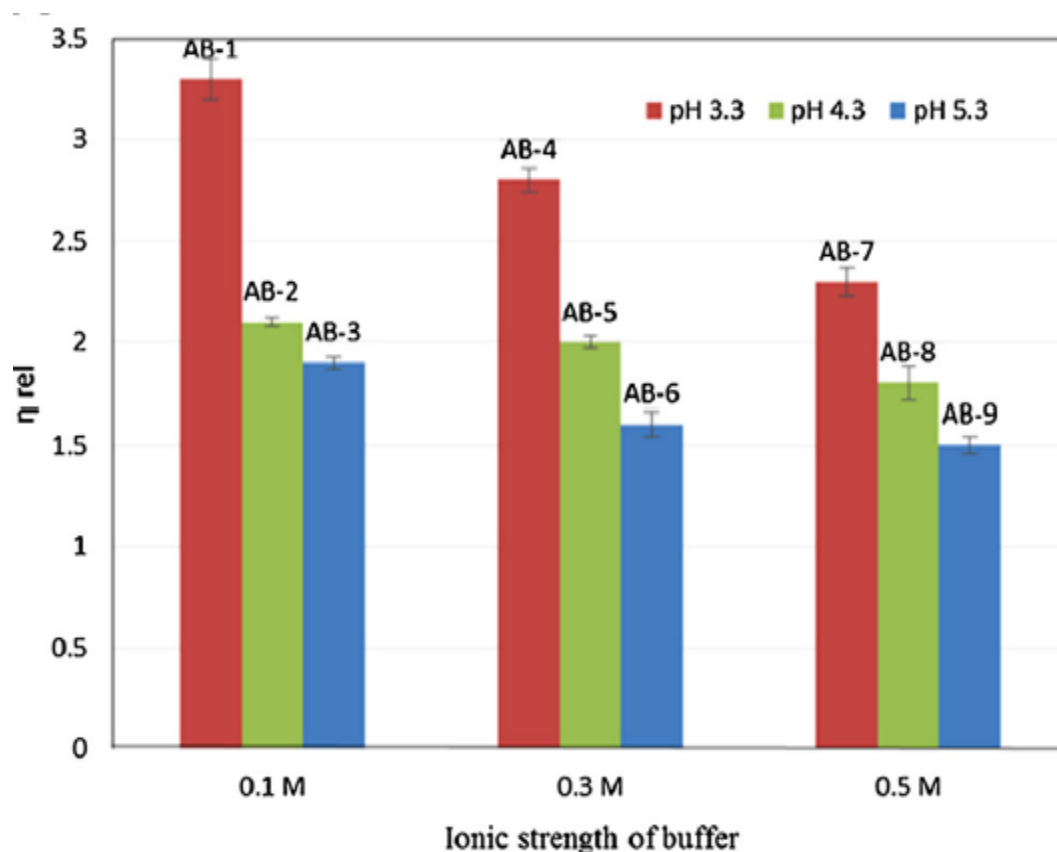


Figure 3.4: Relative viscosities of nine different chitosan solutions (using AB-1 to AB-9) at varying ionic strength and pH values at 25.0 ± 0.1 °C. (Mean \pm SD, n = 10).

The chain flexibility of chitosan molecules in solution can be manipulated by using chitosan with differing solution pH and/or ionic strength. Furthermore, it is known that in acidic media the amino groups of chitosan, NH_2 , are protonated to NH_3^+ groups. This causes electrostatic repulsion between chitosan molecules; meanwhile, there also exists inter-chain hydrogen bonding interactions between chitosan

molecules. The hydrogen bonding occurs between the amino and hydroxyl groups (Fan et al., 2012, Huang et al., 2009).

In low ionic strength solutions (0.1 M), the intramolecular electrostatic repulsion effect, also called the third electroviscous effect, dominates in which the chitosan molecule exists in an extended conformation (Fan et al., 2012, Abodinar et al., 2014). Therefore, more inter-molecular hydrogen bonding occurs in low ionic strength solution (**Figure 3.5**) (Qun and Ajun, 2006). This causes a high resistance to the flow or mobility of the polymer molecules and consequently a high relative viscosity is observed.

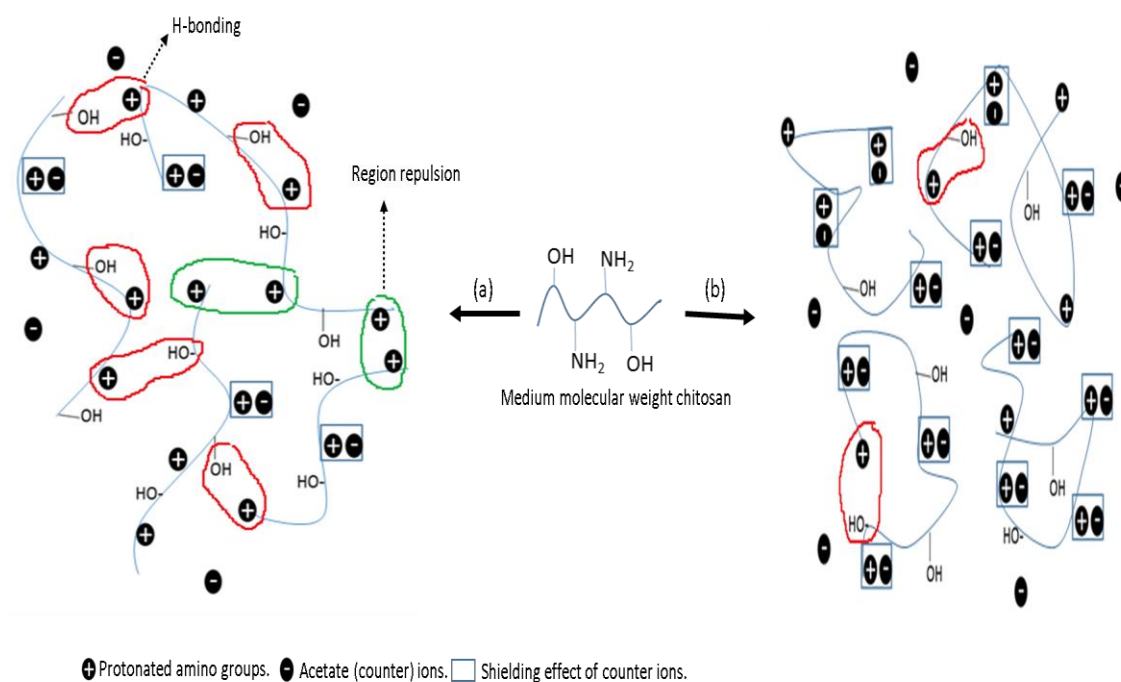


Figure 3.5: Schematic representation of chitosan in (a) low ionic strength and (b) high ionic strength solution (Fan et al., 2012).

However, in high ionic strength solutions (0.5 M), the concentration of acetate ions (CH_3COO^-) is raised which neutralises more NH_3^+ groups. This leads to less

dissolution of chitosan and weaker intermolecular electrostatic repulsion, causing the chitosan polymer chains to become more contracted and lowers the resistance to the flow or mobility of the polymers, resulting in a lower relative viscosity (Hu et al., 2008, Jonassen et al., 2012). In addition, the relative viscosity of chitosan also decreased with increasing pH in solutions with fixed ionic strength. The number of positive charges on CS at I.S 0.1 M will be greater at pH 3.3 of the solvent, leading to a higher degree of expansion of chitosan and a rigid conformation due to electrostatic repulsions (Kasaai et al., 2000). Information on chain expansion of chitosan used in the formulation of microparticles enables the possibility to better control microparticle properties by selecting suitable preparation conditions or starting polymer (Bellich et al., 2016). Because of this, the chitosan molecules disrupt the streamlining of the flow and increases viscosity, which will have an influence on the particle size and particle shape of any chitosan microparticles formed under these conditions (Kawadkar and Chauhan, 2012).

Zeta potential measurement is important to gain knowledge on the surface charge. This charge can affect the interaction between chitosan polymer chains in phenomena such as swelling characterisation, in the interaction with TPP during gelation (Gan et al., 2005) or during the interaction with oily subcutaneous residues (Yamashita and French, 2011). The ionic strength and pH value of the chitosan solution affect this interaction. The effect of pH value and ionic strength of the chitosan solution on zeta potential may be seen:

(i) At variable pH value and fixed ionic strength

It can be seen from **Figure 3.6** that the zeta potential decreases as the pH value increases from 3.3 to 5.3. At pH 3.3, the primary amine groups NH_2 of chitosan are more strongly protonated as NH_3^+ in acetate buffer solution and therefore increased zeta potential. On the other hand, at an increased pH value of 5.3 the NH_3^+ on the chitosan molecules were more neutralised resulting in a decreased zeta potential.

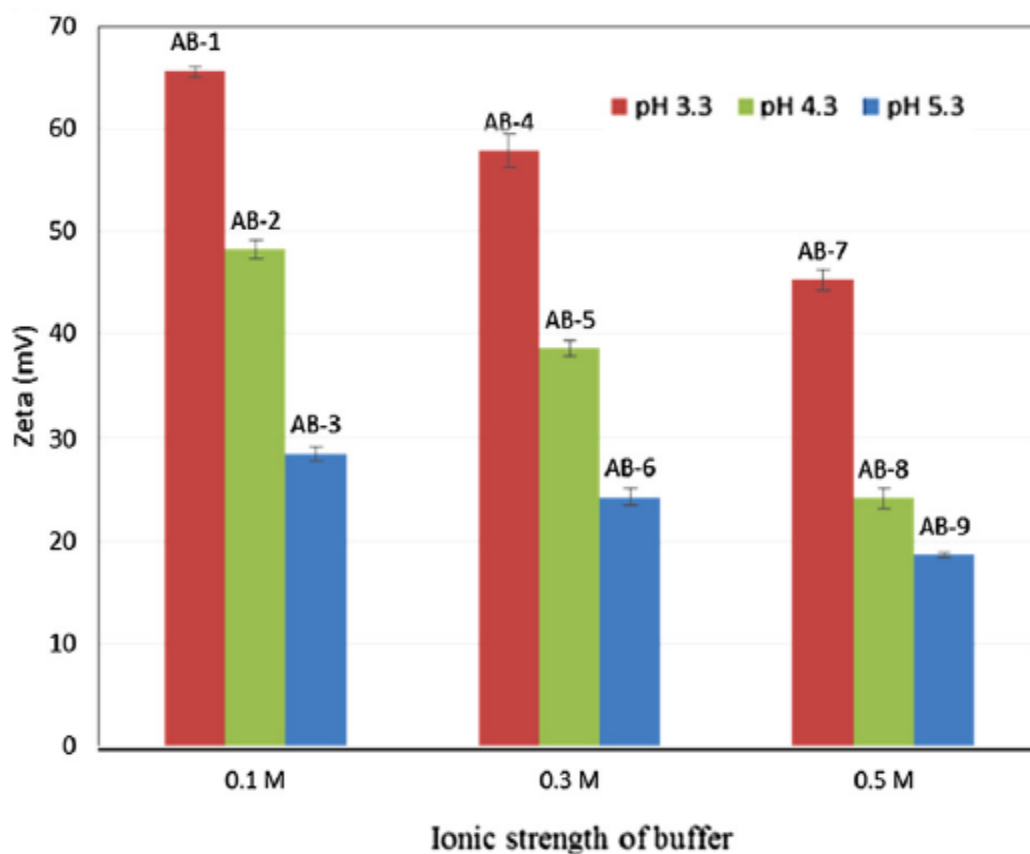


Figure 3.6: Zeta potentials of nine different chitosan solutions (using AB-1 to AB-9) at varying ionic strength and pH values at 25.0 ± 0.1 °C (mean \pm SD, n = 10).

(ii) At the fixed pH value and variable ionic strength (0.1, 0.3 and 0.5 M)

It can be seen from **Figure 3.6** that the zeta potential decreased with an increase in the ionic strength from 0.1 M to 0.5 M. At ionic strength 0.1 M, the primary amine groups NH_2 of chitosan are protonated as $-\text{NH}_3^+$ in acetate buffer solution and therefore an increased zeta potential is seen. Conversely, with an increased ionic strength at 0.5 M, the NH_3^+ on the chitosan molecules were more neutralised by acetate ions (CH_3COO^-) leading to a decreased zeta potential. This is important in terms of the conformation of chitosan chains and how that might influence their interactions with TPP polyanions during ionotropic gelation where the change in zeta potential of chitosan (and indeed all polyelectrolyte biopolymers) can be used to estimate chain stiffness (Abodinar et al., 2014).

3.5.4 Analysis of different ratios of CS: TPP microparticles using scanning electron microscope (SEM)

In this study CS: TPP microparticles formed by ionotropic gelation, were prepared at various ratios, (loaded with red dye for visualisation purposes), by the mixing CS solution with TPP solution under stirring. The particles formed at each ratio were shown to have different chemical and physical properties (**Figure 3.7a–g**). As can be seen in **Figure 3.7**, microparticles prepared with AB-12 at the higher CS: TPP ratios and therefore at higher viscosity and surface charge had more porous surfaces than those of microparticles prepared with the lower CS: TPP ratios which had irregular angular surfaces, this is expected to have an influence strength of interaction and therefore integrity of the particle “walls” and therefore their size and shape (Ponnuraj et al., 2015). The availability of TPP is of course limited at high chitosan ratios and in

excess in those with lower chitosan ratios and this influences the cross-linking density which again has an effect on size, shape and morphology of the particles (Ponnuraj et al., 2015). Furthermore, although it may appear as though some of the particles are fragments of precipitated chitosan this is not the case as this is inconsistent with both the FT-IR and XRD data above.

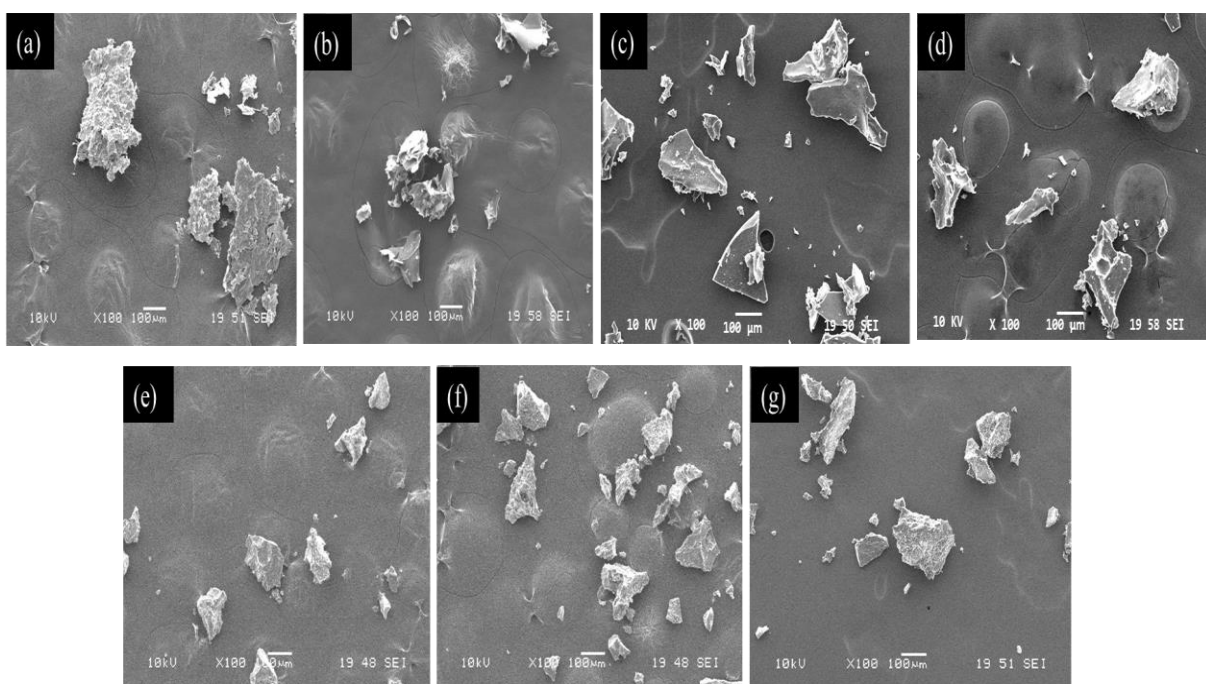


Figure 3.7: Example of SEM images of chitosan microparticles CS: TPP using AB-12 (a) 6:1, (b) 4:1, (c) 2:1, (d) 1:1, (e) 1:2, (f) 1:4 and (g) 1:6. Where the scale bar is 100 μm and the estimated total surface areas (based on the measurement of the sizes and areas of the particles using Image J, version 1.52a (National Institute of Health, Bethesda, USA)) of the particles are approximately ~ 31000 , 14000, 25000, 24000, 10000, 11000 and 12000 μm^2 , respectively.

In terms of potential applications of non-spherical particles, it has been previously reported that flake-like metal particles (aluminium, copper, *etc.*) are more effective than spherical particles in latent fingerprint development (James et al., 1991b) due to increased surface: volume ratios (Yamashita and French, 2011), therefore samples

with a 2:1 CS: TPP ratio were used for further forensic studies in latent fingerprint visualisation with encouraging results, this will depend on total particle surface area, which ranges from $\sim 10000 \mu\text{m}^2$ (**Figure 3.6e**) to $>31000 \mu\text{m}^2$ (**Figure 3.7a**) and on the number of particles per unit area. ImageJ was used to measure surface area of particles. In brief, in the toolbar of ImageJ the line tool has selected to determine how many pixels correspond to scale bar (100 μm). A straight line has drawn along the length of the scale bar of the image. The analyse tool and then set scale has selected. A number 100 was entered in the known distance field and the unit μm has entered in the unit of length field. On the toolbar of ImageJ, file menu has opened, then SEM image of particles has selected. An irregular shape tool has selected then free hand drawn around each of the particles. Under the “analyse tab” measure was selected and the average of surface area was estimated. Measurements were repeated with three another images then the average of surface area was obtained. As the surface area of nanoparticles are greatly influenced by their size similar factors are important in determining the surface area for example: the CS: TPP ratio, the initial chitosan concentration and the degree of de-acetylation of the chitosan (Sreekumar, et al., 2018), the nature (ionic strength, pH, salt content, *etc.*) of the solvent in which the nanoparticles are prepared is also important (Hejjaji, et al., 2017; Sreekumar, et al., 2018). In addition, the drying method is an important parameter which affects the particle size and surface area of chitosan nanoparticles (Kumar and Kar, 2014). Several studies (Gan et al., 2005, Janes and Alonso, 2003, Deng et al., 2006, Yang and Hon, 2009) have concluded that increasing molecular weight of chitosan had a direct effect of chitosan nanoparticles by increasing of particle size, this may be attributed to the increase of chitosan viscosity which led to less solubility of chitosan in acetic acid solution (Bugnicourt et al., 2014) and may form an outer membrane and

leading to effect particle size and surface area (Sarmiento et al., 2007a, Sarmiento et al., 2007b). Furthermore, previous studies reported that there were differences in the particle size and surface areas of chitosan nanoparticles between SEM/TEM and DLS techniques due to the fact that particles swell in aqueous media (through being surrounded solvent molecules). Using DLS, the hydrodynamic diameter of particles is measured, however SEM or TEM provides the dry particle's diameter, where any water or solvent in shell would evaporate and particles therefore shrink in the dry state (Fan et al., 2012, Domingos et al., 2009, Komalam et al., 2012).

In the case of the irregular particles previous research has shown that the shape of chitosan particles depends on the pH at which chitosan and TPP are mixed and the molecular weight (viscosity) of the chitosan (Ko et al., 2002), furthermore in terms of pharmaceutical applications irregular particles with angular features have been shown to decrease drug dissolution (Mosharraf and Nyström, 1995), have a higher drug loading efficiency (Uskokovic et al., 2012), influence phagocytosis (Champion et al., 2007) and to have a greater probability of adhering to cancer cell surfaces (He and Park, 2016) which suggests that chitosan particles formed in this way may have potential in drug delivery formulations.

The relative viscosity of the CS: TPP microparticle suspension is shown in **Figure 3.8**, which indicates that neither pH nor ionic strength have a large influence the relative viscosity at ratios CS: TPP 1:6, 1:4, 1:2, 1:1 and 2:1. It can be attributed to its lesser resistance towards flow due the relatively low charge on chitosan microparticles. At higher ratios (4:1; 6:1), the relative viscosity is higher with an increase in the CS: TPP ratio in the mixture. Moreover, at the fixed pH value and different ionic strength (0.1, 0.3 and 0.5 M), the relative viscosity increased with a

decrease in ionic strength. This behaviour may arise because of the decrease in the repulsion force between charges for the solvent and polymers and not unsurprisingly is dominated by the amount of chitosan in the microparticles.

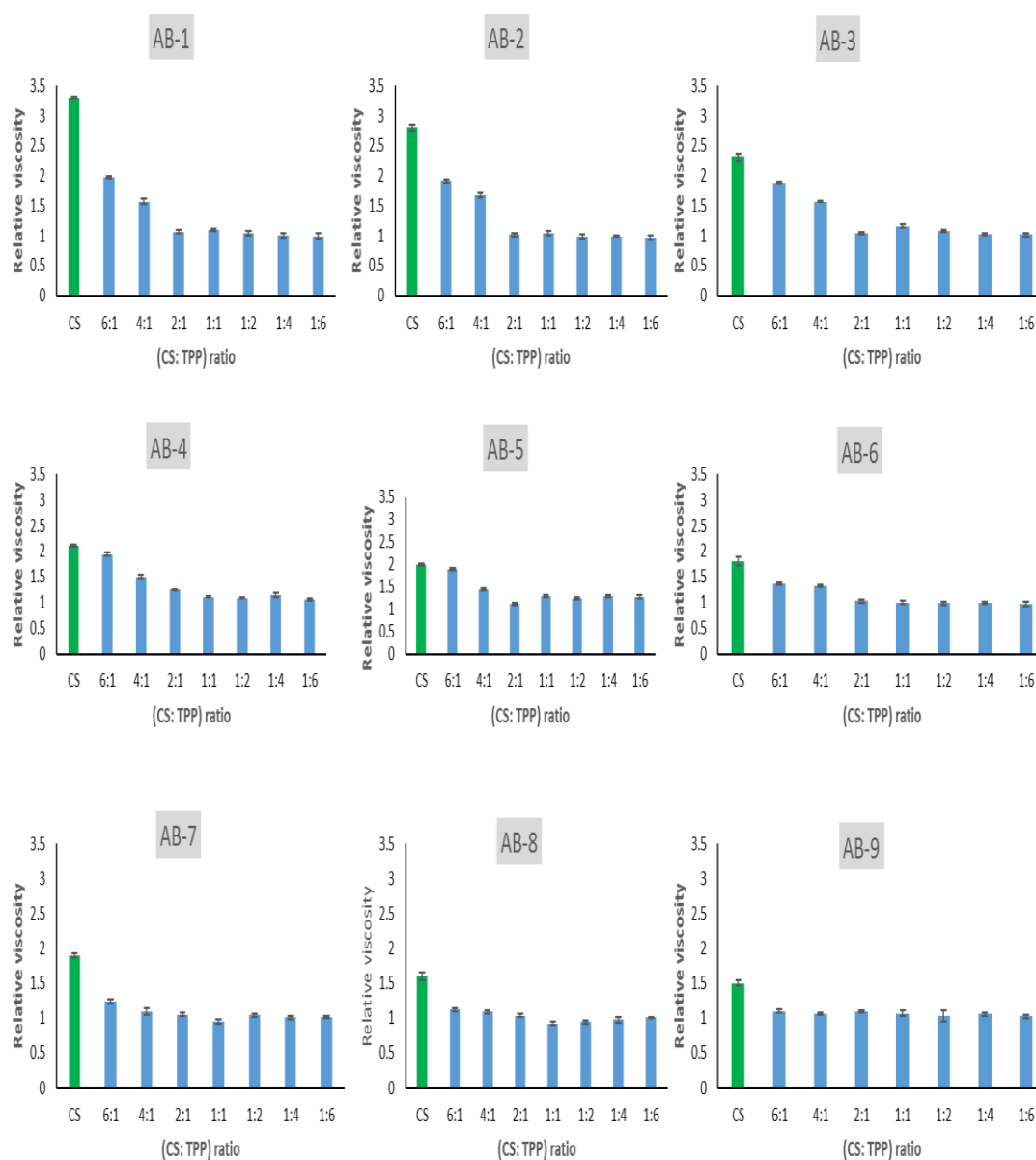


Figure 3.8: Relative viscosities of chitosan (green columns) and CS: TPP microparticles (blue columns) solutions (using AB-1 to AB-9) at varying ionic strength and pH values at 25.0 ± 0.1 °C (mean \pm SD, n = 10).

The effect of ionic strength and pH value on the zeta potential of nine chitosan microparticle formulations was investigated as shown in **Figure 3.9**. When chitosan and TPP were mixed with each other in an acetate buffer, they spontaneously formed microparticles (diameters were in the range 28–445 μm) with an overall positive surface charge which are at least partially within the size range of particles which have been demonstrated to be effective in latent fingerprint visualisation $\sim 1\text{--}50\ \mu\text{m}$ (James et al., 1991b) and may have potential in pulmonary or colonic drug delivery systems (Bellich et al., 2016). The more positively or negatively charged the particles, the more they repel each other and therefore at values of $\pm 30\ \text{mV}$ are required for optimal stability (Tang et al., 2013). As the CS: TPP ratio decreased from 6:1 to 1:6 the zeta potential values decreased from for example $+36.4\ \text{mV}$ to $+5\ \text{mV}$ in buffer AB-1 or from $+13.5\ \text{mV}$ to $+3.0\ \text{mV}$ in buffer AB-9 (**Figure 3.9**).

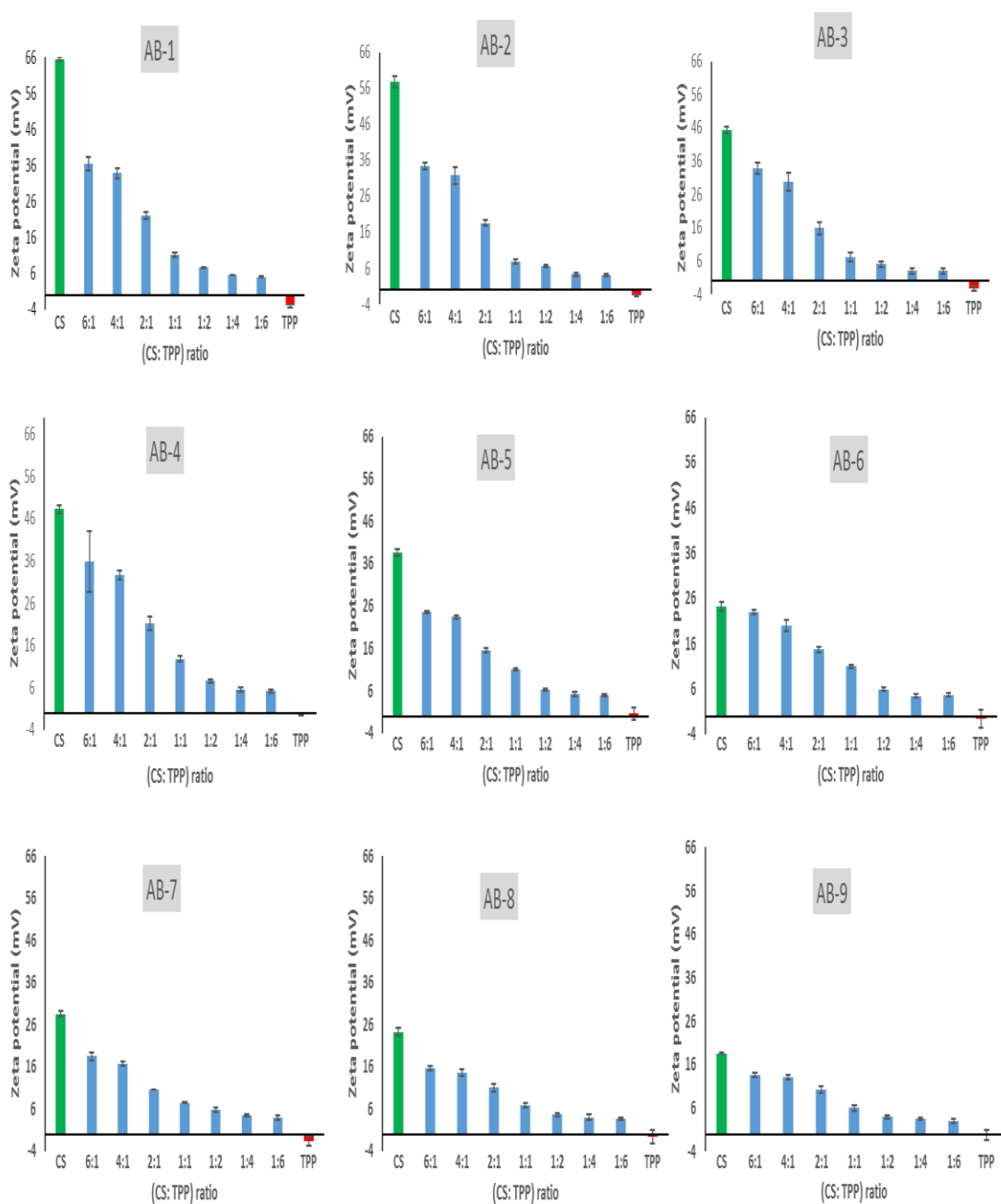


Figure 3.9: Zeta potentials of chitosan (green columns), TPP (red columns) and CS: TPP microparticles (blue columns) solutions (using AB-1 to AB-9) at varying ionic strength and pH values at $25.0 \pm 0.1^\circ\text{C}$ (mean \pm SD, $n = 10$).

It was also observed that with a decrease in the concentration of chitosan the appearance of the system changed from clear viscous liquid to milky dispersion prior

to precipitation. It was demonstrated that, there was no significant difference in the zeta potential values of CS: TPP from 1:2 to 1:6, indicating neutralization of the protonated amino groups on the surface of chitosan microparticles and subsequent loss of repulsive force which led to precipitation of the particles. On the other hand, as the CS: TPP ratio increased from 1:2 to 6:1 the zeta potential increased almost linearly. The large positive surface charge due to the high degree of deacetylation and protonation causes the chitosan molecules to have a large number of potential cross-linking sites. The presence of higher positive charge on the particles indicated that free (non-cross-linked) amino groups remained on the particle surface (Zhang et al., 2004, Fan et al., 2012) which is consistent with an increased viscosity in solution. When the CS: TPP ratio was high at 6:1 and 4:1 (the available quantity of TPP was small) the reaction solution was clear, indicating that the amount of phosphate groups was inadequate to lead to the full cross-linking with the chitosan amino groups (Li and Huang, 2012). As the CS: TPP ratio decreased from 6:1 to 1:1, the particle size decreased due to increased intramolecular and intermolecular cross-linking density between chitosan amino groups and the TPP groups (**Figure 3.10**), this is also due to the decrease in viscosity (**Figure 3.8**) which leads weaker networks and therefore assuming there is no change in shear forces (stirring rate was constant at 600 rpm in all cases) smaller particles (Kawadkar and Chauhan, 2012). It can be inferred that chitosan molecules were almost fully cross-linked at CS: TPP (1:1), which coincided with the smallest particle size range measured. As the CS: TPP ratio decreases further from 1:1 to 1:6 the particle size increased, as more TPP molecules are involved in the formation of the microparticles. This increased concentration of TPP promotes aggregation due to inter-particle cross-linking (bridging effects) which leads to a lower surface charge density of the particles resulting in precipitation (Li and Huang,

2012, Ponnuraj et al., 2015). As we can see in **Figure 3.7** the CS: TPP microparticles are in some cases non-spherical, with aspect ratios ranging from 1:1 to 13:1 and as particle size analysis treats particles as equivalent spheres there is potential for minor discrepancies in the absolute particle sizes, these are expected to be minimal although this will depend on the type of material being measured (Polakowski et al., 2014).

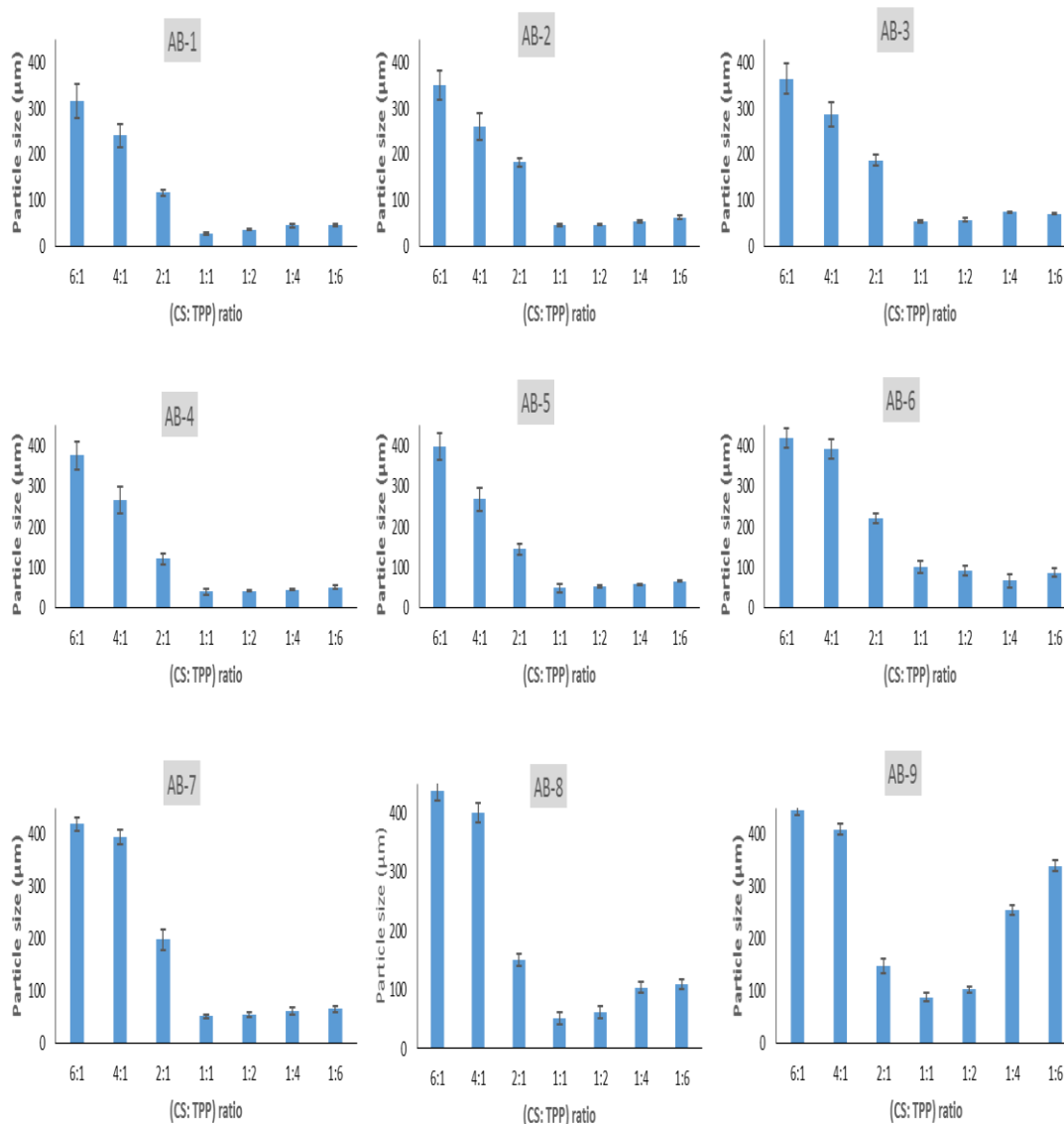


Figure 3.10: Particle size ($D_{[4,3]}$) of CS: TPP microparticles solutions (using AB-1 to AB-9) at varying ionic strength and pH values at $25.0 \pm 0.1^\circ\text{C}$ (mean \pm SD, $n = 10$).

Using multiple regression analysis, the responses (relative viscosity, zeta potential and particle size) were correlated with the three variables studied using second-order polynomials. The coefficients of the model equation and their statistical significance were evaluated using Minitab®17.1.0 software (Minitab Inc., Philadelphia, U.S.A.). The regression model for the responses to relative viscosity (Y_1), zeta potential (Y_2) and particle size (Y_3) in terms of coded factors is given by Eqs. (3.3) – (3.5) respectively.

$$\text{Viscosity (Y1)} = -0.251 + 0.575 X_1 - 0.136 X_2 + 0.3315 X_3 - 0.0631 X_1^2 + 0.008 X_1X_2 - 0.0676 X_1X_3 + 0.232 X_2^2 - 0.178 X_2X_3 + 0.01397 X_3^2 + 0.0213 X_1X_2X_3 \quad \text{Eq. (3.3)}$$

$$\text{Zeta potential (Y2)} = -25.54 + 14.89 X_1 - 35.8 X_2 + 15.00 X_3 - 1.812 X_1^2 + 6.88 X_1X_2 - 1.606 X_1X_3 + 16.5 X_2^2 + 2.32 X_2X_3 - 0.5282 X_3^2 - 1.446X_1X_2X_3 \quad \text{Eq. (3.4)}$$

$$\text{Particle size (Y3)} = 299 - 98.3 X_1 - 271 X_2 - 9.9 X_3 + 12.4 X_1^2 + 54.5 X_1X_2 + 4.23 X_1X_3 + 167 X_2^2 - 12.2 X_2X_3 + 5.50 X_3^2 + 7.1 X_1X_2X_3 \quad \text{Eq. (3.5)}$$

The equations were applied to the responses (Viscosity, Zeta potential and Particle size), to describe the principal effects and interactions amongst the identified variables pH (X_1), ionic strength (X_2) and ratio (X_3). The coefficients with one factor including pH, ionic strength or ratio represent the statistical effect of the particular factor, while the coefficients with two factors (such as X_1X_2), three factors (such as $X_1X_2X_3$), and those with second order terms (such as X_3^2) represent the interaction between the two factors, three factors and quadratic effect, respectively. The positive sign in front of the terms indicates synergistic effect, while negative sign indicates antagonistic effect on the response.

3.5.5 Model validation of relative viscosity, zeta potential and particle size

Four different chitosan microparticle formulations were prepared in different acetate buffers: AB-10, AB-11, AB-12 and AB-13. The relative viscosities, zeta potential and particle size of the four chitosan microparticles were measured (**Table 3.3**). The regression equations were obtained for Eqs. (3.3) – (3.5) which suggests the empirical relationship between the value of response and the independent variable. Therefore, the predicted values were calculated using mathematical model from Eqs. (3.3) – (3.5). For validation of relative viscosity, zeta potential and particle size results, the experimental values of the responses were compared with that of the predicted values (**Table 3.3** and **Figures 3.11**).

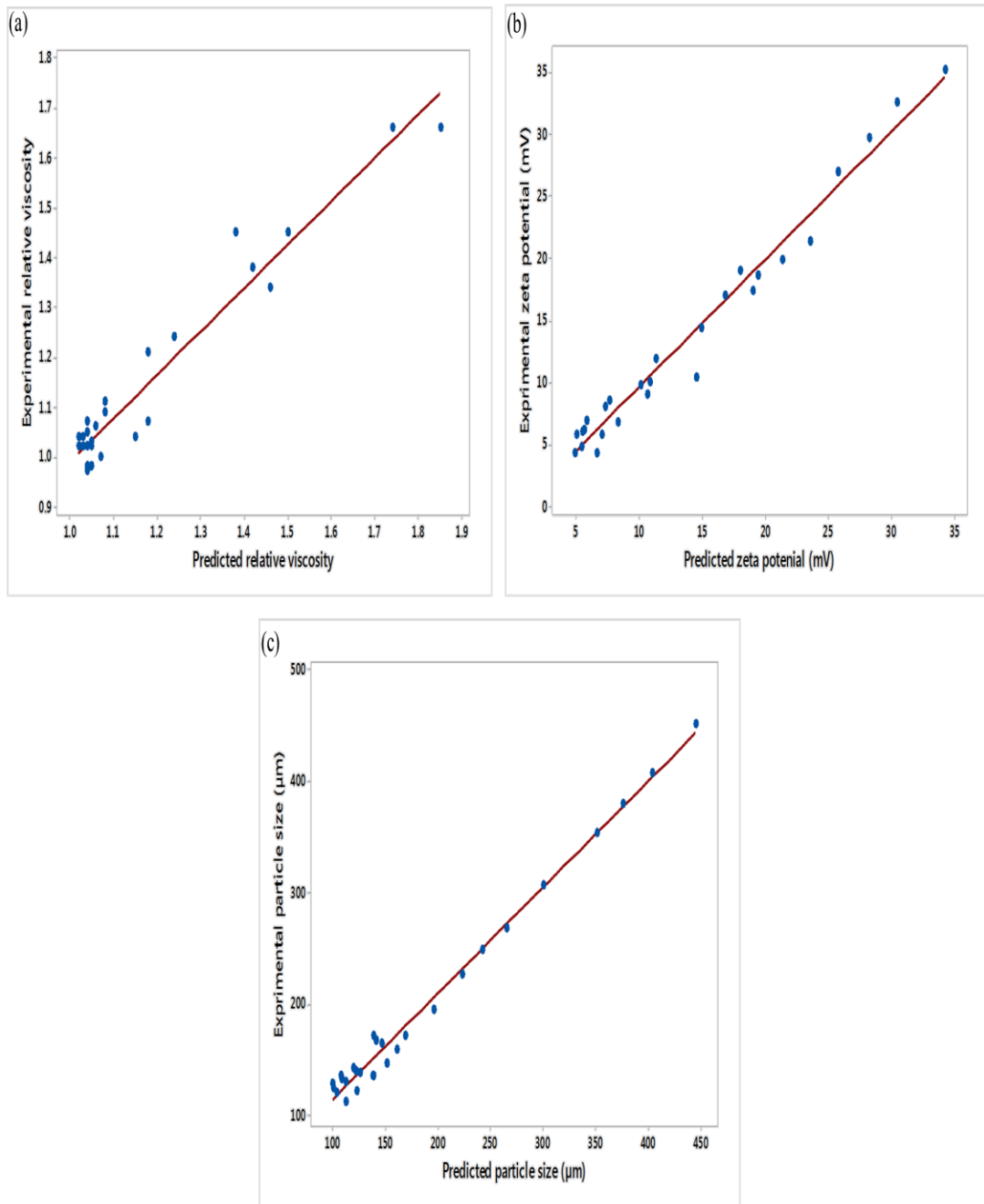


Figure 3.11: Linear correlation plot (scattergram) between the experimental and predicted of relative viscosity (a), zeta potential (b) and practical size (c) for validation data.

Model validation through the analysis of the scattergram plots of expected versus predicted values in **Figures 3.11** were studied. Firstly, with respect to all three scattergram plots, it is clear that these scattergrams exhibit discernible positive correlations from left to right, with all the points more or less adhering to this pattern.

As such, it can be said that the expected responses and predicted values are all positively correlated (Montgomery, 2017). This implies that although not all the points fall precisely on the linear plot itself, there is still a definite correlation that persists between the expected responses and the predicted values (Montgomery, 2017). The outliers are less at lower viscosities because the particle size is low and the density of intramolecular and intermolecular cross-linking between chitosan and TPP is high. Therefore, the viscosity is more predictable for chitosan nanoparticles with small size (**Figure 3.11a**). The experimental zeta potential and predicted zeta potential exhibited a linear relation and outliers were not observed. Such findings suggested that the chitosan nanoparticles were appropriately produced and the surface properties were predictable as a function of the presence of protonated groups. In addition, the findings of the zeta potential were complemented by the findings of the regression line of predicted particle size with experimental particle size. The scattergram reflected strong goodness of fit. Although at the low particle sizes there were certain outliers. However, those outliers were near the goodness of fit (**Figure 3.11b and Figure 3.11c**). Secondly, the correlation coefficient (R^2) values for the plots in **Figures 3.11 – 3.13**, which are 0.91, 0.96, and 0.85, respectively, are all above the minimum acceptable value of 0.85 and all approach unity. As such, the models that were generated during this experiment can be said to be highly linear in addition to exhibiting positive correlations between the x- and y-axes (Montgomery, 2017, Singh and Agarwal, 2002). In turn, the models can be said to be useful for future studies that entail the development of chitosan nanoparticles for a certain application. Furthermore, the variations between the experimental responses and the predicted values have been seen in **Table 3.3**. The least frequent variations between experimental responses and predicted values may be observed for the relative

viscosity measurements. In particular, two of the runs for which percent error relatively high, which were, namely, runs 1 and 3, exhibited a pH of 3.8, an ionic strength of 0.2, and a CS: TPP ratio of 6:1 and 2:1, respectively. The other run for which percent error relatively high, which was run 10, differed from the previous runs in that the ionic strength was 0.4, but it was similar to run 3 in that the CS:TPP ratio was 2:1. Based on these findings, it can be said that higher proportions of chitosan relative to TPP may increase relative viscosity. In support of these results, (Al-Shammari et al., 2011) revealed that polymer concentration significantly affects relative viscosity. Thus, it can be concluded that high concentrations of chitosan may have caused the variations in percent error for the relative viscosity measurements. This could be due to repulsion force decrease between the polymers and the solvent (Harding, 1997). It is observed in **Table 3.3** that the values of zeta potential decreased with decrease in the CS: TPP ratio from 6:1 to 1:6. There is no significant difference between the expected and predicted values by runs 1 – 23. This is a clear indication of protonated amino group neutralization on the chitosan micro-particles' surface and hence, there is repulsive force loss that results to particle precipitation.

Table 3.3: Observed (Exp.) responses and predicted (Pred.) values and percent error (bias^a %) for relative viscosity (Y1), zeta potential (Y2) and particle size (Y3).

Run	Dependant Variables			Y1			Y2			Y3		
	X1	X2	X3	Relative viscosity			Zeta potential (mV)			Particle size [D4,3] (µm)		
	pH	I.S (CS:TPP)		Exp.	Pred.	Bias (%)	Exp.	Pred.	Bias (%)	Exp.	Pred.	Bias (%)
1	3.8	0.2	6:1	1.66 ± 0.01	1.85	11.4	35.2 ± 1.3	34.2	-2.8	354 ± 40	351	0.85
2	3.8	0.2	4:1	1.34 ± 0.01	1.46	9.0	29.7 ± 1.1	28.2	-5.1	226 ± 21	223	1.33
3	3.8	0.2	2:1	1.07 ± 0.01	1.18	10.3	19.0 ± 1.6	18	-5.3	135 ± 6	139	-2.96
4	3.8	0.2	1:1	1.11 ± 0.01	1.08	-2.7	11.8 ± 0.9	11.3	-4.2	111 ± 3	113	-1.80
5	3.8	0.2	1:2	1.05 ± 0.01	1.04	-1.0	8.5 ± 1.3	7.6	-10.6	119 ± 2	104	12.6
6	3.8	0.2	1:4	1.04 ± 0.01	1.03	-1.0	6.1 ± 0.9	5.6	-8.2	124 ± 3	101	18.5
7	3.8	0.2	1:6	1.04 ± 0.01	1.02	-1.9	5.8 ± 0.4	5	-13.8	128 ± 6	100	21.8
8	3.8	0.4	6:1	1.66 ± 0.01	1.74	4.8	32.6 ± 2.9	30.4	-6.7	379 ± 49	376	0.79
9	3.8	0.4	4:1	1.45 ± 0.01	1.38	-4.8	27.0 ± 2.7	25.7	-4.8	248 ± 41	242	2.42
10	3.8	0.4	2:1	1.04 ± 0.01	1.15	10.6	17.0 ± 0.6	16.8	-1.2	146 ± 5	152	-4.11
11	3.8	0.4	1:1	1.00 ± 0.01	1.07	7.0	10.0 ± 0.7	10.8	8.0	121 ± 2	123	-1.65
12	3.8	0.4	1:2	1.02 ± 0.01	1.04	2.0	8.0 ± 1.2	7.3	-8.8	129 ± 5	113	12.4
13	3.8	0.4	1:4	1.02 ± 0.01	1.03	1.0	6.0 ± 1.4	5.5	-8.3	132 ± 4	109	17.4
14	3.8	0.4	1:6	1.02 ± 0.01	1.02	0.0	4.3 ± 0.7	4.9	14.0	135 ± 5	108	20.0
15	4.8	0.2	6:1	1.45 ± 0.01	1.5	3.4	21.3 ± 0.4	23.5	10.3	407 ± 50	404	0.74
16	4.8	0.2	4:1	1.24 ± 0.01	1.24	0.0	19.9 ± 0.8	21.3	7.0	267 ± 31	265	0.75
17	4.8	0.2	2:1	1.09 ± 0.01	1.08	-0.9	14.3 ± 0.6	14.9	4.2	171 ± 4	169	1.17
18	4.8	0.2	1:1	1.03 ± 0.01	1.05	1.9	9.7 ± 0.5	10.1	4.1	135 ± 2	138	-2.22
19	4.8	0.2	1:2	0.98 ± 0.01	1.04	6.1	8.0 ± 0.1	7.3	-8.8	138 ± 2	126	8.70
20	4.8	0.2	1:4	1.07 ± 0.01	1.04	-2.8	6.9 ± 0.4	5.8	-15.9	139 ± 2	122	12.2
21	4.8	0.2	1:6	0.97 ± 0.01	1.04	7.2	4.8 ± 0.1	5.4	12.5	142 ± 6	120	15.4
22	4.8	0.4	6:1	1.38 ± 0.01	1.42	2.9	18.6 ± 0.6	19.4	4.3	451 ± 31	445	1.33
23	4.8	0.4	4:1	1.21 ± 0.01	1.18	-2.5	17.3 ± 0.1	19	9.8	306 ± 29	300	1.96
24	4.8	0.4	2:1	1.06 ± 0.01	1.06	0.0	10.3 ± 0.3	14.5	40.8	194 ± 11	196	-1.03
25	4.8	0.4	1:1	1.02 ± 0.01	1.04	2.0	9.0 ± 0.5	10.6	17.8	158 ± 8	161	-1.90
26	4.8	0.4	1:2	0.98 ± 0.01	1.05	7.1	6.8 ± 0.3	8.3	22.1	164 ± 10	147	10.3
27	4.8	0.4	1:4	1.02 ± 0.01	1.05	2.9	5.7 ± 0.2	7	22.8	167 ± 23	141	15.5
28	4.8	0.4	1:6	0.98 ± 0.01	1.05	7.1	4.2 ± 0.5	6.6	57.1	171 ± 15	139	18.7

^a $Bias (\%) = \frac{\text{Observed value} - \text{Predicted value}}{\text{Observed value}} \times 100$

In general, the percent error variations with the largest magnitude can be discerned at a pH level of 4.8, an ionic strength of 0.4, as well as ratios of chitosan and TPP that are not proportionate, as seen in **Table 3.3**. In fact, it seems that the latter factor has the most significant effect on zeta potential when pH and ionic strength remain unchanged at 4.8 and 0.4, respectively. This trend is best exemplified by runs 26, 27, and 28, wherein the obtained percent error values were 22.1, 22.8, and 57.1, respectively. Such large magnitudes of percent error may be attributed to the changes in CS: TPP, as these runs exhibited polymer: crosslinking agent ratios of 1:2, 1:4, and 1:6, while pH and ionic strength remained constant. Importantly, in their study on the effects of concentration, ionic strength, and pH on zeta potential, (Carneiro-da-Cunha et al., 2011) found that zeta potential increases with increasing chitosan concentration, which was indeed observed for runs 26, 27, and 28. Consequently, it can be said that at the lower pH and the higher ionic strength implemented in this experiment, zeta potential is likely to be decreased with increasing crosslinking agent concentration, thereby resulting in the variations in the zeta potential measurements. There is a decrease in the size of the particle as the ratio of CS: TPP dropped from 6:1 to 1:1 and also within this range, the bias ratio or the difference between the expected and predicted is relatively low. This could be because of increase in the density of intermolecular and intermolecular cross-linking between the TPP and chitosan amino groups; viscosity decrease could also to this (Kawadkar and Chauhan, 2012). It can be noted that there was increase in the particle size as the ratio of CS: TPP dropped from 1:1 to 1:6 and as such, the percentage bias or the difference between the predicted and expected was seen to increase significantly as the ratio dropped from 1:1 to 1:6. The reason for this could be because more molecules of TPP participate in microparticle formation (Li and Huang, 2012). Additionally, as seen in **Table 3.3**, the magnitude of

the variation in percent error increases as the concentration of TPP increases while that of chitosan remains unchanged or constant. To illustrate, for runs 5, 6, and 7 wherein the CS: TPP ratios were 1:2, 1:4, and 1:6, respectively, the obtained percent error values were 12.6, 18.5, and 21.8, respectively. This result appears to imply that greater amounts of a crosslinking agent tend to produce smaller particle sizes. This may occur because the volume of chitosan is lowered when that of TPP is increased. Such a finding is corroborated by the study conducted by (Gan et al., 2005), who explained that controlling the chitosan and TPP weight ratio can lead to the achievement of nanoparticles that possess the desired particle size. Specifically, it was found that smaller volumes of chitosan produced nanoparticles of smaller sizes, while bigger nanoparticles were obtained for larger volumes of chitosan (Choi et al., 2002, Gan et al., 2005, Katas and Alpar, 2006). A possible explanation for this occurrence is that smaller particles form when the unoccupied functional groups are in stoichiometric proportion, whereas large particles tend to form when polymer concentrations are large due to aggregation of polymer molecules (Douglas and Tabrizian, 2005, Quong and Neufeld, 1998, Mandlik and Ranpise, 2017). Thus, it is likely that the CS: TPP ratio caused the variations in the particle size measurements. Finally, **Table 3.3** indicates that ionic strength, pH and CS: TPP ratio are suitable in predicting viscosity, zeta potential and particle size and can therefore be used in future studies to design tuneable microparticles for specific applications.

3.6 Effect of chitosan molecular weight and TPP concentration in acetic acid to formulate CS: TPP nanoparticles

The size of the CS: TPP particles depend basically on molecular weight of chitosan, either concentration of TPP or chitosan and conditions of mixing, *i.e.* chitosan-TPP

volume ratio, stirring speed, pH, sonication or temperature (Giri et al., 2012). The conditions required for these experiments were determined to be (5:1) CS: TPP ratio, 30 °C, 750 rpm (Section 3.4.3). These conditions were selected due to a previous studies described that the particle size of CS: TPP at 5:1 decreases with increased temperature (Jain et al., 2016, Tsai et al., 2008), this is attributed to decrease in intrinsic viscosity and hydrogen bonded water of hydration in chitosan, resulting in an increase in chitosan chain flexibility (Chen and Tsaih, 1998). As a result chitosan chains form a compact structure during cross linking (Fan et al., 2012). Additionally, another previous studies reported that the particle size decreased with increasing stirring speed (Jain et al., 2016, Hassani et al., 2015, Tsai et al., 2008). It can be observed from **Table 3.4** that the concentration of TPP could influence of the particles size. At a fixed concentration of chitosan at 3 mg/mL but different the concentrations of TPP from (0.84 – 1.25, mg/mL), resulted in an increase in particle size for both LMW and MMW samples when TPP concentration was increased. It was noted that the initial increase in TPP concentration (0.84 mg/mL) high degree of cross-linking of chitosan chain, therefore a significant reduction in particle size were formed. Further increase in TPP concentration led to increases in the particles size, this could be due to excessive of interparticle cross-linking (bridging effects) (Li and Huang, 2012). The size of chitosan nanoparticles prepared by different molecular weight chitosan was also studied. **Table 3.4** indicated that the particle size has slightly increased with the molecular weight chitosan due to increased viscosity which led to less solubility of chitosan in diluted acetic acid (Bugnicourt et al., 2014). Therefore, less amino groups on chitosan could be protonated. This could lead to inefficient interaction between positively charged chitosan and negatively charged TPP (Katas and Alpar, 2006). This result is similar to previous studies with reported increases in the particle

size with increases in chitosan molecular weight (Yien et al., 2012, Gan et al., 2005, Janes and Alonso, 2003). The polydispersity index (PDI) reflects the size distribution of nanoparticles and it is documented that the higher PDI value, the wider the range of particle size. The PDI, also, is used to indicate the uniformity of the nanoparticles. As can be seen in **Table 3.4** the PDI ranges from 0.24 ± 0.01 to 0.43 ± 0.01 . This indicates that a narrow size range of nanoparticles, and it in an acceptable range as PDI less than 0.50 indicates a relatively homogenous dispersion (Jardim et al., 2015). PDI of the LMW and MMW samples range from 0.24 ± 0.01 to 0.26 ± 0.01 and 0.34 ± 0.04 to 0.43 ± 0.01 respectively. This suggests that as molecular weight increases the polydispersity of samples also increases, this is due to an increase in particle size distribution, and therefore a homogenous dispersion of chitosan nanoparticles were prepared (Hu et al., 2008). It has been reported in a previous study that the particle size was related to the polymer chain length, and the PDI would tend to procedure particles with a large size range (Bugnicourt et al., 2014) as the molecular weight increases.

Zeta potential of these samples also decreased as the concentration of TPP was increased. Charge ranged from $+36.3 \pm 3.6$ mV to $+34.4 \pm 1.7$ mV. This can be explained by the fact that at a higher concentration of TPP, there are more negatively charged phosphate ions which can form cross linkages with free positively charged amino groups on chitosan. Therefore, the positive charge of these nanoparticles decreases (Dyer et al., 2002, Hassani et al., 2015, Shah et al., 2016). In addition, MMW of chitosan has higher zeta potential than LMW of chitosan. This was due to the MMW of chitosan has more available cationic groups, resulting in the higher positive zeta potential (surface charge) (Hu et al., 2008). Therefore, all chitosan

nanoparticles are stable as a surface charge greater than + 30 mV is in the ideal range (Jardim et al., 2015).

Table 3.4: Change in particle size and zeta potential as concentrations of TPP and molecular weight of chitosan are changed

LMW Chitosan				MMW Chitosan			
Chitosan (mg/mL)	TPP (mg/mL)	Particle Size (nm)	PDI	Z.P (mV)	Particle Size (nm)	PDI	Z.P (mV)
3	0.84	231.3 ± 7.9	0.26 ± 0.01	36.3 ± 3.6	237.4 ± 1.8	0.36 ± 0.02	38.7 ± 1.4
3	1.00	280.3 ± 2.9	0.26 ± 0.01	35.3 ± 1.7	293.7 ± 3.3	0.43 ± 0.01	36.5 ± 1.2
3	1.25	290.6 ± 6.1	0.24 ± 0.01	34.4 ± 1.7	294.7 ± 10.3	0.34 ± 0.04	35.3 ± 1.7

3.7 Summary

In this study, chitosan microparticles of different morphologies were successfully formed by the ionotropic gelation method at method at different CS: TPP ratios and pH/Ionic strength conditions. The particles were characterized by relative viscosity, zeta potential, particle size, FTIR spectroscopy, SEM and XRD. Using experimental design, the relative viscosity, particle size and zeta potential of CS: TPP microparticles under different conditions could be predicted using the mathematical models. The mathematical models obtained showed good relationships between independent variables (pH, ionic strength and CS: TPP ratio) and dependent variables (relative viscosity, zeta potential and particle size) for prediction. This gives us the ability to design tuneable CS: TPP microparticles for specific pharmaceutical or forensic applications more specifically latent fingerprint visualization (see **Chapter 4**).

Chapter 4

The potential of chitosan-tripolyphosphate microparticles in the visualisation of latent fingerprints

4 The potential of chitosan-tripolyphosphate microparticles in the visualisation of latent fingermarks

4.1 Introduction

Chitosan has been investigated widely for its potential in the development of food and drug delivery systems and pharmaceutical applications, however it has not generally been considered in forensic applications for example fingerprints (fingermarks). The identification of fingerprint evidence is widely used in forensic investigations (Becue et al., 2008, Choi et al., 2008). Latent fingerprints are a very common form of physical evidence (Kabklang et al., 2009, Roux et al., 2000). Some new techniques have been enhanced for latent fingerprint identification however, the traditional fingerprint identification technique for treating latent prints is powdering method (metal powders and magnetic powders). The most traditional methods usually used for latent print development are powder dusting (Jones et al., 2010a), iodine fuming, ninhydrin spraying and silver nitrate soaking which are quite effective for numerous surfaces (Garg et al., 2011, Lee and Gaensslen, 2001). On the other hand, these traditional techniques for latent fingermarks detection are not always effective. Therefore, forensic scientists have attempted to improve the existing techniques for the visualization of latent fingermarks (Garg et al., 2011). The most commonly used procedure for revealing the ridge pattern is powder dusting, which relies on the mechanical adherence of fingerprint formulation to the fatty components of the skin deposit that are secreted by sweat pores that exist on friction ridges (Yamashita and French, 2011). Chitosan can form particles by ionic interaction between positively charged amino groups of chitosan and negatively charged counter ions of TPP. Knowledge of viscosity, zeta potential and particle size will have an influence on the

bioadhesion of chitosan: TPP microparticles and hence potential applications in forensic applications such as the development of fingermarks (Il Dueik and Morris, 2013). The factors which effect this interaction are particle size, particle charge, particle shape and relative surface area (James et al., 1991b, Jones et al., 2010b, Yamashita and French, 2011) all of which are controlled by processing parameters such as chitosan concentration, pH and ionic strength of the dissolution media, temperature of cross-linking, stirring rate, *etc* (Wang et al., 2011). There are a number of different powders which have been used to detect fingermarks (**Table 4.1**) including for example, granular carbon particles, lead powder (Graham, 1969), Congo red dye (Sodhi and Kaur, 2001), eosin yellow dye (Sodhi and Kaur, 1999).

Table 4.1: Various chemicals or powders used for development of latent fingerprints (Garg et al., 2011).

Name of powder	Advantages	Disadvantages
Metallic dusting such as grey powder (containing aluminium dust and kaolin); Silver powder (containing aluminium flake and quartz powder)	They have longer shelf lives as compared to the organic-based powders (Sodhi and Kaur, 2001). Grey and silver powder used for dark metallic surfaces and most smooth non-porous surfaces (James et al., 1993)	Silver powder may be hard to see on a reflective surface.
Black powder (Charcoal)	It can develop fingerprints on white and light coloured surfaces (Saferstein, 2004)	Fingerprints may be dotty which more hard to see clear contentious details (Bandey and Gibson, 2006).
Magnetic powder (iron oxide)	It used magnetised rod and there is no conventional brushes such as fibres to touch the print and probably damage it (James et al., 1991a)	Less effective on ferromagnetic surfaces such as steel and nickel metal (James and Nordby, 2003, Yamashita and French, 2011)
Luminescent powders such as acidine yellow, Nile blue, crystal violet	They can be used for developing weak prints and multicoloured surfaces that would present a contrast issues of developed with traditional powders (Menzel and Duff, 1979, Menzel, 1979, Menzel and Fox, 1980)	They are not always suitable for use in a crime scene (Sodhi and Kaur, 2001).
Sudan III	It used primarily for contaminated wet surfaces with beverages, oil, grease, or foods	It caused hazard to user in case of skin contact, and eye contact
Phloxine B dye	It can develop latent fingermarks on a wide range of non-absorbent surfaces (Sodhi and Kaur, 2000)	May cause eye irritation and cause damage to stomach through prolonged or repeated exposure
Rhodamine B dye	It useful for visualisation of latent marks deposited on multi-coloured surfaces (Kapoor et al., 2015)	Hazardous in case of skin, and eye contact (irritant)
Eosin-blue dye	It may develop weak fingermarks under UV-	It may cause eye, skin, and respiratory tract

	light. It gave good fingerprint on laminated and polyethene surfaces (Hawthorne, 2008)	irritation such as eosin dyes
Azure I dye and azure II dye	It can detect latent fingerprints on a wide range of surfaces, porous and non-porous; white and multicoloured (Sodhi and Kaur, 2004)	Harmful
Basic fuchsin dye	It can detect latent fingerprints on wet non-porous surfaces with SPR (Rohatgi and Kapoor, 2016)	Slightly hazardous in case of skin contact (sensitizer)
Molybdenum disulfide	It used for development latent fingerprint on non-porous wet surface	It can cause several irritations of the eyes and skin (Haque et al., 1989)

Other common development techniques as discussed in literature review (section 1.6.6). Titanium dioxide, however, is a white inorganic compound and it is most important widely used in the industry as a white pigment. In addition, it has a higher refractive index than other white pigments (Yang et al., 2004). Furthermore, titanium dioxide for drug delivery have been investigated (Liang et al., 2011, Signoretto et al., 2011, Park et al., 2014, Jia and Kerr, 2013). A previous study (Reynolds et al., 2008) reported that titanium dioxide regularly used in the development of latent fingerprints on dark surfaces, as it contrasts very well, is non-hazardous and nontoxic (Helmus et al., 2008, Pigments, 2008). Titanium dioxide also has a number useful properties such as optical (absorbs ultraviolet light) and photocatalytic ability (it can show photocatalytic activity under ultraviolet light) (Choi et al., 2007, Chen and Mao, 2007). Furthermore, according to literature titanium dioxide is effective for enhancement of bloody prints (Bergeron, 2003) and on wet surfaces. On the other hand, some of chemical substances, which have been used to detect fingermarks, have drawbacks such as high background interference, high toxicity and pose potential health and environment hazards, *e.g.* Congo red is a Group 1 carcinogen (Afkhami and Moosavi, 2010). Therefore, a novel powder for developing latent fingerprints may be used in order to try to minimise these issues, this study has proposed a new fingerprint visualisation powder based on the naturally occurring positively charged polysaccharide chitosan which is cheap, readily available, non-destructive (Islam et al., 2007) and non-toxic (Aramwit et al., 2015). In the previous chapter, seven ratios formulations of CS: TPP microparticles (6:1, 4:1, 2:1, 1:1, 1:2, 1:2, 1:4 and 1:6), were prepared according to ionotropic gelation procedure in a four different acetate buffers (AB-10, AB-11, AB-12 and AB-13). In this chapter, these formulations are optimisation using a 2^3 factorial factor design, with 8 experiments (in triplicate), to

analyse the effects of the three selected factors (pH, ionic strength and CS: TPP ratio), in order to design particles of defined properties for latent fingerprint visualization on glass microscope slide (non-porous surface) and on paper (porous surface). Lipids in fingerprints residue have an important role in forensic science investigations (Girod and Weyermann, 2014). This study will explore capacity of CS: TPP microparticles to associate organic lipid residues in fingerprints for forensic applications. Fingerprints were aged and stored under laboratory conditions, and the effectiveness of a CS: TPP microparticle enhancement method was assessed, following the methodology outlined in (Sears et al., 2012). Moreover, the purpose of using four different conditions of chitosan at various ratios was to find out the optimum conditions of attachment of microparticles to the ridges of latent fingerprints/fingerprint.

4.2 Materials

All the materials that used in this chapter were described in Chapter 3 Section 3.3.

4.3 Factorial design experiment

The experimental design applied in this study. The effect of three different parameters on the ability of chitosan microparticles properties to enhance latent fingerprints were evaluated using a 2^3 factorial design composed of three factors (**Table 4.2**). These factors including: pH value, ionic strength, and CS: TPP ratio were selected as independent variables and set at two levels each (upper and lower). The quality of fingerprint were response parameter or the dependent variable (Y4).

Table 4.2: Parameters used in the factorial design.

Factors	Symbol	Lower level (-)	Upper level (+)
pH value	X ₁	3.8	4.8
Ionic strength	X ₂	0.2	0.4
CS: TPP ratio	X ₃	1:1	2:1

		Assessment quality fingerprint (Fairley et al., 2012)
Dependent variables	Y ₄	4: Over 2/3 clear ridge detail, which is similar to green magnetic powder (Figure 4.1)
		3: Between 1/3 and 2/3 clear ridge detail
		2: Less than 1/3 clear ridge detail
		1: Very few visible ridges, poor quality
		0: No evidence of fingerprint

Assessment of fingermark development quality is basically dependent on an individual's background and experience (Fritz et al., 2015). Additionally, a subjective scale depends on the opinion of the fingerprint examiner to competently identify ridge details (minutiae) (Pounds et al., 1990, Stoilovic, 1993, Wallace-Kunkel et al., 2007, Humphreys et al., 2008) also they are dependent on the scale used (Becue et al., 2009, Fairley et al., 2012, Pulsifer et al., 2013). Previous studies have reported that the evaluation of the quality of a fingermark is difficult due to the subjectivity of the currently used grading systems (Pulsifer et al., 2013) and that these rely entirely on visual assessment. In the original Bandy scale to obtain top a grade of 4, this requires "a full development - whole mark clear with continuous ridges" (Bandey and Gibson, 2006), 3 requires "more than two thirds of marks continues ridges" which can be used for identification, 2 requires about one third to two thirds of the ridge detail, 1 requires signs of contact but without ridge detail. Therefore, it is possible to imagine two or more fingermarks being given the same grade, but not necessarily showing the same level of detail. However in other studies only over two thirds clear ridges details are required for a top grade of 4 (Fairley et al., 2012), and the fingerprint should be usable to identify a person from that fingerprint. The subjective grading system of Bandy is more coarse in comparison to the updated objective grading system presented (Fairley et al., 2012). In this study, following on from (Fairley et al., 2012), the fingermark development was assessed based on clarity ridge detail (de la Hunty et al., 2014), therefore a score of 4 represents over two thirds clear ridge details and can be characterised as potentially identifiable marks. Also, fingermarks with a grade of 3 or 2 may be described as visible fingerprints, whereas finger marks which grade of 1 can be termed as poor quality or very few visible marks (**Table 4.2**). In the present

study, the effectiveness of a development technique can be evaluated in collating and averaging the grade of the fingermarks. When evaluating and comparing methods a high proportion grade of 4 would indicate that the method was performing well (Fairley et al., 2012).

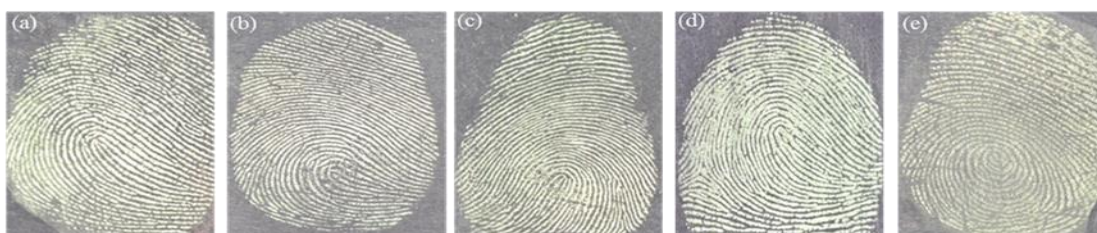


Figure 4.1: Latent fingerprint development using green magnetic powder consisting of iron (I,II) oxide as a control. (a) Donor 1, (b) donor 2, (c) donor 3, (d) donor 4 and (e) donor 5.

4.4 Experimental

4.4.1 Microparticle preparation (CS: TPP)

Following preparation of chitosan, TPP and CS: TPP microparticles at different ionic strengths and pH values (Acetate buffers AB-10 to AB-13) as described in section 3.4.1.3. Buffers AB-10, AB-11, AB-12, and AB-13 were chosen as they have previously been used in model validation in chapter 3 and cover a good range of pH and ionic strength.

4.4.2 Samples preparation and fingermarks development

Two different approaches were used in the experiments. The first approach, was whole fingermarks depletions. Natural latent fingermark were collected from five

donors during the study period. Donors (males and female aged 33-47 years) were asked not to wash their hands for at least thirty minutes prior to fingermark deposition, and rubbed their hands together. This allowed passable fingerprint residue to distribute over fingers, and minimises variability (Sears et al., 2012). Glass microscope slides were used as a “typical” non-porous surfaces during the experiments. The glass slides were washed with detergent and warm water, cleaned with ethanol, to remove any contaminations such as fat soluble or water soluble, and then left to dry prior to deposition (Bacon et al., 2013). Donors were asked to deposit fingermarks using their right thumb (except donor 3 who deposited their left thumb due to an injury to their right thumb) in positions 1, 2, 3, 4, 5 and 6 on glass microscope slides containing the odd numbered fingermarks in a depletion on the left and the even numbered fingermarks on the right, this will be referred to as stage 1. This was repeated but reversing the development process order used on the odd and even numbered fingermarks, referred to as stage 2 (**Figures 4.2**) (Sears et al., 2012, Bandey and Gibson, 2006).

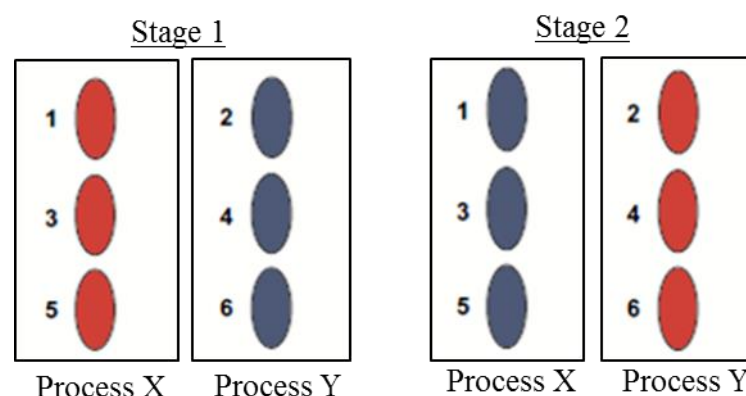


Figure 4.2: Schematic representation depletion method (first approach) (Sears et al., 2012, Bandey and Gibson, 2006).

After deposition, the fingerprints were aged for one day before development, due to the fact that fingerprints found at crime scenes are typically around one day old (James et al., 1991b). Three techniques have been used to develop latent fingerprints: a spray method, suspended chitosan particles in solution and powder method in order to investigate which method is more effective and sensitive for detecting latent fingerprints.

4.4.2.1 First technique (spray)

- 1- Fingerprints deposited on glass slides were sprayed with chitosan solutions using AB-10 at different ratios, slides were then placed in drying oven for 5 minutes at temperature 60 °C.
- 2- TPP solutions using AB-10 with red dye at different volumes were then sprayed on each slide. It was applied five times to confirm the results.
- 3- Steps 1 and 2 were repeated for chitosan and TPP solutions using different acetate buffers (AB-11, AB-12 and AB-13).

4.4.2.2 Second technique (microparticles in solution)

- 1- Fingerprints deposited on glass slides were immersed into the seven working solutions of CS: TPP ratios (AB-10) at 6:1, 4:1, 2:1, 1:1, 1:2, 1:4 and 1:6, for 30 min, 1 hour, 2 hours and 3 hours.
- 2- Slides were then dried at room temperature. It was applied five times to confirm the results.

- 3- Steps 1 and 2 have applied for chitosan microparticles using different acetate buffers (AB-11, AB-12 and AB-13).

4.4.2.3 Third method (microparticles as powder)

The 28 CS: TPP microparticle mixtures prepared using buffers AB-10, AB-11, AB-12 and AB-13 were precipitated by centrifugation (Thermo Fisher scientific - Heraeus biofuge primo R) at 8500 rpm for 60 minutes and then supernatant (liquid) was discarded. The recovered microparticles (remaining solid) were washed three times using deionised water, followed by freeze drying for 24 hours (Alpha 1e4 LD2 freeze drier (Martin Christ GmbH, Osterode am Harz, Germany)). Deposited prints were developed with seven different chitosan particles ratios of CS: TPP (6:1, 4:1, 2:1, 1:1, 1:2, 1:4 and 1:6) formulation for each acetate buffer (AB-10, AB-11, AB-12 and AB-13). The process was repeated five times per formulation (**Figure 4.3**). To confirm these results a further split depletion series (second approach) consisting of six latent fingermarks made by the deposition of prints of three fingers (index, middle and ring finger) from each of the donors were applied as described in section 4.4.2.3.1.



Figure 4.3: An example of CS: TPP particles at ratio of 2:1 using buffer AB-12.

In addition, to further investigate different surfaces, fingermarks were collected from donors on the paper (porous surfaces), then aged for one day and developed using chitosan microparticle powder as described earlier.

4.4.2.3.1 Split print depletion series

- 1- Five donors were asked not to wash their hands for at least thirty minutes before fingermark deposition and they rubbed their fingertips together prior to deposition to minimise variability and distribute sweat evenly in all ridges. To determine the relative sensitivity and limitation of the method, six split depletion series (second approach) of fingermarks were obtained by requesting that each donor deposit fingermarks on the middle of two clean glass microscope slides side-by-side from the index, middle and ring fingers of right hand. The fingermarks were aged for one day before developing (**Figure 4.4**) (Sears et al., 2012).
- 2- Then each fingermark was split into halves. One half slide print of the depletion (left) was developed with CS: TPP at 2:1 ratio using AB-10, while the other half slide print (right) was developed with different CS: TPP at 1:1 ratio using AB-10 for comparison. These two formulations were chosen as they gave satisfactory results in initial experiments (section 4.5.1).
- 3- Step 2 was repeated for CS: TPP at 2:1 and 1:1 ratio using different acetate buffers including AB-11, AB-12 and AB-13. The process was repeated ten times for each of the eight formulations per donor's finger. Bisected slides were placed side by side and imaged together.

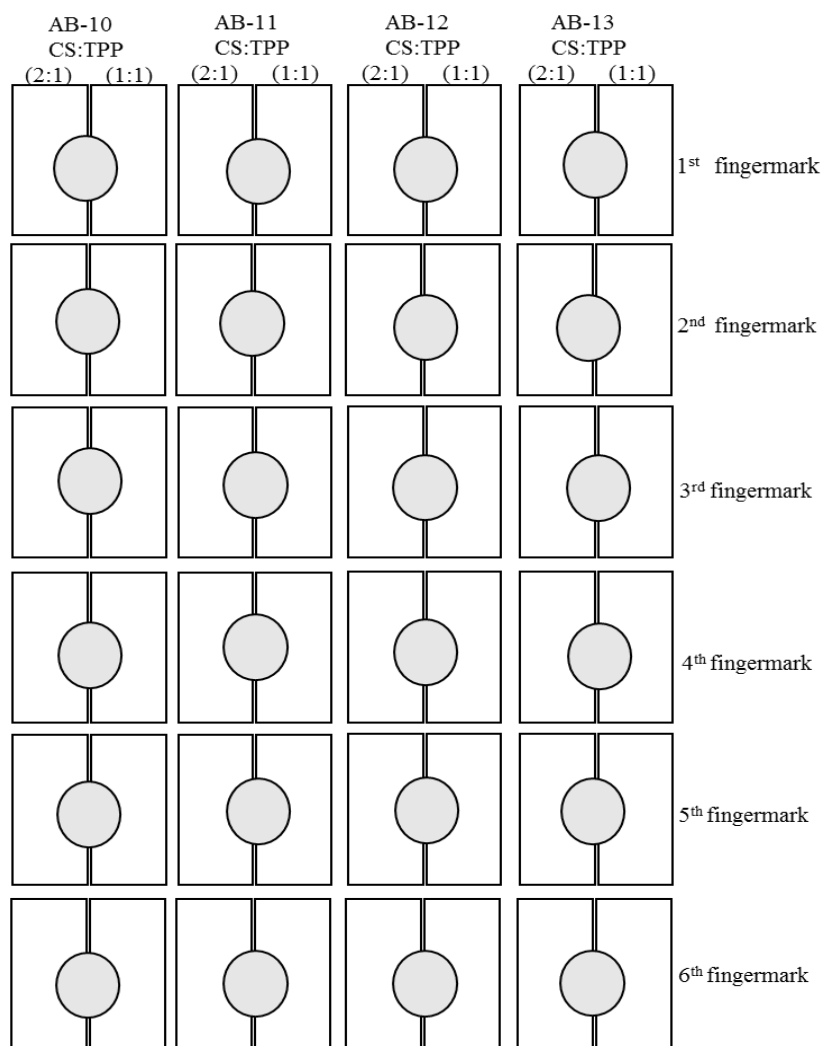


Figure 4.4: Schematic representation of the deposition of a fingerprints the split depletion series (second approach) for four different acetate buffers (AB-10, AB-11, AB-12 and AB-13) at CS:TPP ratios of 2:1 and 1:1 (two techniques per four formulations).

For the aged latent fingerprints study, latent fingerprints deposited in split depletion were collected from each donor (index, middle and ring fingers of their right hand) on cleaned glass microscope slides fingerprints as described earlier and were stored (variable humidity and temperature 20 – 25 °C) for 7 and 14 days respectively in an open tray on the lab bench, where the windows kept closed at all times. Then each fingerprint was split into halves, and the first half (left) was aged for 7 days whereas

the other half (right) was aged for 14 days. Both halves were then developed with chitosan particles as powder CS: TPP at 2:1 in buffer (AB-12).

4.4.3 Photography of Samples

All fingermark samples were visually evaluated and imaged using a Nikon D3100 digital camera (Tokyo, Japan), equipped with an AF-S Micro-NIKKOR 60 mm lens and the camera was mounted on Firenze Mini Repro tripod. Samples, were photographed using a shutter speed of 1/30 seconds, focus mode of AF-S and an ISO sensitivity of Auto. The photographic plane of camera was parallel to the plane of fingermark, and the same angle of incidence, sample positioning and camera aperture. In addition, optical microscopy examination was conducted with two different microscopes (Leica stereo low powered microscope EZ4HD, and Leica high powered microscope DM 500, ICC50 HD) using the same intensity of lighting; Leica LAZ software for image manipulation (Leica Microsystems, Milton Keynes, UK).

4.4.4 Scanning electron microscopy (SEM)

The surface microparticle morphology was characterised using scanning electron microscopy (SEM). The developed fingerprints on glass slides were coated using a Quorum 7920 Sputter coater (Quorum Industries, Laughton, UK) by a thin layer of gold-palladium alloy, before placing onto aluminium stubs using carbon impregnated double sided adhesive tape. The images were obtained using a JEOL JSM 6060 LV Scanning Electron Microscope (Oxford instruments, Abingdon, UK) using the Back Scattered Electron mode at a beam accelerating voltage of 10 kV and under high vacuum. Accelerating voltage was chosen to improve surface sensitivity and obtain

high quality images (Bacon et al., 2013), powdered chitosan microparticles were mounted on aluminium stubs using double sided carbon adhesive tape attached to stub and coated in the same method as described earlier. Scanning electron microscope refers to the surface of the sample by examining it using a beam of electrons of high energy. Backscattered electrons are produced as a result of interaction between the atoms and the electrons and they carry information about the topography of the surface of the sample.

4.5 Results and discussion

The ridge deposits of a fingerprint comprise a complex mixture of natural secretion residues, such as fatty acids, cholesterol, triglyceride and amino acids (Bramble, 1995, Scruton et al., 1975). Lipids on the skin surface come from sebaceous glands (Nicolaidis, 1974). Functionalised nanoparticles have drawn great interest over the last decade in forensic science to detect and as visualising reagents for latent fingerprints (Sametband et al., 2007, Becue et al., 2007). The fingerprints evaluated in these study were aged for 1 day prior to development when preliminary examinations were being conducted, and then for 7 days and 14 days during subsequent comparative studies. The first visualisation technique evaluated fingerprints left on 28 glass microscope slides. Chitosan as solution (AB-10, AB-11, AB-12 and AB-13) were sprayed on to the glass slides, then TPP as solution (AB-10, AB-11, AB-12 and AB-13) was sprayed. This technique did not work for any ratio (**Figure 4.5a**). The second technique was chitosan microparticles in acetate buffer solutions. The fingerprints were immersed into the different microparticle dispersions, removed from the solutions 30 minutes, 1, 2 and 3 hours later, and dried at room temperature. No clear ridges of prints were obtained. As a consequence, using all ratios as a solution, this technique has not yielded any satisfactory results (**Figure 4.5b**).

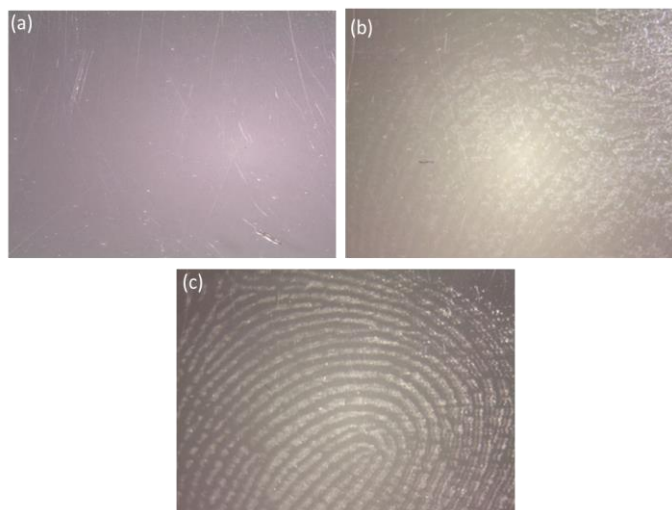


Figure 4.5: An examples of latent fingerprint (donor 1) on glasses slides with different development method utilised, (a) first technique (spraying method), (b) second technique (particles in solution method) and (c) third technique (powder method) (n= 5).

Both techniques (first and second) were unsuccessful, this could be due to low concentrations of chitosan (0.013% - 0.143%) and therefore only limited chitosan microparticles were available and could attached or provide coverage of the lipid residues in latent fingermark. This observation is similar to previous study which reported at low concentrations of chitosan (0.2% - 0.6%) poor quality fingerprints were obtained (Islam et al., 2007). In addition, in the same study it was demonstrated that at higher concentrations of chitosan (> 1.0 %) might cause high viscosity which leads to increased resistance to the flow of chitosan in furrows (between ridges fingermarks) and resulted in a thin chitosan layer over the whole fingermark area, which obscures the ridge details (Islam et al., 2007) and reinforces the importance of particle viscosity in fingermark visualisation. Moreover, in acidic media, some components such as proteins or amino acid within a fingermark can be protonated (Gao et al., 2009, Choi et al., 2008) and therefore become positively charged and will

repulse positively charged chitosan microparticles. As a result, chitosan microparticles were not deposited onto fingerprint ridges. An alternative approach, latent fingerprint developed using third technique (chitosan microparticles as a powder) on glass microscope slides; obtained results which were better than first and second techniques (**Figure 4.5c**). Therefore, this method was used in further studies. However, fingerprints on paper (porous surface), which was developed using CS: TPP powder at ratio of 2:1 in buffer AB-12 was unsuccessful, this is most likely due to the paper absorbing fingerprint residues (**Figure 4.6**). Therefore, the third technique could be sufficient or valid to use on non-porous surfaces (**Figure 4.5c**).



Figure 4.6: An example of development of latent fingerprint (donor 1) on paper using third technique (powder method) (n=5).

4.5.1 Proposed mechanism for interaction

Many researchers have investigated the ability of CS: TPP microparticles to associate with organic compounds such as peptides and proteins for pharmaceutical applications (Hu et al., 2008). However, they have not been widely considered in forensic applications (Il Dueik and Morris, 2013) and it is proposed that chitosan microparticles, which have long carbon chains, deposit on to fingerprints due to the

lipophilic interactions with the lipid residues in fingerprint ridges. Polycationic chitosan molecules with long carbon chains forms an ionotropic gel with the TPP polyanion which results in partially lipophilic microparticles. Then van der Waals interactions occur between the lipophilic (hydrophobic) ends of long carbon chain and the lipid residues of the latent fingerprint (**Figure 4.7**) (Islam et al., 2007). In addition, lipid residues in fingermarks have partially negative charge, whilst CS: TPP microparticles surfaces have positive charge, which can be controlled depending on processing conditions. Therefore, the binding of the chitosan microparticles with lipids may be facilitated by electrostatic and lipophilic interactions and hydrogen bonding (Muzzarelli, 1996, Wydro et al., 2007). Latent fingerprints developed using third technique (chitosan microparticles as a powder) on glass microscope slides (non-porous surface) obtained satisfactory results (although this depends on the pH, ionic strength and CS: TPP ratio at which these particles were prepared). This technique relies on the chitosan microparticles in the fingerprint powder adherence to the oily component of the skin ridge deposits. The effectiveness with which the powder adheres to the ridge depends on the factors such as viscosity, particle size and the charge on the particles (Sodhi and Kaur, 2001).

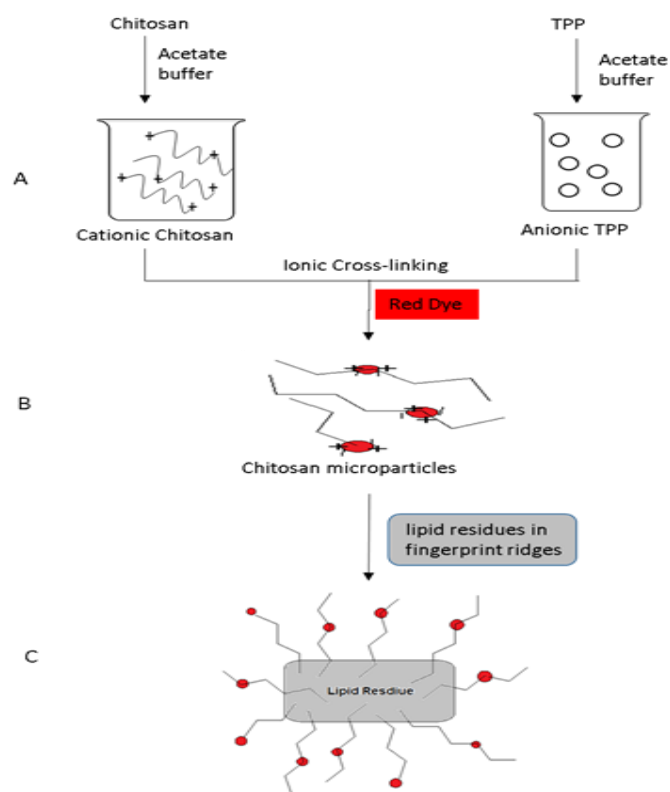


Figure 4.7: Schematic representation of third technique (A) chitosan carbon chains with ionic ends and TPP anions (B) chitosan polycations attraction with TPP polyanions making them lipophilic (C) the hydrophobic (lipophilic) ends of long carbon chains from chitosan microparticles burying themselves into the lipid residues of the latent fingerprint (Islam et al., 2007).

A previous study was conducted using silver nanoparticles which slowly deposited on water insoluble component of sweat, resulted in a black or dark grey print (Burow et al., 2003). This technique is sensitive, however, some forensic laboratories have limited using this technique on a routine basis (Jaber et al., 2012) due to its disadvantages such as solution instability, complexity, and often poor contrast (Becue et al., 2007, Burow et al., 2003, Cantu et al., 2003). Another studies (Stauffer et al., 2007, Schnetz and Margot, 2001) used gold nanoparticles stabilised by citric acid, followed by modification with a physical silver developer. At low pH, gold nanoparticles adhered to fingermark residues due to ionic interactions between

negative charged of gold particles and positive charged of fingerprints component residue (Choi et al., 2006). When using the same finger to deposit fingerprints sequentially the composition of the first deposition mark is different to the second mark, which is different to the third mark and fourth mark *etc.*, this is known as a depletion series (Bandey and Gibson, 2006).

This investigation (third technique) used chitosan microparticle powders prepared using buffers AB-10, AB11, AB-12 and AB-13 at all seven CS: TPP ratios at 6:1, 4:1, 2:1, 1:1, 1:2, 1:4 and 1:6. The results were analysed according to quality of detected fingerprints and sensitivity of the method. The quality of the fingerprint development on seven glass microscope slides (non-porous surface) were first evaluated by visual observation. The results demonstrated that CS: TPP ratios of 2:1 and 1:1 showed ridges than other ratios. Therefore, these ratios (6:1, 4:1, 1:2, 1:4 and 1:6) were withdrawn from the further investigations. Observations of each of the eight developments per donor using CS: TPP at 1:1 and 2:1 ratio as a powder on glasses microscope slides after preparation in the four different acetate buffers: AB-10, AB-11, AB-12 and AB-13 are shown in **Figures 4.8** and **4.9**. The variation in the degree of ridge detail development between donors might be explained in terms of variations in the amount components of deposited residue in latent fingerprints being secreted by different donors (Ramasastry et al., 1970, Downing and Strauss, 1974), also differences in contact time, angle and pressure (Girod et al., 2012, Cadd et al., 2015). Previous studies have reported that the latent residues or the quantity of material deposited, depend on factors such as age (Ramasastry et al., 1970, Buchanan et al., 1997), deposition force (Jasuja et al., 2009), gender (Asano et al., 2002), or diet (Croxtton et al., 2010), the nature of the receiving surface, environment conditions, and the method used in the development of the fingerprints, and it is inevitable for

experimental results involved in fingerprints to reveal some degree of variation (Sauzier et al., 2013). There were a number of fixed parameters in this study:

- all fingerprints collections were made on the same non porous surface (glass microscope slides)
- the forces applied during deposition were carefully controlled throughout the experiments
- dusting was performed under the same environmental conditions
- the same method was used in their development.

The microparticles aggregate on the fingerprint ridges due to lipophilic and electrostatic interactions between the chitosan microparticles and the lipid residues of the latent fingerprints (Choi et al., 2008). These interactions rely on parameters which will be discussed later. In terms of CS: TPP ratios at 2:1 and 1:1, the 1:1 is not best for a good deposition of chitosan microparticles onto the fingerprints (**Figure 4.8**), and all of fingerprints ridges could not be seen clearly using any of four different chitosan microparticles irrespective of the buffer. Although chitosan microparticles cover some of the fingerprint area, there is not enough ridge details for adequate identification (grade 1). Therefore, this method (CS: TPP ratio at 1:1) could not be accepted for identification work.

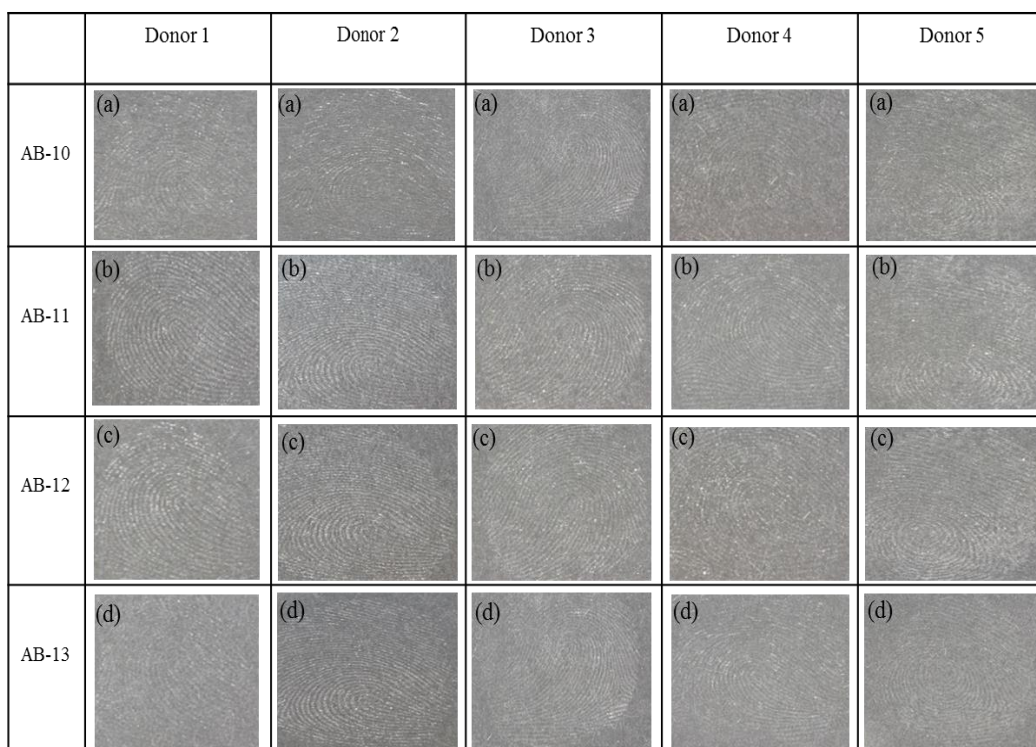


Figure 4.8: Development of first depletion latent fingermarks of CS: TPP at 1:1 ratio as a powder on glass microscope slides (Naked eye) for five donors, using (a) AB-10 (b) AB-11 (c) AB-12 and (d) AB-13. All are poor quality (grade 1) (n=10).

However, as shown in **Finger 4.9**, when latent fingermarks were developed using the buffers (AB-10, AB-11, AB-12 and AB-13) for chitosan microparticles at ratio of 2:1. The images of fingermarks using AB-12 of chitosan microparticle (**Figure 4.8c**) were clear enough and have significant details for comparison and could be used for identification and produced grade 4 fingermarks.

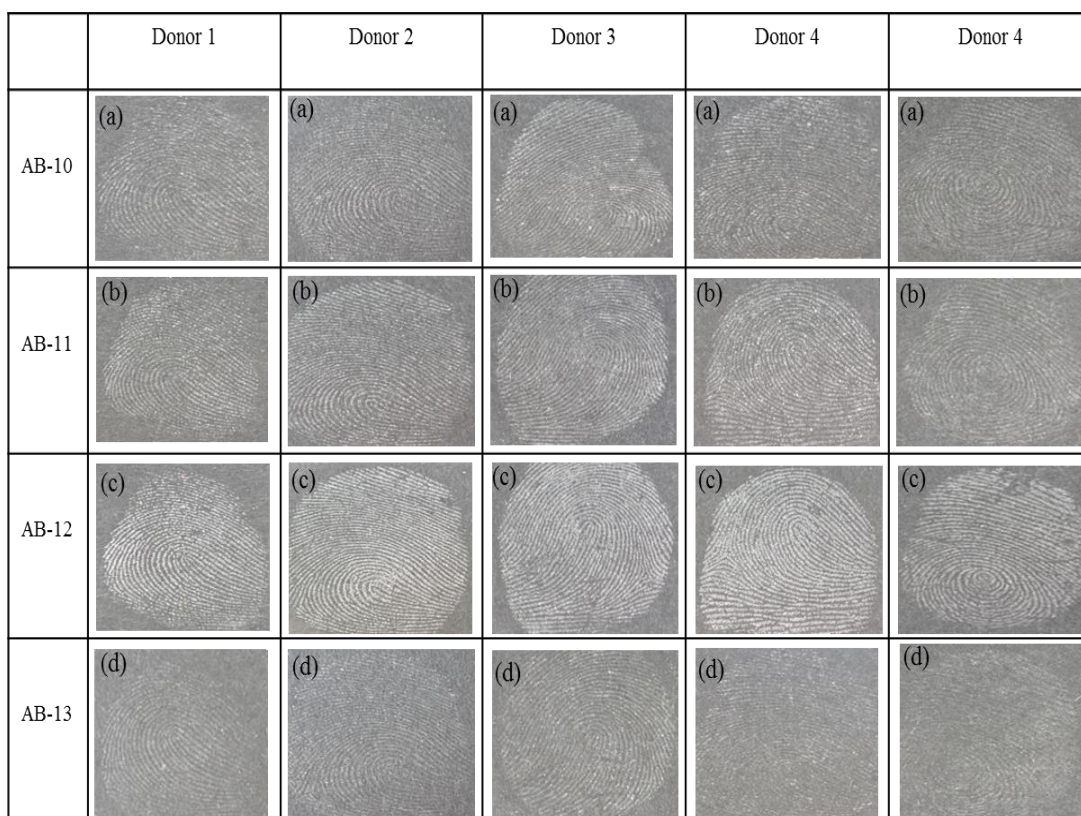


Figure 4.9: Development of first depletion latent fingerprints of CS: TPP at 2:1 ratio as a powder on glasses microscope slides (Naked eye) for five donors, using buffers (a) AB-10 (grade 2) (b) AB-11 (grade 3) (c) AB-12 (grade 4) and (d) AB-13 (grade 1) (n=10).

Additionally, latent fingerprints developed using AB-12 (pH = 4.8 and I.S = 0.2 M), CS: TPP ratio at 2:1 are shown in **Figure 4.9c** and had high capability to enhance the fingerprints for all donors (grade 4). It is thought that these microparticles adsorb more onto the ridges as a result of lipophilic and electrostatic interactions. **Figure 4.10** shows an example of two differences in the development of fingerprint residue by different chitosan microparticles in a depletion series (first approach, section 4.4.2) which had high proportions of grades (3 and 4). As can be seen in **Figure 4.10** that the stage 1 of CS: TPP ratio at 2:1 in buffer 12 (depletions of 1, 3 and 5) and CS: TPP ratio at 2:1 in buffer 11 (depletions of 2, 4 and 6) there is a sequential reduction in

development quality as the deposited fingerprint residue depletes. This is due to decreases in the amount of fingerprint residues on the finger throughout the series. The same observations were seen in stage 2 when repeated but development processes reversed, so that CS: TPP ratio at 2:1 in buffer 11 (depletions of 1, 3 and 5) and the CS: TPP ratio at 2:1 in buffer 12 (depletions of 2, 4 and 6). These observations were consistent with all donors (**Figures 4.10 - 4.13**). The depletion series describes the relative sensitivity or effectiveness of a technique and examination of whole or split fingerprints. Results obtained from 5 donors could give a realistic indication of the method. In addition, a CS: TPP ratio of 2:1 in buffer AB-12 can detect fingerprints until the third depletion, whereas CS: TPP ratio at 2:1 in buffer AB-11 technique can only detect fingerprints until second depletion. This is might be different surface charges on particles which leads to different attractions.

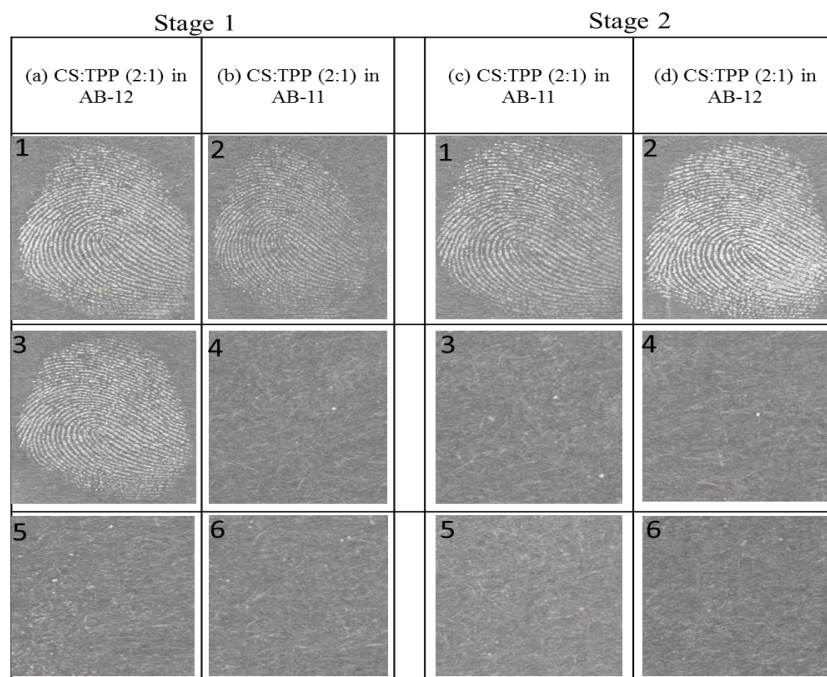


Figure 4.10: Development fingerprints depletion series (donor 1). Stage 1 using CS:TPP at 2:1 (a) in buffer AB-12 (left column), (b) in buffer AB-11 (right column). Stage 2 repeated but development reversed (c) in buffer AB-11 (left column), (d) in buffer AB-12 (right column).

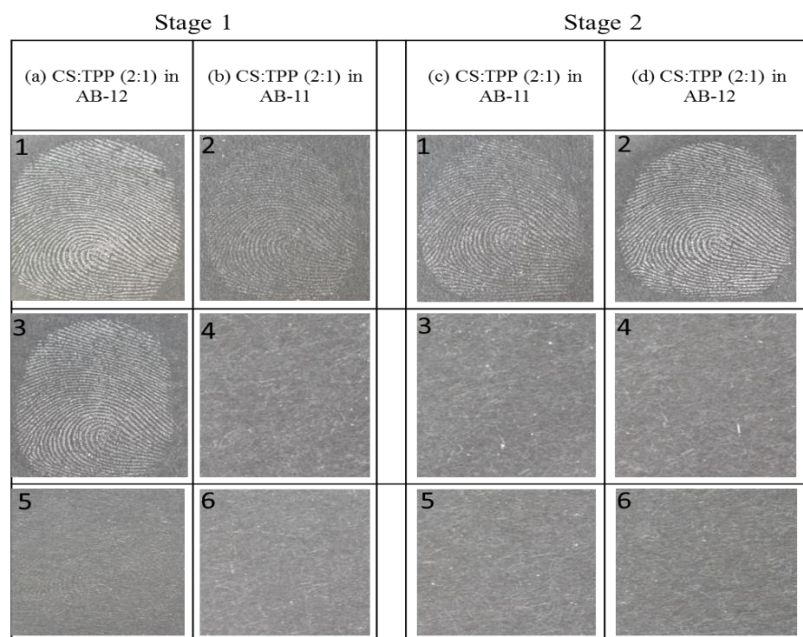


Figure 4.11: Development fingermarks depletion series (donor 2). Stage 1 using CS:TPP at 2:1 (a) in buffer AB-12 (left column), (b) in buffer AB-11 (right column). Stage 2 repeated but development reversed (c) in buffer AB-11 (left column), (d) in buffer AB-12 (right column).

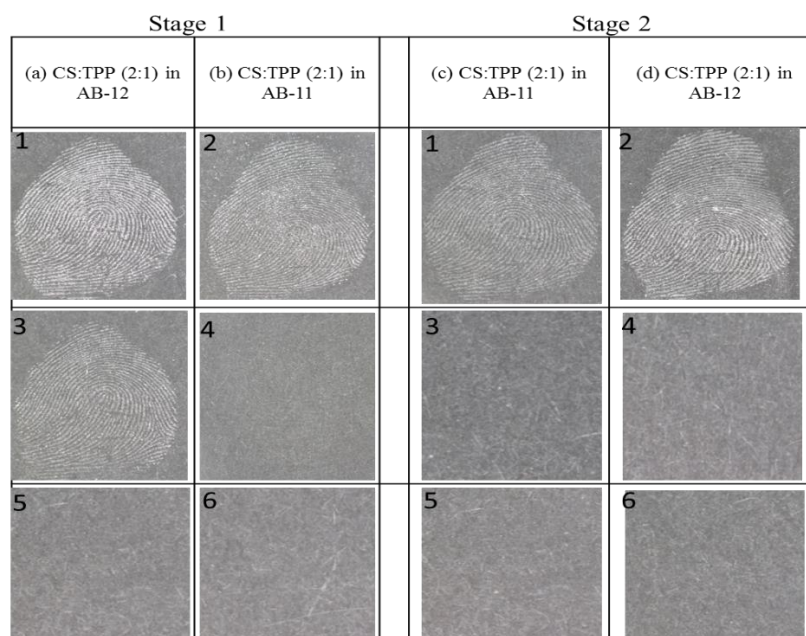


Figure 4.12: development fingermarks depletion series (donor 3). Stage 1 using CS:TPP at 2:1 (a) in buffer AB-12 (left column), (b) in buffer AB-11 (right column). Stage 2 repeated but development reversed (c) in buffer AB-11 (left column), (d) in buffer AB-12 (right column).

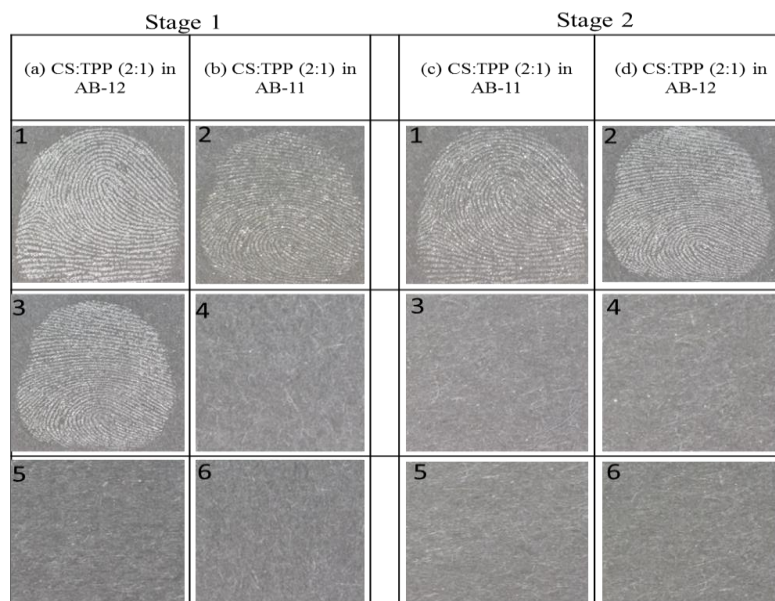


Figure 4.13: development fingermarks depletion series (donor 4). Stage 1 using CS:TPP at 2:1 (a) in buffer AB-12 (left column), (b) in buffer AB-11 (right column). Stage 2 repeated but development reversed (c) in buffer AB-11 (left column), (d) in buffer AB-12 (right column).

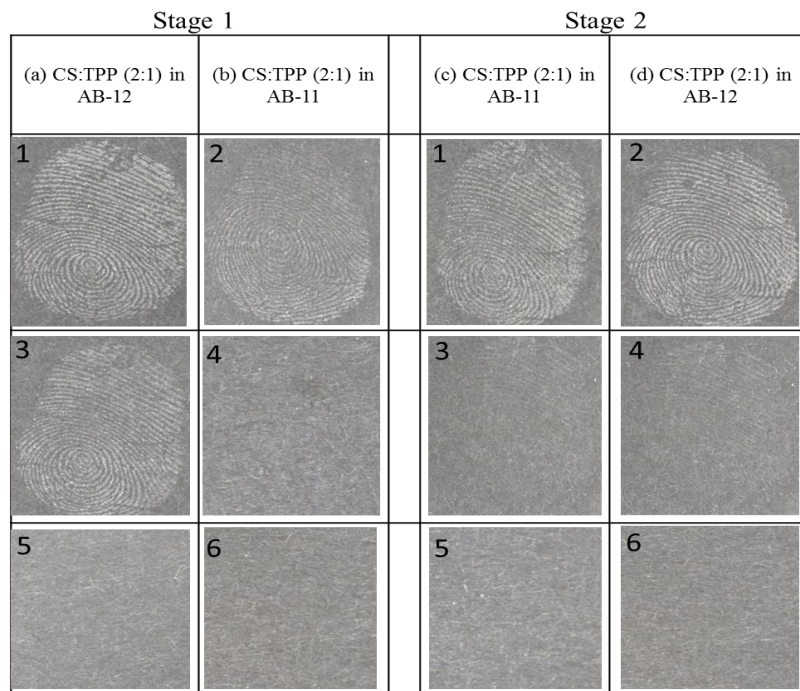
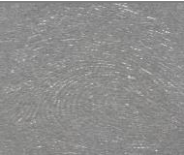









Figure 4.14: Development fingermarks depletion series (donor 5). Stage 1 using CS:TPP at 2:1 (a) in buffer AB-12 (left column), (b) in buffer AB-11 (right column). Stage 2 repeated but development reversed (c) in buffer AB-11 (left column), (d) in buffer AB-12 (right column).

To confirm above results, a further split print depletion series using three fingers from each donor was performed to assess the effect of each development technique and the sensitivity of techniques on the residue fingerprints (second approach, section 4.5.4). Based on those results obtained in preliminary experiments pH, ionic strength and CS:TPP ratio were selected to find the optimised conditions to obtain the best quality fingerprint visualisation using a 2³ factorial design (**Table 4.2**). The formulations (F1 - F8) (**Figure 4.8 and 4.9**) were prepared based on the ionic gelation of positively charged amino groups of CS with TPP anions (**Table 4.3**). An important parameter in the characterization of microparticles is the surface charge of the chitosan microparticles indicated by zeta potential. A higher zeta potential may be related to stronger positive charges of the amino group (NH₃⁺) of chitosan at high level in the factorial design experiment; and the remaining amine groups (non-interacting) would be responsible for the positive zeta potential on microparticles (Zhang et al., 2004). To determine the quality level of fingerprint development; a fingerprints quality scale assessment (0 - 4) was used **Table 4.2** (Fairley et al., 2012). As shown in **Table 4.3 and Figures 4.8, 4.9**, the optimum quality fingerprint was obtained for three formulations: F5 (**Figure 4.8a**), F6 (**Figure 4.9c**) and F7 (**Figure 4.9b**). Formulation F5 (**Figure 4.9a**) had limited development and less than about one third of ridge details were present, and therefore probably could not be used for identification purposes. While, formulation F7 (**Figure 4.9b**) had good development (grade 3) where between one third and two thirds of ridge detail were present. Finally, formulation F6 (**Figure 4.9c**) has the best development (grade 4), as more than two thirds of ridge details were present and it has the potential to be used for identification purposes (Rohatgi and Kapoor, 2016).

Table 4.3: Characteristics of the chitosan microparticles obtained by the factorial design 2^3 for different formulation F1 to F8. Fingerprint quality was assessed using chitosan microparticles on glass microscope slides

Formulation code	Dependent variables			Independent variables, mean \pm SD (N = 3)				Fingerprint image (Donor 2)
	X ₁ : pH	X ₂ : LS	X ₃ : CS:TPP Ratio	Y ₁ : relative viscosity ^a	Y ₂ : zeta potential (mV) ^a	Y ₃ : particle size (μ m) D _[4,3] ^a	Y ₄ : average fingerprint quality ^b (Grade)	
F1 (AB-10)	3.8(-)	0.2(-)	1:1(-)	1.11 \pm 0.01	11.8 \pm 0.9	111 \pm 3	1	
F2 (AB-12)	4.8(+)	0.2(-)	1:1(-)	1.03 \pm 0.01	9.7 \pm 0.5	135 \pm 2	1	
F3 (AB-11)	3.8(-)	0.4(+)	1:1(-)	1.00 \pm 0.01	10.0 \pm 0.7	121 \pm 2	1	

F4 (AB-13)	4.8(+)	0.4(+)	1:1(-)	1.02 ± 0.01	9.0 ± 0.5	158 ± 8	1	
F5 (AB-10)	3.8(-)	0.2(-)	2:1(+)	1.07 ± 0.01	19.0 ± 1.5	135 ± 6	2	
F6 (AB-12)	4.8(+)	0.2(-)	2:1(+)	1.09 ± 0.01	14.3 ± 1.1	171 ± 4	4	
F7 (AB-11)	3.8(-)	0.4(+)	2:1(+)	1.04 ± 0.01	17.0 ± 0.6	146 ± 5	3	
F8 (AB-13)	4.8(+)	0.4(+)	2:1(+)	1.06 ± 0.01	10.3 ± 0.3	194 ± 11	1	

^aChapter 3.

^bY4: Assessment quality fingerprint: (Fairley et al., 2012)

All the chitosan microparticle formulations are positively charged, but the values of charges for F5 (**Figure 4.9a**), F6 (**Figure 4.9c**), and F7 (**Figure 4.9b**) (14.3 - 19.0 mV) are higher than those of the other formulations (9.0 - 11.8 mV). The ionic strength of solution in formulation F7 (**Figure 4.9b**) was at a higher level (**Table 4.3**) and caused an increase in quality of fingerprint compared to F5 (**Figure 4.9a**). Moreover, with an increased ionic strength at 0.4 M, the ammonium ions (NH_3^+) on the chitosan molecules are more shielded by acetate ions (CH_3COO^-) leading to a decreased zeta potential (charge). Increased zeta potential diminished the electrostatic repulsion between the chitosan particles. In general, quality fingerprint increased with increased positive zeta potential (**Table 4.3**) and those samples with a zeta potential of less than +12 mV F1 (**Figure 4.8a**), F2 (**Figure 4.8c**), F3 (**Figure 4.8b**), F4 (**Figure 4.8d**) and F8 (**Figure 4.9d**) produced prints of poor quality (1 on the Fairley scale) (Fairley et al., 2012). Of the three formulations which produced fingerprints of better quality F6 (**Figure 4.9c**) was the best performing (fingerprint quality of 4) and as this sample has a lower zeta potential than both F5 (**Figure 4.9a**) and F7 (**Figure 4.9b**) this suggests that the overall charge on the particles is not the only factor which affects fingerprint quality and that other interactions such as van der Waals interactions with lipid residues of the latent fingerprint are also important, as well as hydrogen bonding (Muzzarelli, 1996, Wydro et al., 2007). The hydrodynamic diameter of particles were measured and this was repeated three times (same formulations) on three different days (different preparations) to produce average values of particle size, and the standard deviations are relatively small therefore particles of similar sizes, at least after suspension in buffer, can be prepared easily with little variation in size (Domingos et al., 2009, Komalam et al., 2012). F6 (**Figure 4.9c**) also had larger particle size ($171 \pm 4 \mu\text{m}$) and great viscosity than both F5 (135

$\pm 6 \mu\text{m}$) (**Figure 4.9a**) and F7 ($146 \pm 5 \mu\text{m}$) (**Figure 4.9b**), which leads to decreased surface area and van der Waals interactions between particles and therefore potentially stronger van der Waals interactions with lipid residues than either F5 (**Figure 4.9a**) or F7 (**Figure 4.9b**). Although the size range of the microparticles are greater than those which have been demonstrated to be the most effective in latent fingerprint visualisation $\sim 50 \mu\text{m}$ (Theaker et al., 2008). However, in the previous chapter the effect of temperature and stirring rates on particle size for example may improve visualisation (Chapter 3, Section 3.6).

In addition, the main (the largest) effect on quality fingerprint (Y4) is the CS: TPP ratio (**Figure 4.15a**). The fingerprint quality increases as we move from low level (1:1) to higher level (2:1) of the factor (CS: TPP ratio). However, the main effects plot also indicates that ionic strength (I.S) has negative effect on quality fingerprint. The fingerprint quality decreases when we move from the low level to the high level I.S which indicates that the net charge on the particles (zeta potential) is important, which is evident from **Table 4.3**. However, pH has no effect on quality fingerprint as the line is horizontal. In brief, an interaction plot basically reveals whether there is an interaction between two different processing conditions for a certain response in the fingerprint quality. When the lines are parallel, interaction effects are zero. The more different the slopes, the more the influence the interaction effect has on the results (Israel et al., 2014). In **Figure 4.15b** the lines of pH and ratio are parallel indicating there are no interactions between them, however the interaction between pH and ionic strength is the most significant as the lines non-parallel and cross. The lines of I.S and ratio are non-parallel indicating there are interactions between the different processing conditions. The two factors interactions are -0.5, -0.25 and 0.0 for pH*I.S, I.S*Ratio and pH*Ratio, respectively.

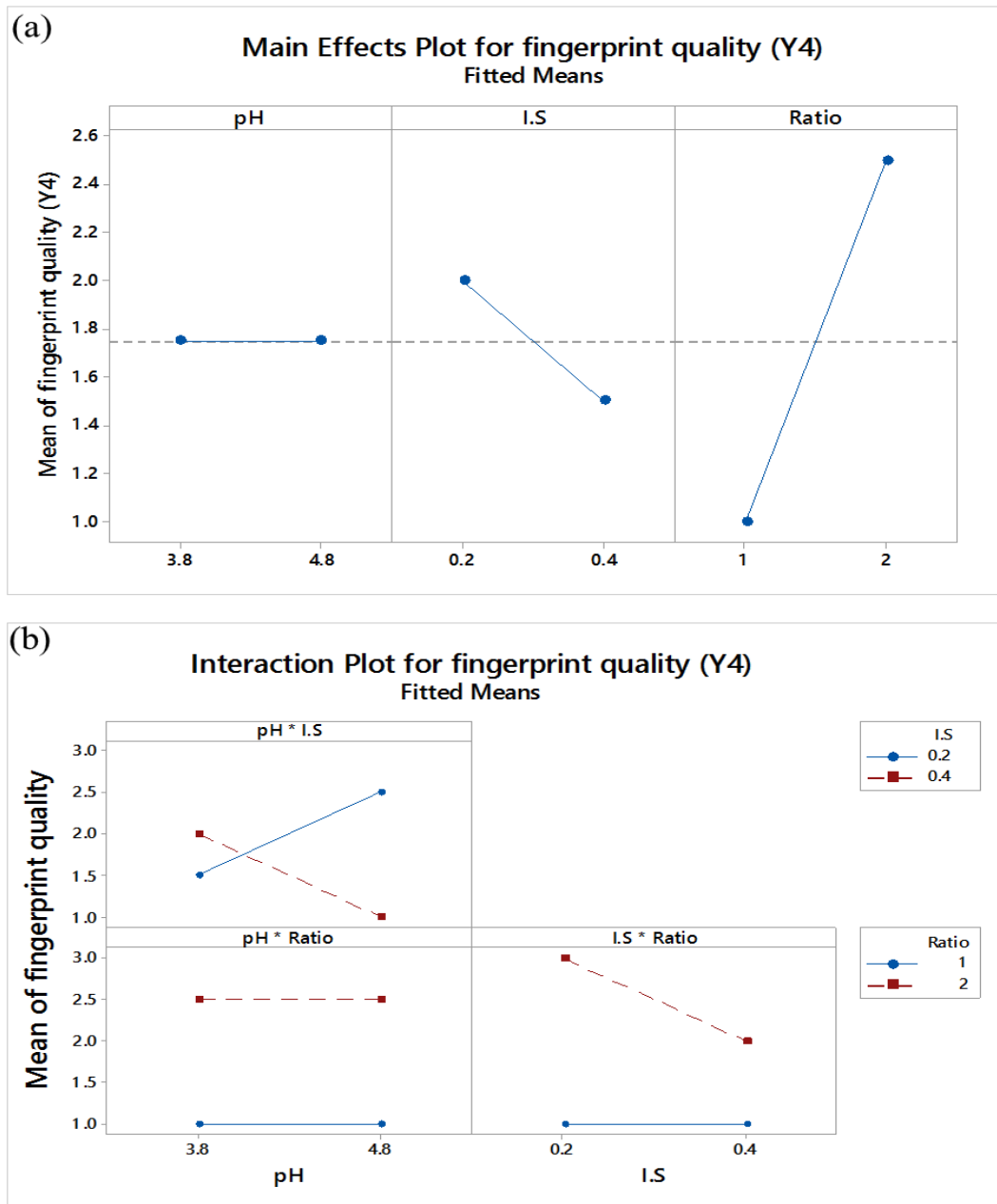


Figure 4.15: (a) The main effect plots for quality fingerprint (Y4): pH; I.S and CS: TPP ratio.

The reference line (1.75) is shown as dotted line and the steeper the slope the greater the effect of a particular parameter. (b) The interactions plot for quality finger. To visualize these effects, the Y-axis scale is always the same for each combination of factors. This graph shows that the pH*IS interaction effect is the largest.

Moreover, the attachment of CS: TPP microparticles to fingermark residues can easily be seen, and revealed clearly visible marks at 2:1 ratio in buffer AB-12 resulting in a high quality fingerprint image where fingerprints are clear enough and have

appropriate details for comparison and identification (**Figures 4.16 - 4.20**). Considering the many features that can be seen when the fingerprint is dusted with the chitosan microparticles and magnified using a low power optical microscope, there may be some potential in further evaluating these materials.

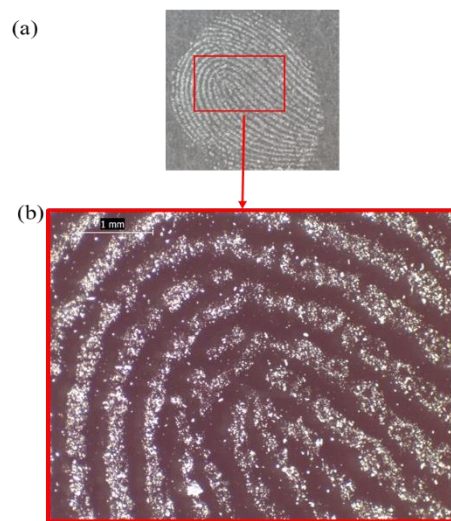


Figure 4.16: (a) A developed latent fingerprint (donor 1) on glass slide using chitosan microparticle as a powder at CS: TPP of 2:1 in buffer AB-12 (Naked eye), (b) chitosan microparticle adsorbed on fingerprint ridges under low power optical microscope, magnification 20x (grade 4).

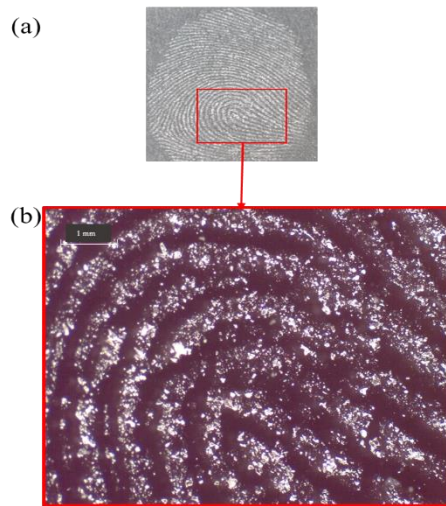


Figure 4.17: (a) A developed latent fingerprint (donor 2) on glass slide using chitosan microparticle as a powder at CS: TPP of 2:1 in buffer AB-12 (Naked eye), (b) chitosan microparticle adsorbed on fingerprint ridges under low power optical microscope, magnification 20x (grade 4).

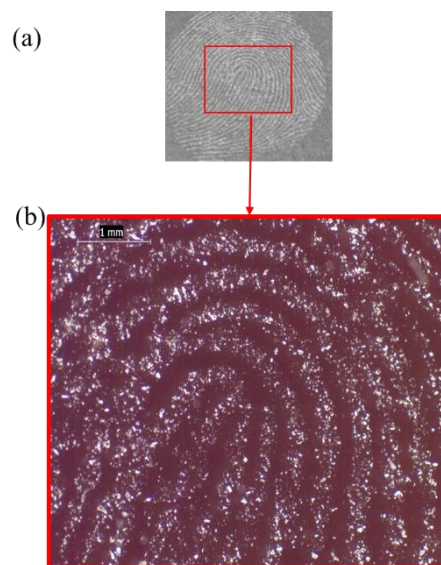


Figure 4.18: (a) A developed latent fingerprint (donor 3) on glass slide using chitosan microparticle as a powder at CS: TPP of 2:1 in buffer AB-12 (Naked eye), (b) chitosan microparticle adsorbed on fingerprint ridges under low power optical microscope, magnification 20x (grade 4).

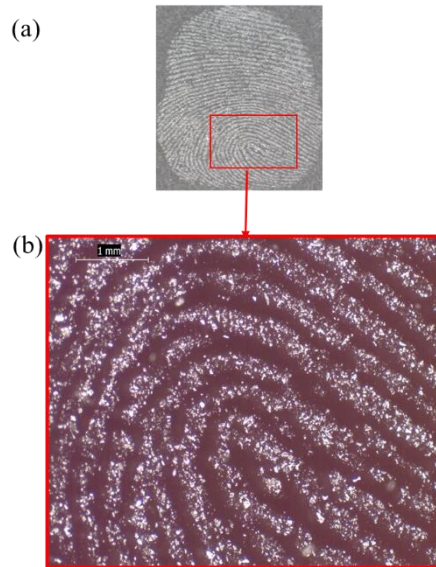


Figure 4.19: (a) A developed latent fingerprint (donor 4) on glass slide using chitosan microparticle as a powder at CS: TPP of 2:1 in buffer AB-12 (Naked eye), (b) chitosan microparticle adsorbed on fingerprint ridges under low power optical microscope, magnification 20x (grade 4).

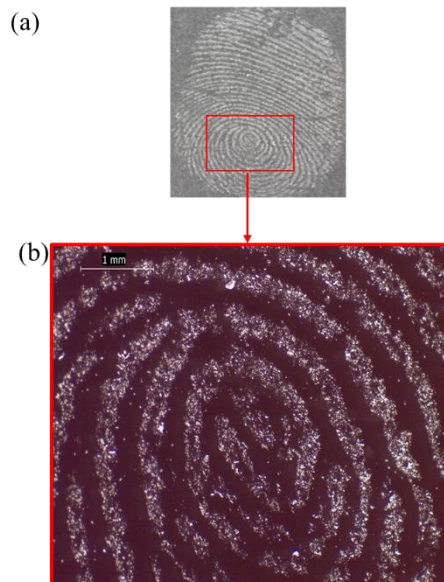


Figure 4.20: (a) A developed latent fingerprint (donor 5) on glass slide using chitosan microparticle as a powder at CS: TPP of 2:1 in buffer AB-12 (Naked eye), (b) chitosan microparticle adsorbed on fingerprint ridges under low power optical microscope, magnification 20x (grade 4).

These results are consistent to results obtained from previous study (Dilag et al., 2009), which used cadmium sulphide/chitosan nanocomposites in the powder dusting method to develop latent fingermarks on non-porous surfaces (aluminium foil). To further compare this new chitosan microparticle formulation with the green magnetic powder (control), fingermarks were split into halves after the donor's deposition on glass microscope slides, therefore that one half (right halves) were developed by green magnetic powder which consisted of iron (II, III) oxide, and the other half (left halves) were developed by CS: TPP particle at 2:1 in buffer AB-12. After development, the latent fingermarks are similar, in terms of quality, for chitosan particle method and the control green magnetic powder, with good details ridge patterns (**Figure 4.21**).

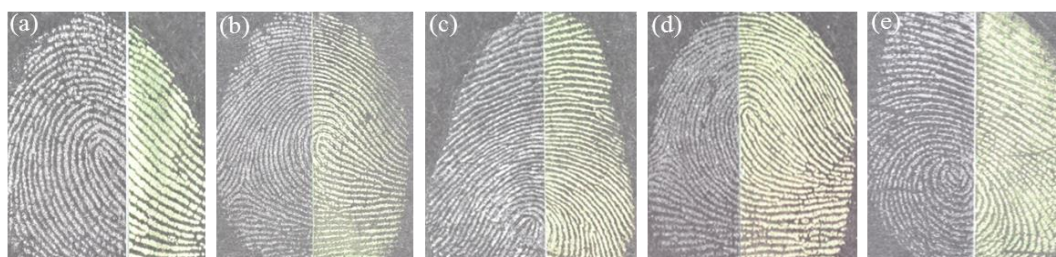
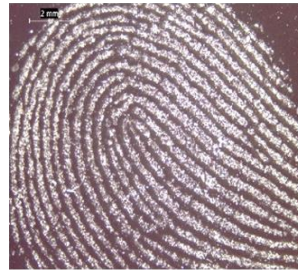


Figure 4.21: Comparison of latent fingermarks development on microscope glass slides between chitosan particles at CS:TPP of 2:1 in buffer AB-12 (left halves) and green magnetic powder as a control (right halves), (a) donor 1, (b) donor 2, (c) donor 3, (d) donor 4 and (e) donor 5.

The typical characteristics of three level features of fingermarks friction ridge developed on glass slides by CS: TPP microparticles using AB-12 at ratio 2:1 under low power optical microscope at different magnification are shown in **Figure 4.22** -

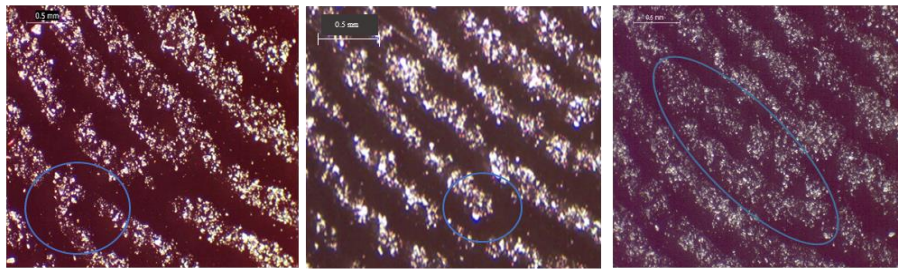
4.26. Importunately, from five donors, first-level feature describes the classification of fingerprints pattern such as loops and whorl features are distinguishable; according to literature, the general information obtained from the level one features are not conclusive (**Figure 4.22a - 4.26a**). Therefore, it cannot be used for identification. The level two features include ridge characteristics and pattern minutiae such as bifurcations, ridge ending, hook, short ridge and enclosure (**Figure 4.22b - 4.26b**). Additionally, the level three features are related to the morphology of a ridge such as pores, and incipient ridges were identifiable (**Figure 4.22c - 4.26c**). As a result level two and three features become strong identification features and can be used in fingerprint matching due to their uniqueness (Ashbaugh, 1999). From **Figure 4.22c**, magnified images of latent fingermarks developed, exhibiting level three details, such as pores. With these images captured under magnification, level two details such as fingerprint endings, ridge bifurcations and enclosures can be seen through the low power microscope(**Figure 4.22b**), and provided high evidential quality which could be used by forensic experts. Moreover, the clarity of the images was such that it is possible to use the level three details, especially the sweat pores (**Figure 4.22c**) running along the ridge pattern, which have been known to be helpful to the identification of partial or damaged fingermarks (Wei et al., 2017).

(a) Level 1 features



Loop

(b) Level 2 features

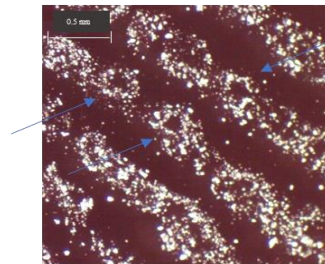


Bifurcation

Ending

Enclosure

(c) Level 3 features



Pores

Figure 4.22: Representative examples of the three levels of features on latent fingerprints developed on glass slides under low power optical microscope (donor 1) using chitosan microparticles at 2:1 in buffer AB-12. Magnification (a) 8x, (b and c) 35x.

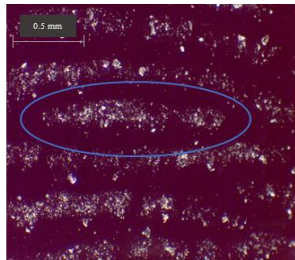
In order to confirm these results, more donors donated their fingerprints for enhancement on glass microscope slides in order to observe all three levels. As shown in **Figure 4.23** to donor 2, there are the details of short ridge, bifurcation and hook were observed (level 2 features) **Figure 4.23b**; incipient ridges were observed (level 3 features) in **Figure 4.23c** which cannot be seen with naked eye.

(a) Level 1 features

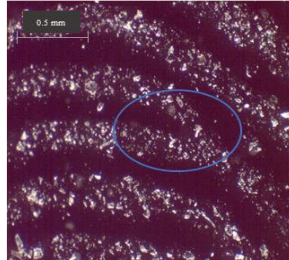


Loop

(b) Level 2 features



Short ridge

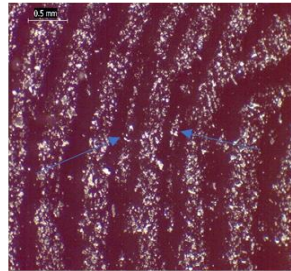


Bifurcation



Hook

(c) Level 3 features

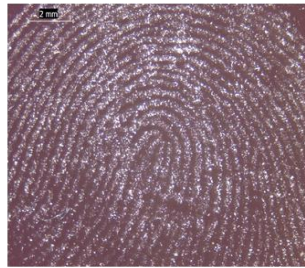


Incipient ridges

Figure 4.23: Representative examples of the three levels of features on latent fingerprints developed on glass slides under low power optical microscope (donor 2) using chitosan microparticles at 2:1 in buffer AB-12. Magnification: (a) 8x, (b and c) 35x.

Moreover, **Figure 4.24** from donor 3 showed a bifurcation, and ending and short ridge (level 2) **Figure 4.24b**, and incipient ridges (level 3) **Figure 4.24c**.

(a) Level 1 features

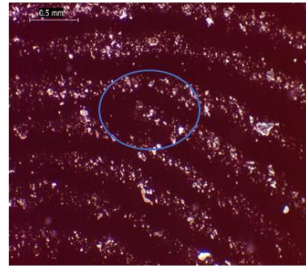


Loop

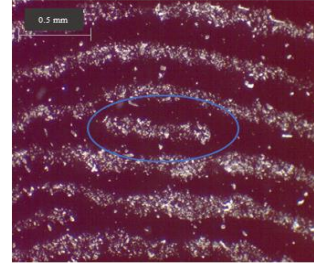
(b) Level 2



Bifurcation

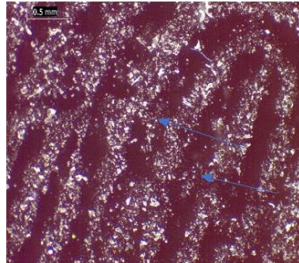


Ending



Short ridge

(c) Level 3 features



Incipient ridges

Figure 4.24: Representative examples of the three levels of features on latent fingerprints developed on glass slides under low power optical microscope (donor 3) using chitosan microparticles at 2:1 in buffer AB-12. Magnification: (a) 8x, (b and c) 35x.

Additionally, **Figure 4.25** from donor 4, showed a bifurcation, a short ridge and an enclosure (level 2) **Figure 4.25b**; incipient ridges (level 3) **Figure 4.25c** were also observed.

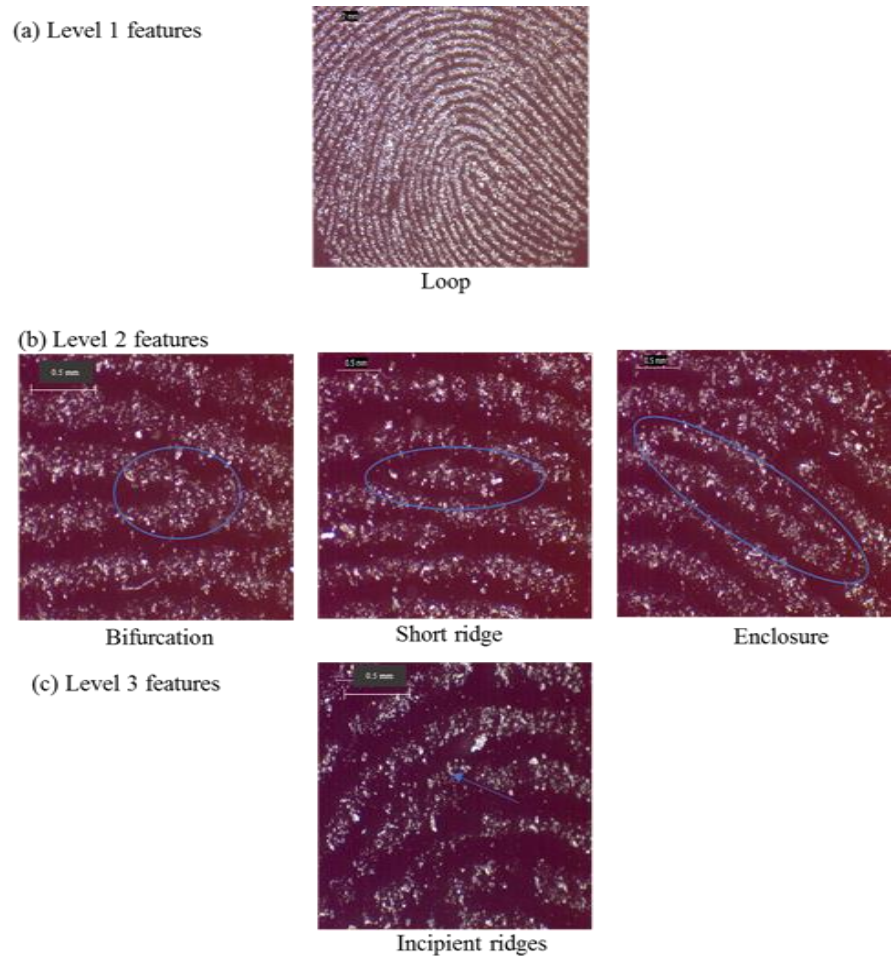
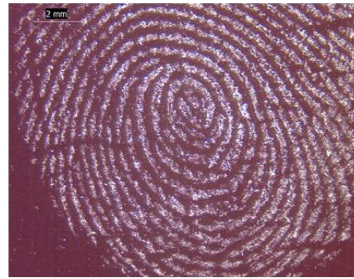


Figure 4.25: Representative examples of the three levels of features on latent fingerprints developed on glass slides under low power optical microscope (donor 4) using chitosan microparticles at 2:1 in buffer AB-12. Magnification: (a) 8x, (b and c) 35x.

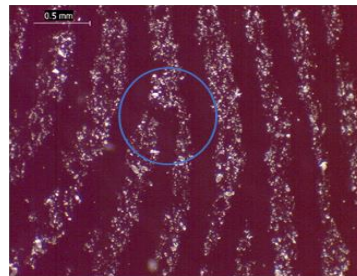
Finally, **Figure 4.26** from donor 5, shows a bifurcation and an ending (level 2) **Figure 4.26b**; pores (level 3) **Figure 4.26c** were also observed.

(a) Level 1 features

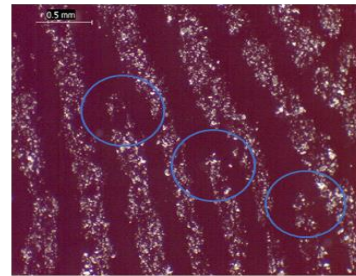


Whorl

(b) Level 2 features

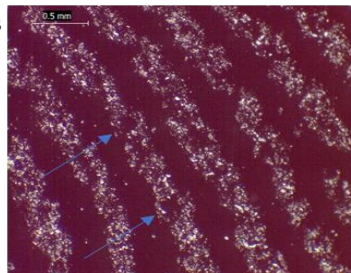


Bifurcation



Ending

(c) Level 3 features



Pores

Figure 4.26: Representative examples of the three levels of features on latent fingerprints developed on glass slides under low power optical microscope (donor 5) using chitosan microparticles at 2:1 in buffer AB-12. Magnification: (a) 8x, (b and c) 35x.

Figure 4.27 shows high power microscope images of at CS: TPP particles at 2:1 using AB-12, applied to the fingerprint in **Figure 4.9c** (donor 1). Aggregates of chitosan microparticles can be clearly seen on residues which form the fingerprint ridges and produced a grade 4 print. This may be due to lipophilic (van der Waals) interactions between alkyl groups of chitosan particles and alkyl chains of the lipid residues (Chen et al., 2009). This result is similar to previous studies (used gold

nanoparticles) with reported increases in quality of developed fingermarks with increases in the length of the alkyl groups, with the longer alkyl group chains obtaining clearer fingermarks due to increasing lipophilic interactions (Sametband et al., 2007, Choi et al., 2007).

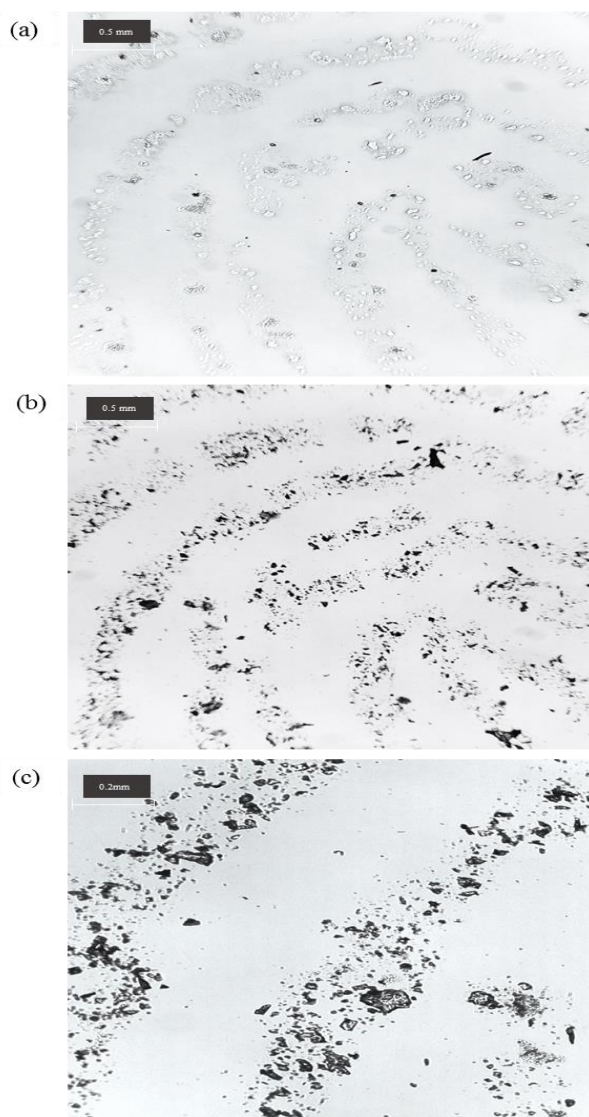


Figure 4.27: (a-c) High power optical microscope magnified images of latent fingermarks (donor 1) on glass microscope slide, (a) before development, magnification 4x, (b) after development chitosan microparticles at CS: TPP of 2:1 in buffer AB-12, magnification 4x (c) a close up view of ridges, magnification 10x shows particles adsorbed on fingermarks ridges (Sametband et al., 2007).

In order to confirm these results, more donors donated their fingermarks for enhancement on glass slides under a high power optical microscope and similar results were obtained and produced grade 4 fingermarks (**Figure 4.28- 4.31**).

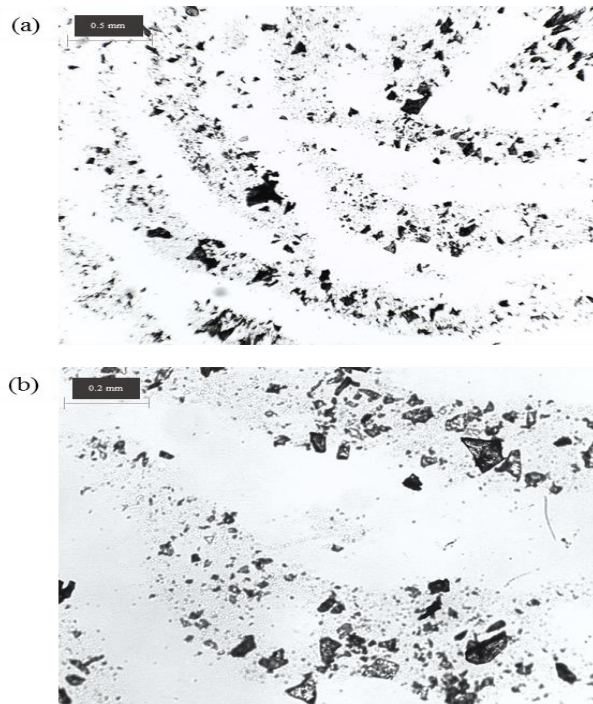


Figure 4.28: High power optical microscope images of latent fingermarks (donor 2) on glass slide; (a) development by chitosan microparticles at CS: TPP of 2:1 in buffer AB-12, magnification 4x; (b) a close up view of ridges, magnification 10x shows particles adsorbed on fingermarks ridges.

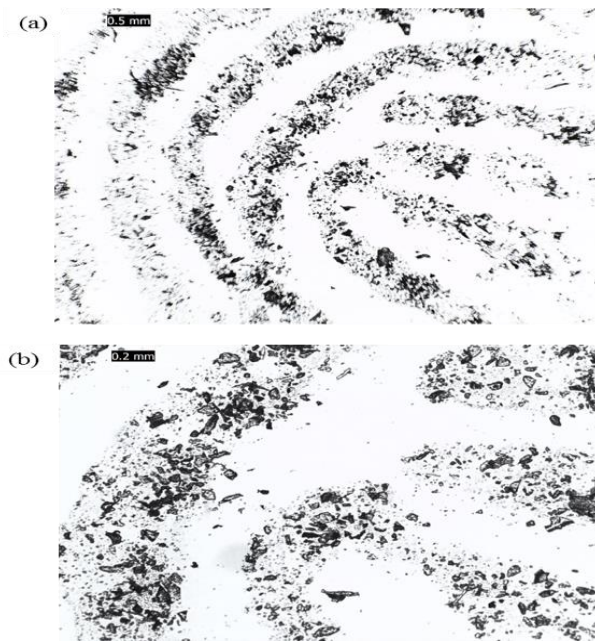


Figure 4.29: High power optical microscope images of latent fingermarks (donor 3) on glass slide; (a) development by chitosan microparticles at CS: TPP of 2:1 in buffer AB-12, magnification 4x; (b) a close up view of ridges, magnification 10x shows particles adsorbed on fingermarks ridges.

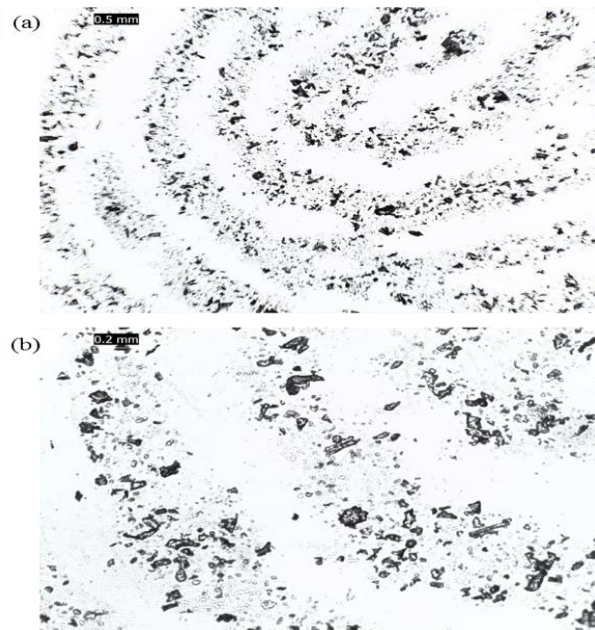


Figure 4.30: High power optical microscope images of latent fingermarks (donor 4) on glass slide; (a) development by chitosan microparticles at CS: TPP of 2:1 in buffer AB-12, magnification 4x; (b) a close up view of ridges, magnification 10x shows particles adsorbed on fingermarks ridges.

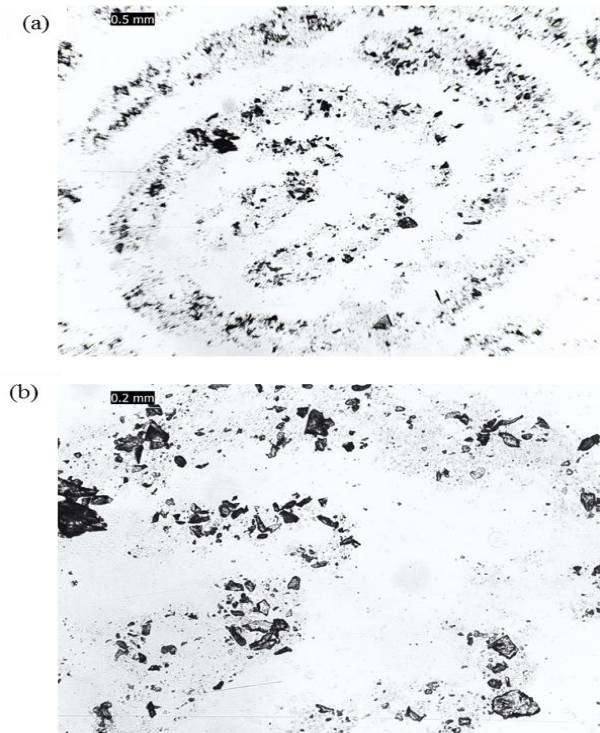


Figure 4.31: High power optical microscope images of latent fingerprints (donor 5) on glass slide; (a) development by chitosan microparticles at CS: TPP of 2:1 in buffer AB-12, magnification 4x; (b) a close up view of ridges, magnification 10x shows particles adsorbed on fingerprints ridges.

On the other hand, fingerprints treated with chitosan microparticles at CS: TPP (1:1) using AB-12 showed weaker development and produced grade 1 fingerprints (**Figure 4.32**) in comparison to those treated with chitosan microparticles at CS: TPP (2:1) using AB-12 produced grade 4 fingerprint (**Figures 4.27, 4.29 and 4.31**).

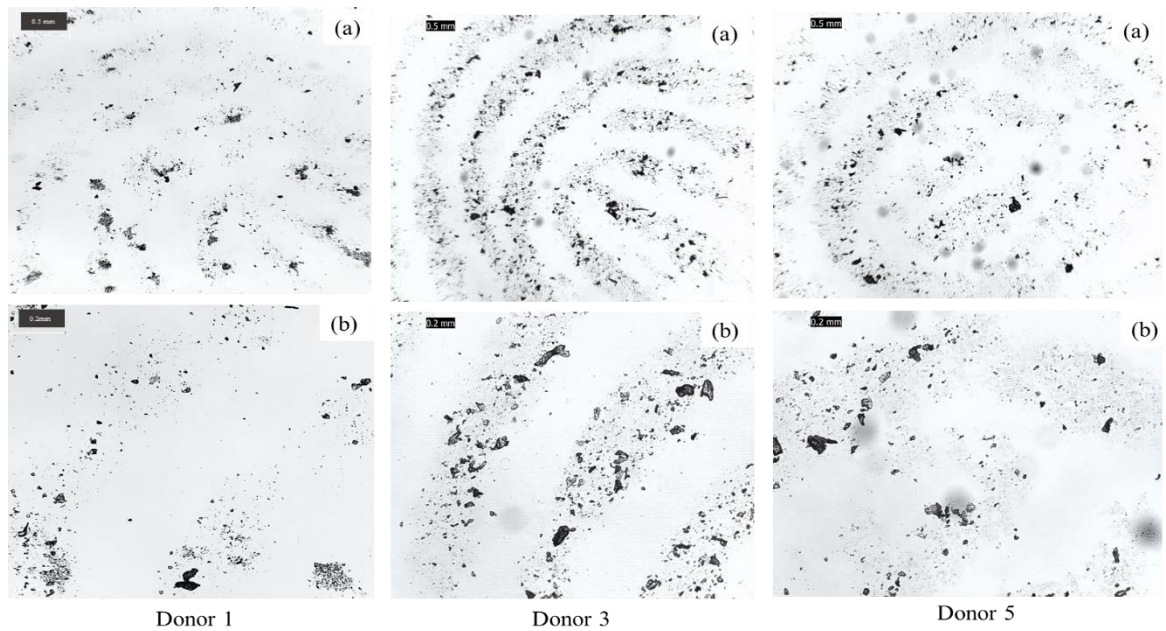


Figure 4.32: High power optical microscope images of latent fingermarks to donor 1, 3 and 5 on glass slides, (a) development by chitosan microparticles at CS: TPP of 1:1 in buffer AB-12, magnification 4x; (b) a close up view of ridges, magnification 10x.

The optical microscope is typically an appropriate technique to observe and obtain information on latent fingermark development (Moret et al., 2015). However, observations with scanning electron microscope can provide further valuable information on detailed morphology and particle attachments.

4.5.2 Scanning electron microscopy (SEM)

To further probe the previous results, scanning electron microscopy was used to examine the treated latent fingermarks. A previous study (Moret et al., 2015) reported that SEM is not suitable to study untreated fingermarks, due to sample processing preparations, including coating with a conductive layer of metal and high vacuum (to

produce a good-quality image), will lead to inevitable and uncontrollable modifications of components. These processes, either coating and high vacuum, will have destructive effects on the fingerprint residue such as evaporation of lipids (Bright et al., 2013). SEM images, **Figure 4.33 and 4.34**, show latent fingerprints deposited on the glass microscope slides developed with different chitosan microparticles from the donor 1. As can be seen in **Figure 4.33a** and **Figure 4.34a** comparison of SEM images from the ridge area of samples developed with CS: TPP at 2:1 using AB-12, and CS: TPP at 2:1 using AB-13, where it is clear that significantly more chitosan microparticles are deposited on fingerprint ridges using CS: TPP at 2:1 prepared with buffer AB-12 (**Figure 4.33a**). Moreover, the microparticles aggregate on the fingerprint ridges creating large clusters, probably due to hydrophobic and electrostatic interactions between the CS: TPP microparticles and the fatty residues of the latent print (Choi et al., 2008). On the other hand, very little chitosan microparticles were deposited between the ridges for CS: TPP at 2:1 using AB-13 (**Figure 4.34a**).

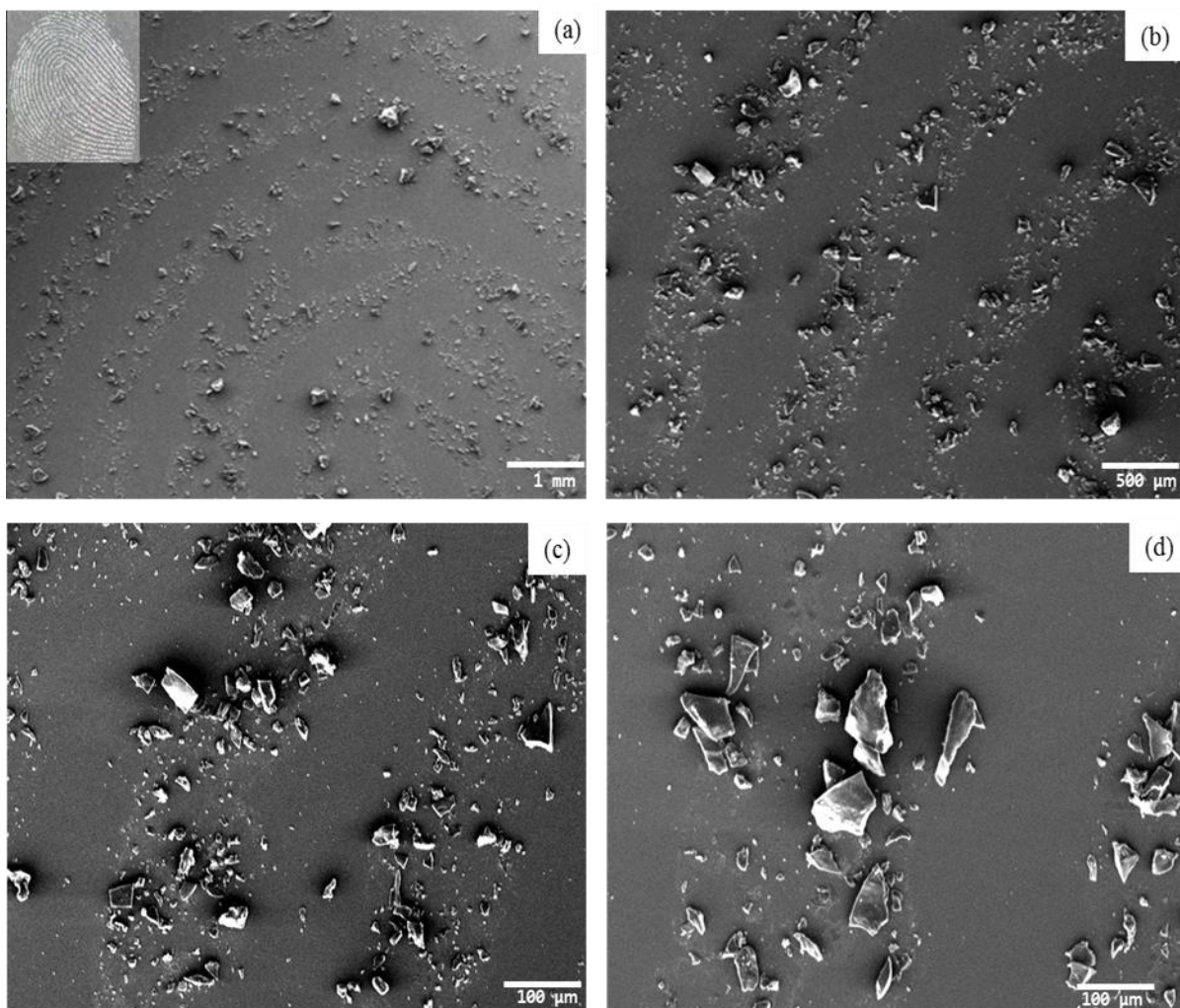


Figure 4.33: SEM images (donor 1) of fingermark development on a glass microscope slide with chitosan microparticles at 2:1 ratio in buffer AB-12; (a) magnification 22x, general overview with digital camera (inset). (b-d) Magnification 50x, 100x and 200x respectively. Representative particles adhered on ridges.

In addition, **Figure 4.33** shows a low magnification SEM image of the developed fingermark, indicating chitosan microparticles adsorbed on ridges and gave a good detail quality. By increasing the magnification, the development ridges of the fingermarks became clearer and evidence for interaction of CS: TPP microparticles is observed on the surface ridges (**Figure 4.33b, c, d**). This result could be attributed to

the particles 2:1 in AB-12 which have a relatively high surface charges which can be attracted to the lipid residue as discussed earlier. In contrast, samples developed with CS: TPP at 2:1 using acetate buffer AB-13, displayed very slight or no associated particles on the fingerprint ridges (**Figure 4.34**). Moreover, **Figure 4.34a** is an SEM image at low magnification, showing unclear developed of the fingerprint. By comparison with developed fingerprint shown in **Figure 4.33a**, limited developed fingerprint ridges. At the same magnifications, **Figure 4.34 b, c, d** display developed fingerprint ridges with no great amounts chitosan particles adsorbed. This result could be attributed to the particles of CS: TPP ratio 2:1 in AB-13 having a low surface charge (lower electrostatic interactions) which could not interact with lipid residues.

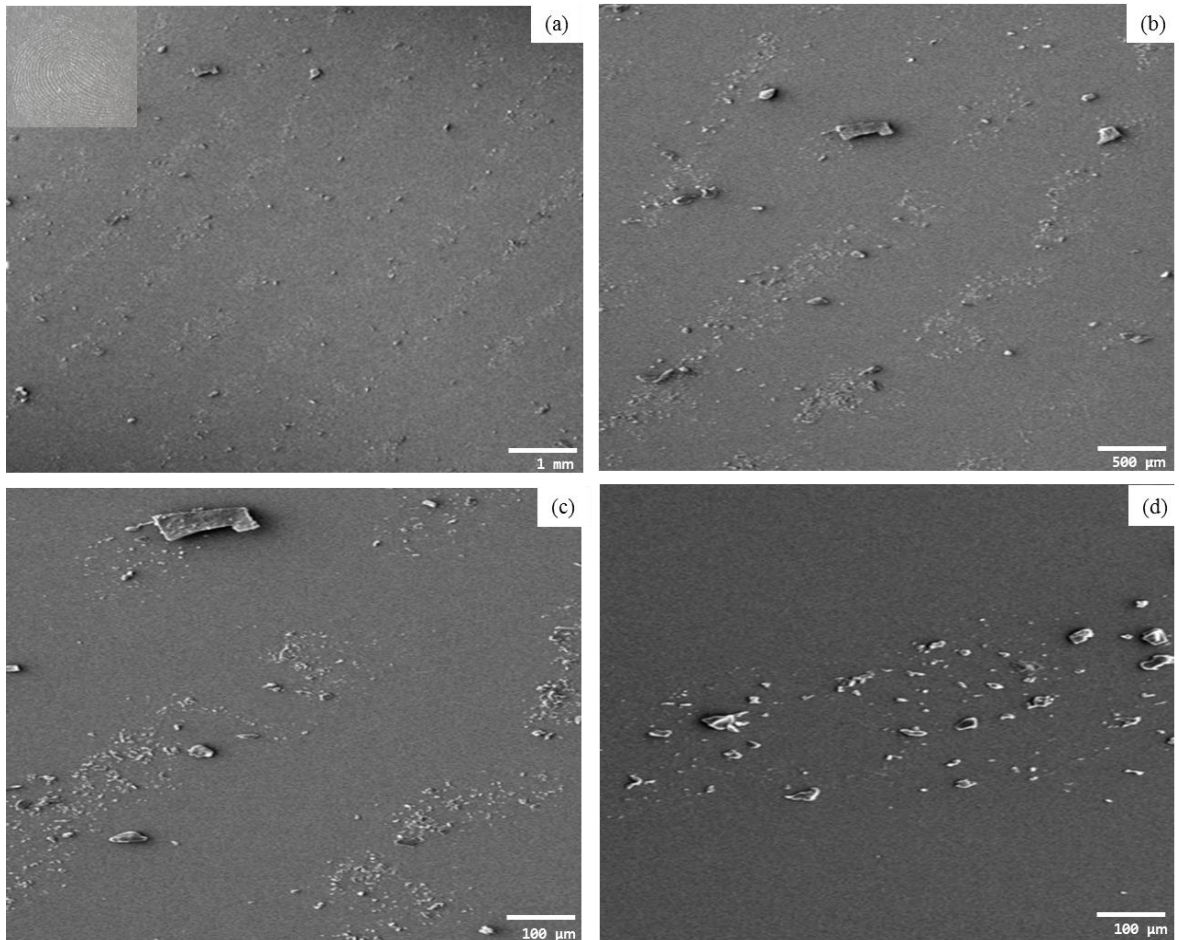


Figure 4.34: SEM images (donor 1) of fingermark development on glass slide with chitosan microparticles at 2:1 ratio in buffer AB-13; (a) magnification 22x, general overview with digital camera (inset). (b-d) Magnification 50x, 100x and 200x respectively.

Additional samples from other donors demonstrated almost the same results (**Figures 4.35 and 4.36**) for donor 2; (**Figures 4.37 and 4.38**) for donor 3, (**Figures 4.39 and 4.40**) for donor 4, (**Figure 4.41 and 4.42**) for donor 5.

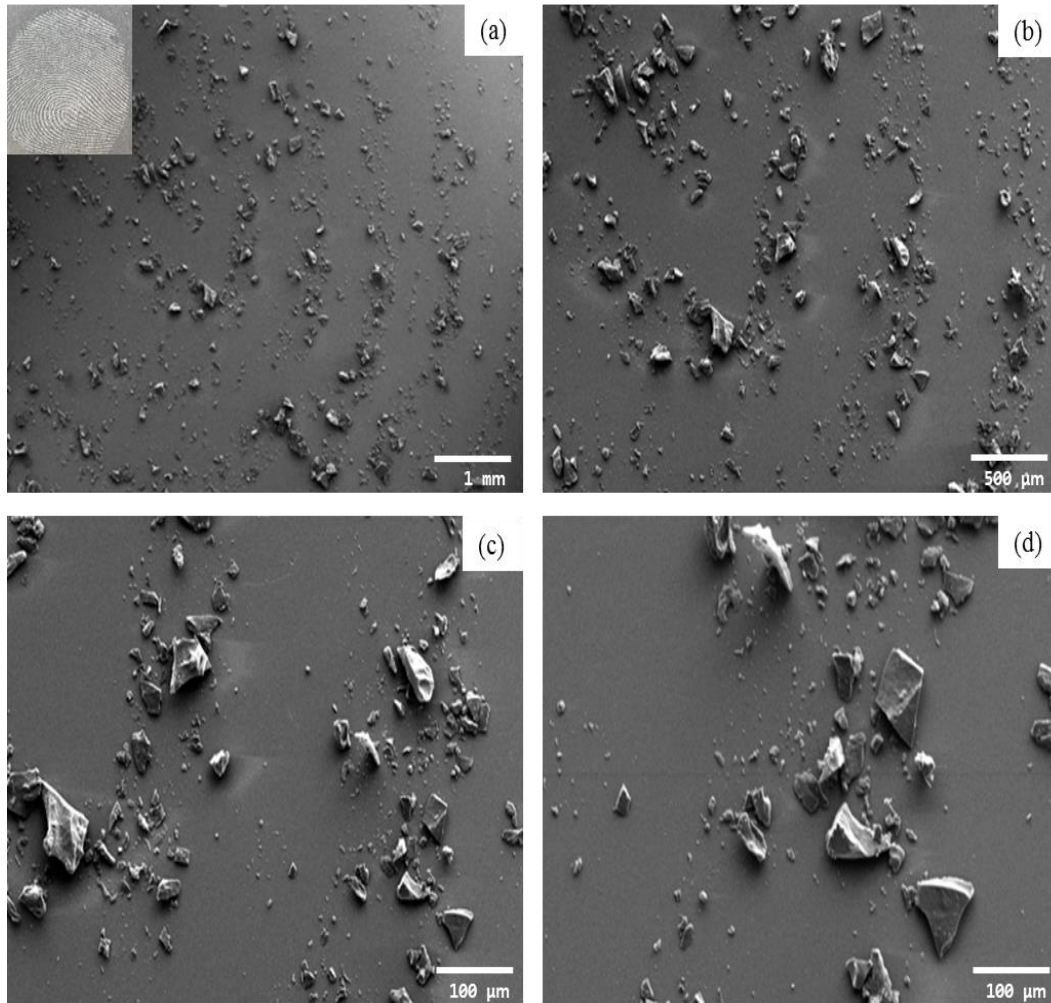


Figure 4.35: SEM images (donor 2) of fingermark development on glass microscope slide with chitosan microparticles at 2:1 ratio in buffer AB-12; (a) magnification 22x, general overview with digital camera (inset). (b-d) Magnification 50x, 100x and 200x respectively. Representative particles adhered on ridges.

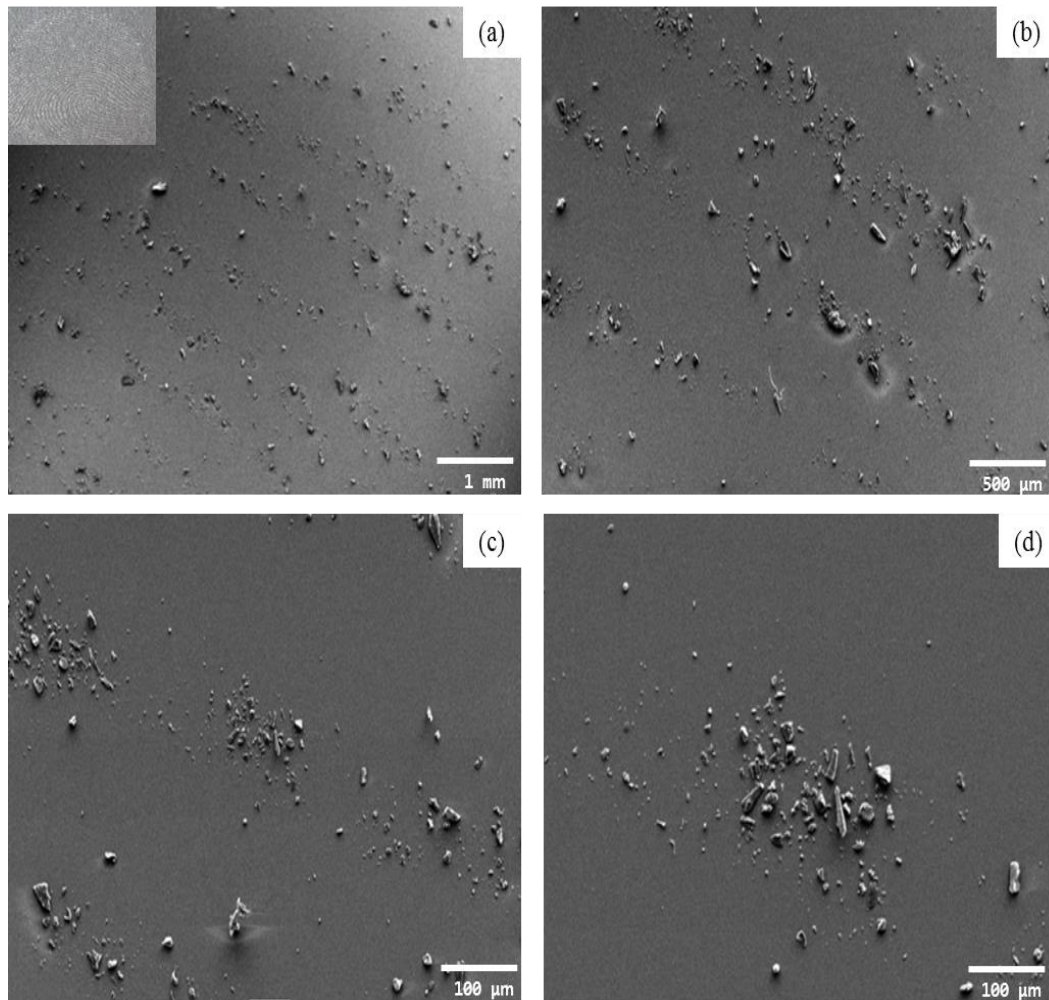


Figure 4.36: SEM images (donor 2) of fingermark development on glass microscope slide with chitosan microparticles at 2:1 ratio in buffer AB-13; (a) magnification 22x, general overview with digital camera (inset). (b-d) Magnification 50x, 100x and 200x respectively.

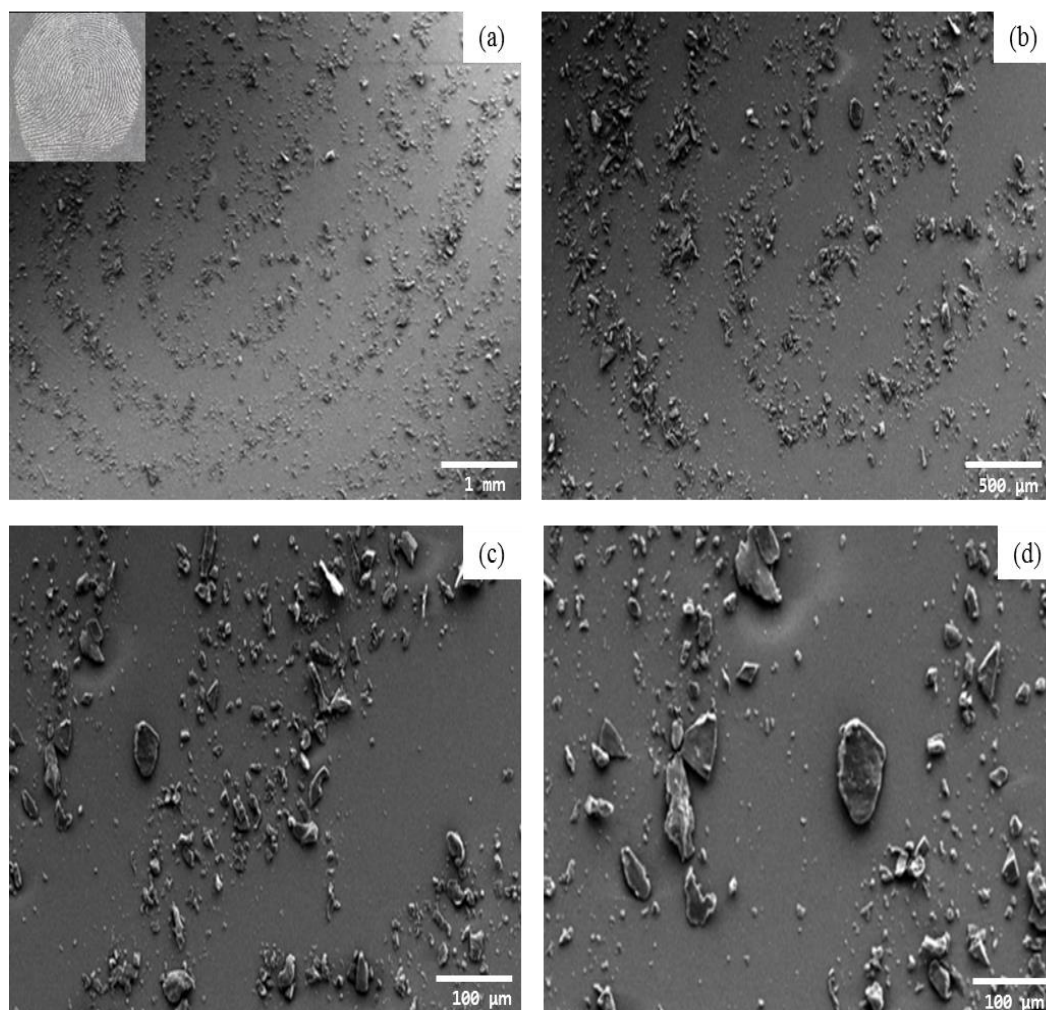


Figure 4.37: SEM images (donor 3) of fingermark development on glass microscope slide with chitosan microparticles at 2:1 ratio in buffer AB-12; (a) magnification 22x, general overview with digital camera (inset). (b-d) Magnification 50x, 100x and 200x respectively. Representative particles adhered on ridges.

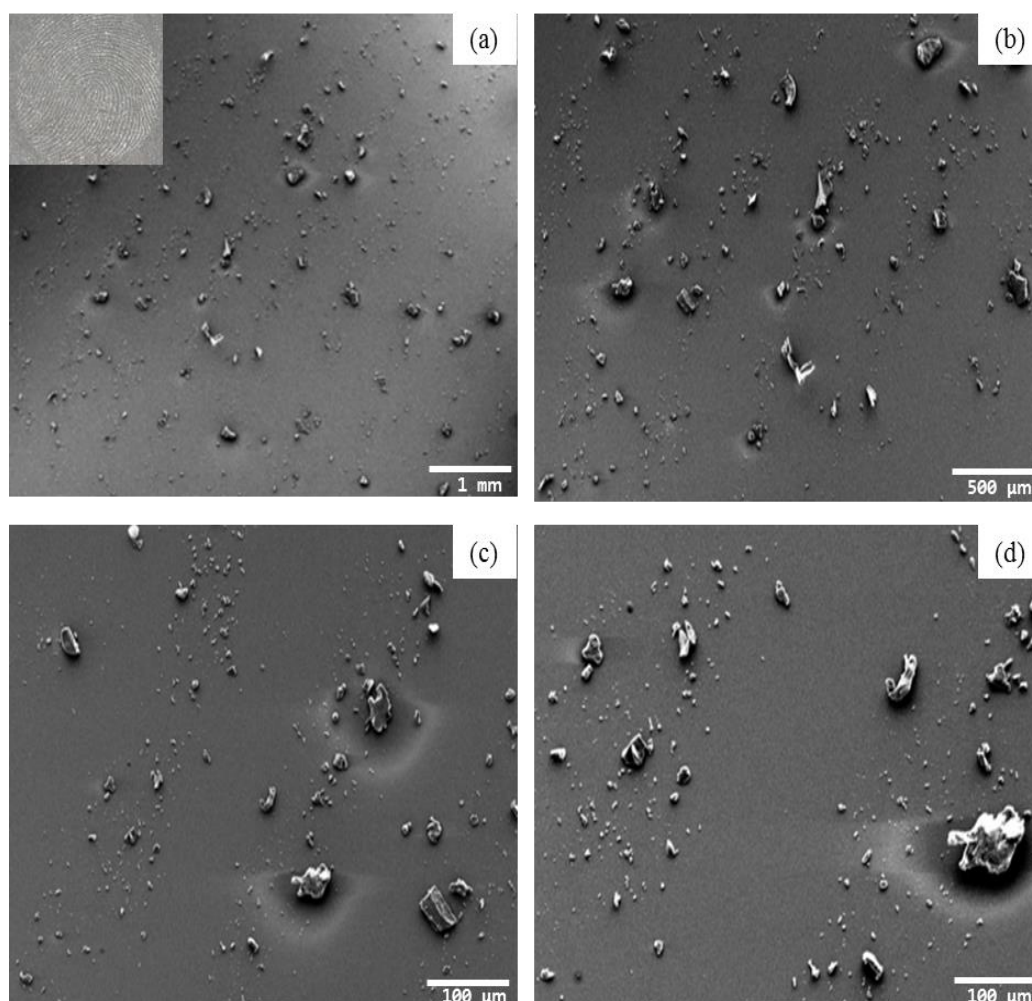


Figure 4.38: SEM images (donor 3) of fingermark development on glass microscope slide with chitosan microparticles at 2:1 ratio in buffer AB-13; (a) magnification 22x, general overview with digital camera (inset). (b-d) Magnification 50x, 100x and 200x respectively.

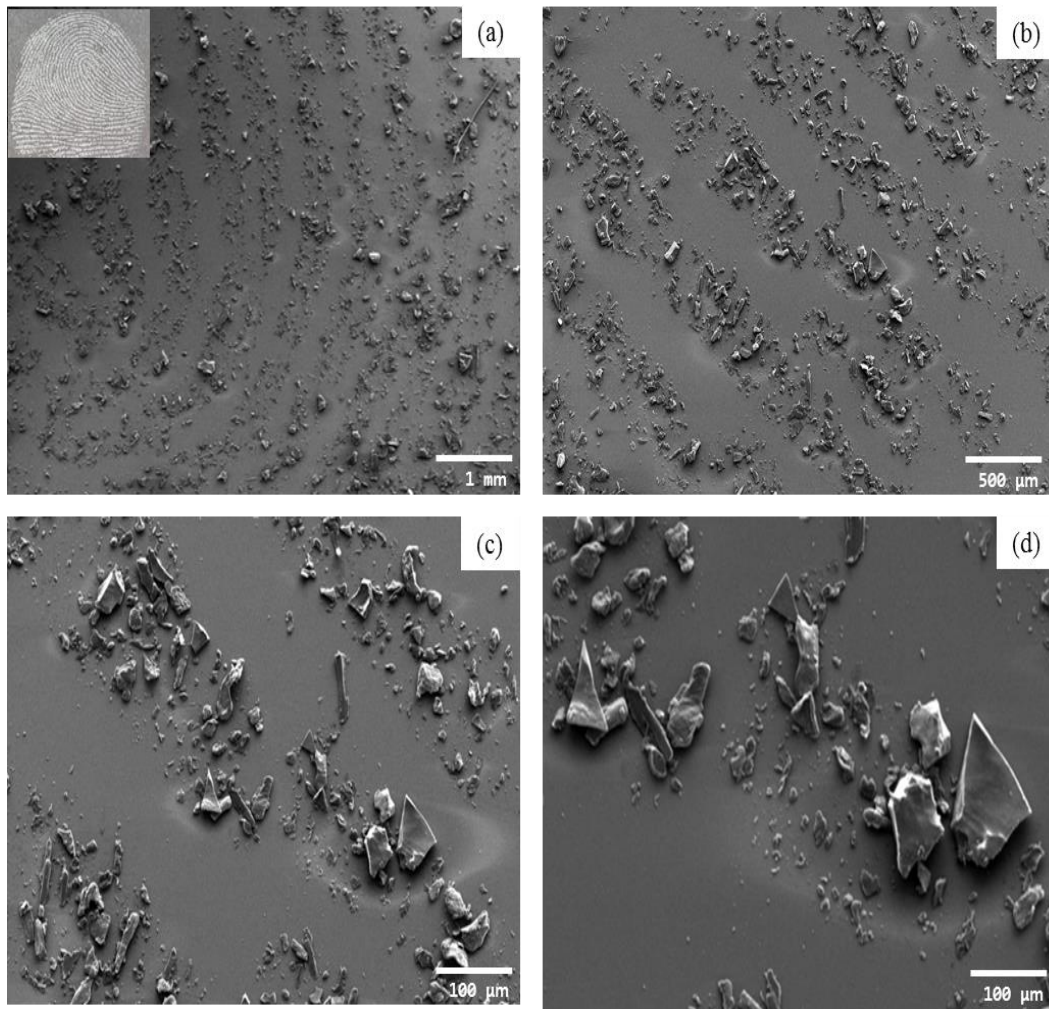


Figure 4.39: SEM images (donor 4) of fingermark development on glass microscope slide with chitosan microparticles at 2:1 ratio in buffer AB-12; (a) magnification 22x, general overview with digital camera (inset). (b-d) Magnification 50x, 100x and 200x respectively. Representative particles adhered on ridges.

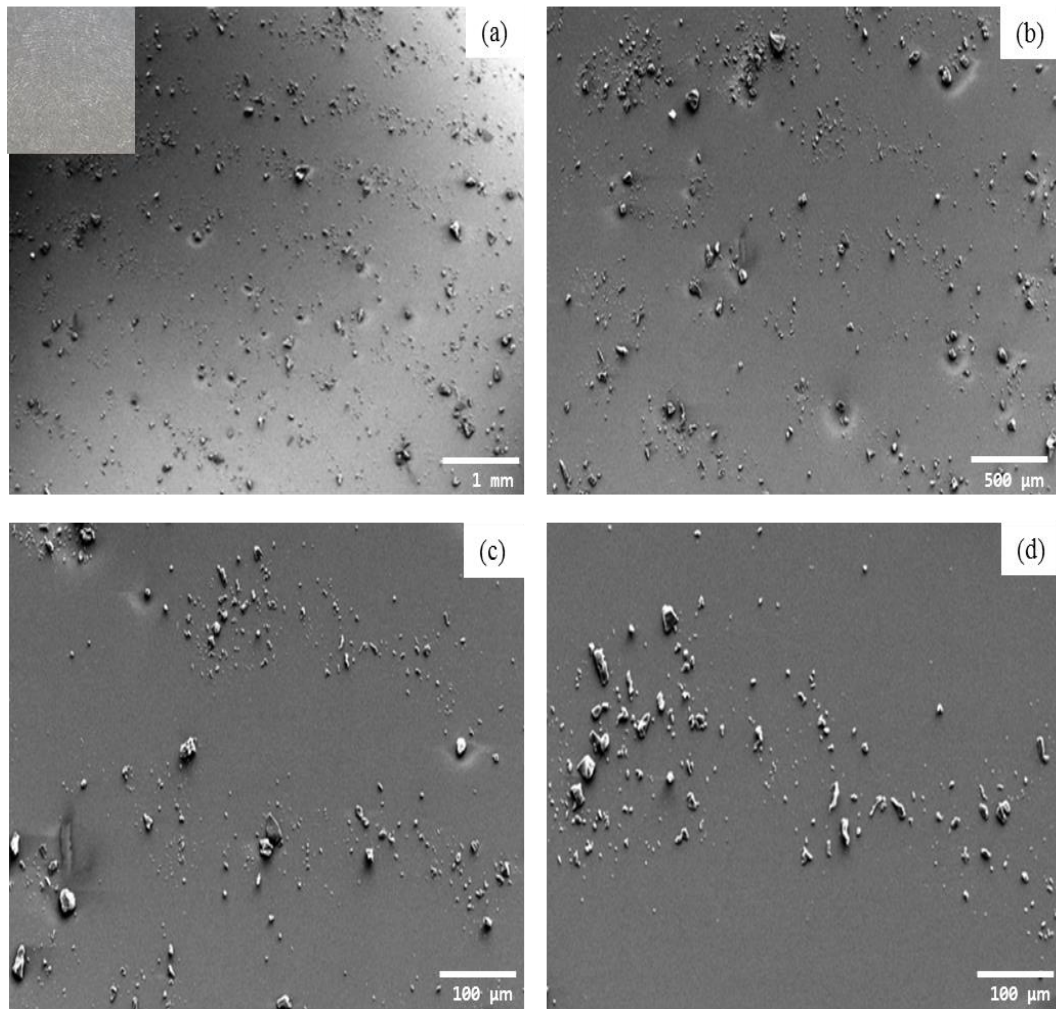


Figure 4.40: SEM images (donor 4) of fingermark development on glass microscope slide with chitosan microparticles at 2:1 ratio in buffer AB-13; (a) magnification 22x, general overview with digital camera (inset). (b-d) Magnification 50x, 100x and 200x respectively.

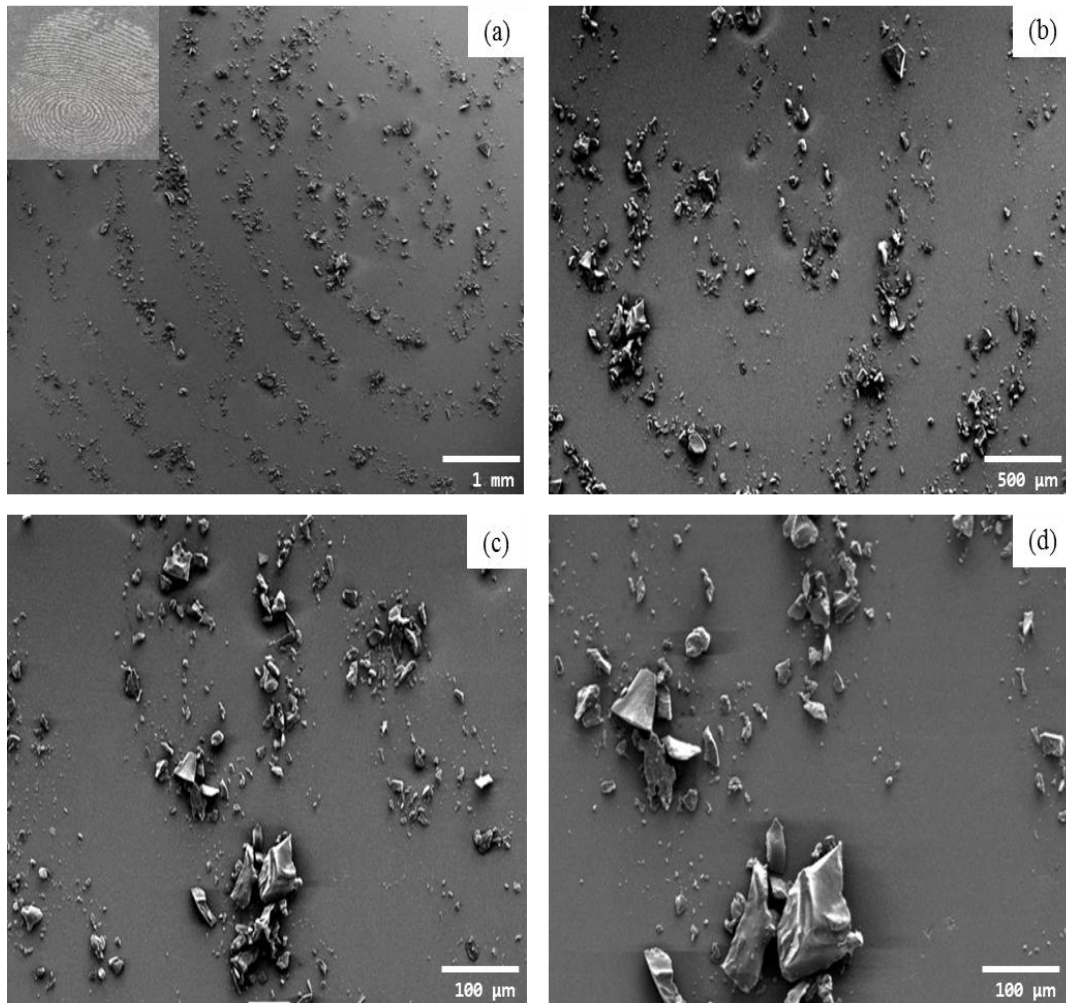


Figure 4.41: SEM images (donor 5) of fingermark development on glass microscope slide with chitosan microparticles at 2:1 ratio in buffer AB-12; (a) magnification 22x, general overview with digital camera (inset). (b-d) Magnification 50x, 100x and 200x respectively. Representative particles adhered on ridges.

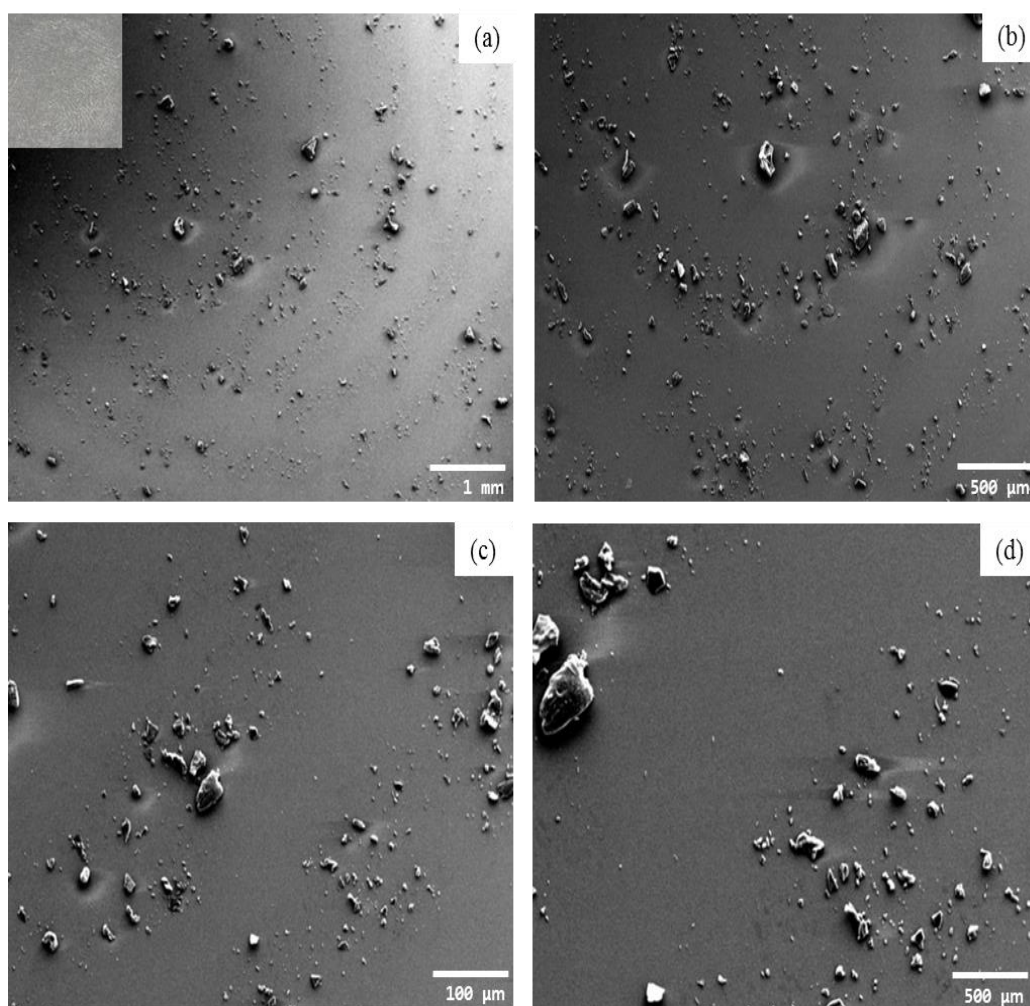


Figure 4.42: SEM images (donor 5) of fingermark development on glass microscope slide with chitosan microparticles at 2:1 ratio in buffer AB-13; (a) magnification 22x, general overview with digital camera (inset). (b-d) Magnification 50x, 100x and 200x respectively.

Furthermore, the morphology which has potential to improve interactions to the latent fingermarks can effect on quality of development fingermarks with increasing TPP has studied. For comparison purposes with high TPP ratio of CS: TPP particles, SEM images of developed latent fingermarks on glass microscope slide using CS: TPP ratio at 1:6 and 2:1 using buffer AB-12 are shown in **Figure 4.43**.

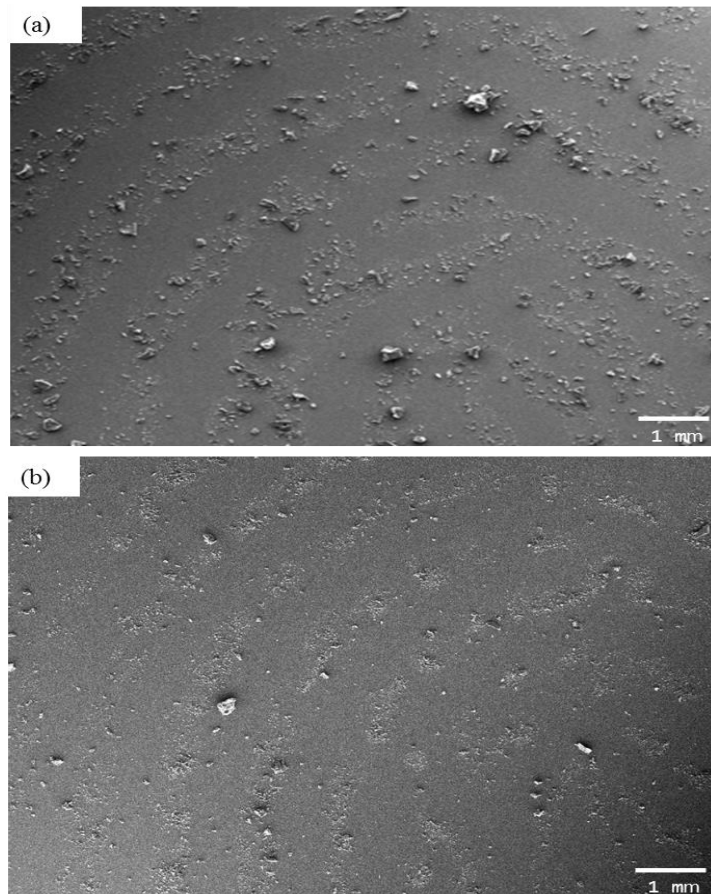


Figure 4.43: SEM images (donor 1) latent fingerprint developed of CS:TPP microparticles in buffer AB-12 on glass slides (Magnification 22x) at ratio (a) 2:1 and (b) 1:6.

It is observed that chitosan microparticles are adhere on fingerprint ridges using CS: TPP ratio at 2:1 prepared using AB-12 (**Figure 4.43a**). The microparticles bind on the fingerprint ridges making large clusters, maybe due to hydrophobic and electrostatic interactions between the fatty residues of the latent print and the chitosan particles (Wydro et al., 2007). In contrast, fewer chitosan microparticles were adheres on fingerprint ridges for CS: TPP ratio at 1:6 (**Figure 4.43b**). This result may be attributed to the surfaces of chitosan microparticles. The surface morphologies of chitosan microparticles were examined using scanning electron microscopy analysis (**Figure 4.44a**). SEM images allow observations on the morphology of particles and is

dependent on CS: TPP ratio. The effectiveness with which the microparticle powder attract to the ridges depends on surface morphology of the particles; relatively fine smooth microparticles probably adhere more easily to fingerprint residues than rough larger, coarse ones (Wilshire, 1996). Furthermore, the results indicated that the microparticles prepared with AB-12 (pH 4.8 and I.S 0.2 M) at the higher CS: TPP ratio 2:1 had highly smoother surface (**Figure 4.44a**) than those of microparticles prepared with the lower CS: TPP ratio 1:6 which had a rougher surface (**Figure 4.44b**). This result could be attributed to the particles 1:6 have lower surface charge (zeta potential is 4.8 ± 0.1 mV), which lead to decreasing electrostatic interactions.

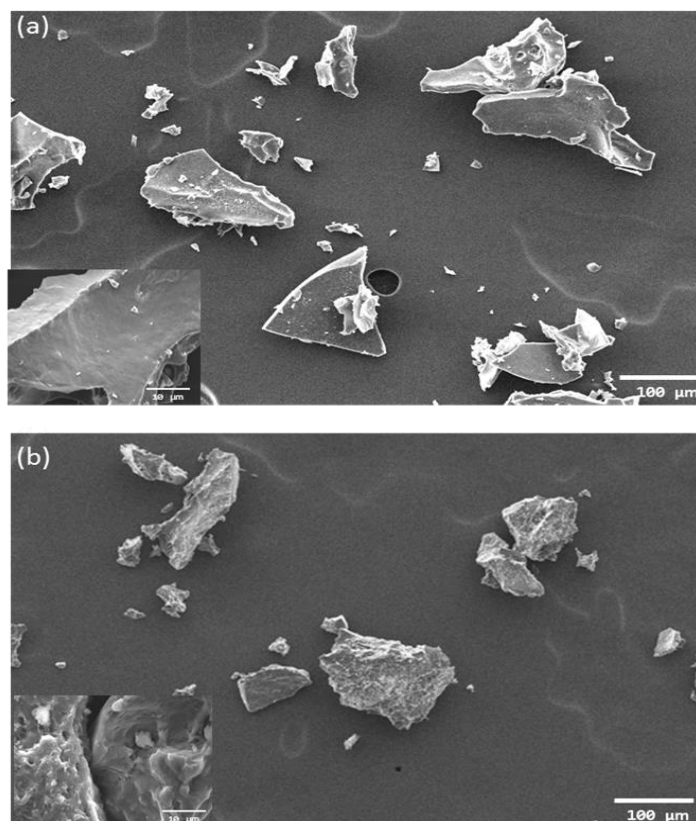


Figure 4.44: SEM images of the surface of CS: TPP microparticles using buffer AB-12 at CS:TPP ratio of (a) 2:1 and (b) 1:6. The insert of each SEM images display high magnified images (the scale bar was 10 μm).

Furthermore, as can be seen in **Figure 4.45**, the rough particles (1:6 ratio, using AB-12) are poorly adhered on to the developed fingerprint ridges, which is in agreement with previous study (Wilshire, 1996). Additionally, **Figure 4.45** shows that particles were attached on some ridges, due to reduced electrostatic interactions; and at increased magnification were found to have rough particles surfaces.

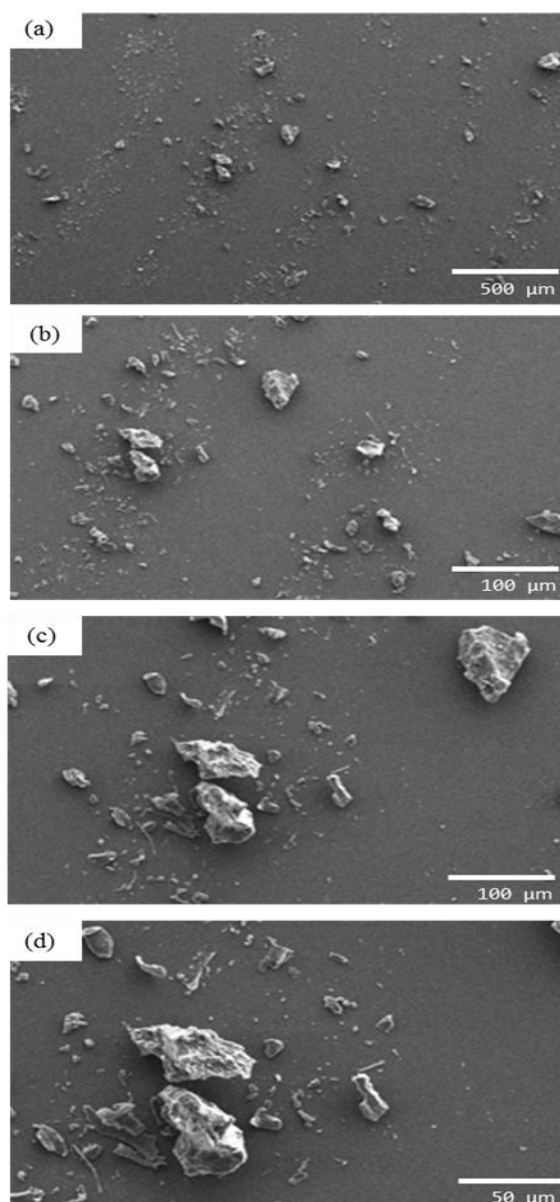


Figure 4.45: (a) SEM image low magnification (donor 1) of fingerprint development by CS:TPP particles in buffer AB-12 at ratio 1:6 on glass slide from **Figure 4.43b**. (b) Increased magnification SEM image from the centre of (a). (c, d) Two more increased in magnification.

It has been reported in a previous study that the particle size has a large influence on the adhesion efficiency to fingerprints and that fine particles adhere better than larger ones. Small flake-like particles (around 1 - 10 μm) have also good adhesion to the fingerprint ridges (Wilshire, 1996). Furthermore, poor fingerprint development was observed with powder particles which were $\sim 50 \mu\text{m}$ in diameter (James et al., 1991b). However, another study reported that particle sizes of 45 - 63 μm obtained the best result in fingerprint development (Theaker et al., 2008). Previous studies (Choi et al., 2008, Dilag et al., 2009, Dilag et al., 2013, Choi et al., 2007, Ma et al., 2011, Becue et al., 2008, Wang et al., 2009) applied different methods to visualise fingerprints using nanoparticles (small particle size) and obtained a good results. On the other hand, most of these methods applied luminescent techniques, which require specialist technical development, and expensive instruments, therefore they are inappropriate for immediate use in a crime scene (Theaker et al., 2008). In a present study the relative large particle size could be explained as the reason for aggregation of chitosan microparticles which may occurred by two processes. The first reason has been described in a previous study that the particles were increasing in size after centrifugation due to smaller particles adsorbing on to the surface of larger particles through partial physical interactions to form agglomerates (Yien et al., 2012). Secondly, it has been postulated by (Dilag et al., 2009) that drying particles using the freeze drying process could definitely cause the CdS/chitosan particles to become aggregated, thus increasing the particle size. However, based on previous results, it can be demonstrated that the surface charge of particles is most effective in latent fingerprint visualisation than particle size. Pharmaceutical sieves could be used as a cheap and simple approach to prepare particles of defined sizes for example in the range 40-65 μm .

4.5.3 Ageing study of latent fingerprints

Based on previous results which demonstrated that chitosan particles at CS: TPP ratio of 2:1 in buffer AB-12 give the best results (clear fingerprint features) in latent fingerprint development. A further set of experiments were carried out to investigate the ageing of latent fingerprints deposited on glass slides. Split fingerprints, which is a fingerprint was deposited and physically divided in two prints at centre line, were used due to estimate the inherent variability in fingerprints composition from the same donor (intra variability) and also between donors (inter variability). This led to potential comparison half prints with the same quality of material, pressure at time of deposition and the same chemical components (Sears et al., 2012). In the series of experiments, a set of fifteen split fingerprints depletion (5 donors per 3 their fingers involved index, middle and ring) were taken. The left halves of fingerprints were left to age for 7 days, while the right halves fingerprints were left to age for 14 days. Both halves were then developed with chitosan particles as powder CS: TPP at 2:1 in buffer AB-12. As can be seen in **Figure 4.46**, the comparisons of two aged fingerprints (7 days and 14 days old prints) using split depletion produced a blurred images and very weak development. This method has therefore been shown to produce poor quality fingerprints development on fingerprints aged for 7 days and 14 days, this is most likely due to loss of lipid component residues of the fingerprints. This result is similar to previous studies which reported a reduction in the fatty acid (lipid) with the time after deposition (Archer et al., 2005, Bright et al., 2013, Weyermann et al., 2011). Therefore, the chitosan microparticles were unsuccessful in developing the aged (7 and 14 days) fingerprints on glass slides, with inadequate ridge definition.

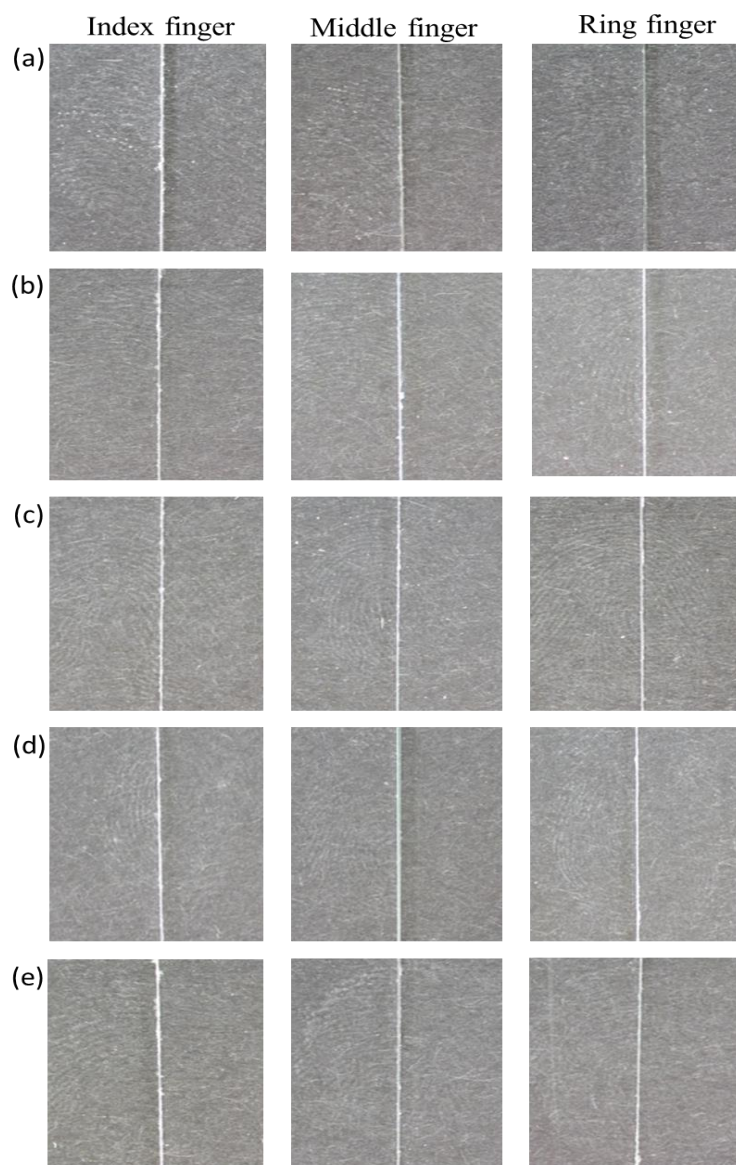


Figure 4.46: Split depletion of dusted fingerprints aged on glass slides for 7 days (left halves) and 14 days (right halves) using CS:TPP at 2:1 in buffer AB-12, (a) donor 1, (b) donor 2, (c) donor 3, (d) donor 4, (e) donor 5; where index finger (left column), middle finger (medium column) and ring finger (right column).

However, when the same method of CS: TPP particles at 2:1 in buffer AB-12 were applied to the fingerprints after aged for 1 day on glass slides (left halves of split depletion series), the development technique was effective in fingerprint development, possibly due to the relatively high amount of lipids present in the

fingermark residue resulting in clear development (grade 4). Therefore, it can be demonstrated that this method is effective on one day aged fingermarks and details can be observed with the naked eye. The results were consistent for all donors as per all their three fingers (**Figure 4.48a, Figure 4.49a and Figure 4.50a**) for donor 5; (**Figure 4.51a, Figure 4.52a and Figure 4.53a**) for donor 4; (**Figure 4.54a, Figure 4.55a and Figure 4.56a**) for donor 3; (**Figure 4.57a, Figure 4.58a and Figure 4.59a**) for donor 2; (**Figure 4.60a, Figure 4.61a and Figure 4.62a**) for donor 1.

A previous study reported that the stability (in terms of particle size) of chitosan nanoparticles (CS: TPP) after one year storage at 25 °C the size of nanoparticles remained similar to those of the freshly prepared samples (Morris et al., 2011). The effective of chitosan particles degradation after the development fingermarks ageing were examined. All fingermark development for five donors were collected and stored together under the same environmental conditions (Moret et al., 2015) **Figure 4.47**. As can be seen **Figure 4.47** shows a comparison between two fingerprints (thumbs), one which is 24 hours old after developed, that had clear ridge detail across the whole mark (**Figure 4.47a**), and the other was taken two months after development and still retains most of the details and ridges (**Figure 4.47b**). As a result, this method allowed the developed marks to be seen by naked eye for long periods of time. Therefore, one further advantage of this technique is that they do not quickly fade. This may be due to the strong attractive binding between chitosan particles and lipid residues in latent fingermarks which leads to chitosan-lipid interactions. This interactions are consistent with the findings reported in previous study (Wydro et al., 2007) and concluded that a number of possible processes may be contributed to these interactions including (i) lipophilic interactions between lipid residues of the latent fingerprint and ends of long

carbon chain of chitosan particles, (ii) chitosan microparticles may bind with fatty acids through interactions of their ammonium groups with carboxylic groups of fatty acids, and possibly (iii) hydrogen bonds between hydroxyl groups of cholesterol and chitosan may be formed.

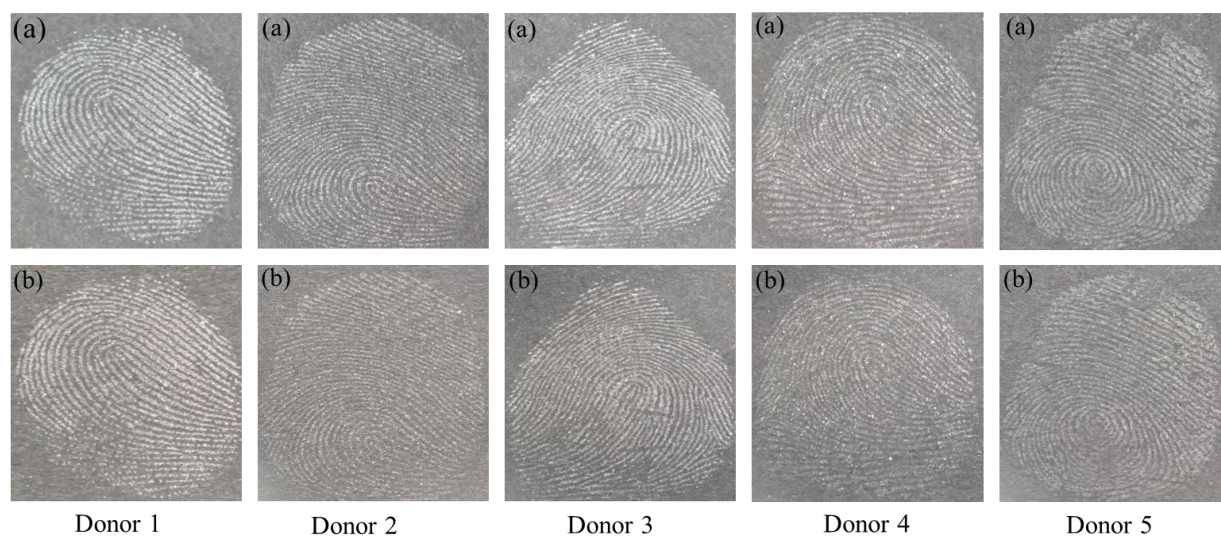


Figure 4.47: Latent fingerprints deposited on glass slides and developed using chitosan microparticle as a powder at CS: TPP (2:1) in buffer AB-12 for five donors. Those pictures have been observed and taken: (a) after the 24 h post-development (upper row) and (b) after two months post-development (lower row).

4.5.4 Method limitation (Split fingerprints depletion series)

There is variability in fingerprints composition from the same donor (intra variability) or between donors (inter variability), therefore, split prints were used to reduce the possible effect of this variability on interpretation of the results. In addition, split depletion series (second approach, section 4.4.2.3.1) was used to assess the sensitivity of the method and they were commonly compared with the influence of a

development method on the residue depleted fingermark (Almog et al., 2014). For confirmation of the earlier observations (**Figures 4.8 and 4.9**), the results were further analysed according to limitation of the methods. CS: TPP particles of 2:1 in buffer AB-12 consistently produce more potentially identifiable fingermarks (grade 4) than CS: TPP of 1:1 in buffer AB-12 (grade 1) across all surfaces evaluated, this is shown in **Figures 4.48a - 4.62a**. To determine the sensitivity and capability of the third technique (chitosan particles as a powder), five donors were asked to deposit a six split depletion series on non-porous glass microscope slides, which consisted of multiple successive contacts down the glass slides with a right three fingers (index, middle and ring). When a sequence of fingermarks is left on glass slides each successive fingermark in the depletion could be predicted to contain less sweat residue than the previous one (Fairley et al., 2012). This gives an indication of the sensitivity of the method and its limitation to continue to develop fingermarks with gradually decreasing the amounts of residue, prior to dusting with the CS: TPP powders. Comparisons of the two CS: TPP particles ratios involving 2:1 and 1:1 at four different formulations including AB-10, AB-11, AB-12 and AB-13 by split depletion series shown in **Figures 4.48 - 4.62**. According to donor's metabolism they will deposit different levels of secretions which will also have different compositions, therefore the development of fingermarks will vary from individual to individual. This is not controlled but is reflected by the fact that the detection of fingermarks differs depending on persons (Becue et al., 2008). The fingermarks development for ratios CS: TPP at 2:1 (left halves) and 1:1 (right halves) show that 2:1 is much clearer as compared to 1:1 (**Figures 4.48 - 4.62**). Significant differences in sensitivity were observed between the two halves developed by chitosan particles formulations including AB-10, AB-11, and AB-12 (**Figures 4.48 a, b, c - 4.62 a, b, c**). Whereas,

no differences in sensitivity were observed between the two halves developed by chitosan particles by AB-13 which both produced a fingerprint grade of 1 (**Figure 4.48d - 4.62d**). In general, CS: TPP ratios at 1:1 were a very poor quality (grade 1) with very few clear visible ridge details (right halves) (AB-10, AB-11, AB-12 and AB-13). Additionally, chitosan particles using AB-13 (both ratios at 2:1 and 1:1) does not give any useful ridge detail. The series of depletion cannot be traced past the first depletion level, and it becomes difficult to visualise the fingermarks developed at ratios 2:1 and 1:1, as it displays blurred prints whose ridges details cannot be recognized (**Figure 4.48d - 4.62d**). Furthermore, using CS: TPP (2:1) particles in buffer AB-10 (grade 2) was not sensitive enough to developed fingermarks past the first depletion (**Figure 4.48c - 4.62c**). When using CS: TPP (2:1) particles in buffer AB-11 (grade 3) fingermarks were developed up to the second depletion. On the other hand, strong ridges clear seen in the development using CS: TPP particles at 2:1 in buffer AB -12 (grade 4), the developed fingermarks also can be traced down to greater levels with the series of depletion considered. At the beginning, the fingerprint development is clear and adequate ridge details were still obtained even with the naked eye until third depletion and are identifiable fingermarks (left halves) (**Figure 4.48a - 4.62a**). Other donors produced similar results (clear ridges visible print) using CS: TPP particles at 2:1 in buffer AB-12 and development grades of 4 were obtained.

However, the reduction in effectiveness, where the features of the fingerprint unclear and difficult to define were observed by the fourth depletion, due to the decline in the amount of residue present along the fingermarks ridges (de la Hunty et al., 2015) (**Figure 4.48a - 4.62a**). These results were consistent with each repetition of the experiments for each donor. Therefore, it can be demonstrated that limitation method

(sensitivity) for fingerprint visualization for chitosan microparticles prepared as a powder using a buffer AB-12 (pH 4.8, IS 0.2M) at CS: TPP of 2:1 (left halves) is third depletion level which can be observed with the naked eye.

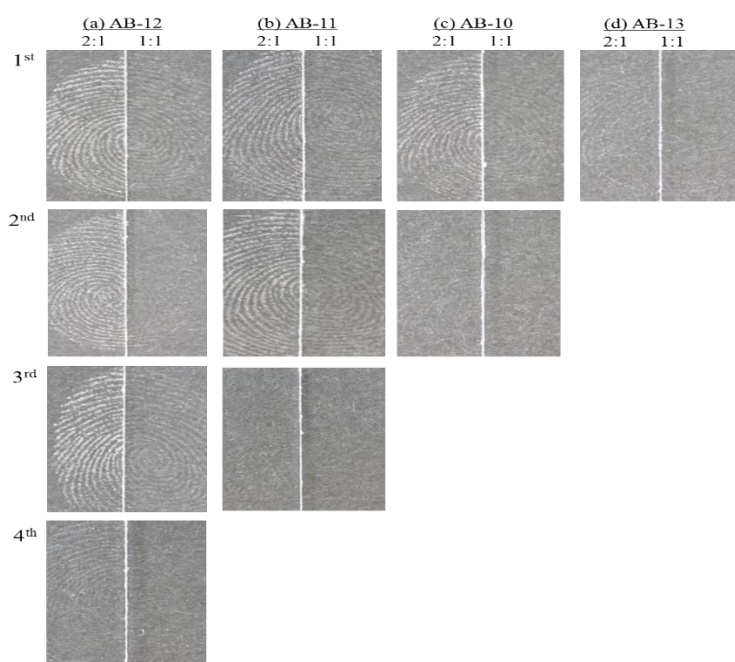


Figure 4.48: Depletion series (donor 5 index finger), with split halves developed by chitosan microparticle CS:TPP ratio at (a) 2:1 (left) vs 1:1 (right) using AB-12; (b) 2:1 (left) vs 1:1 (right) using AB-11; (c) 2:1 (left) vs 1:1 (right) using AB-10; and (d) 2:1(left) vs 1:1 (right) using AB-13. (n=10).

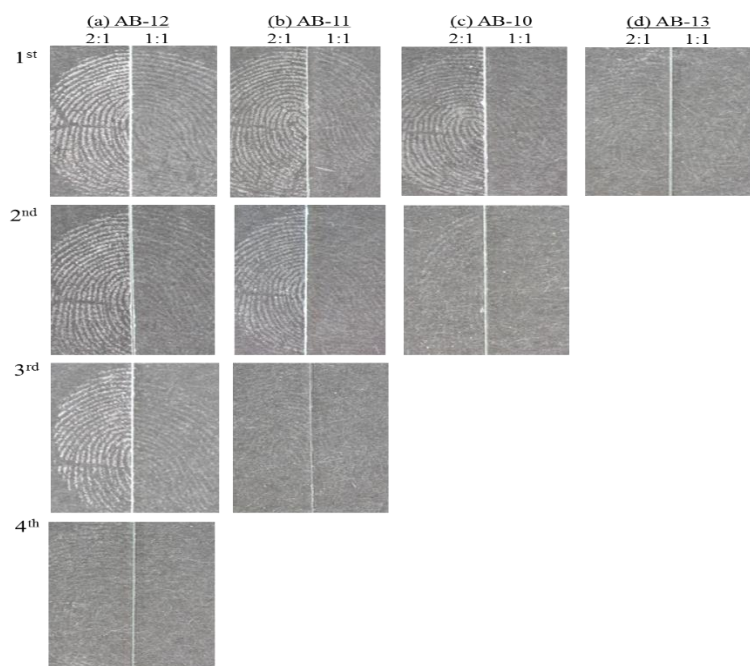


Figure 4.49: Depletion series (donor 5 middle finger), with split halves developed by chitosan microparticle CS:TPP ratio at (a) 2:1 (left) vs 1:1 (right) using AB-12; (b) 2:1 (left) vs 1:1 (right) using AB-11; (c) 2:1 (left) vs 1:1 (right) using AB-10; and (d) 2:1(left) vs 1:1 (right) using AB-13. (n=10).

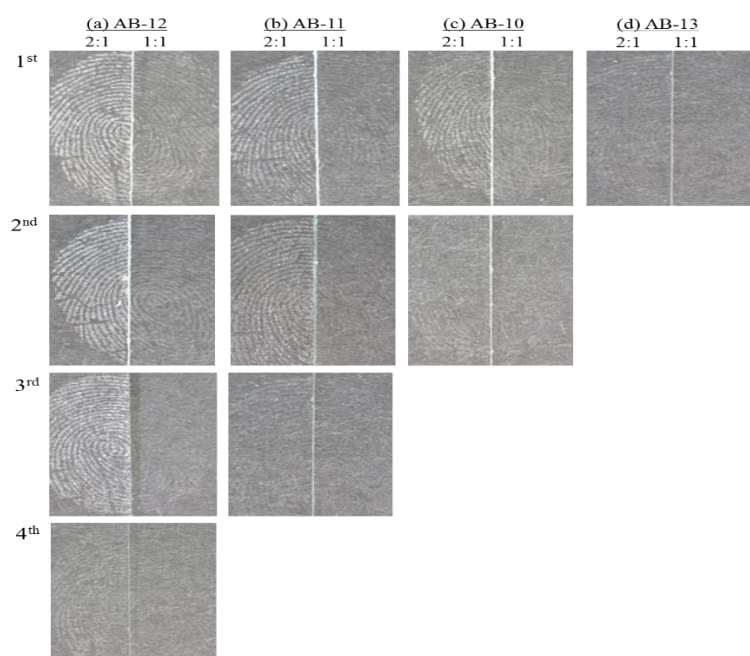


Figure 4.50: Depletion series (donor 5 ring finger), with split halves developed by chitosan microparticle CS:TPP ratio at (a) 2:1 (left) vs 1:1 (right) using AB-12; (b) 2:1 (left) vs 1:1 (right) using AB-11; (c) 2:1 (left) vs 1:1 (right) using AB-10; and (d) 2:1 (left) vs 1:1 (right) using AB-13. (n=10).

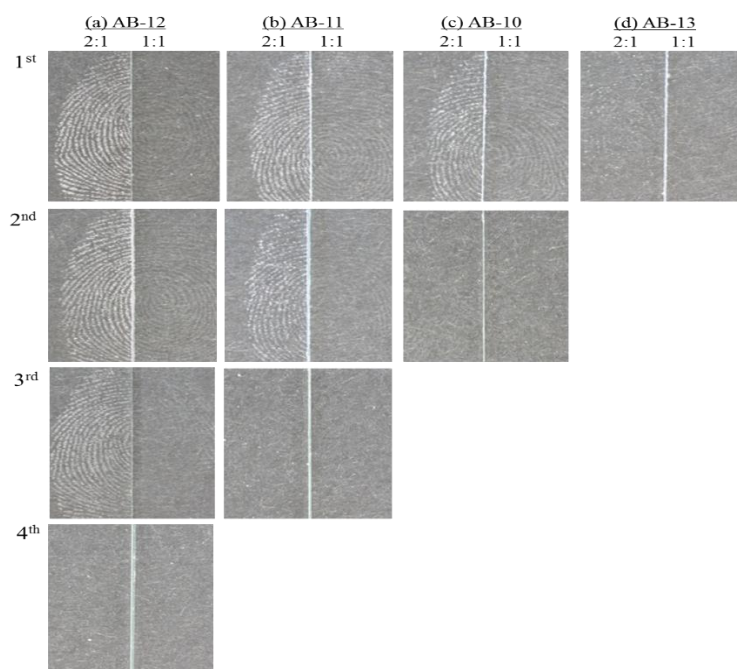


Figure 4.51: Depletion series (donor 4 index finger), with split halves developed by chitosan microparticle CS:TPP ratio at (a) 2:1 (left) vs 1:1 (right) using AB-12; (b) 2:1 (left) vs 1:1 (right) using AB-11; (c) 2:1 (left) vs 1:1 (right) using AB-10; and (d) 2:1 (left) vs 1:1 (right) using AB-13. (n=10).

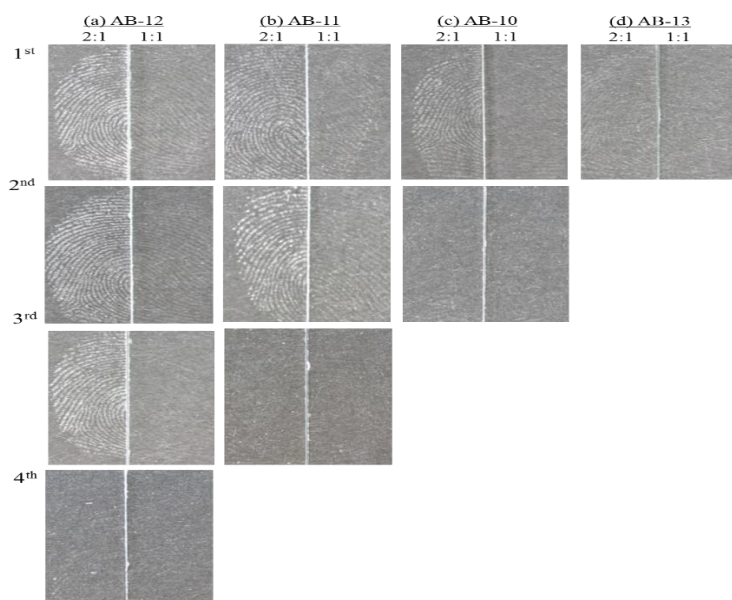


Figure 4.52: Depletion series (donor 4 middle finger), with split halves developed by chitosan microparticle CS:TPP ratio at (a) 2:1 (left) vs 1:1 (right) using AB-12; (b) 2:1 (left) vs 1:1 (right) using AB-11; (c) 2:1 (left) vs 1:1 (right) using AB-10; and (d) 2:1 (left) vs 1:1 (right) using AB-13. (n=10).

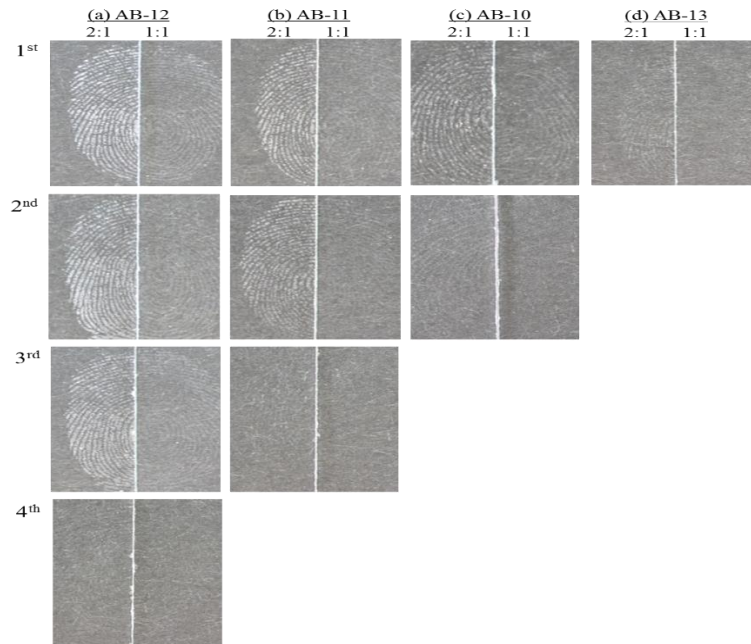


Figure 4.53: Depletion series (donor 4 ring finger), with split halves developed by chitosan microparticle CS:TPP ratio at (a) 2:1 (left) vs 1:1 (right) using AB-12; (b) 2:1 (left) vs 1:1 (right) using AB-11; (c) 2:1 (left) vs 1:1 (right) using AB-10; and (d) 2:1 (left) vs 1:1 (right) using AB-13. (n=10).

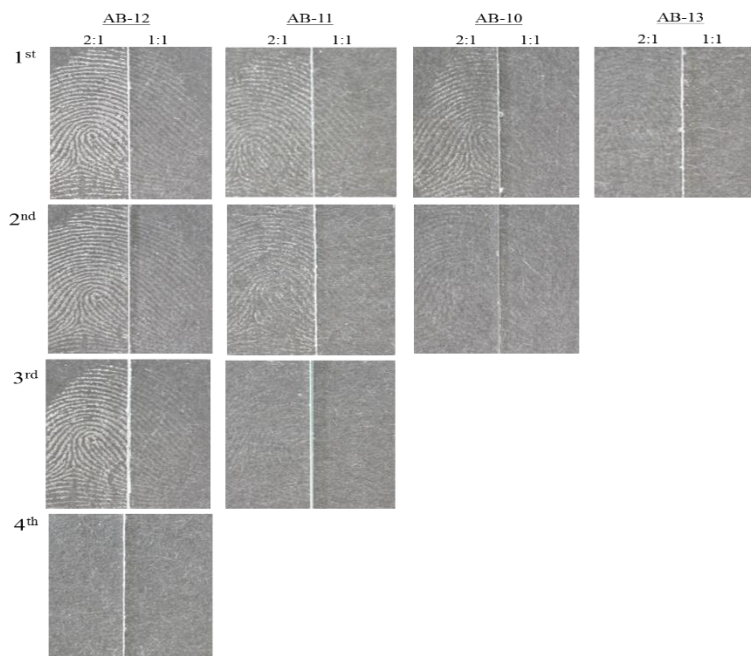


Figure 4.54: Depletion series (donor 3 index finger), with split halves developed by chitosan microparticle CS:TPP ratio at (a) 2:1 (left) vs 1:1 (right) using AB-12; (b) 2:1 (left) vs 1:1 (right) using AB-11; (c) 2:1 (left) vs 1:1 (right) using AB-10; and (d) 2:1 (left) vs 1:1 (right) using AB-13. (n=10).

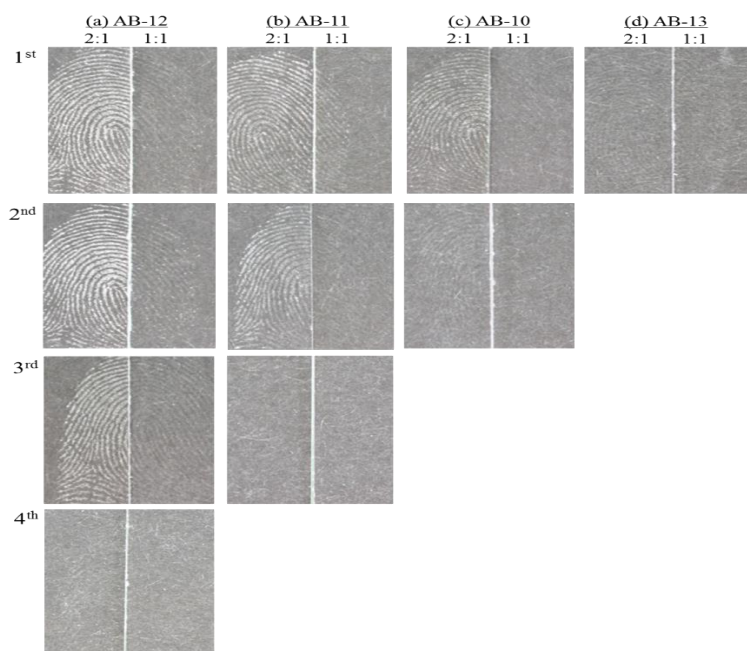


Figure 4.55: Depletion series (donor 3 middle finger), with split halves developed by chitosan microparticle CS:TPP ratio at (a) 2:1 (left) vs 1:1 (right) using AB-12; (b) 2:1 (left) vs 1:1 (right) using AB-11; (c) 2:1 (left) vs 1:1 (right) using AB-10; and (d) 2:1 (left) vs 1:1 (right) using AB-13. (n=10).

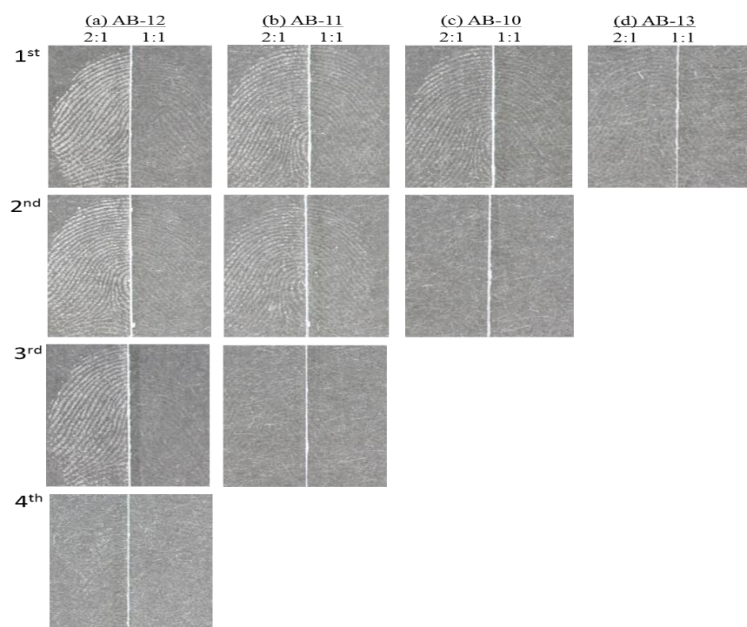


Figure 4.56: Depletion series (donor 3 ring finger), with split halves developed by chitosan microparticle CS:TPP ratio at (a) 2:1 (left) vs 1:1 (right) using AB-12; (b) 2:1 (left) vs 1:1 (right) using AB-11; (c) 2:1 (left) vs 1:1 (right) using AB-10; and (d) 2:1 (left) vs 1:1 (right) using AB-13. (n=10).

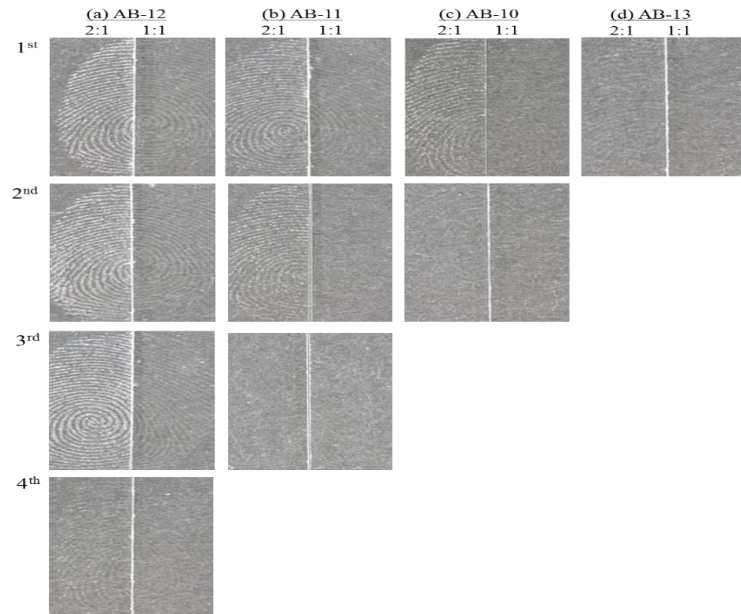


Figure 4.57: Depletion series (donor 2 Index finger), with split halves developed by chitosan microparticle CS:TPP ratio at (a) 2:1 (left) vs 1:1 (right) using AB-12; (b) 2:1 (left) vs 1:1 (right) using AB-11; (c) 2:1 (left) vs 1:1 (right) using AB-10; and (d) 2:1(left) vs 1:1 (right) using AB-13. (n=10).

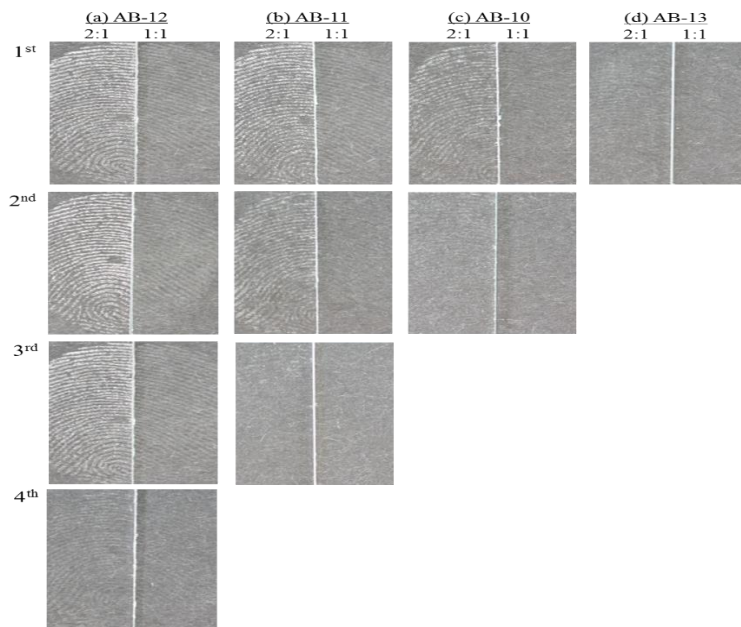


Figure 4.58: Depletion series (donor 2 Middle finger), with split halves developed by chitosan microparticle CS:TPP ratio at (a) 2:1 (left) vs 1:1 (right) using AB-12; (b) 2:1 (left) vs 1:1 (right) using AB-11; (c) 2:1 (left) vs 1:1 (right) using AB-10; and (d) 2:1 (left) vs 1:1 (right) using AB-13. (n=10).

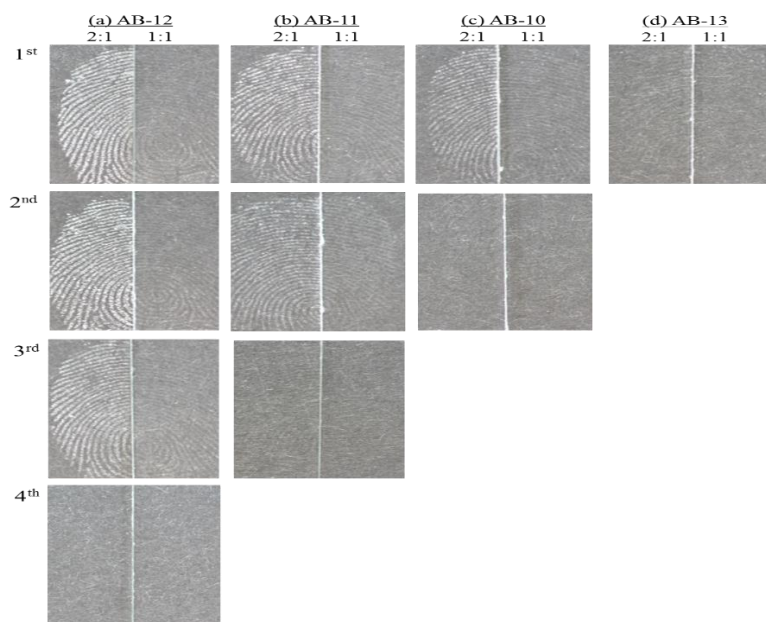


Figure 4.59: Depletion series (donor 2 ring finger), with split halves developed by chitosan microparticle CS:TPP ratio at (a) 2:1 (left) vs 1:1 (right) using AB-12; (b) 2:1 (left) vs 1:1 (right) using AB-11; (c) 2:1 (left) vs 1:1 (right) using AB-10; and (d) 2:1 (left) vs 1:1 (right) using AB-13. (n=10).

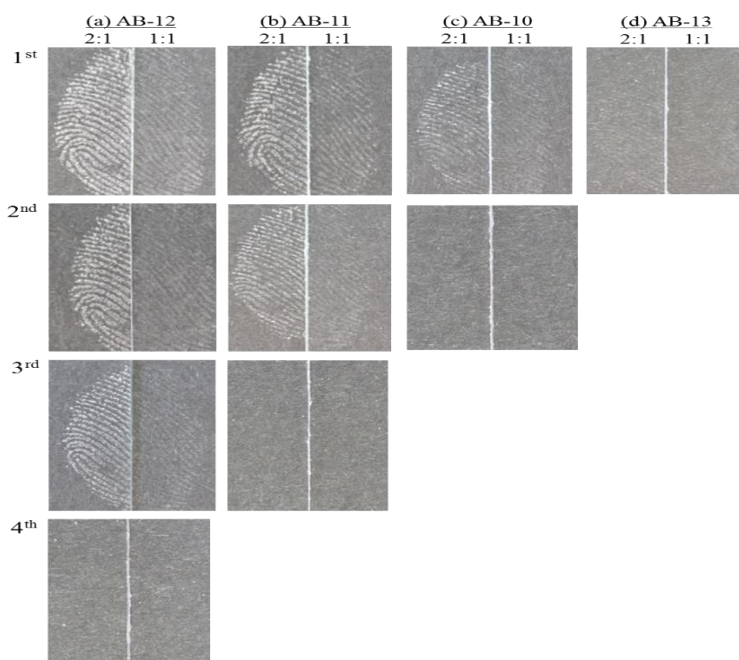


Figure 4.60: Depletion series (donor 1 index finger), with split halves developed by chitosan microparticle CS:TPP ratio at (a) 2:1 (left) vs 1:1 (right) using AB-12; (b) 2:1 (left) vs 1:1 (right) using AB-11; (c) 2:1 (left) vs 1:1 (right) using AB-10; and (d) 2:1 (left) vs 1:1 (right) using AB-13. (n=10).

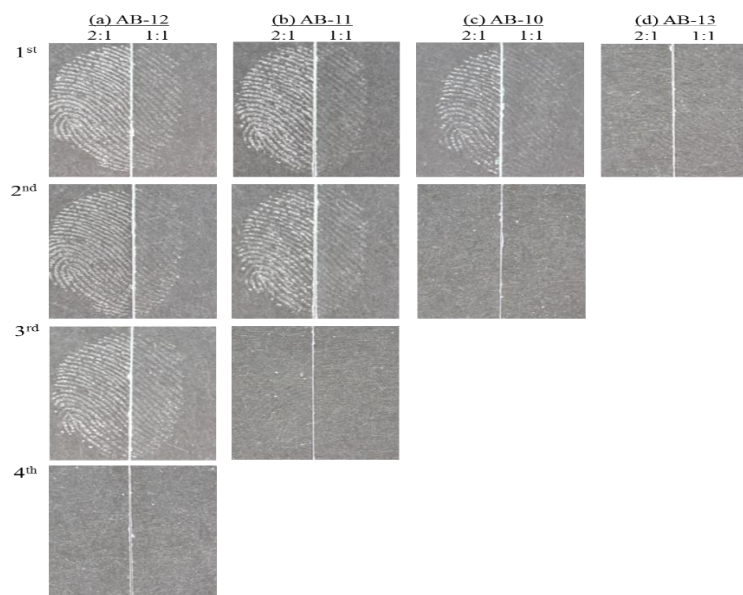


Figure 4.61: Depletion series (donor 1 middle finger), with split halves developed by chitosan microparticle CS:TPP ratio at (a) 2:1 (left) vs 1:1 (right) using AB-12; (b) 2:1 (left) vs 1:1 (right) using AB-11; (c) 2:1 (left) vs 1:1 (right) using AB-10; and (d) 2:1(left) vs 1:1 (right) using AB-13. (n=10).

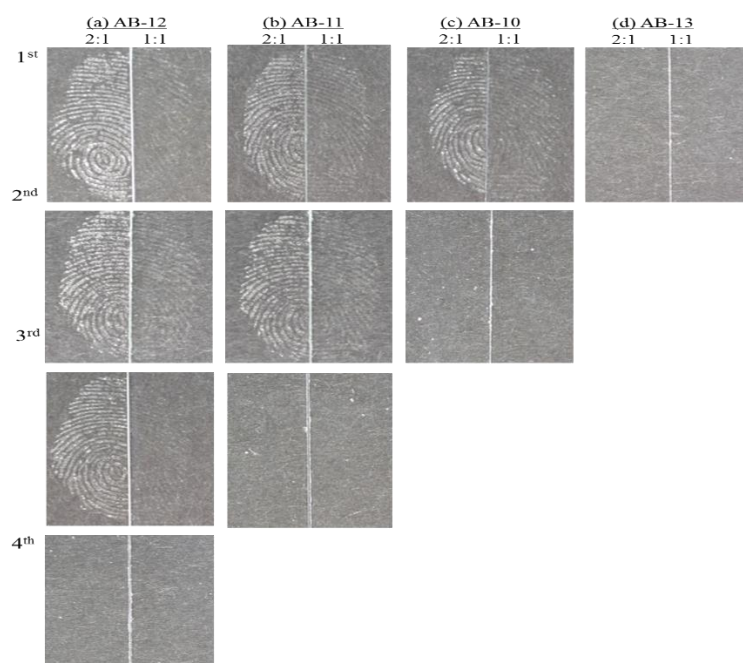


Figure 4.62: Depletion series (donor 1 ring finger), with split halves developed by chitosan microparticle CS:TPP ratio at (a) 2:1 (left) vs 1:1 (right) using AB-12; (b) 2:1 (left) vs 1:1 (right) using AB-11; (c) 2:1 (left) vs 1:1 (right) using AB-10; and (d) 2:1 (left) vs 1:1 (right) using AB-13. (n=10).

4.6 Summary

In this study chitosan microparticles were successfully obtained from the ionotropic gelation method using different processing conditions. This method gives us the ability to design tuneable CS: TPP microparticles for specific forensic applications. It is proposed the CS: TPP particles deposit onto fingerprints due to the lipophilic and electrostatic interaction with the fatty components in fingerprint ridges. Latent fingerprints were developed using chitosan microparticles as a powder (third technique) on glass microscope slides obtained variable degrees of success depending on how the microparticles were prepared. A clear relationship between size and charge on the microparticles and the fingerprint quality was found. In the present study it was demonstrated that CS: TPP ratio has the strongest effect on quality fingerprint. Microparticles were obtained (pH 4.8, CS: TPP of 2:1 and 0.2 M of ionic strength using AB-12) with average diameter of 171.3 μm and a zeta potential of +14.3 mV which may have good potential for applications in fingerprint development on non-porous surfaces (glass slides). The effectiveness of an enhancement method was evaluated and limitation to detecting fingerprints (sensitivity) by this method which is third depletion level for one day aged. The advantages of using chitosan microparticles as a powder technique are that they are non-toxic (Aramwit et al., 2015) sustainable (Yan and Chen, 2015), underutilised (it is the second most abundant polymer on the planet (Matlack, 2010) and therefore poses less potential health and environmental hazards, quick, easy to apply and able to produce good quality fingerprints under the conditions studied. As well as the developed marks can be easily visualised and remain visible for a long period of time (2 months) there is therefore no requirement that the fingerprints need to be photographed immediately. Furthermore, this method of visualisation is non-destructive and therefore avoiding

potential degradation of the physical evidence and unlike some other recent developments in fingerprint visualisation this method is not dependent on prior knowledge of any materials handled by the subject/suspect. Disadvantage of this method is that it is not effective on aged fingerprints. To our knowledge this is the first time that particle size, shape, viscosity and zeta potential have been used as a way of predicting latent fingerprint quality.

Chapter 5

Formulation, characterization and *in vitro* evaluation of ibuprofen loaded chitosan-TPP nanoparticles as a model pharmaceutical application

5 Formulation, characterization and *in vitro* evaluation of ibuprofen loaded chitosan-TPP nanoparticles as a model pharmaceutical application

5.1 Introduction

Chitosan, has been widely investigated in drug delivery systems for pharmaceutical applications (Qandil et al., 2009). Furthermore, low molecular weight (LMW) drugs can be incorporated into chitosan nanoparticles which can be used to control the release of drugs. Nanoparticles are sub-micron particles with size less than 1000 nm, and with several morphologies, such as nanocapsules, nanospheres, nanoliposomes, and nanodrugs. Nanoparticles have been widely applied in drug delivery systems to deliver drugs or biomolecules (Liu et al., 2008b). Among the numerous methods developed for preparation of nanoparticles, the ionic gelation method is simple to process and can also be used to optimize the required particle sizes such that any encapsulated drug can penetrate the epithelial membrane (Nanda et al., 2012). Particles sizes for example in the range of 10-500 nm are believed to be acceptable for intravenous injection (Koo et al., 2011). This is because these particles can spend longer in circulation and can also be retained longer in the body and may deposit in tumor tissue through active targeting or by the improved permeation and retention effect (Danhier et al., 2010, Jonassen et al., 2012). However, It has been observed that the number of microspheres which can cross the epithelium is lesser than the number of nanoparticles (McClellan et al., 1998) and a range of 10-200 nm is more suitable as it is more efficient in penetrating different biological membranes such as the mucosal membrane (Krasnici et al., 2003, Mitra et al., 2001, Masarudin et al., 2015). Therefore, all things being considered, there are not any major issues associated to the presence of nanoparticles in the general circulation. In this study, LMW chitosan was

used because of the fact that an increase in molecular weight increases the particle size, as the solubility of higher molecular weight chitosan is lower, and consequently, an increase in particle diameter or even aggregates may be obtained (Wu et al., 2005). In addition, high molecular weight (HMW) chitosan has slow dissociation and release of drug. To overcome these problems of HMW chitosan, several studies have been conducted by using LMW chitosan (Choi et al., 2016). Furthermore, LMW chitosan and its concentration should be within range of 1.0 – 3.0 mg/mL and for 1 mg/mL of TPP cross linker to form nanoparticles of the CS: TPP (see Chapter 3, section 3.6) (Wu et al., 2005, Xu and Du, 2003). Moreover, LMW chitosan concentration should increase drug encapsulation (Li and Huang, 2012). Therefore, a chitosan concentration of 3 mg/mL was used in this study. Considering the possible pharmaceutical applications of ibuprofen loaded nanoparticles in drug delivery systems, small particles, relatively high drug entrapment efficiency of nanoparticles and continuous drug release should be taken into consideration. Ibuprofen, (RS)-2-methyl-4-(2-methylpropyl) phenyl propanoic acid, is an effective non-steroidal anti-inflammatory drug (NSAID) (Ganesh and Lee, 2013) used for relief from headaches, dental pain, menstrual cramps, muscle aches, fever, symptoms of rheumatoid arthritis and osteoarthritis.. Ibuprofen is usually completely excreted after less than 24 hours and its biological half-life is 2 hours (Ganesh and Lee, 2013, Abioye et al., 2016) and is a biopharmaceutical classification system (BCS) class II drug (Al-Hamidi et al., 2015). Moreover, ibuprofen is absorbed at greater than 95 % in the plasma of the human body and may be completely bound to plasma proteins (Najafabadi et al., 2014, Abioye and Kola-Mustapha, 2015). However, ibuprofen has a free carboxylic acid group (COOH) in the chemical formula which leads to side effects in the

gastrointestinal (GI) tract such mild dyspepsia and gastric bleeding, therefore its use is often limited (Depan et al., 2009, Kamari and Ghiaci, 2016) (**Figure 5.1**).

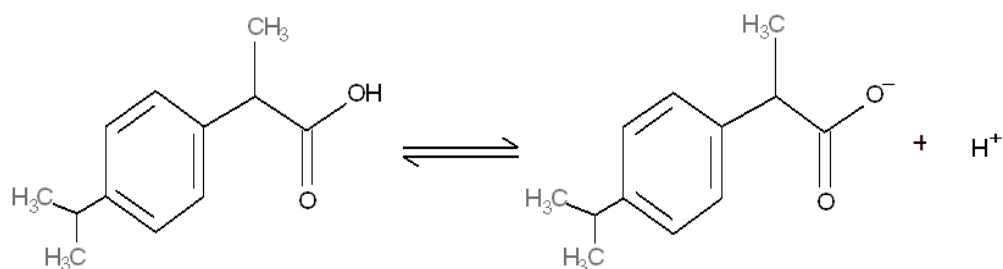


Figure 5.1: Ibuprofen dissociation

Hydrophobic ibuprofen is a weakly acidic drug; therefore it can be easily dissolved in alkaline solution $\text{pH} > 7.0$. Whereas, it is almost insoluble in water ($49 \mu\text{g/mL}$ at 25°C) with a pK_a of 4.5 and it has a low solubility in acidic solution at $\text{pH} 1.2$ ($53 \mu\text{g/mL}$ at 25°C) (Lin et al., 2005, Abioye and Kola-Mustapha, 2015). Ibuprofen is generally marketed as tablets such as NurofenTM and as liquid formulations such as CalprofenTM with different potencies. The main advantage of a chitosan-TPP formulation is that the ibuprofen in the chitosan particles remains unaltered chemically and is the same as the native ibuprofen, after being released (Win et al., 2005). In this study ibuprofen is used as a model drug to prepare drug loaded chitosan nanoparticles using two different ionotropic gelation methods (see section 5.2.5.1 and 5.2.5.2 which differ in the order mixing) to investigate the drug entrapment efficiency (DEE) of chitosan nanoparticles. The factors that influence the formulation of nanoparticles including CS: TPP ratios and different concentrations of ibuprofen on DEE of the chitosan nanoparticles were investigated. The obtained ibuprofen-loaded

chitosan-TPP nanoparticles were characterized in terms of particle size determination, zeta potential, and ibuprofen loading to determine the optimum ratio to be used in drug release. Finally, *in vitro* drug release profile of drug-loaded chitosan nanoparticles were studied during incubation in phosphate buffer saline (PBS).

5.2 Methods and materials

5.2.1 Chemicals

Chitosan of low molecular weight (LMW ~ 50,000 g/mol as determined by viscosity using equations 5.1-5.4 (see section 5.2.2.1) was purchased from Sigma–Aldrich (Gillingham, UK) and was reported to have an average degree of deacetylation (DD) of ~90 % as determined by FT-IR using the equation 5.5 (see section 5.2.2.2). Glacial acetic acid and TPP sodium salt was also obtained from Sigma–Aldrich (Gillingham, UK). Ibuprofen powder (Ibuprofen 38) was obtained from BASF (Germany), phosphate buffer saline (PBS) pH 7.4 was obtained from Fisher Scientific (Loughborough, UK). Dialysis tubing cellulose membrane (molecular weight cut off 14,000 g/mol) was purchased from Sigma–Aldrich. All materials were used without any further purification.

5.2.2 Sample preparation

5.2.2.1 Viscosity analysis of chitosan

The relative viscosity (η_{rel}) of chitosan solution was tested at $37.0 \pm 0.1^\circ\text{C}$ by a Bohlin Gemini HR Nano Rheometer (Malvern Instruments, Worcestershire, UK) using 1 mm

gap and 55 mm parallel plate geometry at a constant shear rate of 500 s^{-1} under precise temperature control, according to the following equation:

$$\eta_{rel} = \left(\frac{\eta}{\eta_0} \right) \quad \text{Eq. (5.1)}$$

where η is the average viscosity of the sample and, η_0 is the viscosity for the reference solvent *i.e.* dilute acetic acid. All measurements were performed in triplicate. The specific (η_{sp}), viscosity is defined as follows:

$$\eta_{sp} = \eta_{rel} - 1 \quad \text{Eq. (5.2)}$$

A useful method for measuring the intrinsic viscosity is to calculate the relative and specific viscosities at one concentration and utilise the Solomon-Ciută approximation (Solomon and Ciută, 1962, Harding, 1997). The intrinsic viscosity can then be accurately estimated (error generally $\sim 1 \%$) by a single measurement at low concentration approximately $\leq 0.5 \%$.

$$[\eta] \approx \frac{(2\eta_{sp} - 2\ln(\eta_{rel}))^{1/2}}{c} \quad \text{Eq. (5.3)}$$

The intrinsic viscosities can then be converted to molar mass using the following Mark–Houwink–Kuhn–Sakurada (MHKS) power law relationship (Morris et al., 2009):

$$M_w = \left(\frac{[\eta]}{0.0074} \right)^{1/0.95} \quad \text{Eq. (5.4)}$$

5.2.2.2 Fourier transform infrared (FTIR)

Spectroscopy FTIR spectra of chitosan, ibuprofen, CS: TPP nanoparticle (blank) and CS-IBU-TPP nanoparticle samples were recorded using a Fourier transform infrared spectrophotometer (Thermo Nicolet 380 FT-IR spectrometer, Thermo Electron Corporation), operating from 4000 to 500 cm^{-1} . FTIR spectra depend on the interaction of electromagnetic radiation with sample and it is a surface sensitive technique. The ATR (Attenuated total reflectance) crystal was cleaned with isopropyl alcohol. A background check was performed prior to obtaining sample spectra. Powdered samples were placed on the crystal using micro-spatula and force was applied by twisting top of the arm of sample stage. The test sample spectra were collected. The degree of deacetylation (DD) was calculated from equation 5.5 (Czechowska-Biskup et al., 2012).

$$DD (\%) = 100 - \left(\frac{\left(\frac{A_{1655 \text{ cm}^{-1}}}{A_{2945 \text{ cm}^{-1}}} \right) \times 100}{1.33} \right) \quad \text{Eq. (5.5)}$$

where $A_{1655\text{ cm}^{-1}}$ and $A_{3450\text{ cm}^{-1}}$ are the absorbances of the C=O and OH stretches of chitosan respectively. Each sample was run in triplicate.

5.2.2.3 Preparation of chitosan and TPP samples

1 mg/mL solution of TPP was prepared by weighing out 250 mg of TPP and making up to 250 mL using deionized water. However, the pH of this solution was controlled by adding 0.1 N hydrochloric acid (HCl) until a final pH of 5.0 was obtained. 3.0 mg/mL solution of chitosan was prepared by weighing out 750 mg of chitosan then added to glacial acetic acid solution (0.5 %) and this was left stirring overnight at room temperature. The solution was then filtered under Gooch crucible (AG 1 X 3) vacuum filtration to discard any undissolved chitosan then pH was adjusted to 5.0 using 0.1 N sodium hydroxide (NaOH).

5.2.2.4 Preparation of ibuprofen samples

Five different concentrations of ibuprofen solutions 0.5, 1.0, 1.5, 2.0 and 2.5 mg/mL were prepared using phosphate buffer saline PBS pH 7.4 (sodium chloride 137 mM, potassium chloride 2.7 mM, disodium hydrogen phosphate 10 mM and potassium dihydrogen phosphate 2.0 mM).

5.2.3 Ibuprofen assay

The amounts of ibuprofen entrapped in the chitosan nanoparticles as well as the amounts of ibuprofen released from the chitosan nanoparticles were determined by UV-Vis spectrophotometer (Shimadzu UV-160A, Wolverton, UK).

5.2.3.1 Wavelength of maximum absorbance

The UV absorption spectra of ibuprofen (1.5 mg/mL) in phosphate buffered saline PBS (pH 7.4) was obtained by scanning a wide range of wavelengths (200 – 300 nm) in optically homogeneous quartz cuvettes. The wavelength of maximum absorbance (peak value) was recorded for ibuprofen and used in all analytical determinations of ibuprofen in this study.

5.2.3.2 Standard curve

A stock solution of ibuprofen was prepared by weighing 80 mg accurately and dissolving it in 100 mL phosphate buffer saline (PBS) pH 7.4 produce a 0.80 mg/mL solution. This stock solution was further diluted to produce a series of ibuprofen solutions containing 0.5, 0.4, 0.3, 0.2, 0.15, 0.12, 0.09, 0.07, 0.05, 0.02 and 0.01 mg/mL ibuprofen, respectively. The phosphate buffer saline used as a reference solution (or blank). The measured absorbance of each solution was plotted as a function of the concentration of each solution to produce a standard curve. Linear regression analysis was performed on this curve using Microsoft Excel® 2013 (Microsoft Corporation, Redmond, USA).

5.2.3.3 Validation of Analytical Method

UV-Visible spectrophotometric method for dissolution studies was validated. Validation of dissolution method was done in terms of curve linearity, precision, accuracy, limit of detection and limit of quantification.

5.2.3.4 UV light absorbance by chitosan and TPP

To determine if there is any interference caused by chitosan and TPP molecules during the spectroscopic analysis of ibuprofen, the UV absorbance profiles of chitosan and TPP used in this study were measured. This was done by scanning solutions of the chitosan and TPP over a range of wavelengths ranging from 200 nm to 300 nm.

5.2.4 Preparation of blank chitosan-TPP nanoparticles

CS: TPP nanoparticles were produced by the drop wise addition of an appropriate volumes of chitosan solution to appropriate volumes of TPP solutions under magnetic stirring at 600 rpm for 60 min, making CS: TPP ratios be 3:1, 4:1, 5:1, 6:1 and 7:1 respectively (Appendix B). All operations above were conducted at room temperature and were sonicated for 5 min (the cycle and amplitude was adjusted to 0.5 and 80 % respectively; Hielscher Ultrasonics GmbH, Teltow, Germany) before being subjected to further analysis.

In acidic medium there are two forces between chitosan molecules. First is electrostatic repulsion due to the ammonium groups of chitosan; second is inter-chain hydrogen bonding interactions between chitosan molecules. The CS: TPP ratio is an important parameter in effecting the zeta potential and particle size of chitosan nanoparticles. If the amount of TPP is small it is unable to a cross-link of chitosan chains. Whereas, when the available quantity of TPP is high, this leads to more chitosan chains being cross-linked, as a result, particles aggregate then precipitate (Fan et al., 2012). It has reported that to obtain a smaller size and higher zeta potential ($> \pm 30$ mV) of chitosan nanoparticles, the chitosan to TPP ratio is from 3:1 to 7:1

(Chapter 3, section 3.6) (Gan et al., 2005, Hu et al., 2008, Gokce et al., 2014).

Therefore, these ratios have chosen.

5.2.5 Preparation of drug loading/incorporation into chitosan nanoparticles (CS-IBU-TPP)

The ibuprofen loading in chitosan nanoparticle system can be done by two methods as described in the sections 5.2.5.1 and 5.2.5.2 depending on whether the ibuprofen is first added to the chitosan or to the TPP. It is proposed that ibuprofen will be entrapped into the chitosan matrix during the ionotropic gelation process making chitosan to TPP ratios of 3:1, 4:1, 5:1, 6:1 and 7:1. For both methods, ibuprofen solution was prepared by dissolving 1.5 mg/mL of ibuprofen in PBS (pH 7.4).

5.2.5.1 Internal entrapment of ibuprofen into chitosan matrix (ibuprofen first mixed with chitosan), referred to as (IBU+CS)/TPP

Ibuprofen-chitosan nanoparticles can be formed according to **Figure 5.2**, by adding 10.1 mL of ibuprofen to 50 mL of chitosan solution and magnetically stirred for 30 min. Then a 30 mL aqueous solution of TPP has been added drop-wise to the chitosan-ibuprofen mixture while stirring with magnetic stirrer for 60 minutes at 600 rpm. The cross-linked chitosan nanoparticles were then isolated by ultra-centrifugation at 40,000 x g (Beckman Coulter Optima L-100K, 50Ti rotor) for 60 min, followed by freeze drying for 24 hours (Alpha 1- 4 LD2 freeze drier, Germany).

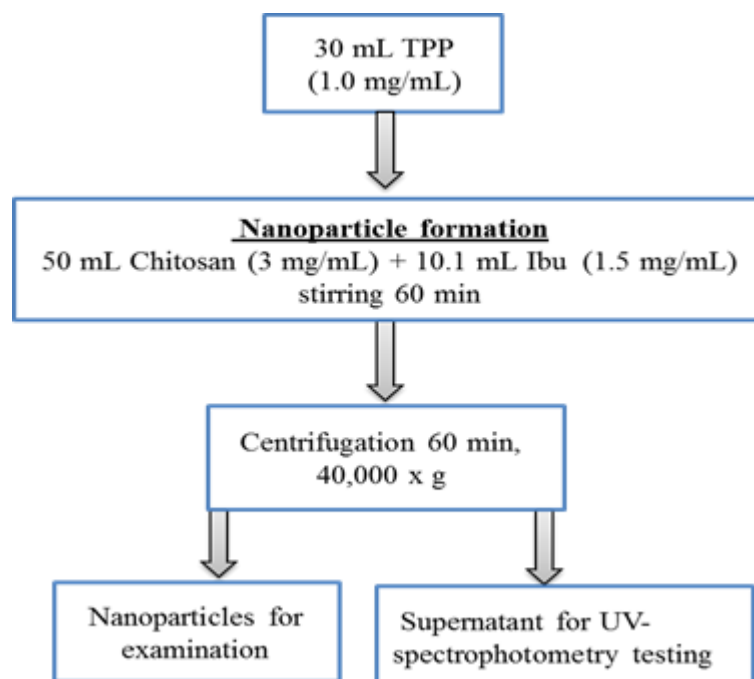


Figure 5.2: First method an internal entrapment of ibuprofen into chitosan nanoparticles, ibuprofen first mixed with chitosan: (IBU+CS)/TPP.

5.2.5.2 Internal entrapment of ibuprofen into chitosan matrix (ibuprofen first mixed with TPP), referred to as CS/(TPP+IBU)

For the association of ibuprofen with CS: TPP nanoparticles, 10.1 mL of ibuprofen solution (1.5 mg/mL) was premixed with 30 mL of TPP solution before adding drop-wise into the chitosan solution (50 mL) under magnetically stirred for 60 min at 600 rpm as shown below in **Figure 5.3**. The cross-linked chitosan nanoparticles were then separated by ultra-centrifugation at 40,000 x g (Beckman Coulter Optima L-100K, 50Ti rotor) for 60 min, followed by freeze drying for 24 hours (Alpha 1- 4 LD2 freeze drier, Germany).

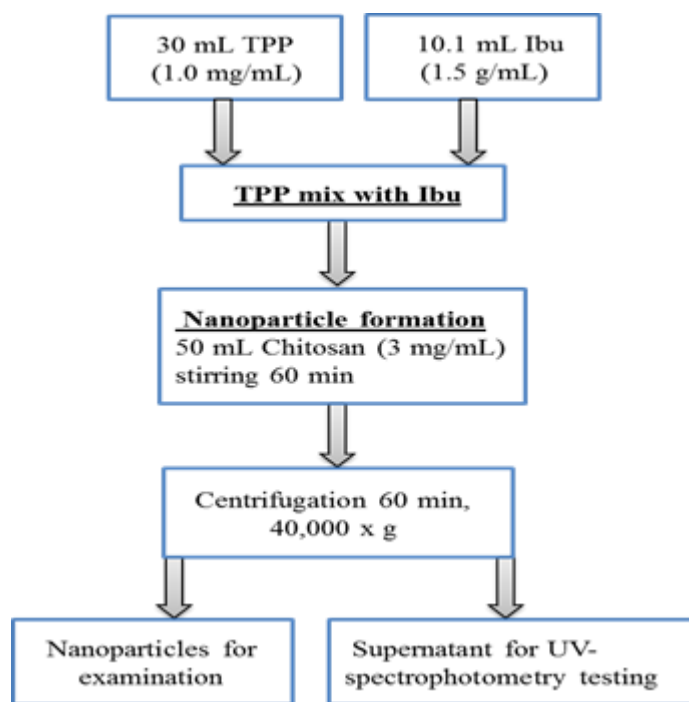


Figure 5.3: Second method an internal entrapment of ibuprofen into chitosan nanoparticles, ibuprofen first mixed with TPP: CS/(TPP+IBU).

5.2.6 Effects of CS: TPP ratio on CS-IBU-TPP nanoparticles

A 10.1 mL of ibuprofen (1.5 mg/mL) were mixed with 30 mL of TPP and stirred for 30 min. Then CS-IBU-TPP nanoparticles were formed by the drop-wise addition of a suitable volume of chitosan solution at selected chitosan to TPP ratios of 3:1, 4:1, 5:1, 6:1 and 7:1 respectively. The nanoparticle suspensions were gently stirred for 60 min at room temperature and were then sonicated for 5 min before being subjected to further analysis and applications (Appendix C). The CS-IBU-TPP nanoparticles collected by ultra-centrifugation at 40,000 x g (Beckman Coulter Optima L-100K, 50Ti rotor) for 60 min, followed by freeze drying for 24 hours (Alpha 1- 4 LD2 freeze drier, Germany).

5.2.7 Effects of ibuprofen concentration on CS-IBU-TPP nanoparticle

A 30 mL of TPP solution was mixed with different concentrations of ibuprofen solutions including 0.5, 1.0, 1.5, 2.0, and 2.5 mg/mL and stirred for 30 min. Then CS-IBU-TPP nanoparticles with the CS: TPP ratio 5:1 were produced by the drop-wise addition of 50 mL chitosan solution under constant stirring (600 rpm for 60 min) and were then sonicated for 5 min. The CS-IBU-TPP nanoparticles collected by ultracentrifugation at 40,000 x g (Beckman Coulter Optima L-100K, 50Ti rotor) for 60 min, followed by freeze drying for 24 hours (Alpha 1- 4 LD2 freeze drier, Germany).

5.2.8 Characterization of chitosan nanoparticles

Measurement of the mean particle diameter (z-average), polydispersity (size distribution) and zeta potential of CS: TPP and CS-IBU-TPP nanoparticles in the suspension were performed using Malvern Zetasizer NANO-Z (Malvern Instruments Limited, Malvern, UK) on the basis of DLS techniques. The dispersion medium (water) and refractive index of particles was set at 1.330 and 1.6 respectively. An angle scattering of 173° was utilized. To determine particle size a glass cuvette was used. Approximately 1.0 mL of sample was pipetted into the cuvette and three readings were taken. An average of these readings was then recorded. Zeta potential of samples was measured using the same instrument used to determine particle size. Measurements were performed using a folded capillary zeta cell. To determine the zeta potential approximately 1.0 mL of sample was pipetted into a folded capillary cell by using a syringe and measurements were performed at 25 ± 0.1 °C in triplicate to obtain data value an average of 3 measurements.

5.2.9 Drug entrapment efficiency (DEE) of ibuprofen in CS-IBU-TPP nanoparticles

Drug entrapment efficiency (DEE) indicates the efficiency of the preparation method to incorporate the drug into the carrier system as it expresses the amount of the drug entrapped within the nanoparticle compared to the initial drug loading. Where 100% DEE means that the entire drug quantity added, has been incorporated into the nanoparticle (Gomathi et al., 2017). DEE depends on the physicochemical properties and the interactions between the drug, carrier and the surrounding medium. After nanoparticle formation, as described in section 5.2.5, the DEE can be determined from the supernatant. In order to determine DEE of nanoparticles, CS-IBU-TPP nanoparticles were isolated from solution ultra-centrifugation at 40,000 x g (Beckman Coulter Optima L-100K, 50Ti rotor) for 60 min, at 25 °C. Based on the absorbance of the samples determined using the UV spectrophotometer the ibuprofen concentration in the supernatant can be determined. A standard curve (concentration vs. UV absorbance) was prepared according to section 5.2.3.2. Drug entrapment efficiency were calculated according to the following equations (Adebisi and Conway, 2014):

$$\text{Drug content} \left(\% \frac{w}{w} \right) = \frac{\text{amount of drug in sample (mg)}}{\text{sample weight (mg)}} \times 100 \quad \text{Eq. (5.1)}$$

$$\text{DEE (\%)} = \frac{\% \text{ drug content}}{(\% \text{ theoretical drug content})} \times 100 \quad \text{Eq. (5.2)}$$

Drug entrapment efficiency describes the quantity of the ibuprofen entrapped within the chitosan nanoparticle as it is related to the initial drug loading.

5.2.10 *In vitro* release of ibuprofen from CS-IBU-TPP nanoparticles

In vitro ibuprofen release profiles from chitosan nanoparticles were implemented over time in release media (PBS pH 7.4) (Figure 5.4). After ultra-centrifugation, the supernatant was discarded from the ibuprofen-loaded chitosan nanoparticles. The *in vitro* release studies were conducted using dialysis tubing to contain the ibuprofen-loaded chitosan nanoparticles in order to minimize the effect that nanoparticles and other large molecules could have on the spectrophotometric absorbance of the samples. Drug release from chitosan nanoparticles formulations was carried out in pH 7.4 phosphate buffered saline PBS. The dialysis tubing was first soaked for 10 minutes in deionized water. 500 mg of ibuprofen-loaded nanoparticle formulations were placed into the dialysis tubing. Then were immersed in 200 mL media at 37 ± 1 °C under 20 dips per minute (DPM) using the USP XXII apparatus 3 (BIO-DIS Dissolution Test Station, Vankel Industries, Chatham, US). To maintain the original volume, 5 ml sample media were withdrawn at predetermined time intervals and replaced with fresh, warm dissolution media of equal volume. The quantity of ibuprofen in the release media was assessed by absorption using UV-spectrophotometric examination at λ_{max} 263.9 nm. From the equation fitted to the standard curve (section 5.2.3.2) the amount of free ibuprofen in the release media was calculated. The *in vitro* release studies were performed in triplicate for each of the samples.

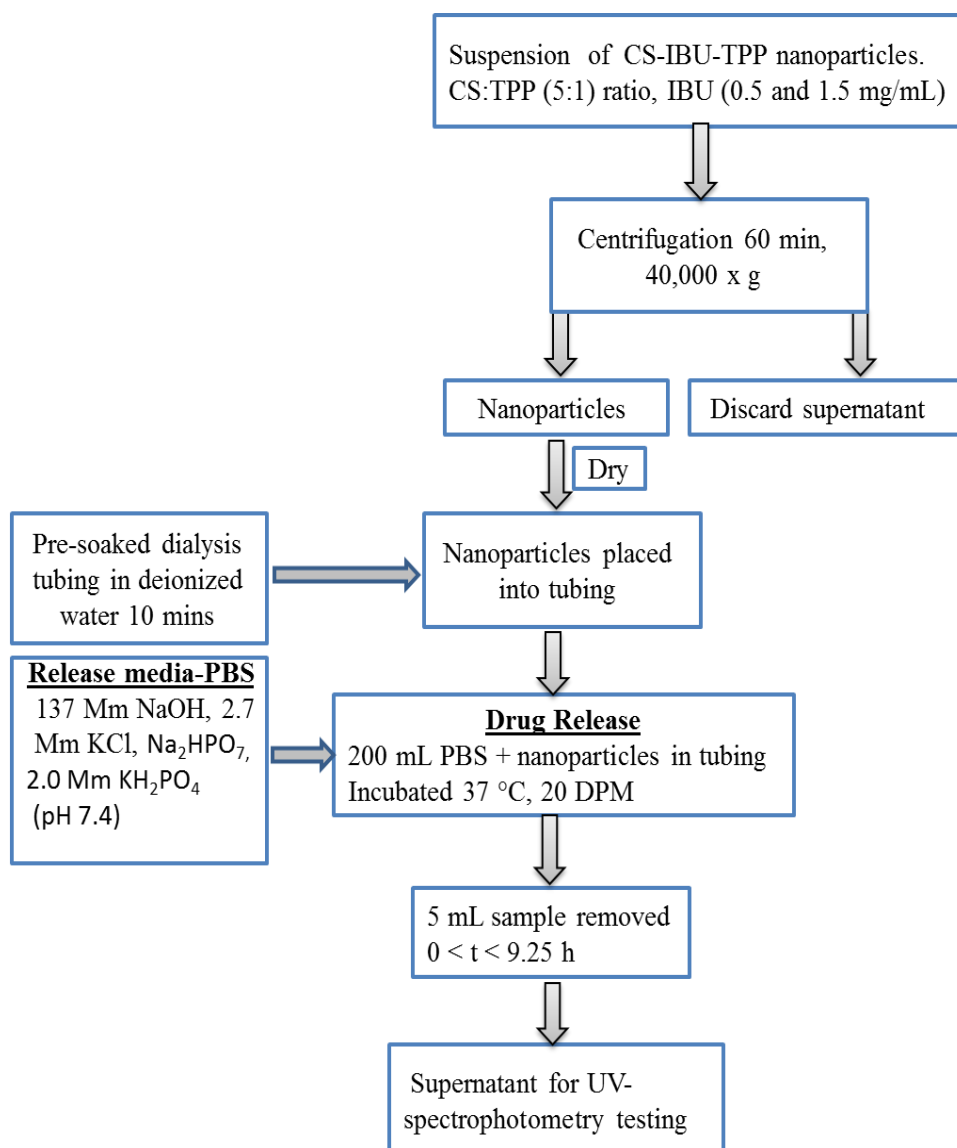


Figure 5.4: Method summary for drug release experiment.

5.2.11 Statistical analysis

All experiments were expressed as the mean value \pm standard deviations (SD) of at least three readings. Statistical significance (p value less than 0.05) between test groups was performed by one-way analysis of variance (ANOVA) or Tukey post-hoc test using Primer of Biostatistics version.

5.3 Results and discussion

5.3.1 Ibuprofen assay

5.3.1.1 Wavelength of maximum absorbance

Ibuprofen (1.5 mg/mL) was dissolved in phosphate buffer saline PBS (pH 7.4), above its pKa 4.5 to produce a highly soluble carboxylate species. **Figure 5.5** shows the UV absorption spectra of chitosan and ibuprofen solution. These solutions were scanned over a wavelength range of 200 – 300 nm. The absorbance (Abs) was expressed as a function of wavelength and this graph was used to determine the wavelength of maximum absorbance (peak values).

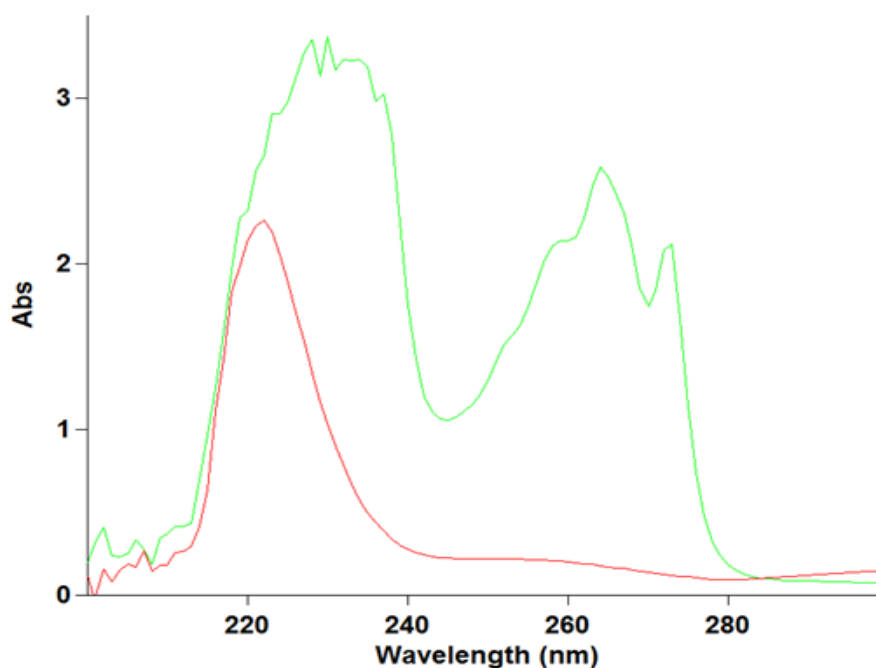


Figure 5.5: UV- absorption spectrum of chitosan (red) and ibuprofen (green).

As can be seen in **Finger 5.5** there is interference between chitosan and ibuprofen over a wavelength range from 200 nm to 240 nm. Therefore, the solutions were scanned over other a wavelength range of 240 – 300 nm (**Figure 5.6**).

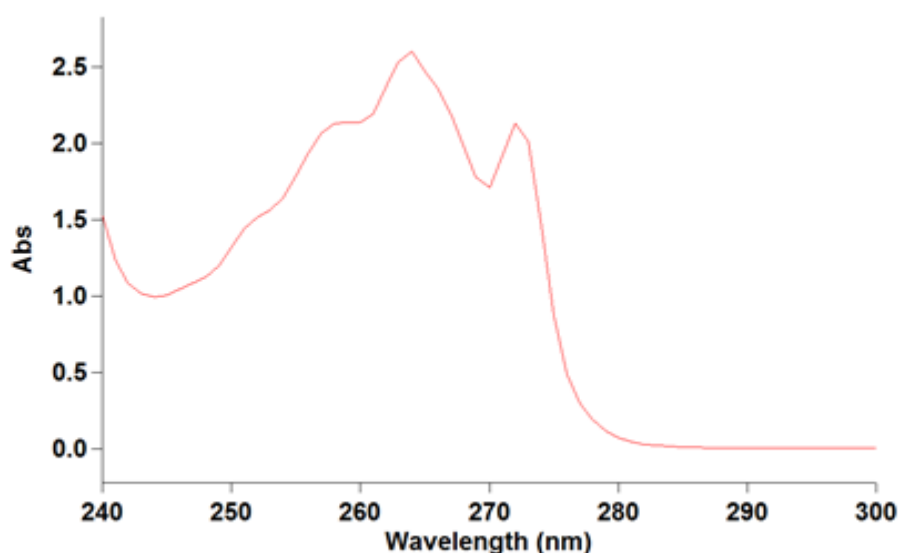


Figure 5.6: UV- absorption spectrum of ibuprofen in PBS (pH 7.4); the maximum absorbance wavelength (λ_{max}) of ibuprofen in PBS was found to be value at 263.9 nm.

5.3.1.2 UV light absorbance by chitosan and TPP

This was done to determine if any interference caused by chitosan and TPP molecules during the spectroscopic analysis of ibuprofen, the UV absorbance profiles of chitosan and TPP used in this study were determined by scanning a solution of each compound over a wavelength range from 240 nm to 300 nm.

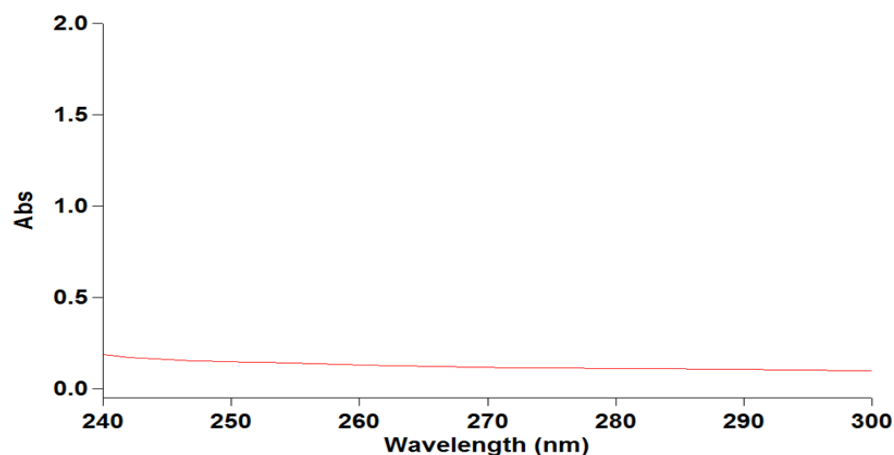


Figure 5.7: UV- absorbance scan for chitosan.

The UV scan of 3.0 mg/mL chitosan solution in diluted acetic acid and 1.0 mg/ml TPP in deionised water showed no absorbance at wavelengths ranging from 240 nm to 300 nm. It is clear from **Figures 5.7 and 5.8** that chitosan and TPP would not significantly interfere with the absorbance of ibuprofen at a wavelength of 263.9 nm which is in agreement with the previous studies (Zhao et al., 2014, Lu et al., 2005, Liu et al., 2014, Ji et al., 2011, Ganesh and Lee, 2013).

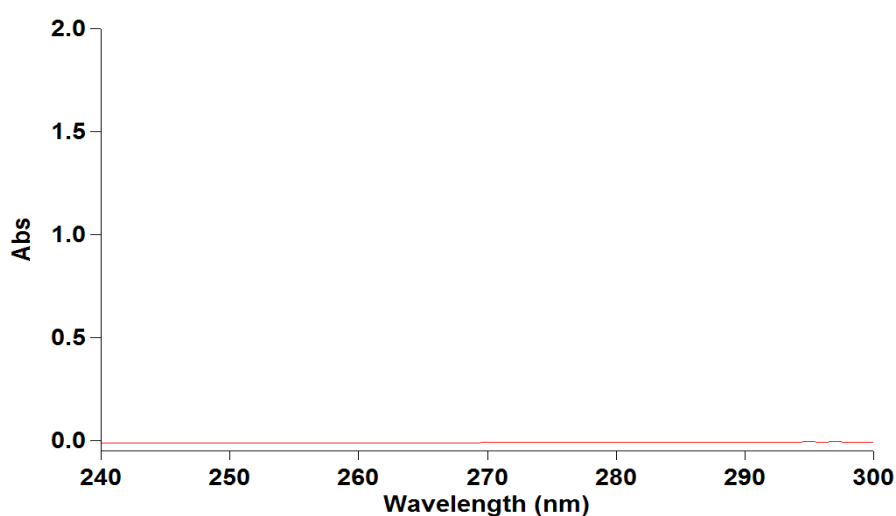


Figure 5.8: UV- absorbance scan for TPP

5.3.1.3 Standard curve and validation for ibuprofen

The method linearity can be determined by evaluation of the calibration curve. The linearity for the ibuprofen assay was determined by performing a linear regression analysis of the absorbance against ibuprofen concentration plot (standard curve). The standard curve was acquired setting the UV wavelength to 263.9 nm. The correlation coefficient (R^2) with a value of 0.9999 indicates a good regression within the given range of 0.01 to 0.8 mg/mL concentrations, which will be analysed in this study (**Figure 5.9**). The data of standard curve is best described by a linear equation:

$$y = 1.6893x + 0.0053 \quad \text{Eq. (5.3)}$$

Therefore, this equation was used to calculate the concentration of ibuprofen in the samples drawn from the dissolution experiments and drug entrapment efficiency experiments.

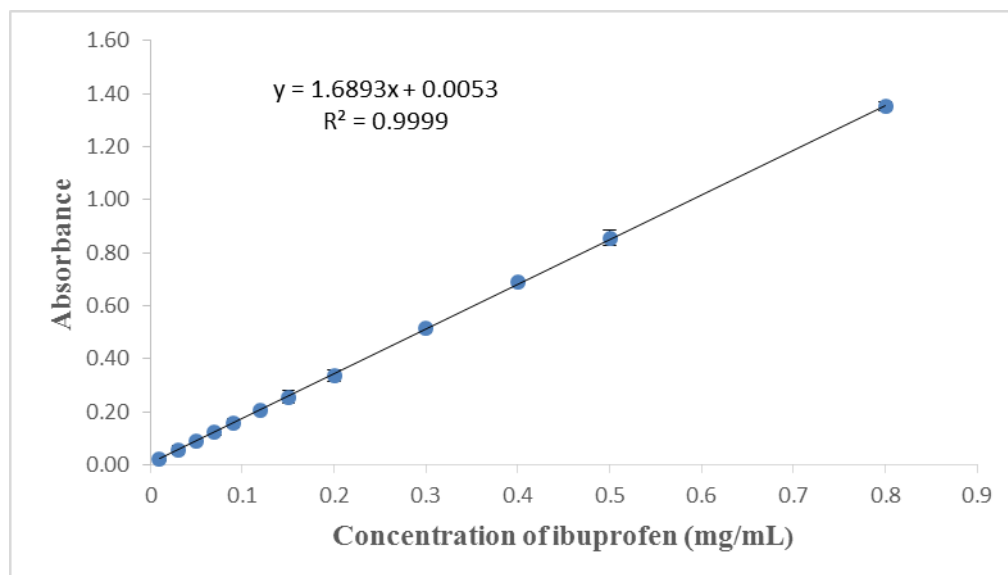


Figure 5.9: Mean calibration curve for ibuprofen preparation in PBS (pH 7.4). Values represent mean \pm SD (n=3).

In this study, besides method linearity there are other parameters including precision, accuracy, limit of detection and limit of quantification which were carried out for analytical method validation. Precision is defined as the closeness of replicate measurements on a single sample. Precision may be considered at two levels: repeatability and reproducibility. Repeatability consists of multiple replicates of the analysis of samples on the same day and with the same instruments by one analyst, on the other hand reproducibility is assessed by different conditions, such as different days, different instruments, different analyst and a different laboratory. Precision is determined by using the process to examine a sample for an adequate number of times to gain statistically valid results, and this is done by analysing samples of each concentration between 3 and 5 times. Moreover, to determine the precision, the mean, standard deviation and relative standard deviation (RSD) are calculated for replicate measurements.

The relative standard deviation is:

$$(\% \text{ RSD}) = (\text{SD} / \text{Mean}) \times 100\% \quad \text{Eq. (5.4)}$$

The method precision for this study was determined by reproducibility (inter-day). It was evaluated by triplicate measurements at three concentration levels (low, medium and high) on different three days. The precision was calculated from the percentage of relative standard deviation (% RSD). For precision the RSD for all samples were within the satisfactory range ($\text{RSD} < 1 \%$). Accuracy is defined according to how far or close a measured experimental value is to the true value. Accuracy shows the

deviation between the mean value found and the true value. Therefore, the accuracy of the test results is calculated as a percentage of the analyte recovered by the assay. Like precision, for all samples, it was found that the RSD < 1 % which is accepted as a satisfactory value for RSD.

Limit of detection (LOD) and limit of quantification (LOQ) are, also, important parameters. LOD is defined as the minimal concentration of sample of interest which can be detected from the background noise with a certain degree of confidence. LOQ is the lowest concentration of an analyte which can provide a quantitative result within specified limits of accuracy and precision. The LOQ and LOD have been determined from calibration curve data. The LOD and LOQ were calculated by statistical methods using standard error (SE) for intensity and concentration and the slope of the calibration curve for caffeine. The LOD value was predicted by using the formula $[3.3 \times SE / \text{Slope}]$. Meanwhile, the LOQ was predicted by using the formula $[10 \times SE / \text{Slope}]$ (Bushra et al., 2014). The UV method validation for the ibuprofen assay presented in **Table 5.1**.

Table 5.1: UV-Spectrophotometric method validation for ibuprofen assay

Wavelength	$\lambda = 263.9 \text{ nm}$
Slope	1.6893
Intercept	0.0053
Correlation coefficient (R^2)	0.9999
Precision and accuracy	RDS < 1 %
LOD	8 $\mu\text{g/mL}$
LOQ	24 $\mu\text{g/mL}$

5.3.1.3.1 Nanoparticle formation observations

Chitosan was dissolved in glacial acetic acid at pH 5, below its pKa 6.3, to produce a reactive positively charged ammonium group (NH_3^+) (protonated amine D-glucosamine monomeric unit). Due to the different pKa values 0.9, 1.9, 5.3, 7.7 and 9.5 (Pati et al., 2011, Bhumkar and Pokharkar, 2006), multiple anions ($\text{P}_3\text{O}_{10}^{5-}$, $\text{HP}_3\text{O}_{10}^{4-}$, $\text{H}_2\text{P}_3\text{O}_{10}^{3-}$, $\text{H}_3\text{P}_3\text{O}_{10}^{2-}$ and $\text{H}_4\text{P}_3\text{O}_{10}^{-}$) may be present in solution depending on the pH when TPP is dissolved in water, which is undesirable as they can competitively react with the protonated ammonium groups (NH_3^+) of chitosan solution (pH 5.0). Therefore, the pH of TPP was adjusted to 5.0 to make sure that predominantly $\text{H}_2\text{P}_3\text{O}_{10}^{3-}$ (~67%) ions exist in solution; this is also beneficial in producing less polydisperse nanoparticles (Sullivan et al., 2018). Moreover, the solutions pH of TPP and chitosan were adjusted to the same value (pH = 5.0) to reduce the alteration of resulting nanoparticle suspension pH. The formation of chitosan nanoparticles by ionic gelation occurs spontaneously upon the interaction with the TPP anion solution (phosphate groups $\text{H}_2\text{P}_3\text{O}_{10}^{3-}$) with the cation chitosan solution (ammonium groups, NH_3^+). The results appearance of the solution changed from clear to one that is opalescent and colloidal upon the contact of chitosan and TPP. This change in solution appearance signified a modification of the physical state of the chitosan to form nanoparticles. Furthermore, ibuprofen (IBU) molecular carrier one negative charge. In the present study we selected ibuprofen as a model drug in the development of controlled drug delivery system (Ganesh and Lee, 2013). Ionized ibuprofen species adsorb onto poly-chitosan nanoparticles containing ammonium groups, through their hydrophilic carboxylic groups leading to, electrostatic interactions or hydrogen bonding (Abioye et al., 2015). The addition of ibuprofen to either the chitosan solution or TPP solution before the chitosan interaction with TPP resulted in a final

solution that was more opalescent, due to the ions of the carboxylate anion (COO^-) of ibuprofen and $\text{H}_2\text{P}_3\text{O}_{10}^{3-}$ of TPP binding to the ammonium group NH_3^+ of chitosan (**Figure 5.10**) (Qandil et al., 2009). As a result, the electrostatic interaction of a strong polycation chitosan, with the ibuprofen or with a mixture of TPP/ ibuprofen should result in a poly cation–multivalent anion complex by ionotropic gelation.

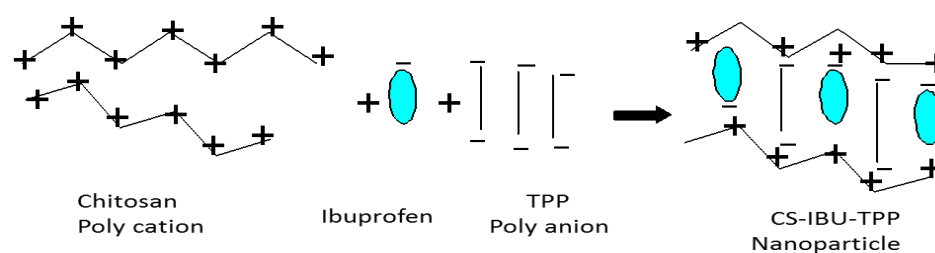


Figure 5.10: Scheme illustration ibuprofen loading/incorporation into chitosan nanoparticles (CS-IBU-TPP).

5.3.1.4 Fourier transform infrared (FT-IR) studied

The FTIR spectra characteristics of pure ibuprofen, blank chitosan nanoparticles and loaded ibuprofen chitosan nanoparticles (CS-IBU-TPP) are shown in **Figure 5.11**.

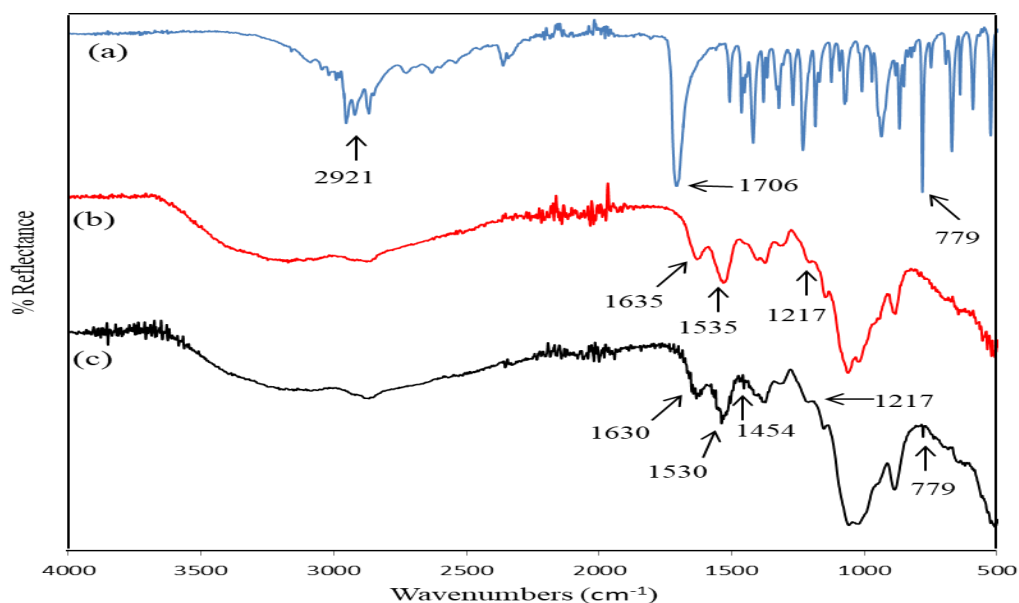


Figure 5.11: FT-IR spectra of (a) Pure ibuprofen, (b) blank CS-TPP nanoparticles (c) ibuprofen loaded chitosan nanoparticles (CS-IBU-TPP).

The spectra were compared to that of pure ibuprofen, unloaded ibuprofen chitosan nanoparticles (CS: TPP) and loaded ibuprofen chitosan nanoparticles (CS-IBU-TPP). The spectrum of ibuprofen exhibited characteristic peak at 2921 cm^{-1} , which can be attributed to O-H group stretching from carboxylic acid (COOH), and an intense absorption at 1706 cm^{-1} absorption bands for the carbonyl (C=O) (Nokhodchi et al., 2015). Moreover, a strong absorption at 779 cm^{-1} represents the aromatic C-H stretching due to the presence of para (1,4-)disubstituted benzene ring (Liu et al., 2014). The spectrum of blank CS: TPP nanoparticles shows absorption bands at 1635 cm^{-1} and 1535 cm^{-1} , corresponding to the linkage between the ammonium ions (NH_3^+) and phosphate ions ($\text{H}_2\text{P}_3\text{O}_{10}^{3-}$) (Bhumkar and Pokharkar, 2006). In addition, the spectrum of CS-TPP nanoparticles also shows a peak at 1217 cm^{-1} which may be attributed to the P=O stretching from TPP (Qi and Xu, 2004). Compared with the

spectrum of ibuprofen (**Figure 5.11a**), in the spectrum of ibuprofen loaded chitosan nanoparticles (CS-IBU-TPP) (**Figure 5.11c**), the absorption peak of 1706 cm^{-1} disappears and a new peak at 1454 cm^{-1} (salt of carboxyl) appears (Wu et al., 2005). However, two peaks at 1635 cm^{-1} and 1535 cm^{-1} in CS: TPP nanoparticles (**Figure 5.11b**), slightly shifted to a sharp peaks at 1630 cm^{-1} and 1530 cm^{-1} in (CS-IBU-TPP) nanoparticles (**Figure 5.11c**), suggesting that the carboxylic group of ibuprofen electrostatic interacts with amino groups of chitosan nanoparticles (Abioye et al., 2016, Dudhani and Kosaraju, 2010). Furthermore, the FT-IR spectrum of ibuprofen loaded chitosan nanoparticles (CS-IBU-TPP) show the peak at 779 cm^{-1} , providing evidence that ibuprofen presence in the chitosan nanoparticles (Liu et al., 2014).

5.3.2 Ibuprofen entrapment results using two methods UV-spectrophotometry

Iontropic gelation is a popular and widely used preparation method, especially when chitosan particulate systems are involved in *in vitro* drug delivery (Mohammadpour Dounighi et al., 2012). Such a great extent of usage is due to the method's simplicity, mildness, effectiveness without organic solvents, and mitigation of toxicity, which afford ionotropic gelation with a distinct advantage above other chemical crosslinking procedures (Mohammadpour Dounighi et al., 2012, Dash et al., 2011). In particular, ionotropic gelation is predicated on the occurrence of electrostatic forces between the positive charge of a polycation with the negative charge of a polyanion (Dung et al., 2007, Sailaja et al., 2010). In the case of this experiment, the polycation was chitosan and the anion was ibuprofen (IBU), while TPP was introduced as a crosslinking agent. TPP in its sodium salt form is commonly used as a crosslinking agent because of its nontoxicity, stabilisation of chitosan, as well as its promotion of gel formation (Gan et al., 2005, Gan and Wang, 2007, Zhang et al., 2013). However, in practice, it has been

shown that crosslinking agents such as TPP can compete with polyanions such as IBU for the limited number of binding sites on chitosan, which could adversely affect drug entrapment efficiency (Zhang et al., 2013). Additionally, it is possible that chitosan and ibuprofen molecules could interact when they are close together, which could eventually have a negative impact on crosslinking. Entrapment efficiency of ibuprofen reflects the amount of ibuprofen that is adsorbed on the chitosan nanoparticles that are prepared by different methods (Manjanna, Shivakumar, & Pramod, 2009, Xu et al., 2003). Thus, (Zhang et al., 2013) maintain that material addition sequences are among the most important factors that influence the preparation of drug-polymer complexes via ionotropic gelation. The significance of material addition sequence as mentioned above is seen clearly in the findings of this experiment. To illustrate, as seen in **Figures 5.12** and **5.13**, the method involving the ibuprofen was first mixed with chitosan prior to incorporation with TPP solution, referred to as (IBU+CS)/TPP and the addition of IBU into TPP prior to these two chemicals are added to chitosan, referred to as CS/(TPP+IBU). Upon mixing either chitosan or TPP with ibuprofen there is an initial dilution, however when the TPP is added to chitosan (IBU+CS)/TPP or chitosan is added to TPP CS/(TPP+IBU) the subsequent dilution of the added material results in nanoparticles which are of the same final CS: TPP ratios in both **Figure 5.12** and **Figure 5.13**.

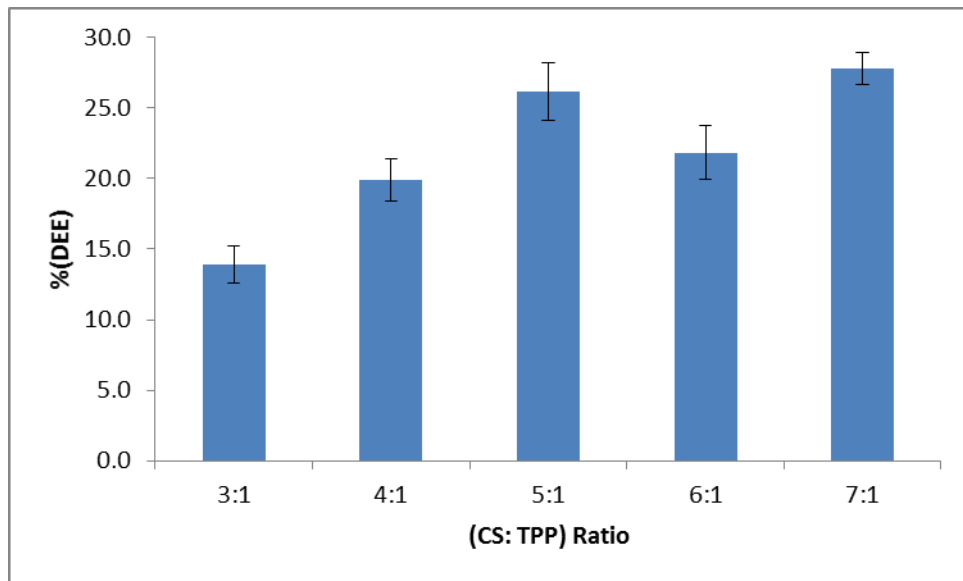


Figure 5.12: First method an internal entrapment of ibuprofen into chitosan nanoparticles, ibuprofen first mixed with chitosan: (IBU+CS)/TPP. The entrapment efficiency of ibuprofen generally increased with CS:TPP ratio for the CS+IBU/TPP design.

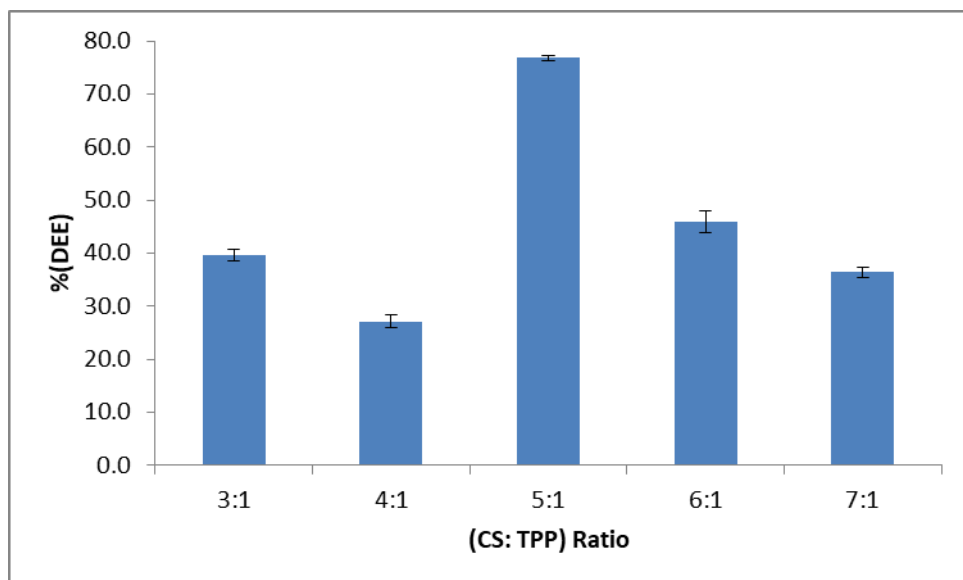


Figure 5.13: Second method an internal entrapment of ibuprofen into chitosan nanoparticles, ibuprofen first mixed with TPP: CS/(TPP+IBU). The entrapment efficiency of ibuprofen differed greatly and appeared to be independent of CS:TPP ratio in the CS/(TPP+IBU) design.

In **Figure 5.12** the result may be explained due to chitosan and ibuprofen prematurely interacted in the (IBU+CS)/TPP solutions. Moreover, it is possible that ibuprofen could have formed a preferential complex with chitosan due to the close proximity in which they were placed. In this way, it is also plausible to infer that the amount of free cationic chitosan sites with which the anionic sites of TPP could interact were lessened. In turn, this occurrence may have lowered the chances that chitosan and TPP had to interact and subsequently form a tightly bound matrix upon addition of the latter. The sequence of material addition in the (CS+IBU)/TPP solution resulted in decreased amounts of effectively entrapped ibuprofen due to late addition of the crosslinking agent TPP, which is reflected by the low DEE% values (**Figure 5.12**). Furthermore, the trends in DEE% may also be explained by the concentration of chitosan (Patel and Patel, 2014, Kunjachan and Jose, 2010). When ibuprofen is first mixed with chitosan before the addition of TPP, concentration of chitosan solution was initially diluted, then the DEE% increases with increasing CS: TPP ratio and therefore increasing concentration of chitosan, as seen in **Figure 5.12**. In addition, in **Figure 5.12**, as the maximum percentage drug entrapment efficiency is with ratio of 7:1, which is 27.8%. Other CS: TPP ratios 3:1, 4:1, 5:1, and 6:1 show entrapment efficiencies of 13.9%, 19.9%, 26.2% and 21.8% respectively. The graph clearly shows that if the drug is first mixed with the chitosan, then the results will not exceed above 28%. In fact, the CS: TPP ratio of 7:1 produced the highest DEE% for this material addition sequence. Such a result may have occurred due to the greater availability of free chitosan molecules that have not formed preferential complexes with ibuprofen as CS: TPP rises, which are then free to interact with TPP when it is added. Hence, a direct relationship between chitosan concentration and DEE% for this material addition sequence may be discerned (Kunjachan and Jose, 2010). However, the 5:1

ratio exhibits the second highest DEE% value for this material addition sequence. As such, it can be said that this ratio of CS to TPP is the one at which the DEE% for this drug delivery system can be optimised for the material addition sequence of (IBU+CS)/TPP (Kunjachan and Jose, 2010). When ibuprofen is first mixed with TPP (**Figure 5.13**), concentration of chitosan before mixing is 3 mg/mL and graph presenting percentage drug entrapment efficiency (%DEE) with relation to CS: TPP, maximum percentage obtained is approximately 76.8% with the ratio used of 5:1 of CS: TPP, respectively. Other ratios used from 3:1, 4:1, 6:1 and 7:1 showed percentage of drug entrapment efficiency 39.6%, 27.1%, 45.9% and 36.4% respectively. It was hypothesized that loading ibuprofen into TPP solution prior to incorporation with chitosan solution, the anionic of ibuprofen molecules were further negatively charged carboxylate group (COO^-) in the TPP solution as the pH of the solution around 7.4, which favours the electrostatic reaction between the ions of carboxylate (COO^-) and the NH_3^+ of chitosan and consequential higher drug entrapment efficiency. Across both of the material addition sequences that were implemented, it is evident that the CS: TPP ratio of 5:1 in the CS/(TPP+IBU) solutions can provide the greatest effectivity of drug entrapment, as reflected by the calculated DEE% value of 76.8 for this condition. Moreover, previous studies (Jelvehgari et al., 2011, Patel and Patel, 2014) conducted further corroborate these findings, as the authors discovered that drug: polymer ratio and crosslinking agent concentration have a significant impact on % entrapment efficiency. At a CS: TPP ratio of 5:1, it is possible that the amounts of drug, polymer, and crosslinking agent that were present may have been optimised. However, the DEE% decreases with CS: TPP increasing from 6:1 – 7:1. This result may be attributed to the carboxylate group of ibuprofen is present in lower amounts, as the pH of the solution reduced, therefore little ibuprofen is able to interact when

added to chitosan (Al-Hamidi et al., 2015). There are some factors which may cause decrease or increase in percentage drug entrapment efficiency such as entrapment conditions. The change in these parameters can affect the entrapment efficiency (Garlea et al., 2007). Moreover, the water insoluble drugs, usually have lesser drug entrapment efficiency than that of soluble. About 65% to 85% of the efficiency is obtained by encapsulation of fat-soluble drug by cross-linking technique of immobilization (Sinha et al., 2004).

5.3.3 Characterization of chitosan nanoparticles and effects of CS-TPP ratio on CS-IBU-TPP nanoparticles

In this study, the influence of different CS: TPP ratios (3:1, 4:1, 5:1, 6:1 and 7:1) on CS-IBU-TPP nanoparticles were investigated by measuring the particle size, zeta potential and DEE of CS-IBU-TPP nanoparticles. The Malvern Zetasizer NANO-Z was used to measure the particle size and zeta potentials characteristics of both ibuprofen-loaded chitosan-TPP (CS-IBU-TPP) nanoparticles and chitosan-TPP (CS: TPP) nanoparticles.

5.3.3.1 Dynamic light scattering (DLS)

Particle size is common analysis, which determined the biocompatibilities and bioactive of nanoparticles, as well as small nanoparticles have cross epithelia and have the higher intracellular uptake than microparticles (Wu et al., 2005). Therefore, to improve intracellular uptake, it was better to reduce particle size as much as possible. In addition, the particle size investigation is a very important factor

characterization process for nanoparticles since it helps understanding their dispersion and aggregation method (Desai et al., 1997). As shown in **(Figure 5.14a)** five ratios (3:1, 4:1, 5:1, 6:1 and 7:1) of CS: TPP were chosen to study its effect on the features of chitosan nanoparticles. The other parameters were fixed at chitosan concentration is 3 mg/mL and ibuprofen concentration is 1.5 mg/mL. The ability of chitosan to interact with TPP depends on the formation of inter- and intramolecular cross-linking between ammonium groups (NH_3^+) and phosphate groups. When the CS: TPP ratio was small, the available quantity of TPP was high, as a result increased cross-linking density between chitosan and TPP. The particle size characteristics found to influence the biological performance of chitosan nanoparticles (Papadimitriou et al., 2008). For this reason, before ibuprofen encapsulation into CS: TPP nanoparticles, the effect of CS: TPP ratio on the particle size characteristics was studied in order to find the best ratio which results in nanoparticles of relatively low size and narrow size distribution. With an increase in CS: TPP ratio, the particle size increases due to decreased cross-linking density between chitosan and TPP (Liu and Gao, 2009), an increase in viscosity can also increase particle size (Kawadkar and Chauhan, 2012). This result is similar to previous study with reported increases in the particle size with increases in CS: TPP ratio (Gan et al., 2005). It appears from **(Figure 5.14a)** that, drug loading affects the size of the chitosan nanoparticles. Ibuprofen (1.5 mg/mL) loading decreased particle size in comparison to the “native” nanoparticles. These differences are statistically significant ($p < 0.05$) at all CS: TPP ratios.

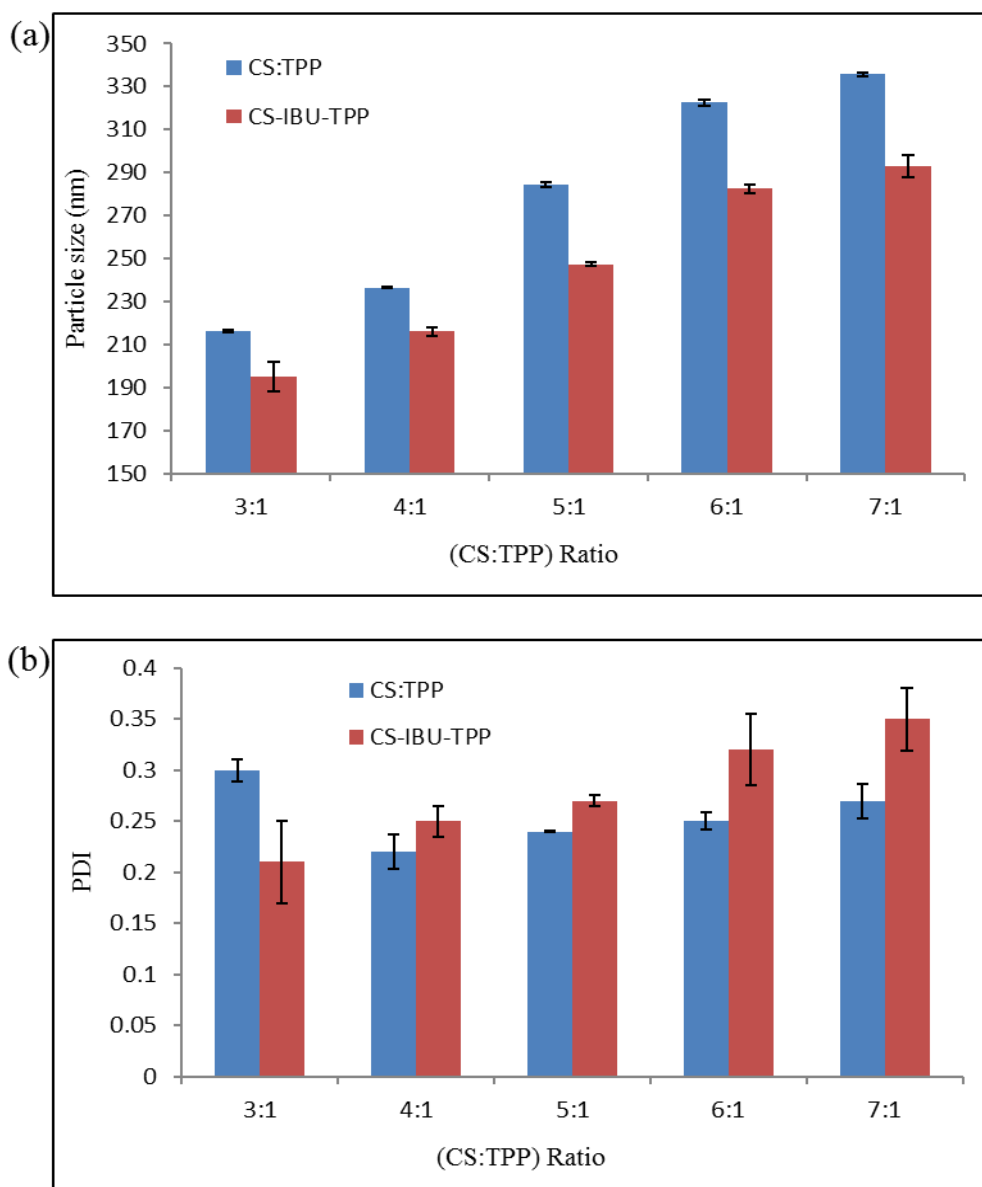


Figure 5.14: The effect of (CS: TPP) ratio on the (a) particle size and (b) polydispersity index (PDI), ibuprofen free nanoparticles (blue columns); ibuprofen loaded nanoparticle (brown columns). All data are the mean \pm SD for n = 3 replicates.

It is interesting to notice that when CS: TPP ratio changes from 3:1 to 6:1 a significant increase of particle size is observed ($p < 0.05$). When CS: TPP ratio increased, the presence of ibuprofen starts to play a dominant role. It should be noted that with the addition of ibuprofen the particle size was reduced, suggesting that the presence of an

additional negatively charged carboxylate groups (COO^-) in the mixture. Within the tested chitosan to TPP ratio range conditions, ibuprofen (1.5 mg/mL) loading increased the particle size following a linear relationship (**Figure 5.14a**) with increase in chitosan to TPP ratio: 195 ± 4 , 216 ± 2 , 247 ± 1 , 283 ± 2 , and 293 ± 5 for 3:1, 4:1, 5:1, 6:1 and 7:1, respectively (Appendix D).

Polydispersity index (PDI) is a parameter used to define the particle size distribution of chitosan nanoparticles. In addition, the PDI value of 0.1 to 0.25 refers a narrow size distribution, whereas, a PDI of more than 0.5 indicates to a broad size distribution (Wu et al., 2011). The PDI measured for each ibuprofen loading as well as the empty chitosan nanoparticles was more than 0.2 as exhibited in (**Figure 5.14b**). The empty nanoparticles (native) have polydispersity index of 0.22 ± 0.02 to 0.30 ± 0.01 , and the ibuprofen loaded nanoparticles have polydispersity index of 0.21 ± 0.04 to 0.35 ± 0.03 , as shown in (**Figure 5.14b**) indicating a narrow size polydispersity. In addition, all the values of PDI were below 0.35, indicating that a homogenous dispersion of nanoparticles were obtained (Hu et al., 2008).

Zeta potential is another key parameter providing the density of the surface charge, and can inflects the stability of nanoparticle in suspension. High zeta potential ($> +30$ mV) indicates high stability of nanoparticles due to the electrostatic repulsion amongst nanoparticles (Müller et al., 2001, Hu et al., 2008). As shown in **Figure 5.15**, the chitosan nanoparticles with all ratios demonstrated high zeta potential values, suggesting that these nanoparticles can be stable for long-term storage. Increases in the zeta potential was observed as the CS: TPP ratio increased. Furthermore, the

ibuprofen loaded chitosan nanoparticles did not cause a significant reduction in the zeta potential at all ratios compared to the “native” nanoparticles ($p > 0.05$).

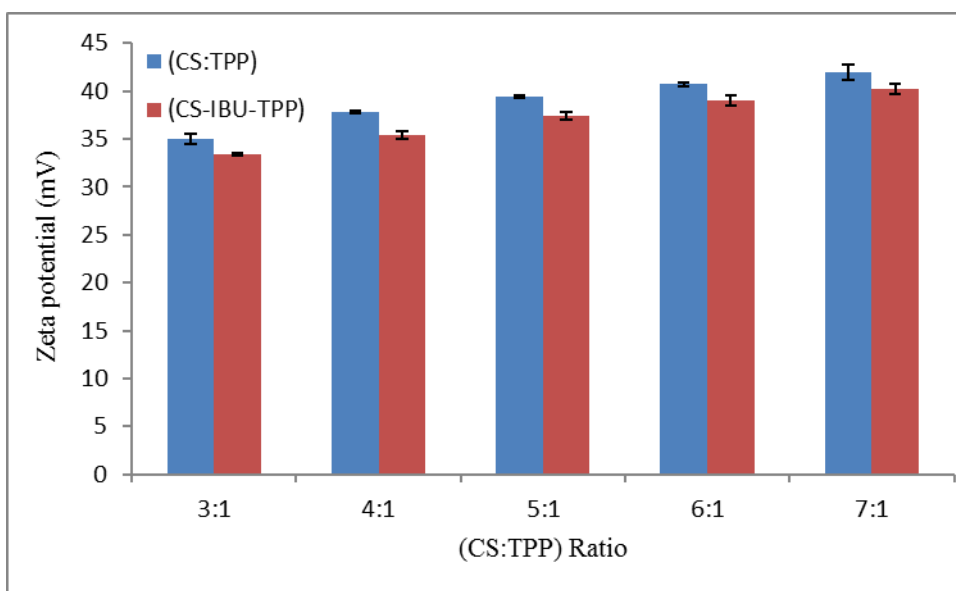


Figure 5.15: The effect of (CS:TPP) ratio on zeta potential, ibuprofen free nanoparticles (blue columns); ibuprofen loaded nanoparticle (brown columns). All data are the mean \pm SD for $n = 3$ replicates.

5.3.4 Effects of CS: TPP ratio on CS-IBU-TPP nanoparticles

CS: TPP ratio is an important factor, which affects the characteristics of CS-IBU-TPP nanoparticles. Drug entrapment efficiency (DEE) of CS-IBU-TPP nanoparticles is defined as a percentage of ibuprofen loading content that can be entrapment into CS: TPP nanoparticles. As shown in **Table 5.2**, DEEs of CS-IBU-TPP nanoparticles ranged from 27.1 % to 76.8 % at variable CS-TPP ratios and the highest DEE was 76.8 % corresponding to the CS: TPP ratio at 5:1. In addition, when CS-IBU-TPP nanoparticles were prepared at CS: TPP ratio at 5:1, the zeta potential ($+37.4 \pm 0.4$

mV) indicated that the solution of CS-IBU-TPP nanoparticles can maintain a stable suspension for a long time, furthermore, the particle size of CS-IBU-TPP nanoparticles was 247.3 ± 1.0 nm. However, when the CS: TPP ratio is over (5:1), the aggregation of nanoparticles occurs, which indicated the reduction of drug entrapment efficiency.

Table 5.2: The particle size, zeta potential, drug content (DC) and DEE of CS-IBU-TPP nanoparticles at variable CS: TPP ratios.

CS-TPP ratio	Particle size (nm)	PDI	Zeta potential (mV)	DC (%)	DEE (%)
3:1	195.0 ± 4.2	0.21 ± 0.04	$+33.4 \pm 0.1$	4.4 ± 1.2	39.6 ± 7.4
4:1	216.0 ± 1.9	0.25 ± 0.02	$+35.4 \pm 0.3$	2.7 ± 0.4	27.1 ± 2.5
5:1	247.3 ± 1.0	0.27 ± 0.01	$+37.4 \pm 0.4$	7.0 ± 0.2	76.8 ± 1.3
6:1	282.5 ± 2.1	0.32 ± 0.03	$+39.0 \pm 0.5$	3.9 ± 0.8	45.9 ± 6.4
7:1	293.0 ± 5.3	0.35 ± 0.03	$+40.2 \pm 0.6$	2.9 ± 0.9	36.4 ± 7.9

Moreover, the DEE of CS-IBU-TPP nanoparticles was highest therefore, CS: TPP ratio at 5:1 would be used in the subsequent experiments to study the influences of ibuprofen concentration on the characteristics of CS-IBU-TPP nanoparticles and *in vitro* release study of ibuprofen from CS-IBU-TPP nanoparticles.

5.3.5 Effects of ibuprofen concentration on CS-IBU-TPP nanoparticles

In this section, a series of ibuprofen concentrations were set to study its effect on the characteristics of CS: TPP nanoparticles. The particle size, zeta potential and drug

entrapment efficiency (DEE) of CS-IBU-TPP nanoparticles at different concentrations of ibuprofen (0, 0.5, 1.0, 1.5, 2.0 and 2.5 mg/mL) were summarized in **Table 5.3**. As shown, the increased particle size and decreased zeta potential of CS-IBU-TPP nanoparticles is a good indication of the entrapment of ibuprofen in the chitosan nanoparticles. The particle size of CS-IBU-TPP nanoparticles increased from 284.1 nm to 348.3 nm with the increase of ibuprofen concentration in the range of 0.5 – 2.5 mg/mL. The particle size distribution for the CS-IBU-TPP nanoparticles are represented in Appendix E. It can be observed that when the concentration of ibuprofen was lower than or equal to 1.5 mg/mL, the particle size of CS-IBU-TPP nanoparticles was smaller than that of the size of “native” nanoparticles (CS: TPP) (unloaded drug). This phenomenon may be attributed to a greater cross-linking density of the CS-IBU-TPP nanoparticles, which caused by the interactions between chitosan and ibuprofen. On the other hand, when the concentration of ibuprofen was higher than or equal to 2.0 mg/mL, the particle size of CS-IBU-TPP nanoparticles was larger than that of the “native” CS: TPP nanoparticles (unloaded drug). It is thought that at higher ibuprofen loading concentration, ibuprofen adsorbed on the particles, leading to rise of particle size. This may be confirmed by the reduced in zeta potential. Moreover, the PDI of the CS-IBU-TPP nanoparticles suspension increased (more than 0.4) at higher ibuprofen loading concentration, which might be caused by the formation of linkages or aggregation of the nanoparticles.

Table 5.3: The particle size, zeta potential, drug content (DC) and DEE of CS-IBU-TPP nanoparticles at variable concentrations of ibuprofen (IBU).

IBU (mg/mL)	Particle size (nm)	PDI	Zeta potential (mV)	DC (%)	DEE (%)
0	293.6 ± 4.2	0.30 ± 0.04	+39.4 ± 0.1	n/a	n/a
0.5	284.1 ± 4.1	0.36 ± 0.02	+38.6 ± 0.5	3.2 ± 0.4	86.6 ± 9.3
1.0	256.9 ± 3.4	0.27 ± 0.01	+37.4 ± 1.0	3.8 ± 0.8	60.2 ± 11.7
1.5	247.3 ± 1.0	0.27 ± 0.04	+36.3 ± 0.4	7.0 ± 0.2	76.8 ± 1.3
2.0	378.7 ± 9.2	0.49 ± 0.03	+34.1 ± 1.3	3.3 ± 0.5	27.8 ± 6.9
2.5	348.3 ± 9.9	0.43 ± 0.02	+33.8 ± 1.3	4.2 ± 0.8	29.0 ± 3.6

As shown in **Table 5.3**, all the zeta potentials of CS-IBU-TPP nanoparticles at different concentrations of ibuprofen were greater than +30 mV, due to repulsive forces between particles and therefore leads to minimal aggregation, indicating a high stability of CS-IBU-TPP nanoparticles (Parida et al., 2013). It appears from **Table 5.3** that, the ibuprofen concentration did affect the zeta potential of the CS-IBU-TPP nanoparticles significantly ($p < 0.05$). Therefore, there is a clear decrease in charge. The effect of ibuprofen concentration on drug entrapment efficiency (DEE) was studied at the concentrations of (0, 0.5, 1.0, 1.5, 2.0 and 2.5 mg/mL), and summarized in **Table 5.3**. The DEEs of CS-IBU-TPP nanoparticles ranged from 27.8 % to 86.6 % and the highest DEE was obtained at ibuprofen concentration of 0.5 mg/mL. It should be noted that, at high concentrations of ibuprofen 2.0 mg/mL and 2.5 mg/mL, the DEE % was 27.8 % and 29.0 % respectively, which may be attributable to the limited availability of loading sites for the higher concentration of ibuprofen (Sogias et al., 2012, Alshehri et al., 2016). Considering the possible pharmaceutical application of

nanoparticles in drug delivery system, smaller particle size, relatively high DEE and ibuprofen release are more effective in improving the bioavailability of ibuprofen (Hu et al., 2008, Wang et al., 2011). In this study, when the concentrations of ibuprofen were 0.5 mg/mL and 1.5 mg/mL, the particle size of CS-IBU-TPP nanoparticles were 284.1 nm and 247.3 nm, respectively; and the higher DEE were 86.6 % and 76.8 %, respectively. Therefore, ibuprofen concentrations of 0.5 mg/mL and 1.5 mg/mL were chosen to determine *in vitro* release profiles of ibuprofen in subsequent experiments. High concentration of loaded ibuprofen caused increased in PDI values, indicating wider piratical size distribution (Appendix E).

5.3.6 *In vitro* release of ibuprofen (IBU) from CS-IBU-TPP nanoparticles

In this study, the ibuprofen was not chemically reacted with chitosan, but the interactions were due to electrostatic attractions, also it is entrapped within the chitosan nanoparticles. Thereby, the ibuprofen remains in a biologically active form and can use its effect upon the body as soon as it is released from the polymer matrices (Win et al., 2005). In this section ibuprofen was studied *in vitro* as a model drug in drug release study from chitosan-TPP nanoparticles using pH 7.4 PBS for 9 hours at 37 °C. *In vitro* release of ibuprofen from chitosan nanoparticles with respect to different concentrations of ibuprofen (0.5 mg/mL and 1.5 mg/mL) were shown in **Figure 5.16**. 500 mg of ibuprofen-loaded nanoparticle formulations were weighed and injected in the dialysis membranes, which were placed in basket and immersed in 200 mL of PBS. The ibuprofen-loaded chitosan nanoparticles provided a sustained release of ibuprofen releasing between 35 – 50 % of drug during 9 hour period of study.

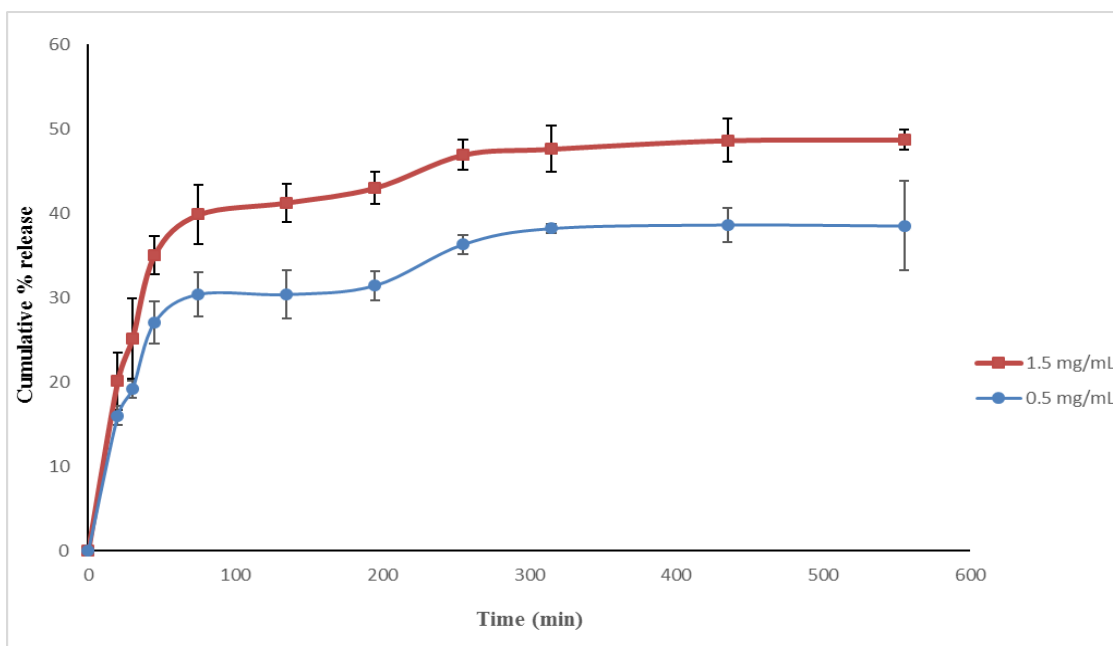


Figure 5.16: *In vitro* release profiles of ibuprofen from CS-IBU-TPP nanoparticles with respect to different concentration of ibuprofen, carried out in phosphate buffer at pH 7.4 maintained at 37 °C. (Mean ± SD, n=3).

The drug release curves resemble those that are obtained when diffusion controlled-release is involved (Siegel and Rathbone, 2012). This observation is to be expected given the use of chitosan nanoparticles, which act as a matrix for the drug. In this experiment, the chitosan nanoparticles provide surfaces from which the drug particles dissociate, surround themselves with solvent, then diffuse, which prolongs the half-life of ibuprofen (Irvine et al., 2018, Islam and Ferro, 2016). However, a lag period from 100 to 300 minutes exists wherein the % release slowed down after an initial burst. The initial burst followed by the lag periods can be attributed to the difference in dissolution speeds of surface-associated drug particles as compared to those that are located further inside (Siegel and Rathbone, 2012). The mechanism of ibuprofen release is therefore explained by the diffusion of ibuprofen localized at the particle

surface. The diffusion of ibuprofen was enhanced at PBS (pH 7.4) (Lin et al., 2005) due to the deprotonation of chitosan, as a consequence, the interaction between the polycation chitosan and the polyanion TPP weakened or disappeared. So, ibuprofen was released quickly, and then followed by a slow drug release (Zhao et al., 2014). Also ibuprofen is readily soluble above pH 7.2 therefore initial dissolution from the surface would be expected. Higher ibuprofen loading causes increased total particle surface area available for burst release from particles. The drug release reflected that the cumulative release of ibuprofen from CS-IBU-TPP nanoparticles of concentration 1.5 mg/mL (drug content 2.5%) was higher than their nanoparticle counterparts 0.5 mg/mL (drug content 3.2%) for different time periods. Such observations were consistent with respect to time. The drug release also reflected that the release of ibuprofen (1.5 mg/mL) from chitosan nanoparticles was significantly higher at the start which was maintained until the termination of release. Such findings complement the binding profile of ibuprofen on the chitosan nanoparticles (Luo and Wang, 2014). The two ibuprofen formulations exhibited slow release profiles under the given test conditions. This is because the official threshold of 85% cumulative release (Popa et al., 2014) was not met, even when 555 minutes was reached. Nevertheless, within the first 20 minutes of observation, the 1.5 mg/ml ibuprofen solution displayed a greater extent of release when compared to the 0.5 mg/ml ibuprofen solution, a difference which was emphasised with time. Ibuprofen was not chemically bound to chitosan, but remained entrapped within chitosan through electrostatic interactions. The results from this release study are similar to those found using chitosan as a reservoir for ibuprofen. (Tang et al., 2014) reported that around 70 % of ibuprofen was released from ibuprofen loaded chitosan films over 460 min. Another study conducted using chitosan/IB-MSNs (embedded mesoporous silica

nanoparticles), and the results showed that 65 % of ibuprofen released (Zhao et al., 2014). Several factors can be attributed to the observed drug release characteristics of the two test solutions. The low degradability and solubility of chitosan at pH 7.4 may be among the causes of the slow and less than 50% release of ibuprofen (Agnihotri et al., 2004, Popat et al., 2012). Unfortunately, some studies (Jin-gou et al., 2012, Jayakumar et al., 2010) show that although chitosan nanoparticles have advantages such as biocompatibility and nontoxicity, several drawbacks persist. One such drawback entails the insufficient entrapment of a poorly water-soluble drug such as ibuprofen within the chitosan matrix due to the insolubility of chitosan at neutral pH, under which the dissolution studies were performed (Jin-gou et al., 2012). However, had the dissolution study been undertaken at the isoelectric point of chitosan (pH 6.5) rather than pH 7.4, then loading efficiency may have improved (Bowman and Leong, 2006). Ibuprofen is ionised in alkaline solutions leading to an increase in solubility of the ibuprofen at high pH. As the pH increased, the solubility of the ibuprofen increased and production a highly soluble carboxylate ions due to increase in the ionization of the ibuprofen (Hadgraft and Valenta, 2000) (**Figure 5.1**). Solubility has been reported to be very poor 0.059 mg/mL at low pH (0.1 N HCl) (Al Masum et al., 2012), however, the solubility of the drug dramatically increased, with increasing pH (Abioye and Kola-Mustapha, 2015). Another previous study reported the solubility of Ibuprofen in PBS at pH 7.4 to be 6.02 mg/ml (Levis et al., 2003). Previous studies have suggested that small size of the chitosan nanoparticles produce greater surface area for entrapment of ibuprofen. As a result of greater surface area, the release of ibuprofen from the small-sized chitosan nanoparticles is faster than their large-sized counterparts (Nokhodchi et al., 2010). Hence, ibuprofen at higher doses small size (247.3 ± 1.0 nm) and greater surface area, therefore, got effectively trapped and

released from (1.5 mg/mL) ibuprofen loaded chitosan nanoparticle (DC 2.5%). On the contrary, the (0.5 mg/mL) of ibuprofen loaded chitosan nanoparticle (DC 3.2%) could have presented lesser surface area and higher size (284.1 ± 4.1 nm). Hence, the loading dose and release of ibuprofen from such nanoparticles were lower compared to their 1.5 mg/mL ibuprofen loaded chitosan nanoparticle counterparts. Due to the low solubility of ibuprofen and the large volume of dissolution media, it is most certainly in sink conditions, the total amount of drug that was added to the dissolution bath were 0.025 mg and 0.034 mg for 0.5 and 1.5 mg/mL of ibuprofen solution respectively, and with solubility of ibuprofen 6.02 mg/mL, this demonstrates sink conditions were present in the experiment. In particular, saturation solubility of a drug in the dissolution medium should be at least three times that of the drug concentration in order to maintain sink conditions (Phillips et al., 2012). However, for poorly water-soluble compounds such as ibuprofen (Faruki et al., 2013, Irvine et al., 2018), aqueous media cannot create such conditions. As such, lowered levels of drug release and slow release rates are not uncommon (Phillips et al., 2012). Also, poor sorption of ibuprofen onto the chitosan nanoparticles could be another cause of the observed drug release characteristics (Faruki et al., 2013). It is possible that the presence of chemicals such as NaOH, KCl, Na₂HPO₇, and KH₂PO₄ resulted in the dissociation of ibuprofen to the anionic form and therefore insufficient amounts of ibuprofen interacted with the chitosan nanoparticles (Oh et al., 2016). With regards to the 0.5 mg/ml ibuprofen solution, since the drug concentration was lower, it is likely that fewer drug molecules interacted with the chitosan nanoparticles, thereby yielding slower release rates and % release relative to the 1.5 mg/ml ibuprofen solution. Studies further suggest that the release of ibuprofen from the chitosan polymers was dependent on pH. Low pH inhibits the release of the ibuprofen from chitosan (Khan et

al., 2011). This is because low pH reduces the swelling of chitosan nano-conjugates in experimental media or body fluids and ibuprofen is poorly soluble at low pH. For example, release of ibuprofen from chitosan is not mediated in the stomach. Hence, the chitosan-mediated ibuprofen release incurs a bypass at the stomach, a property that reduces the chances of peptic ulcer (Vieira et al., 2013). The overestimation of drug content could have been caused by the use of centrifugation to separate the chitosan nanoparticles and drug molecules. This is because the application of centrifugal forces could have resulted in premature release of the drug as well as a greater drug content (Moreno-Bautista and Tam, 2011). In this study ultracentrifuge at 40,000 g for 60 min was used to separate all ibuprofen loaded chitosan nanoparticles. Some studies, however, reported speed at 16,000 rpm for 30 min (Ji et al., 2011), 10,000 rpm for 5 min (Qiu et al., 2001), 9000 rpm for 20 min (Varga et al., 2014), 15,000 rpm for 30 min (Thakur et al., 2013), 5000 rpm for 60min (Abioye et al., 2016), 25,000g for 30 min (Jain and Banerjee, 2008), 13000 g for 10 min (Katas and Alpar, 2006), 20,000 g for 30 minutes (Mohammadpour Dounighi et al., 2012) to separate particles. Additionally, the USP apparatus used in the experiment has been found to be inappropriate when smaller medium volumes are used for poorly water-soluble drugs. Larger vessels of capacities up to 1000-mL may reduce the chances of errors in future experiments (Pezzini et al., 2015).

5.3.6.1 Comparison of Drug Release Profiles: f_2 Analysis

f_2 is logarithmic reciprocal square root transformation of one plus the mean squared (the average sum of squares) differences of drug percent dissolved between test solution and reference solution (**equation 5.5**) (Costa and Lobo, 2001).

$$f_2 = 50 \times \log \left\{ \left[1 + \frac{1}{n} \sum_{t=1}^n (R_j - T_j)^2 \right]^{-0.5} \times 100 \right\} \quad \text{Eq. (5.5)}$$

Where, f_2 is similarity factor, T_j is average percentage drug dissolved from test formulation, R_j is average percentage drug dissolved from reference formulation and n is the number of sampling time. The drug release profiles of the two test solutions can be further compared using f_2 analysis (Costa and Lobo, 2001). f_2 evaluation was to compare the dissolution between ibuprofen which was loaded on 1.5 mg/mL and 0.5mg/mL chitosan nanoparticle respectively. In the present experiment, the calculated f_2 value for the 0.5 mg/ml and 1.5 mg/ml IBU solutions is 52.5. According to (Pillay and Fassihi, 1998), an f_2 value between 50 and 100 shows that the test and reference solutions are equivalent or the same, with a value of 100 representing total equivalence or sameness. The obtained f_2 value for the test solutions is above 50, which suggests that the two test solutions appear to be equivalent for two nanoparticle concentrations (Costa and Lobo, 2001, Pillay and Fassihi, 1998, Polli et al., 2004).

5.4 Summary

It has been previously reported that using ibuprofen as pharmaceutical drug can be prepared by the interaction of cationic chitosan with ibuprofen using many different methods including chitosan microparticles (Lu et al., 2005, Kulkarni et al., 2007), chitosan hydrogels (Liu et al., 2014) chitosan with ibuprofen (Qandil et al., 2009). In this chapter, chitosan nanoparticles were successfully prepared using the polyanion TPP to create ionic cross-linking with amino groups of chitosan using the ionotropic gelation method at different CS: TPP ratios including 3:1, 4:1, 5:1, 6:1 and 7:1. The CS and TPP ratio is important and controls the size of the nanoparticles. Moreover, it has been demonstrated that chitosan nanoparticles can incorporate appreciable quantities of ibuprofen into nanoparticles CS-IBU-TPP using two methods. The carboxylate ions (COO^-) of ibuprofen and $\text{H}_2\text{P}_3\text{O}_{10}^{3-}$ ion of TPP should bind strongly to the NH_3^+ of chitosan, thereby forming more drug-loaded in chitosan nanoparticles. Ibuprofen (1.5 mg/mL) was entrapped during preparation of the nanoparticles system at different CS: TPP ratios either by mixed ibuprofen with chitosan then TPP added referred to as (CS+IBU)/TPP (first method) or by mixed ibuprofen with TPP then chitosan added referred to as CS/(IBU+TPP) (second method). The second method has obtained relatively high DEE of ibuprofen and was selected to carry out further experiments. The ibuprofen-loaded nanoparticles exhibited relatively narrow particle size distribution, as the relatively low polydispersity index (PDI) values. The particle size of the drug-loaded nanoparticles was affected by the CS: TPP ratio. It is obvious that the incorporation of ibuprofen into CS nanoparticles leads to CS-IBU-TPP a decrease of their size compared with the non-loaded or “native” CS: TPP nanoparticles. It may be attributed to the increases of ionic interactions between CS and TPP during nanoparticle formation because of the presence of the ibuprofen

molecules. It was observed that the optimum CS-IBU-TPP ratio among these studied here is CS: TPP at 5:1 ratio, which leads to the highest DEE (76.8 %). At this ratio, CS-IBU-TPP nanoparticles with sizes 247.3 ± 1.0 nm, with PDI 0.27 ± 0.01 and with zeta potential $+37.4 \pm 1.0$ are produced. Thus, this ratio (5:1) was selected for the preparation of drug-loaded nanoparticles at various ibuprofen concentrations. During the experiment, CS: TPP ratio at 5:1 and ibuprofen concentration of 0.5 and 1.5 mg/mL, were supposed to be most effective in delivering ibuprofen. Increasing concentration of ibuprofen from 0.5 to 1.5 mg/mL caused an increasing CS: TPP interaction, leading to decreasing nanoparticle size. In these conditions, the particle sizes of CS-IBU-TPP nanoparticles were 284.1 ± 4.1 nm and 247.3 ± 1.0 nm respectively; the zeta potentials were $+38.6 \pm 0.5$ mV and $+35.3 \pm 0.4$ mV, indicating high stability of CS-IBU-TPP nanoparticles; the DEE of nanoparticles were 86.6 % and 76.8 %; the cumulative release of ibuprofen *in vitro* were 38.5 % and 48.7 %. These results suggested that the potential of ibuprofen loaded chitosan nanoparticles (CS-IBU-TPP) is expected to have potential as a method in pharmaceuticals applications.

Chapter 6

Evaluation of mucoadhesive properties
of chitosan nanoparticles prepared
using different chitosan to
tripolyphosphate (CS: TPP) ratios

6 Evaluation of mucoadhesive properties of chitosan nanoparticles prepared using different chitosan to triphosphate (CS: TPP) ratios

6.1 Introduction

Chitosan is highly considered in the medicinal world, for use in drug delivery systems especially in those which target specific delivery sites as it demonstrates mucoadhesive characteristics (Lehr et al., 1992, Lueßen et al., 1997). Chitosan and other mucoadhesive polysaccharides are highly sought after as they can be formulated into transmucosal drug delivery systems that can achieve and enhance the local and prolonged effect of active drugs over for example 12 - 24 h. Mucoadhesion is often defined as where two materials, one of which is a mucosal surface, adhere to each other. It is generally understood that electrostatic interactions can occur between chitosan's positively charged NH_3^+ groups and the negatively charged sialic acid residue on mucin (Fiebrig et al., 1995). In addition, in an aqueous environment, the interaction between porcine stomach mucin and chitosan, when different additives were present confirmed that electrostatic interaction was taking place and being aided by hydrogen bonding (Harding et al., 1999). Hydrophobic and hydrophilic interactions are also very important (Harding et al., 1999). Depending on the physiological conditions and physiochemical properties such as pH, the carboxylate group of sialic acid residues on mucin can interact with the positive charge on the chitosan particles, due to the protonated amino group (NH_3^+) to form electrostatic and hydrogen bonds (Morris et al., 2010). If such interactions occur, it would be useful to test particle size and zeta potential (surface charge) to gain a better understanding of the interactions of mucin with the chitosan nanoparticles. Moreover, the mucoadhesiveness was evaluated by measuring the mucin binding efficiency. It is therefore clear that the surface charge (zeta potential), the size and occupied space

(viscosity) of the nanoparticles will have an influence on their interactions with mucin. Previous studies in to altering the charge on the nanoparticles have involved modification with poly-ethylene glycol for example (Wu et al., 2005) and have clearly demonstrated that mucin binding and drug release are influenced by nanoparticle charge (Wu et al., 2005, Xu et al., 2015).

In this study, once the different ratios (CS: TPP) ratios of chitosan nanoparticles were formulated their physico-chemical properties (viscosity, zeta potential, particle size and particle size distribution) were measured prior to being mixed with mucin. The physico-chemical properties were then determined after mixing, in order to examine the interaction between the chitosan nanoparticles and mucin. This provided an indication into how CS: TPP nanoparticles may act *in vivo* and which ratios of CS: TPP show potential as drug delivery. Moreover, the mucoadhesiveness was then evaluated by measuring the mucin binding efficiency. It is therefore our hypothesis that by preparing CS: TPP nanoparticles of controlled viscosity, size and charge (Hejjaji et al., 2017, de Pinho Neves et al., 2014, Hashad et al., 2016, Silva et al., 2017) it will be possible to determine whether a minimum CS: TPP ratio or net charge is required for mucoadhesion and from this gain a greater understanding of the mucoadhesive process. This will provide important information for designing tunable mucoadhesive systems for specific applications, where for example, the degree of mucin binding can be controlled.

6.2 Methods and materials

6.2.1 Chemicals

Chitosan of low molecular mass (LMW) of $\sim 50,000$ g/mol as determined by viscosity (see section 5.2.2.1), was purchased from Sigma–Aldrich (Gillingham, UK) and has an average degree of acetylation (DD) of ~ 90 % as determined by FT-IR (see section 5.2.2.2). Glacial acetic acid and TPP sodium salt were also obtained from Sigma–Aldrich (Gillingham, UK). Extensively degraded pig gastric mucin was kindly gift from Biofac A/S (Kastrup, Denmark) and has been fully characterized previously in our group (Abodinar et al., 2016). All materials were used without any further purification.

6.3 Experimental

6.3.1 Preparation of chitosan-TPP nanoparticles

Chitosan-TPP nanoparticles were prepared at seven different ratios (CS: TPP) as described in sections 5.2.2.3 and 5.2.4.

6.3.2 Mucin sample preparation

A 3.5 % (w/v) mucin stock solution was formulated using 3.5 g mucin to 100 mL of deionised water (pH 4.2). This was magnetically stirred overnight at room temperature (~ 20 °C). The solution was then filtered through filter paper (Whatman No.1, Sigma–Aldrich Gillingham, UK) to isolate a larger particles of mucin and reduce aggregation.

6.3.3 Evaluation of the mucoadhesive properties of chitosan-TPP nanoparticles

6.3.3.1 Adsorption of mucin on to chitosan-TPP nanoparticles (CS: TPP)

Mucin solution (1 mL) was added to each CS: TPP nanoparticle preparation (19 mL), with magnetic stirring at 600 rpm and mixtures were incubated at 37 °C for 1 hour prior to analysis, this will be referred to as first stage preparation. To further test the interactions of these nanoparticles, it was decided to test mix equal volumes of different CS: TPP ratios (10 mL) with mucin (10 mL), referred to as second stage preparation, and whether these nanoparticles best interact with mucin for suitable pharmaceutical applications. Then the mucin-nanoparticle mixtures were centrifuged at 40,000 x g (Beckman Coulter Optima L-100K, 50Ti rotor) for 60 min and the supernatant was used for the measurement of the free mucin concentration using the standard calibration curve (section 6.3.4.1). In addition, the mucoadhesiveness was expressed as the mucin binding efficiency of the nanoparticles and was calculated from the following equation:

$$\text{Mucin binding efficiency (\%)} = \frac{(C_o - C_s)}{C_o} \times 100 \quad \text{Eq. (6.1)}$$

Where C_o is the initial concentration of mucin used for incubation, and C_s is the concentration of free mucin in the supernatant (Papadimitriou et al., 2008, Andersen et al., 2015).

6.3.3.1.1 Viscosity analysis of chitosan nanoparticles-mucin mixtures

The relative viscosity (η_{rel}) of all samples (chitosan solution, mucin solution and chitosan nanoparticle-mucin mixtures) were tested at 37.0 ± 0.1 °C by a Bohlin Gemini HR Nano Rheometer (Malvern Instruments, Worcestershire, UK) using 1 mm gap and 55 mm parallel plate geometry at a constant shear rate of 500 s^{-1} under precise temperature control, according to the following equation:

$$\eta_{rel} = \left(\frac{\eta}{\eta_0} \right) \quad \text{Eq. (6.2)}$$

where η is the average viscosity of the samples and, η_0 is the viscosity for the reference solvent *i.e.* dilute acetic acid. All measurements were performed in triplicate. A change in relative viscosity of nanoparticles indicates the interaction with mucin (Menchicchi et al., 2014).

6.3.3.1.2 Zeta potential of chitosan nanoparticles-mucin mixtures

The zeta potential of the chitosan solution (0.3 %), mucin solution (3.5 %) and chitosan nanoparticle-mucin mixtures were measured with a Malvern Zetasizer NANO-Z (Malvern Instruments Limited, Malvern, UK) using the capillary cell. All samples were taken at 37 ± 0.1 °C and the mean values and standard deviations of triplicate measurements were calculated. Mucin solutions were measured at pH 4.2 and CS: TPP nanoparticle-mucin mixtures were at pH 5. To determine the zeta potential approximately 1.0 mL of sample was pipetted into a folded capillary cell by using a syringe and measurements were performed at 37 ± 0.1 °C in triplicate to

obtain data value an average of ten measurements. Laser, the source of light, Doppler electrophoresis is a technique of taking zeta potential measurements. The laser is divided to give a reference and an incident beam. The latter (incident beam) goes through the sample cell centre, then the forward angle is used to spot and observe scattered light. Immediately the measurement of zeta potential commences, reference beam's intensity is taken. This technique takes into account the speed with which particles can move in liquids after an application of electric field (its velocity). As soon as the applied electrical field and the particle's velocity are known in advance and by use of sample constants; dielectric and viscosity constant, zeta potential now becomes determinable

6.3.3.1.3 Particle Size analysis of chitosan nanoparticles-mucin mixtures

The particle diameter of mucin solution (3.5 %) and chitosan nanoparticle-mucin mixtures were measured by dynamic light scattering (DLS) using Malvern Zetasizer NANO-Z (Malvern Instruments Limited, Malvern, UK). The dispersion medium (water) and refractive index of particles was set at 1.330 and 1.6 respectively. A glass cuvette was used and an angle scattering of 173° was utilized. Approximately 1.0 mL of sample was pipetted into the cuvette. The laser is used to provide a light source to illuminate the sample particles. Some of the laser beam scattered by the particles within the sample then the detector measures the intensity of the scattered light. The samples were measured in triplicate and the results represent the mean particle diameter at 37.0 ± 0.1 °C.

6.3.4 Mucin adsorption assay

Mucin adsorption was studied using a periodic acid /Schiff colorimetric method described by Mantle and Allen (Mantle and Allen, 1978) to determine the free mucin concentration following incubation with chitosan nanoparticles.

6.3.4.1 Calibration curve of mucin using PAS/Schiff colorimetric assay

Standard calibration curves for mucin were prepared from 2 mL of mucin standard solutions of concentrations (0.01 % – 0.08 %). Mucin concentrations were quantified by colorimetric method of the glycoprotein based on the periodic acid/Schiff reagent (PAS) (Mantle and Allen, 1978). This method was divided by into two parts: firstly, coupling of the oxidised mucin (glycoprotein) using periodic acid reagent (periodate anion) to aldehyde (**Figure 6.1**).

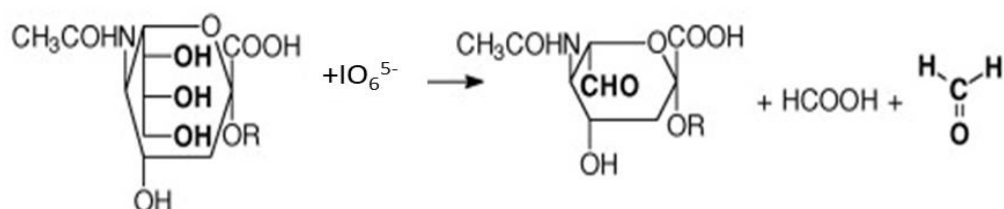


Figure 6.1: Periodate oxidation of sialic acid to aldehyde (Matsuno and Suzuki, 2008).

Periodic acid reagent was prepared by adding 10 μL of 50 % of periodic acid solution to 7 mL of 7 % acetic acid solution (Mantle and Allen, 1978). Secondly, the preparation of the Schiff reagent was prepared by adding 1 % basic Fuschin aqueous solution to 20 mL of 1 M HCl, and twice mixing the resulting solution with 300 mg of activated charcoal, then shaking for 5 min and filtering to remove the charcoal. The resulting solution was stored in an amber glass bottle at room temperature. Sodium

metabisulphite (0.1 g) was added to every 6 mL of Schiff reagent directly before use and the resultant solution was incubated at 37 °C until it became colourless or pale yellow (about 90 minutes). A standard calibration curve was constructed by adding 200 µL of freshly periodic acid reagent to 2 mL of mucin standard solutions (0.01 % – 0.08 %), solutions then were incubated at 37 °C for 2 hours in a water bath to complete periodate oxidation. Then 200 µL of the colourless Schiff reagent was added at room temperature in order to react with the aldehyde (from first step) to form a pink colour solution. Colour development was complete after 30 minutes and the absorbance of the standard solutions were recorded at 555 nm using UV-Vis spectrophotometer (Shimadzu UV-160A, Wolverton, UK) (da Silva et al., 2007, Rossi et al., 1995). Samples were prepared for analysis as per section 6.3.3.1.

6.4 Statistical analysis

All experiments were expressed as the mean value \pm standard deviations (SD) of at least three readings. Statistical significance ($p < 0.05$) between test groups was performed by one-way analysis of variance (ANOVA) and a Tukey post-hoc test.

6.5 Results and discussion

Five different ratios of (CS: TPP) nanoparticles (3:1, 4:1, 5:1, 6:1 and 7:1) were spontaneously obtained upon addition of a TPP (polyanion) solution to the chitosan solution (polycation), according to the procedure previously developed by chapter five. These formulations resulted in positively charged chitosan nanoparticles, which helps to facilitate electrostatic interactions with the negatively charged carboxylic acid groups of the mucin. Pig gastric mucin was used as the pig is physiology similar to humans. A lot of similarities clearly exist between pigs and humans, thereby making swine an experimental model system that is very essential in conducting investigations in a range of scientific parameters (Patterson et al., 2008). In addition, the physiological resemblance to human intestines and mechanisms of human disease are advantages of pig models advantages which these studies highlighted (Gonzalez et al., 2015). There are several distinct advantages that pigs possess which make them become a useful translational research animal model (Gonzalez et al., 2015). Specifically pigs possess important anatomical and physiological structures that are similar to human beings (Shu et al., 2001, Labib et al., 2004, Douglas, 1972). The pig possesses a genome with extensive homology that is comparative to that of human. The sequence homology that the pig genome has is 60% that of human, in contrast to rodents with only 40% homology (Thomas et al., 2003, Humphray et al., 2007). Furthermore, the pig chromosomal structure, in contrast to mouse, rat, dog, cat or horse, is more like that of human's (Murphy et al., 2005, Meyers et al., 2005). Just like humans, pigs, are omnivores in nature and, as such, share identical physiological processes with regards to their metabolism and intestine (Meyers et al., 2005, Deglaire and Moughan, 2012, Patterson et al., 2008). The small intestine structure is very similar in humans and pigs, and this includes macroscopic features like the

intestinal length ratio for every kilogram bodyweight (Block et al., 2011). Furthermore, pigs, just like humans, are real omnivores, while other potential mammalian models like dogs, cats, ruminants, rabbits and rodents have undergone evolution in the development of their alternative digestive strategies (Kararli, 1995). The rapid growth rate and size of pigs once they become fully matured, as well as their differences in gut-associated lymphoid tissue, are other essentials being taken into consideration when pigs are being utilised as animal models in the study of human development and disease (Heinritz et al., 2013, Sinkora et al., 2011).

Extensively degraded pig gastric mucin may differ slightly from the native porcine mucus gel due to the manufacturing process. However, off-the-shelf mucin formulations are often used research as they have similar functionality (Fefelova et al., 2007, Takeuchi et al., 2005) and it is expected that batch-to-batch variability would be less of an issue compared to freshly prepared material (Fefelova et al., 2007). In this study, a 3.5 % pig gastric mucin solution was used because this concentration is almost equivalent to mucin concentration in gastric mucus (Bansil et al., 2013). The preparation of digested gastric mucins and degradation process were made in the form of a by-product derived from large scale pharmaceutical quality pepsin preparation in the city of Copenhagen, Denmark at Orthana Kemiske Fabrik A/S (a division of the Biofac group). Red lining derived porcine stomachs came from abattoirs in the US (Farmland) and kept at a frozen temperature of -18°C until it was brought into the production area to be utilised. First, a large meat crusher (screen 18 mm) was used in crushing approximately 1000 kg of frozen linings. The crushed raw material was placed in a stirred tank prior to a 100 kg of RO water added into it. Concentrated hydrochloric acid was used in adjusting the pH to 2.0 prior to heating it to a temperature of 38°C . Then concentrated sodium hydroxide was used in adjusting

the pH to 2.8 after 4.5 hours. There was transfer of the processed liquid to a precipitation tank and cooled down to a temperature of $-5\text{ }^{\circ}\text{C}$. The precipitation of the crude mucin was then performed by slowly adding 97% acetone until a concentration of 61% w/w was reached. Mild agitation was used in mixing the precipitation liquid, held at a temperature of $-5\text{ }^{\circ}\text{C}$, for 30 minutes. The separation of the processed liquid into liquid and solid phases was then made on a Flotweg decanter (1500 rpm inner speed, 6000 rpm outer speed), where the solid phase consisted of fat and mucins. By adding approximately 5 volumes of water, the precipitate became solubilised. Evaporation of acetone remnants was undertaken under vacuum. The liquid was then left for 3 days to sediment, prior to pumping out of the clear liquid top phase. Cellulose and filter aid based filter plates (at first T2600, T1000 and lastly K250, every one of them coming from Seitz, Pall Corporation, New York, USA) covered with filter aid (Hyflo Super Cel) were used three times in filtering the crude mucin on a Seitz Orion plate and frame filter press. The mucin concentration was then made to 5% solid content with 3 volumes of RO water used in washing it prior to adjusting pH to 3–4 and then frozen at a temperature of $-18\text{ }^{\circ}\text{C}$ and lyophilized (Abodinar et al., 2016). Studies on native pig gastric mucin have previously shown an isoelectric point at $\sim\text{pH } 2\text{--}2.5$ (Caicedo and Perilla, 2015) and sialic acid has a pKa of 2.6 (Hurd, 1970). Therefore there is potential to interact with the positive charged amino groups of chitosan nanoparticles (De Campos et al., 2004) when both sialic acid and chitosan are oppositely charged at therefore $\sim\text{pH } 4.5 - 5$. However, there are other contributions such as hydrogen bonding and hydrophobic effects might have an effect.

6.5.1 Mucoadhesion Studies

The mucoadhesive properties and the influences of different CS-TPP ratio at 3:1, 4:1, 5:1, 6:1 and 7:1 nanoparticles were evaluated by measuring the relative viscosity, particle size and zeta potential on interaction with negatively charge mucin. Different volumes mixing (two preparations) were used to assess the stability and interaction of nanoparticles prepared using various CS: TPP ratios and mucin which could lay the foundations for potential future use as a drug carrier and/or other pharmaceutical applications (**section 6.3.3.1**). Both preparations were based on the measurements of the viscosity, zeta potential (surface charge) and particle size of chitosan nanoparticles before and after incubation with mucin at 37° C under moderate stirring.

6.5.1.1 First preparation incubation with mucin

6.5.1.1.1 Assessment of chitosan nanoparticle-mucin interactions by relative viscosity

The interactions between chitosan nanoparticles (CS: TPP) and mucin were initially studied by relative viscosity (η_{rel}) (**Figure 6.2**). Chitosan solution (0.3 %) and mucin solution (3.5 %) were prepared in order to produce relative viscosity (η_{rel}) close to 1.8. Relative viscosities of this order of magnitude are required as at higher relative viscosities for example > 2 the onset in polymer entanglement is observed. Therefore, the relative viscosities were kept below 2 with the aim of minimising these polymer entanglement effects which would obscure changes in viscosity due to interactions with mucin (Goycoolea et al., 1995).

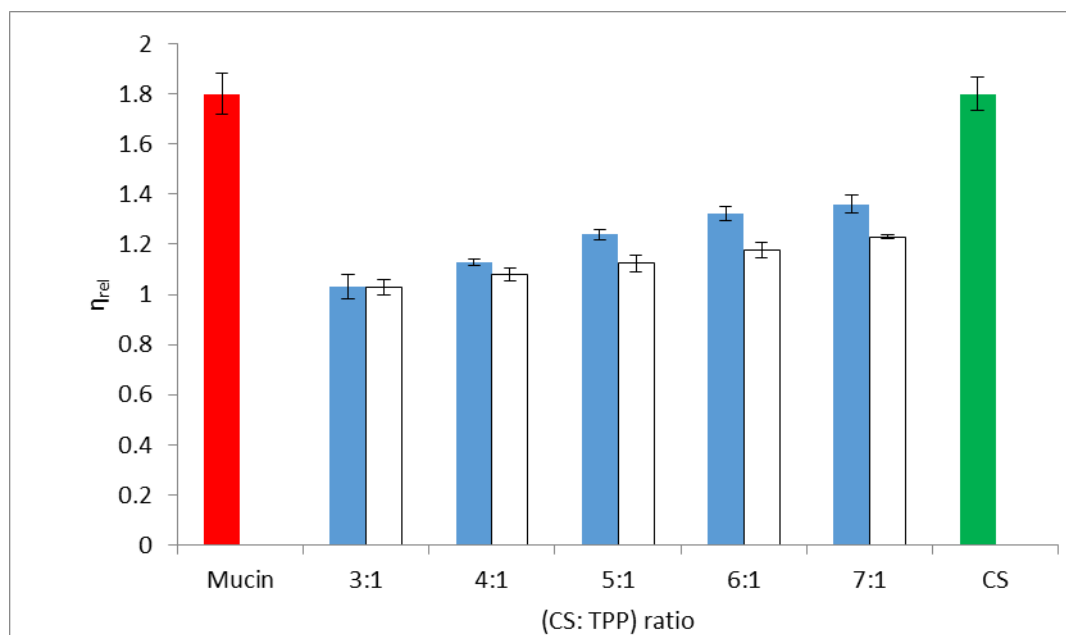


Figure 6.2: Relative viscosity of mucin (red column), chitosan (green column), a native chitosan nanoparticles (blue columns) and chitosan nanoparticle-mucin mixtures-mucin (white columns) at 37 °C (mean values \pm SD, n=3).

It can be seen in **Figure 6.2**, chitosan nanoparticles were mixed with mucin at different CS: TPP ratios (3:1, 4:1, 5:1, 6:1 and 7:1), then the relative viscosities of the mixed solutions were determined. The formation of chitosan nanoparticles-mucin interactions products were determined on the basis of the changes in relative viscosities of the nanoparticle-mucin mixtures (Rossi et al., 2001). The relative viscosity of chitosan nanoparticles (CS: TPP)-mucin mixtures increased with increasing CS: TPP ratios (**Figure 6.2**). Increasing CS: TPP ratios (no mucin), caused an increase in relative viscosity which was expected due to the increased concentration of chitosan used (higher charge on chitosan nanoparticles) (Casettari et al., 2013, Perinelli et al., 2018). It was observed however, that chitosan nanoparticle-mucin mixtures decreased the relative viscosities in compared with CS: TPP nanoparticles (blank). This could be due to the electrostatic interactions between positively charged ammonium group on the chitosan nanoparticles and the negatively

charged sialic acid residue on mucin (Fiebrig et al., 1995, Deacon et al., 1999), perhaps with a contribution from hydrogen bonds (Fiebrig et al., 1995). The difference between the native chitosan nanoparticle and chitosan nanoparticle-mucin mixture was not statistically significant ($p > 0.05$) on relative viscosity at (CS: TPP) 3:1. This could be attributed to a small amount of chitosan nanoparticles interacting with the mucin causing a limited viscosity change. However, other CS: TPP ratios (4:1, 5:1, 6:1 and 7:1) did significantly affect relative viscosity ($p < 0.05$). This suggests an important interaction occurring between chitosan nanoparticles and mucin. This is most likely due to a conformational change to a more compact structure (*i.e.* a reduction in the hydrodynamic volume (Mackie et al., 2017)) for one or more of the macromolecules due to an interaction (Mackie et al., 2017, Menchicchi et al., 2014, Silva et al., 2017). Moreover, this would also be consistent with a decrease in net charge/ zeta potential (Abodinar et al., 2014). A decrease in viscosity may also be advantageous from a formulation point of view, for example in ocular delivery systems where an increase in viscosity would be unacceptable due the blink process requiring low shear viscosities in order to avoid unnecessary damage to the corneal epithelium (De Campos et al., 2004), low viscosity aids the spray ability of liquid nasal formulations (Morris et al., 2010, Mackie et al., 2017). Although not explicitly evaluated, changes in viscosity are related to the swelling and stiffness of polymeric systems and could therefore be probed further, this would be influenced greatly by the CS: TPP ratio and the pH at which nanoparticles were formed (Bhumkar and Pokharkar, 2006) where chain stiffness has been shown to influence mucin interactions (Mackie et al., 2017, Menchicchi et al., 2014).

6.5.1.1.2 Zeta potential of chitosan nanoparticles-mucin mixtures

In order to further support the interactions between chitosan nanoparticles and mucin, zeta potential was investigated. Determination of the zeta potential of chitosan nanoparticles in the presence of mucin has been demonstrated to be a good means of studying the mucoadhesive interactions of the chitosan nanoparticles–mucin mixtures (Fefelova et al., 2007, Takeuchi et al., 2005, Menchicchi et al., 2014). Furthermore, zeta potentials of less than +30 mV indicate lower nanoparticle stabilities due to the lower electrostatic repulsion (Hunter, 1993), zeta potential of native chitosan nanoparticles increased as the CS: TPP ratio increased (**Figure 6.3**) which is a highly attractive property amongst nanoparticles. Furthermore, this would theoretically allow the preparation of nanoparticles of controlled zeta potential in the range +34 - +42 mV by varying the CS: TPP ratio. Nanoparticles outside of this range could be prepared under different pH conditions or by using different CS: TPP ratios, for example.

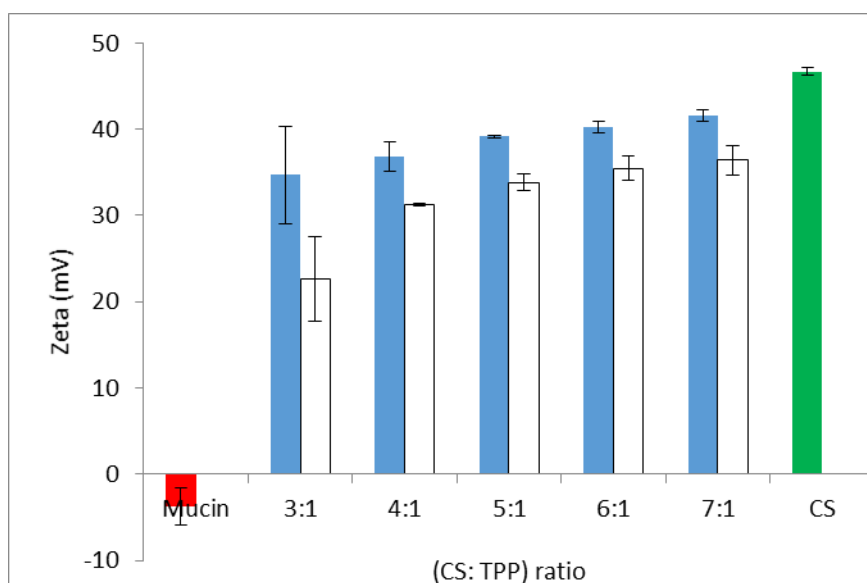


Figure 6.3: Zeta potential values obtained for mucin (red column), chitosan (green column), native chitosan nanoparticles (blue columns) and chitosan nanoparticle-mucin mixtures (white columns) at 37 °C. All values represent the mean \pm SD (n = 3).

Chitosan has a mucoadhesive properties, therefore it would be expected that the surface charge of chitosan nanoparticles might be changed by the adhesion of the mucin and in this case a decrease in zeta potential was observed upon mixing with mucin at all CS:TPP ratios (**Figure 6.3**). The occurrence of such change was detected by measuring the changes in the zeta potential of chitosan nanoparticle-mucin mixtures with different of CS: TPP ratios. The zeta potential of mucin and chitosan were determined to be -4.0 ± 3.1 and $+46.7 \pm 0.4$ mV, respectively. It is known that chitosan has positive charge at pH 5.0 due to presence of ammonium ions (NH_3^+) (Vilasaliu et al., 2010). The negative charge, however, of mucin is as a result of the ionization of sialic acid (COO^-). Therefore, chitosan nanoparticles could lead to a strong electrostatic interaction with the mucin. An addition of mucin to the different ratios of CS: TPP nanoparticles results in a significant ($p < 0.05$) decrease in zeta potential for all CS: TPP ratios (**Figure 6.3**). The reduction of zeta potentials could be

due to the ionic reaction between negatively charged sialic acid in mucin and positively charged amino groups in chitosan nanoparticles (Grießinger et al., 2015). Moreover, as shown in **Figure 6.3**, the zeta potential decreased sharply as the CS: TPP ratio decreased from mixtures 4:1 to 3:1, which might be caused by decrease amount in these nanoparticles which leads to most of NH_3^+ groups interacting with COO^- groups on the of sialic acid. These results were in agreement with lowest relative viscosity of 3:1 mixture (**Figure 6.2**). Furthermore, this may be attributed to the fact that native (3:1) ratio nanoparticles had lower zeta potential values ($+34.7 \pm 5.6$ mV) than other ratios including 4:1, 5:1, 6:1 and 7:1. On the other hand, a small increase in zeta potential of chitosan nanoparticles-mucin mixtures were observed as the CS: TPP ratio increased from 5:1 to 7:1, which might be due to increase positive charge surfaces on the particles. This may also be confirmed by the changes in particle size and polydispersity index (PDI) of native CS: TPP nanoparticles. At all CS: TPP ratios greater than 3:1 the zeta potential decreased by ~ 5 mV which is in the range of the overall charge on mucin and may be indicative of the majority of the mucin being bound to the nanoparticles at these ratios.

6.5.1.1.3 Particle size of chitosan nanoparticle-mucin mixtures

In all cases there is an increase in particle size upon addition of CS: TPP nanoparticles to mucin, clearly indicating an interaction (**Figure 6.4**), although this increase in particle size is generally not as pronounced when the CS: TPP nanoparticles are larger *i.e.* those containing greater amounts of chitosan (Sosnik et al., 2014). In order to remove residues of insoluble mucin molecules and reduce mucin aggregation, the suspension was filtrated and the particle size was obtained at 41 ± 5 nm. The change in zeta potential is related to a change particle size (Morris et al., 2010) and it is clear

that as the CS: TPP ratio increases both the zeta potential and particle size also increase. This is true both in the presence and absence of mucin which is related to the reduction in TPP available to interact with chitosan and therefore a decrease in the density internal cross-linking and hence larger particles (Masarudin et al., 2015) (**Figure 6.4**). Nanoparticles at all ratios, other than 3:1, were in the optimal range (200 – 500 nm) for mucosal interaction (Krogstad et al., 2014). When the mucin solution were mixed with different CS: TPP ratios of chitosan nanoparticles from 3:1 to 7:1, the particle size increased significantly (**Figure 6.4**). This is probably due to adsorption (binding) of mucin on the chitosan nanoparticles surfaces (Fefelova et al., 2007). The modification of the particle size was a result of electrostatic interactions between the negative charge of mucin and positive charge of chitosan particles. In addition, the increase in particle size, together with a decrease in zeta potential demonstrates that the mucin is binding to the surface of the chitosan nanoparticles, when the CS: TPP ratios varied from 3:1 to 7:1.

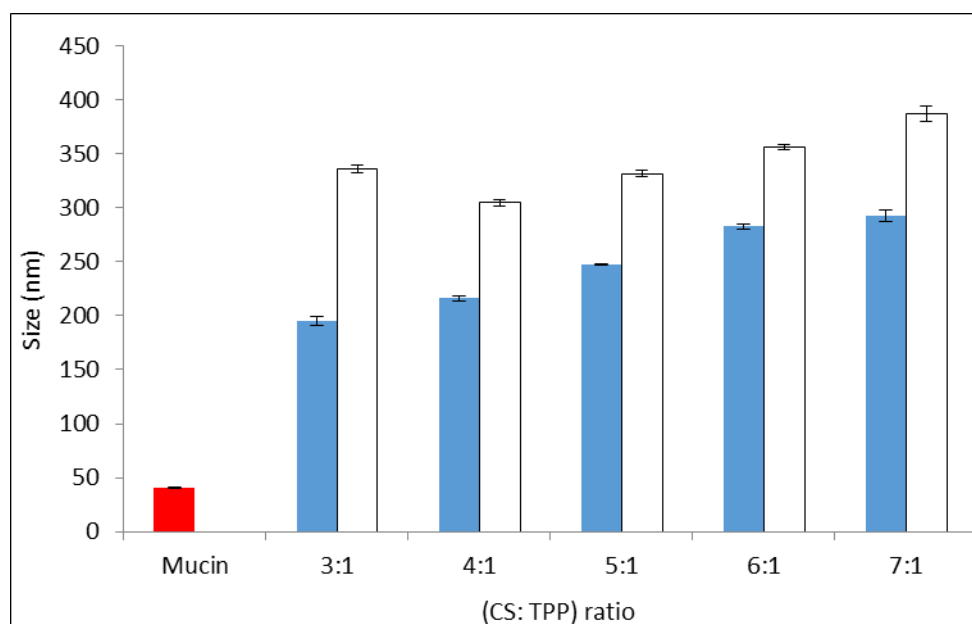


Figure 6.4: Particle size of mucin (red column), a native chitosan nanoparticles (blue columns) and chitosan nanoparticle–mucin mixtures (white columns) at 37 °C. All values represent the mean \pm SD (n = 3).

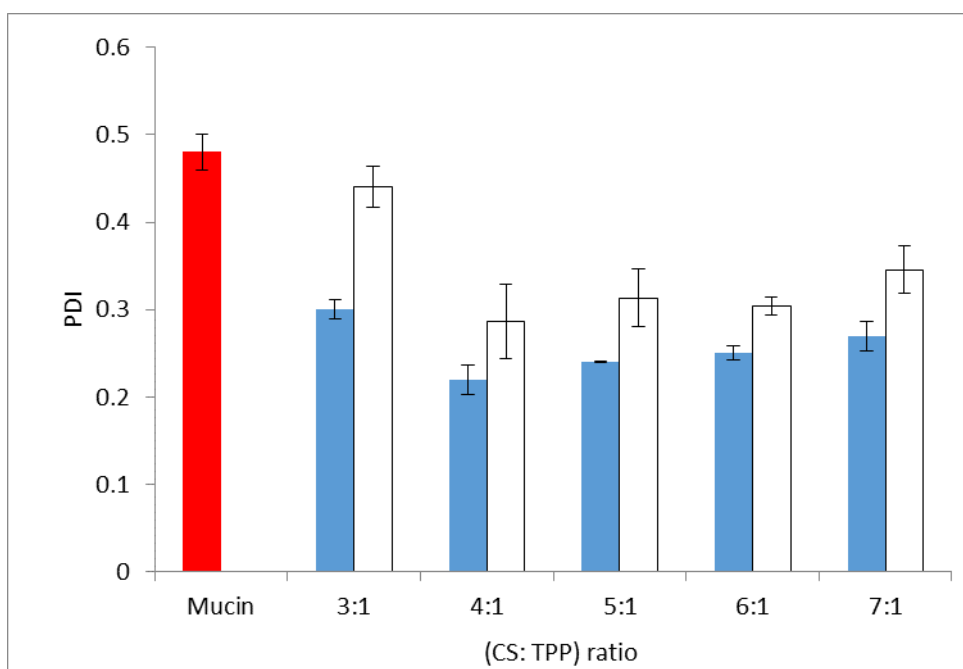


Figure 6.5: PDI of mucin (red column), a native chitosan nanoparticles (blue columns) and chitosan nanoparticles–mucin mixtures (white columns) at 37 °C. All values represent the mean \pm SD (n = 3).

This result may be attributed to the overall negative charge of mucin, due to the presence of sialic acid, and the overall positive charge of the chitosan nanoparticles. The interaction at ratio CS: TPP (4:1) between chitosan nanoparticles and mucin can was the strongest as the nanoparticles binding the mucin more strongly and hence reducing the particle size. Furthermore, this increase in interaction is important in respect to potential applications as increased interaction with mucin is indicative of increased mucoadhesion, which depending on the specific application may not always be optimum. At the lowest CS: TPP ratio (3:1) mucin in mixture is potentially available in greater amounts. Therefore we would expect more mucin to be adsorbed on to the chitosan nanoparticle surface, which would increase aggregation due to, for example, the formation of mucin bridges between chitosan nanoparticles (Fefelova et al., 2007), or the aggregation of nanoparticles due to their instability the latter is

consistent with the low zeta potential value of the 3:1 mixture ($+22.6 \pm 4.9$ mV). The PDI value was used as a reflection for uniformity and stability of particles (Masarudin et al., 2015). Moreover, **Figure 6.5** shows the highest value (0.44 ± 0.02) of PDI at CS: TPP ratio 3:1 mixture indicates a wider range of particle size distribution in chitosan nanoparticle-mucin mixtures relative to other CS: TPP ratios (Appendix F). At a CS: TPP ratio of 4:1 mixture, chitosan nanoparticles with the smallest size and lower PDI were formed. Above the CS: TPP ratio 4:1 mixture, a clear increase in chitosan nanoparticle-mucin mixture size is obtained, thereby confirming the adsorption of negative mucin onto the surfaces chitosan nanoparticles. In addition, as can be shown in **Figure 6.5**, the CS: TPP ratio from 5:1 to 7:1 mixtures have PDI values of 0.30 - 0.35, indicating a narrow size range and a homogenous dispersion of chitosan nanoparticle-mucin mixture were obtained (Appendix F) (Hu et al., 2008) which is important in terms of the movement/ diffusion of nanoparticles through a mucosal layer *in vivo* (Abdulkarim et al., 2015). On the basis of these observations, the strongest interaction, which can be related to the smallest particle size was a CS: TPP ratio of 4:1.

6.5.1.1.4 Mucin binding test (adsorption) as indicator of mucoadhesiveness

Mucin colorimetric assay and calibration curve

Proteins are commonly measured at ultraviolet region at 280 nm (Layne, 1957), nevertheless mucins absorb ultraviolet light poorly, since they generally have no or negligible aromatic amino acid content (Wang and Granados, 1997, Christlet and Veluraja, 2001). A colorimetric assay, however, provides an effective method of detection and analysis of mucin glycoproteins.

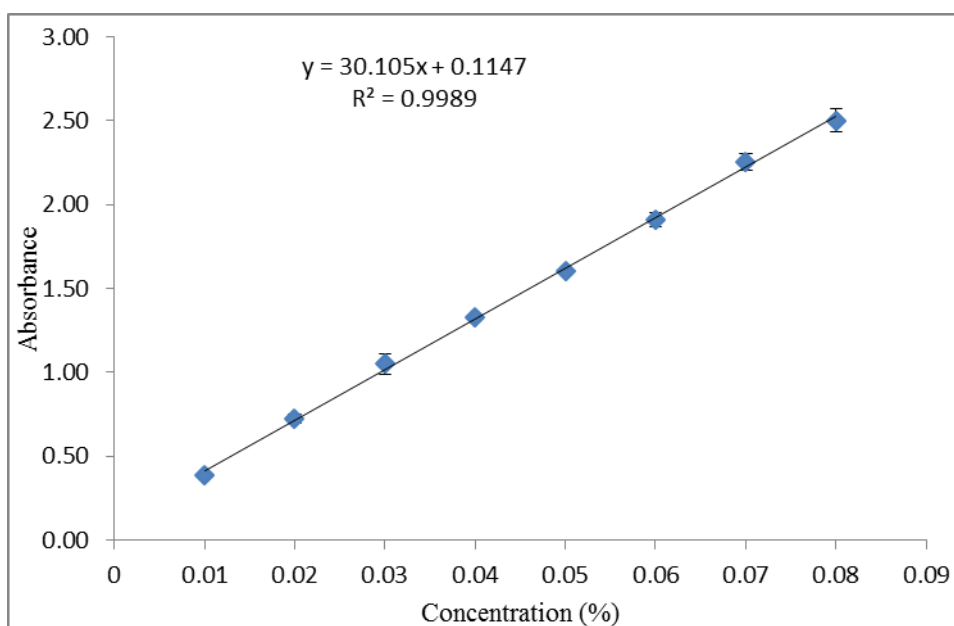


Figure 6.6: Calibration curve of mucin. (n=3; mean \pm SD).

From the **Figure 6.6**, it can be concluded that the assay showed a high sensitivity with LOD and LOQ being 0.006 ± 0.05 % and 0.019 ± 0.02 %, respectively with a high linearity ($R^2 > 0.99$) and reproducibility with RSD < 3.7 %.

Mucin is predicted to spontaneously adsorb onto the surface of the chitosan nanoparticles (Hu et al., 2015). The mucoadhesive behaviour of chitosan nanoparticles was assessed by the suspension of different CS: TPP ratios in fixed amount of mucin in aqueous solutions at 37°C . Furthermore, the amount of mucin adsorbed was measured from the change in free concentration of mucin in the reaction mixtures according to Eq. 6.1, Section 6.3.3.1.

After confirming the high surface charge (zeta potentials $> +30$ mV) for all native CS: TPP ratios (**Figure 6.3**), a mucin binding efficiency test was applied to confirm the system's adhesiveness (**Figure 6.7**).

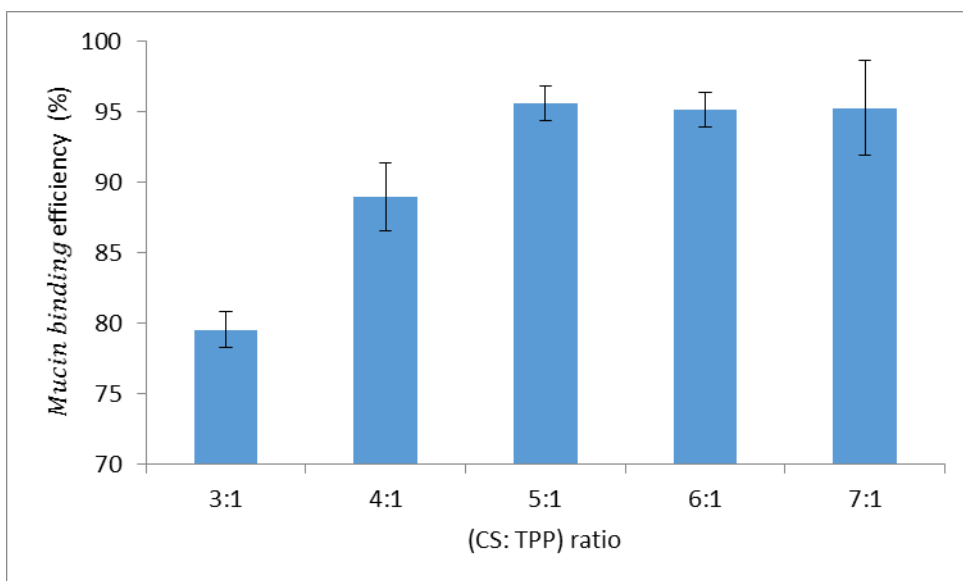


Figure 6.7: Mucin binding efficiency (adsorption) of different chitosan nanoparticles of different CS:TPP ratios. All values represent the mean \pm SD (n = 3).

The mucin binding efficiency (mucin adsorbed onto the chitosan nanoparticle surface) increased from 79.5 ± 1.3 % to 88.9 ± 2.4 % ($p < 0.05$) as CS: TPP ratios increased from 3:1 to 4:1 respectively (**Figure 6.7**). However, it was demonstrated that, there was no significant differences ($p > 0.05$) in the mucin binding efficiency values (~ 95 %) when increase in CS: TPP ratios from 5:1 to 7:1. This result may be attributed to more NH_3^+ functional groups being present to interact with the sialic acid residues on mucin. This also agrees with the finding from zeta potential which suggests a large amount of mucin has been bound to the nanoparticles at CS: TPP ratios greater than 3:1 and that native CS: TPP nanoparticles of ratios from 5:1 to 7:1 were shown to have available surface charges ($> +39$ mV).

It is known that the smaller particles are able to penetrate to the sub-mucosal layers whereas the larger particles localised in the epithelial lining (Gan et al., 2005). Based on these results an optimal minimum chitosan nanoparticle CS: TPP ratio of 4:1 is required to interact with mucin, nanoparticles with lower amounts of chitosan are unstable and prone to aggregation. The zeta potential of 4:1 mixture is $+31.3 \pm 0.06$ mV (**Figure 6.3**), its particle size is the smallest (**Figure 6.4**) and has lowest PDI value (**Figure 6.5**). At CS: TPP ratio of 4:1 there are sufficient levels of CS: TPP particles for the mucin to interact with. This result may be attributed to a critical point of binding sialic acid being saturated at the CS: TPP ratio of 4:1 and all the mucin being adsorbed on to the particles.

6.5.1.2 Second preparation incubation with mucin

6.5.1.2.1 Assessment of chitosan nanoparticles-mucin interactions by relative viscosity, zeta potential and particle size

In this stage equal volumes solutions of chitosan nanoparticles and mucin were mixed (Section 6.3.1.1). **Table 6.1** compares results which obtained from second preparation tests. As be seen from the table below, the relative viscosity, zeta potential and particle size of different chitosan nanoparticles ratios were determined upon their incubation in the present and absent of mucin.

Table 6.1: Second stage measurements of relative viscosity, zeta potential and particle size of different CS: TPP nanoparticles before and after incubation with mucin.

(CS:TPP) ratio	Relative viscosity		Zeta potential		Particle size	
	Control (CS:TPP)	(CS:TPP + Mucin)	Control (CS:TPP)	(CS:TPP + Mucin)	Control (CS:TPP)	(CS:TPP + Mucin)
3:1	1.03 ± 0.05	1.16 ± 0.02	33.4 ± 3.62	-3.0 ± 1.44	195.0 ± 4.2	▼
4:1	1.13 ± 0.01	1.17 ± 0.03	35.4 ± 1.70	-2.2 ± 0.95	216.0 ± 1.9	▼
5:1	1.24 ± 0.02	1.17 ± 0.02	37.4 ± 0.88	-1.5 ± 0.60	247.3 ± 1.0	▼
6:1	1.32 ± 0.04	1.17 ± 0.01	39.0 ± 0.73	-1.0 ± 0.33	282.5 ± 2.1	▼
7:1	1.36 ± 0.03	1.18 ± 0.02	40.2 ± 0.74	-0.6 ± 0.17	293.0 ± 5.3	▼

▼ : Aggregation/ precipitation of particles

The physical state of chitosan nanoparticle-mucin mixtures at different CS: TPP ratios (3:1, 4:1, 5:1, 6:1 and 7:1) were visual observed. When observing the samples visually, it is noted that there was an increase in the presence of milkiest mixtures then observed previously (first preparation). This is indication more mucin binding to the particles, where the particles were most noticeable; however, this observation did affect ($p < 0.05$) the results of the viscosity, zeta potential and particle size tests. The results, as shown in **Table 6.1**, indicate that by decreasing in CS: TPP mixture from 7:1 to 5:1, decreased in the specific viscosity. This is caused by the precipitation of the chitosan nanoparticles-mucin interaction product. On the other hand, by a further decreasing in CS: TPP mixture from 4:1 to 3:1, an increase in the specific viscosity was observed. This was due to the excess mucin which has not interacted with the chitosan nanoparticles. These results confirmed with surface charge of particles (**Table 6.1**). Moreover, the results exhibited that an excess of mucin was adsorbed (interaction) on all different ratios of CS: TPP nanoparticles surfaces and potentially caused further aggregation (**Figure 6.8**). This result may be explained by the fact that the hydrogen bonding occurred which formation of bridges between nanoparticles (bridging effect) (Fefelova et al., 2007, Sogias et al., 2008).

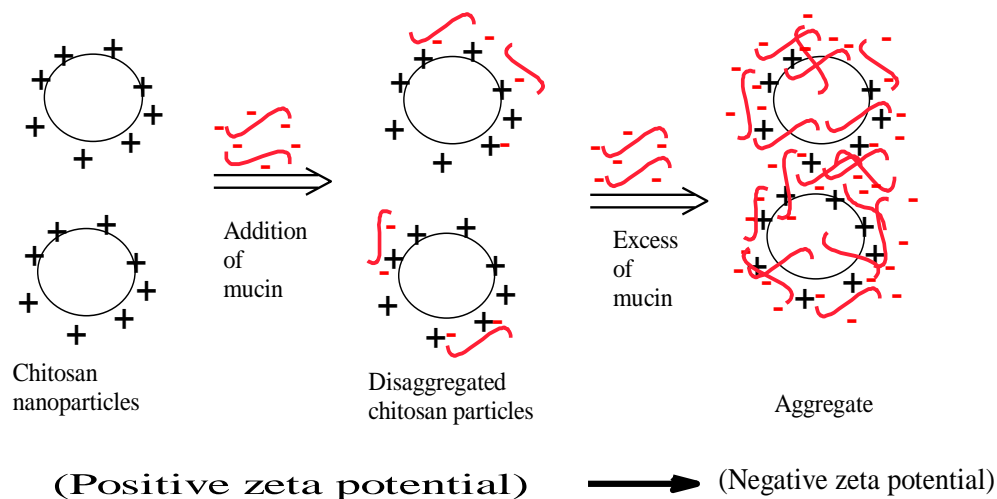


Figure 6.8: Diagrammatic representation of adsorption of mucin on CS:TPP nanoparticles and aggregation of nanoparticles in the presence of an excess of mucin (Sogias et al., 2008).

In order to confirm the above observation model we have studied the interactions between chitosan nanoparticles and mucin using zeta potential measurements. When chitosan nanoparticles were mixed with mucin solution, the resultant zeta potential of chitosan nanoparticles shifted to a negative values because of the negative charge of the mucin **Table 6.1**. Therefore, the particles in suspension were unstable as zeta potential less than ± 30 mV, and aggregates were present due to loss repulsive forces. This is due to the adsorption (binding) of fully mucin molecules on the chitosan nanoparticles were responsible for the aggregation (**Figure 6.8**), due to mucin bridges between nanoparticles (Sogias et al., 2008) or due to nanoparticle instability if the zeta potential is in the ranges -30 mV - +30 mV. As a result, second preparation test for all chitosan nanoparticles-mucin mixture are not stable systems and the charges are not sufficient to prevent aggregation of the particles.

6.6 Summary

In this study, it has been demonstrated that different CS: TPP nanoparticle ratios, prepared by the ionotropic gelation method, were evaluated for their mucoadhesive properties for potential use as in pharmaceutical applications. The incubation of different ratios of CS: TPP nanoparticles solutions including 3:1, 4:1, 5:1, 6:1 and 7:1 with mucin did lead to a modification in their physiochemical properties. Positively charged chitosan nanoparticles, which is one of the main factors responsible for its mucoadhesive properties, had the ability to adsorb mucin (Andersen et al., 2015). A strong interaction between chitosan nanoparticles and mucin in aqueous solution was measured using relative viscosity, zeta potentials and particle size. In addition, a mucin colorimetric assay was performed to determine the amount of mucin adsorbed on chitosan nanoparticles. The results of this study support the idea the alterations in physiochemical properties of nanoparticles after incubation with mucin such as decreased in zeta potential and increased in particle size. The experiments were conducted at 37 °C, as this is closer to physiological conditions. The first stage has obtained better mucoadhesion results. For all CS: TPP ratios examined, a minimum value of viscosity was reached for a 3:1 CS: TPP ratio, however chitosan nanoparticles at this ratio (3:1) was not stable as its zeta potential was $+22.6 \pm 4.9$ mV). Whereas a CS: TPP ratio of 4:1 mixture displayed the strongest interaction with mucin. This result may be attributed to a critical point of binding carboxylate groups being saturated at the CS: TPP ratio of 4:1 and a possible of all mucin adsorbed on particles. Taken all together we can conclude that a minimum CS: TPP ratio of 4:1 is required to produce stable nanoparticles able to form strong interactions with mucin, which is consistent with a greater mucin binding efficiency at CS:TPP ratios of 4:1 and higher.

Chapter 7

General Conclusions and Future Recommendations

7 General Conclusions and Future Recommendations

The purpose of this research was to prepare chitosan micro/nanoparticles at different CS: TPP ratios then investigation the potential of these particles for forensic and pharmaceutical applications. To achieve this purpose, the physicochemical properties of chitosan particles must be characterized. Furthermore, the aims of this thesis, as stated in Chapter 1 (Section 1.7) were successfully achieved and summarised in the following sections.

Chapter 3 discussed their physicochemical properties extensively. Firstly, chitosan microparticles in a nine different acetate buffers (AB-1 to AB-9) were successfully formed by the ionotropic gelation method at different CS: TPP ratios (6:1, 4:1, 2:1, 1:1, 1:2, 1:4 and 1:6), pH values (3.3, 4.3 and 5.3) and ionic strength (0.1, 0.3 and 0.5 M) conditions. Secondly, 63 chitosan microparticles formulation prepared at different conditions were studied by determining relative viscosity, zeta potential and particle size. Thirdly, for model validation, further formulations of CS: TPP microparticles (6:1, 4:1, 2:1, 1:1, 1:2, 1:4 and 1:6), were prepared in a four different acetate buffers (AB-10, AB-11, AB-12 and AB-13). The characterisation of particles including relative viscosity, zeta potential, particle size, FTIR, XRD and SEM were investigated. Finally, using experimental design, the relative viscosity, particle size and zeta potential of CS: TPP microparticles under different conditions could be predicted using the mathematical models. The mathematical models obtained showed good relationships between independent variables (pH, ionic strength and CS: TPP ratio) and dependent variables (relative viscosity, zeta potential and particle size) for prediction.

Chapter 4 focused on forensic application in specific latent fingerprint visualization. Seven ratios formulations of CS: TPP microparticles (6:1, 4:1, 2:1, 1:1, 1:2, 1:4 and 1:6), were prepared in a four different acetate buffers (AB-10, AB-11, AB-12 and AB-13). These formulations optimised using a 2^3 factorial factor design, in order to design particles of defined properties for latent fingerprint visualization on nonporous surfaces (glass microscope slides). Particles characteristics (such as surface charge and size) had effect on the fingerprint quality. One of the more significant finding to emerge from this study is that CS: TPP ratio has strong effect on quality fingerprint. The optimum conditions of attachment of microparticles to the ridges of latent fingermarks/fingerprint on glass are pH 4.8, CS: TPP ratio of 2:1 and 0.2 M of ionic strength using AB-12. With these conditions, particles were obtained with average diameter of 171.3 μm and the zeta potential of +14.3 mV. The limitation to detecting fingerprints (sensitivity) using CS: TPP particles as a powder is the third depletion level for one day aged. There is further work that could be done to make small changes to the formulation conditions (pH, ionic strength, CS: TPP ratio for example) this could potentially enable the fine tuning of nanoparticles in terms of size and charge to produce better or even bespoke particles for specific applications rather than one size fits all approach, such as visualisation of latent prints on surfaces which have thus far proven difficult for example skin.

Chapter 5 highlighted the formation of chitosan nanoparticles (LMW chitosan in acetic acid), through ionic cross-linkages with TPP for potential pharmaceutical applications. From the analysis of the ibuprofen loaded chitosan nanoparticles by FT-IR spectrometry, it is evident that chitosan nanoparticles with ibuprofen involves ionic interaction between the positive ammonium groups of chitosan nanoparticles and the

carboxylate anion of ibuprofen. Firstly, the ibuprofen was entrapped during preparation of the nanoparticles system by mixed ibuprofen with chitosan then TPP added referred to as (CS+IBU)/TPP (first method) or by mixed ibuprofen with TPP then chitosan added referred to as CS/(IBU+TPP) (second method). The findings of this results show that the second method obtained relatively high DEE of nanoparticles and was selected to carry out further experiments and reinforces the importance of the order addition in formulation preparation. Secondly, the effects of different CS: TPP ratios (3:1, 4:1, 5:1, 6:1 and 7:1) on ibuprofen loaded chitosan nanoparticles was studied. We demonstrated that the optimum CS: TPP ratio amongst those studied is CS: TPP at 5:1 ratio, which leads to the highest DEE (76.8 %). At this ratio, CS-IBU-TPP nanoparticles with sizes 247.3 nm, with PDI 0.27 and with zeta potential +37.4 are produced. Thirdly, effects of ibuprofen concentration (0.5, 1.0, 1.5, 2.0 and 2.5 mg/mL) on ibuprofen loaded chitosan nanoparticles were investigated. During the experiment, CS: TPP ratio at 5:1 and ibuprofen concentration of 0.5 and 1.5 mg/mL, were proposed to be most effective in delivering ibuprofen. Increasing concentration of ibuprofen from 0.5 to 1.5 mg/mL caused an increasing high of CS: TPP interaction, leading to decreasing nanoparticle size. In these conditions, the particle sizes of CS-IBU-TPP nanoparticles were 284.1 nm and 247.3 nm respectively; the zeta potentials were +38.6 mV and +35.3 mV, indicating high stability of CS-IBU-TPP nanoparticles; the DEE of nanoparticles were 86.6 % and 76.8 % respectively. Finally, the cumulative release of ibuprofen in vitro were 38.5 % and 48.7 % respectively. There is further work that could be done to further develop this formulation that includes optimisation of the particle and studying the effect different pH values of formulations and also the effect of the pH of the media on ibuprofen release. This study has suggested that the potential of ibuprofen loaded

chitosan nanoparticles (CS-IBU-TPP) was expected be a new method using in pharmaceuticals applications.

Chapter 6 focused on evaluating the interaction between different ratios (CS: TPP) chitosan nanoparticles including 3:1, 4:1, 5:1, 6:1 and 7:1 and mucin based on relative viscosity, zeta potentials and particle size. We demonstrated that interaction between chitosan nanoparticle and mucin occurred. CS: TPP nanoparticles were evaluated for their mucoadhesive properties for potential use in pharmaceutical applications. The experiments were conducted at 37 °C, as this is closer to physiological conditions. The changes in relative viscosity, surface charge and particle size of nanoparticles indicated an interaction with mucin. The CS: TPP nanoparticles were better at the ratio of 4:1 mixture due to the strongest interaction with mucin. This result may be attributed to a critical point of binding carboxylate groups being saturated at the ratio of 4:1 and a possible of all mucin adsorbed on particles. Mucoadhesion of chitosan nanoparticles were obtained with relative viscosity of 1.08 and zeta potential of +31.3 mV, particle size of 304.6 nm and mucin binding efficiency of 90 %. Further work can be done by mixing different mucin concentrations (*i.e.* 1.0 %, 1.5 %, 2.0 %, 2.5 % and 3%) with CS: TPP of 4:1, as well as different pH to determine a change in viscosity, surface charge and particle size, as this would indicate the occurrence of interaction.

Taking all of the above into account, when a new researcher continues on this work I would suggest they investigate trends in fingerprint development which could include the encapsulation of for example, florescent dyes inside the particles which may improve contrast. If I had time I would like to have done the formulation,

characterization and *in vitro* evaluation of ibuprofen loaded chitosan-TPP nanoparticles at ratio 5:1 - 7:1 using different chitosan concentrations with relatively high ibuprofen concentrations.

8 References

- ABDULKARIM, M., AGULLÓ, N., CATTOZ, B., GRIFFITHS, P., BERNKOP-SCHNÜRCH, A., BORROS, S. G. & GUMBLETON, M. 2015. Nanoparticle diffusion within intestinal mucus: Three-dimensional response analysis dissecting the impact of particle surface charge, size and heterogeneity across polyelectrolyte, pegylated and viral particles. *European Journal of Pharmaceutics and Biopharmaceutics*, 97, 230-238.
- ABIOYE, A. O., ARMITAGE, R. & KOLA-MUSTAPHA, A. T. 2016. Thermodynamic changes induced by intermolecular interaction between ibuprofen and chitosan: Effect on crystal habit, solubility and *in vitro* release kinetics of ibuprofen. *Pharmaceutical Research*, 33, 337-357.
- ABIOYE, A. O., ISSAH, S. & KOLA-MUSTAPHA, A. T. 2015. *Ex vivo* skin permeation and retention studies on chitosan–ibuprofen–gellan ternary nanogel prepared by in situ ionic gelation technique—a tool for controlled transdermal delivery of ibuprofen. *International journal of pharmaceutics*, 490, 112-130.
- ABIOYE, A. O. & KOLA-MUSTAPHA, A. 2015. Controlled electrostatic self-assembly of ibuprofen-cationic dextran nanoconjugates prepared by low energy green process—a novel delivery tool for poorly soluble drugs. *Pharmaceutical research*, 32, 2110-2131.
- ABODINAR, A., SMITH, A. M. & MORRIS, G. A. 2014. A novel method to estimate the stiffness of carbohydrate polyelectrolyte polymers based on the ionic strength dependence of zeta potential. *Carbohydrate Polymers*, 112, 6-9.
- ABODINAR, A., TØMMERAAS, K., RONANDER, E., SMITH, A. M. & MORRIS, G. A. 2016. The physicochemical characterisation of pepsin degraded pig gastric mucin. *International journal of biological macromolecules*, 87, 281-286.
- ADEBISI, A. O. & CONWAY, B. R. 2014. Lectin-conjugated microspheres for eradication of *Helicobacter pylori* infection and interaction with mucus. *International journal of pharmaceutics*, 470, 28-40.
- AFKHAMI, A. & MOOSAVI, R. 2010. Adsorptive removal of Congo red, a carcinogenic textile dye, from aqueous solutions by maghemite nanoparticles. *Journal of Hazardous Materials*, 174, 398-403.
- AGARWAL, M., NAGAR, D., SRIVASTAVA, N. & AGARWAL, M. 2015. Chitosan Nanoparticles based Drug Delivery: an Update. *International Journal of Advanced Multidisciplinary Research*, 2, 1-13.
- AGNIHOTRI, S. A. & AMINABHAVI, T. M. 2004. Controlled release of clozapine through chitosan microparticles prepared by a novel method. *Journal of Controlled Release*, 96, 245-259.
- AGNIHOTRI, S. A., MALLIKARJUNA, N. N. & AMINABHAVI, T. M. 2004. Recent advances on chitosan-based micro-and nanoparticles in drug delivery. *Journal of controlled release*, 100, 5-28.
- AIBA, S.-I. 1992. Studies on chitosan: 4. Lysozymic hydrolysis of partially N-acetylated chitosans. *International journal of biological macromolecules*, 14, 225-228.

- AL-HAMIDI, H., ASARE-ADDO, K., DESAI, S., KITSON, M. & NOKHODCHI, A. 2015. The dissolution and solid-state behaviours of coground ibuprofen–glucosamine HCl. *Drug development and industrial pharmacy*, 41, 1682-1692.
- AL-SHAMMARI, B., AL-FARISS, T., AL-SEWAILM, F. & ELLEITHY, R. 2011. The effect of polymer concentration and temperature on the rheological behavior of metallocene linear low density polyethylene (mLLDPE) solutions. *Journal of King Saud University-Engineering Sciences*, 23, 9-14.
- AL MASUM, M. A., ISLAM, S. A. & REZA, M. S. 2012. Enhancement of solubility and dissolution characteristics of ibuprofen by solid dispersion technique. *Dhaka University Journal of Pharmaceutical Sciences*, 11, 1-6.
- ALI, S. W., RAJENDRAN, S. & JOSHI, M. 2011. Synthesis and characterization of chitosan and silver loaded chitosan nanoparticles for bioactive polyester. *Carbohydrate Polymers*, 83, 438-446.
- ALMOG, J., CANTU, A. A., CHAMPOD, C., KENT, T. & LENNARD, C. 2014. Guidelines for the assessment of fingerprint detection techniques International Fingerprint Research Group (IFRG). *Journal of Forensic Identification*, 64, 174-200.
- ALMOG, J., SEARS, V. G., SPRINGER, E., HEWLETT, D. F., WALKER, S., WIESNER, S., LIDOR, R. & BAHAR, E. 2000. Reagents for the chemical development of latent fingerprints: scope and limitations of benzo [f] ninhydrin in comparison to ninhydrin. *Journal of Forensic Science*, 45, 538-544.
- ALONSO-SANDE, M., CUÑA, M., REMUÑÁN-LÓPEZ, C., TEJEIRO-OSORIO, D., ALONSO-LEBRERO, J. L. & ALONSO, M. J. 2006. Formation of new glucomannan– chitosan nanoparticles and study of their ability to associate and deliver proteins. *Macromolecules*, 39, 4152-4158.
- ALSHEHRI, S. M., AL-LOHEDAN, H. A., CHAUDHARY, A. A., AL-FARRAJ, E., ALHOKBANY, N., ISSA, Z., ALHOUSINE, S. & AHAMAD, T. 2016. Delivery of ibuprofen by natural macroporous sporopollenin exine capsules extracted from *Phoenix dactylifera* L. *European Journal of Pharmaceutical Sciences*, 88, 158-165.
- ALTEKAR, M., HOMON, C. A., KASHEM, M. A., MASON, S. W., NELSON, R. M., PATNAUDE, L. A., YINGLING, J. & TAYLOR, P. B. 2007. Assay optimization: a statistical design of experiments approach. *Clinics in laboratory medicine*, 27, 139-154.
- ANAL, A. K., STEVENS, W. F. & REMUÑÁN-LÓPEZ, C. 2006. Iontropic cross-linked chitosan microspheres for controlled release of ampicillin. *International journal of pharmaceuticals*, 312, 166-173.
- ANDERSEN, T., BLEHER, S., EIDE FLATEN, G., THO, I., MATTSSON, S. & ŠKALKO-BASNET, N. 2015. Chitosan in Mucoadhesive Drug Delivery: Focus on Local Vaginal Therapy. *Marine drugs*, 13, 222-236.
- ANDREWS, G. P., LAVERTY, T. P. & JONES, D. S. 2009. Mucoadhesive polymeric platforms for controlled drug delivery. *European Journal of Pharmaceutics and Biopharmaceutics*, 71, 505-518.
- ANITHA, A., DEEPA, N., CHENNAZHI, K., NAIR, S., TAMURA, H. & JAYAKUMAR, R. 2011. Development of mucoadhesive thiolated chitosan nanoparticles for biomedical applications. *Carbohydrate Polymers*, 83, 66-73.
- ARAMWIT, P., EKASIT, S. & YAMDECH, R. 2015. The development of non-toxic ionic-crosslinked chitosan-based microspheres as carriers for the controlled release of silk sericin. *Biomedical microdevices*, 17, 1-9.

- ARANAZ, I., MENGÍBAR, M., HARRIS, R., PAÑOS, I., MIRALLES, B., ACOSTA, N., GALED, G. & HERAS, Á. 2009. Functional characterization of chitin and chitosan. *Current Chemical Biology*, 3, 203-230.
- ARCHER, N. E., CHARLES, Y., ELLIOTT, J. A. & JICKELLS, S. 2005. Changes in the lipid composition of latent fingerprint residue with time after deposition on a surface. *Forensic science international*, 154, 224-239.
- ARTURSSON, P., LINDMARK, T., DAVIS, S. S. & ILLUM, L. 1994. Effect of chitosan on the permeability of monolayers of intestinal epithelial cells (Caco-2). *Pharmaceutical research*, 11, 1358-1361.
- ASANO, K. G., BAYNE, C. K., HORSMAN, K. M. & BUCHANAN, M. V. 2002. Chemical composition of fingerprints for gender determination. *Journal of Forensic Science*, 47, 1-3.
- ASHBAUGH, D. R. 1999. Quantitative-qualitative friction ridge analysis: an introduction to basic and advanced ridgeology. (ed.) *New York: CRC press, Boca Raton*.
- ATKINS, P. & DE PAULA, J. 2011. Physical chemistry for the life sciences. Second edition. *USA: Oxford University Press*.
- ATTARD-MONTALTO, N., OJEDA, J. J., REYNOLDS, A., ISMAIL, M., BAILEY, M., DOODKORTE, L., DE PUIT, M. & JONES, B. J. 2014. Determining the chronology of deposition of natural fingermarks and inks on paper using secondary ion mass spectrometry. *Analyst*, 139, 4641-4653.
- AU, C., JACKSON-SMITH, H., QUINONES, I., JONES, B. & DANIEL, B. 2011. Wet powder suspensions as an additional technique for the enhancement of bloodied marks. *Forensic science international*, 204, 13-18.
- AVADI, M. R., SADEGHI, A. M. M., MOHAMMADPOUR, N., ABEDIN, S., ATYABI, F., DINARVAND, R. & RAFIEE-TEHRANI, M. 2010. Preparation and characterization of insulin nanoparticles using chitosan and Arabic gum with ionic gelation method. *Nanomedicine: Nanotechnology, Biology and Medicine*, 6, 58-63.
- AYDIN, Z. & AKBUĞA, J. 1996. Chitosan beads for the delivery of salmon calcitonin: preparation and release characteristics. *International journal of pharmaceuticals*, 131, 101-103.
- AZOFEIFA, D. E., ARGUEDAS, H. J. & VARGAS, W. E. 2012. Optical properties of chitin and chitosan biopolymers with application to structural color analysis. *Optical materials*, 35, 175-183.
- BACON, S. R., OJEDA, J. J., DOWNHAM, R., SEARS, V. G. & JONES, B. J. 2013. The effects of polymer pigmentation on fingerprint development techniques. *Journal of forensic sciences*, 58, 1486-1494.
- BAHL, B. & TULI, G. D. 2010. Essentials of Physical Chemistry, *S Chand & Co Ltd*.
- BAILEY, M. J., BRIGHT, N. J., CROXTON, R. S., FRANCESE, S., FERGUSON, L. S., HINDER, S., JICKELLS, S., JONES, B. J., JONES, B. N. & KAZARIAN, S. G. 2012. Chemical characterization of latent fingerprints by matrix-assisted laser desorption ionization, time-of-flight secondary ion mass spectrometry, mega electron volt secondary mass spectrometry, gas chromatography/mass spectrometry, X-ray photoelectron spectroscopy, and attenuated total reflection Fourier transform infrared spectroscopic imaging: an intercomparison. *Analytical chemistry*, 84, 8514-8523.
- BANDEY, H. & GIBSON, A. P. 2006. Fingerprint development and imaging newsletter: the powders process, study 2. *Sandridge, UK: Police Scientific Development Branch, Home Office*, 8, 1-16.

- BANERJEE, T., MITRA, S., SINGH, A. K., SHARMA, R. K. & MAITRA, A. 2002. Preparation, characterization and biodistribution of ultrafine chitosan nanoparticles. *International Journal of Pharmaceutics*, 243, 93-105.
- BANIUK, K. 1990. Determination of age of fingerprints. *Forensic Science International*, 46, 133-137.
- BANSIL, R., CELLI, J., HARDCASTLE, J. & TURNER, B. 2013. The influence of mucus microstructure and rheology in *Helicobacter pylori* infection. *Frontiers in immunology*, 4, 1-12.
- BANSIL, R. & TURNER, B. S. 2006. Mucin structure, aggregation, physiological functions and biomedical applications. *Current Opinion in Colloid & Interface Science*, 11, 164-170.
- BARBOSA-CANOVAS, G. V. & IBARZ, A. 2014. Introduction to food process engineering. First edition. CRC Press: Boca Raton.
- BARRON, A. R., ALLEN, J., BOTT, S., JEBB, M., JIANG, C. & KIENAST, W. 2012. Physical methods in chemistry and nano science. SEM and its Applications for Polymer Science. (ed.) Texas, USA. *Connexions Rice University: Houston*,
- BECUE, A., CHAMPOD, C. & MARGOT, P. 2007. Use of gold nanoparticles as molecular intermediates for the detection of fingermarks. *Forensic science international*, 168, 169-176.
- BECUE, A., MORET, S., CHAMPOD, C. & MARGOT, P. 2009. Use of quantum dots in aqueous solution to detect blood fingermarks on non-porous surfaces. *Forensic Science International*, 191, 36-41.
- BECUE, A., SCOUNDRIANOS, A., CHAMPOD, C. & MARGOT, P. 2008. Fingermark detection based on the in situ growth of luminescent nanoparticles—Towards a new generation of multimetal deposition. *Forensic science international*, 179, 39-43.
- BELLICH, B., D'AGOSTINO, I., SEMERARO, S., GAMINI, A. & CESÀRO, A. 2016. “The good, the bad and the ugly” of chitosans. *Marine drugs*, 14, 1-31.
- BENTON, M., CHUA, M., GU, F., ROWELL, F. & MA, J. 2010a. Environmental nicotine contamination in latent fingermarks from smoker contacts and passive smoking. *Forensic science international*, 200, 28-34.
- BENTON, M., ROWELL, F., SUNDAR, L. & JAN, M. 2010b. Direct detection of nicotine and cotinine in dusted latent fingermarks of smokers by using hydrophobic silica particles and MS. *Surface and interface analysis*, 42, 378-385.
- BERGER, J., REIST, M., MAYER, J., FELT, O., PEPPAS, N. & GURNY, R. 2004. Structure and interactions in covalently and ionically crosslinked chitosan hydrogels for biomedical applications. *European Journal of Pharmaceutics and Biopharmaceutics*, 57, 19-34.
- BERGERON, J. 2003. Development of bloody prints on dark surfaces with titanium dioxide and methanol. *Journal of forensic Identification*, 53, 149.
- BERRY, J. & STONEY, D. A. 2001. The history and development of fingerprinting. *Advances in fingerprint Technology*, 2, 13-52.
- BERTHOLD, A., CREMER, K. & KREUTER, J. 1996. Preparation and characterization of chitosan microspheres as drug carrier for prednisolone sodium phosphate as model for anti-inflammatory drugs. *Journal of Controlled Release*, 39, 17-25.

- BHARDWAJ, V., SHUKLA, V., GOYAL, N., MALVIYA, R. & SHARMA, P. 2010. Formulation and evaluation of different concentration chitosan based periodontal film of ofloxacin. *J. Pharmacy Res*, 3, 528-532.
- BHUMKAR, D. R. & POKHARKAR, V. B. 2006. Studies on effect of pH on cross-linking of chitosan with sodium tripolyphosphate: a technical note. *AAPS PharmSciTech*, 7, E138-E143.
- BLOCK, T., ISAKSSON, H. S., ACOSTA, S., BJÖRCK, M., BRODIN, D. & NILSSON, T. K. 2011. Altered mRNA expression due to acute mesenteric ischaemia in a porcine model. *European Journal of Vascular and Endovascular Surgery*, 41, 281-287.
- BOBEV, K. 1995. Fingerprints and factors affecting their condition. *Journal of Forensic Identification*, 45, 176-183.
- BODDUPALLI, B. M., MOHAMMED, Z. N., NATH, R. A. & BANJI, D. 2010. Mucoadhesive drug delivery system: An overview. *Journal of advanced pharmaceutical technology & research*, 1, 381-387.
- BODMEIER, R., OH, K.-H. & PRAMAR, Y. 1989. Preparation and evaluation of drug-containing chitosan beads. *Drug development and industrial pharmacy*, 15, 1475-1494.
- BOONSONGRIT, Y., MITREVEJ, A. & MUELLER, B. W. 2006. Chitosan drug binding by ionic interaction. *European journal of pharmaceutics and biopharmaceutics*, 62, 267-274.
- BOWMAN, K. & LEONG, K. W. 2006. Chitosan nanoparticles for oral drug and gene delivery. *International journal of nanomedicine*, 1, 117-128.
- BRAMBLE, S. 1995. Separation of latent fingerprint residue by thin-layer chromatography. *Journal of Forensic Science*, 40, 969-975.
- BRIGHT, N. J., WILLSON, T. R., DRISCOLL, D. J., REDDY, S. M., WEBB, R. P., BLEAY, S., WARD, N. I., KIRKBY, K. J. & BAILEY, M. J. 2013. Chemical changes exhibited by latent fingerprints after exposure to vacuum conditions. *Forensic science international*, 230, 81-86.
- BROWN, S. D., NATIVO, P., SMITH, J.-A., STIRLING, D., EDWARDS, P. R., VENUGOPAL, B., FLINT, D. J., PLUMB, J. A., GRAHAM, D. & WHEATE, N. J. 2010. Gold nanoparticles for the improved anticancer drug delivery of the active component of oxaliplatin. *Journal of the American Chemical Society*, 132, 4678-4684.
- BUCHANAN, M. V., ASANO, K. & BOHANON, A. Chemical characterization of fingerprints from adults and children. *Forensic Evidence Analysis and Crime Scene Investigation, 1997. International Society for Optics and Photonics*, 89-96.
- BUGNICOURT, L., ALCOUFFE, P. & LADAVIÈRE, C. 2014. Elaboration of chitosan nanoparticles: Favorable impact of a mild thermal treatment to obtain finely divided, spherical, and colloidally stable objects. *Colloids and Surfaces A: Physicochemical and Engineering Aspects*, 457, 476-486.
- BUROW, D., SEIFERT, D. & CANTU, A. A. 2003. Modifications to the silver physical developer. *Journal of forensic sciences*, 48, 1094-1100.
- BUSCHMANN, M. D., MERZOUKI, A., LAVERTU, M., THIBAUT, M., JEAN, M. & DARRAS, V. 2013. Chitosans for delivery of nucleic acids. *Advanced drug delivery reviews*, 65, 1234-1270.
- BUSHRA, M. U., AKTER, N., HASSAN, M. R., ISLAM, A. & HOSSAIN, M. R. 2014. Development and validation of a simple UV spectrophotometric method

- for the determination of cefotaxime sodium in bulk and pharmaceutical formulation. *IOSR J. Pharm*, 4, 74-77.
- CADD, S., ISLAM, M., MANSON, P. & BLEAY, S. 2015. Fingerprint composition and aging: a literature review. *Science & Justice*, 55, 219-238.
- CAICEDO, J. & PERILLA, J. E. 2015. Effect of pH on the rheological response of reconstituted gastric mucin. *Ingeniería e Investigación*, 35, 43-48.
- CALVO, P., REMUNAN-LOPEZ, C., VILA-JATO, J. & ALONSO, M. 1997a. Novel hydrophilic chitosan-polyethylene oxide nanoparticles as protein carriers. *Journal of applied polymer science*, 63, 125-132.
- CALVO, P., REMUÑAN-LÓPEZ, C., VILA-JATO, J. L. & ALONSO, M. J. 1997b. Chitosan and chitosan/ethylene oxide-propylene oxide block copolymer nanoparticles as novel carriers for proteins and vaccines. *Pharmaceutical research*, 14, 1431-1436.
- CANTU, A. 2001. Silver physical developers for the visualization of latent prints on paper. *Forensic Science Review*, 13, 29-64.
- CANTU, A. A., LEBEN, D. A. & WILSON, K. Some advances in the silver physical development of latent prints on paper. Sensors, and Command, Control, Communications, and Intelligence (C3I) Technologies for Homeland Defense and Law Enforcement II, 2003. *International Society for Optics and Photonics*, 5071, 164-168.
- CARAMELLA, C. M., ROSSI, S., FERRARI, F., BONFERONI, M. C. & SANDRI, G. 2015. Mucoadhesive and thermogelling systems for vaginal drug delivery. *Advanced drug delivery reviews*, 92, 39-52.
- CARNEIRO-DA-CUNHA, M. G., CERQUEIRA, M. A., SOUZA, B. W., TEIXEIRA, J. A. & VICENTE, A. A. 2011. Influence of concentration, ionic strength and pH on zeta potential and mean hydrodynamic diameter of edible polysaccharide solutions envisaged for multilayered films production. *Carbohydrate polymers*, 85, 522-528.
- CARVALHO, F. C., BRUSCHI, M. L., EVANGELISTA, R. C. & GREMIÃO, M. P. D. 2010. Mucoadhesive drug delivery systems. *Brazilian Journal of Pharmaceutical Sciences*, 46, 1-17.
- CASETTARI, L., CESPI, M., PALMIERI, G. F. & BONACUCINA, G. 2013. Characterization of the interaction between chitosan and inorganic sodium phosphates by means of rheological and optical microscopy studies. *Carbohydrate polymers*, 91, 597-602.
- CHAMPION, J. A., KATARE, Y. K. & MITRAGOTRI, S. 2007. Particle shape: a new design parameter for micro-and nanoscale drug delivery carriers. *Journal of Controlled Release*, 121, 3-9.
- CHAMPOD, C., LENNARD, C., MARGOT, P. & STOILOVIC, M. 2004. Fingerprints and Other Ridge Skin Impressions. *International forensic science and investigation series*. (ed.) London, New York, Washington. *CRC Press: Boca Raton*.
- CHANDY, T. & SHARMA, C. P. 1996. Effect of liposome-albumin coatings on ferric ion retention and release from chitosan beads. *Biomaterials*, 17, 61-66.
- CHELLAT, F., TABRIZIAN, M., DUMITRIU, S., CHORNET, E., RIVARD, C. H. & YAHIA, L. H. 2000. Study of biodegradation behavior of chitosan-xanthan microspheres in simulated physiological media. *Journal of Biomedical Materials Research*, 53, 592-599.

- CHEN, M.-C., MI, F.-L., LIAO, Z.-X. & SUNG, H.-W. 2011. Chitosan: its applications in drug-eluting devices. *Chitosan for Biomaterials I*. Springer. 243, 185-230.
- CHEN, Q., KERK, W. T., SOUTAR, A. M. & ZENG, X. T. 2009. Application of dye intercalated bentonite for developing latent fingerprints. *Applied Clay Science*, 44, 156-160.
- CHEN, R. H. & TSAIH, M. L. 1998. Effect of temperature on the intrinsic viscosity and conformation of chitosans in dilute HCl solution. *International journal of biological macromolecules*, 23, 135-141.
- CHEN, X. & MAO, S. S. 2007. Titanium dioxide nanomaterials: synthesis, properties, modifications, and applications. *Chemical reviews*, 107, 2891-2959.
- CHENG, K. H., AJIMO, J. & CHEN, W. 2008. Exploration of functionalized CdTe nanoparticles for latent fingerprint detection. *Journal of nanoscience and nanotechnology*, 8, 1170-1173.
- CHEON, J. W. & CHUNG, S. J. 2009. Original Articles: Effect of Tripolyphosphate (TPP) on the Controlled Release of Cyclosporin A from Chitosan-coated Lipid Microparticles. *J. Kor. Pharm. Sci*, 39, 59-63.
- CHHABRA, R. P. & RICHARDSON, J. F. 2008. Non-Newtonian flow and applied rheology: engineering applications. Second edition. UK: *Butterworth-Heinemann*.
- CHOI, C., NAM, J.-P. & NAH, J.-W. 2016. Application of chitosan and chitosan derivatives as biomaterials. *Journal of Industrial and Engineering Chemistry*, 33, 1-10.
- CHOI, J., KWAK, S. Y., KANG, S., LEE, S. S., PARK, M., LIM, S., KIM, J., CHOE, C. & HONG, S. 2002. Synthesis of highly crosslinked monodisperse polymer particles: effect of reaction parameters on the size and size distribution. *Journal of Polymer Science Part A: Polymer Chemistry*, 40, 4368-4377.
- CHOI, M. J., MCDONAGH, A. M., MAYNARD, P. & ROUX, C. 2008. Metal-containing nanoparticles and nano-structured particles in fingerprint detection. *Forensic science international*, 179, 87-97.
- CHOI, M. J., MCDONAGH, A. M., MAYNARD, P. J. & WUHRER, R. 2006. Preparation and evaluation of metal nanopowders for the detection of fingerprints on nonporous surfaces. *Journal of Forensic Identification*, 56, 756-768.
- CHOI, M. J., SMOOTHER, T., MARTIN, A. A., MCDONAGH, A. M., MAYNARD, P. J., LENNARD, C. & ROUX, C. 2007. Fluorescent TiO₂ powders prepared using a new perylene diimide dye: Applications in latent fingerprint detection. *Forensic Science International*, 173, 154-160.
- CHRISTIAN, G. D. & O'REILLY, J. E. 1988. Instrumental analysis, Second edition. United states: *Allyn and Bacon, Inc*.
- CHRISTIAN, P., VON DER KAMMER, F., BAALOUSHA, M. & HOFMANN, T. 2008. Nanoparticles: structure, properties, preparation and behaviour in environmental media. *Ecotoxicology*, 17, 326-343.
- CHRISTLET, T. H. T. & VELURAJA, K. 2001. Database analysis of O-glycosylation sites in proteins. *Biophysical journal*, 80, 952-960.
- COSTA, P. & LOBO, J. S. 2001. Influence of dissolution medium agitation on release profiles of sustained-release tablets. *Drug development and industrial pharmacy*, 27, 811-817.

- CROXTON, R. S., BARON, M. G., BUTLER, D., KENT, T. & SEARS, V. G. 2010. Variation in amino acid and lipid composition of latent fingerprints. *Forensic Science International*, 199, 93-102.
- CUCE, P., POLIMENI, G., LAZZARO, A. & DE FULVIO, G. 2004. Small particle reagents technique can help to point out wet latent fingerprints. *Forensic science international*, 146, S7-S8.
- CZECHOWSKA-BISKUP, R., JAROSIŃSKA, D., ROKITA, B., ULAŃSKI, P. & ROSIAK, J. M. 2012. Determination of degree of deacetylation of chitosan—comparison of methods. *Progress on Chemistry and Application of Chitin and its Derivatives*, 17, 5-20.
- DA SILVA, C., MARTINS, F. & SANTANA, M. H. 2007. Adsorption isotherms of mucin on granules containing chitosan microspheres. *Adsorption Science & Technology*, 25, 781-789.
- DALRYMPLE, B., DUFF, J. M. & MENZEL, E. 1977. Inherent fingerprint luminescence—detection by laser. *Journal of Forensic Science*, 22, 106-115.
- DANHIER, F., FERON, O. & PRÉAT, V. 2010. To exploit the tumor microenvironment: passive and active tumor targeting of nanocarriers for anti-cancer drug delivery. *Journal of controlled release*, 148, 135-146.
- DASH, M., CHIELLINI, F., OTTENBRITE, R. M. & CHIELLINI, E. 2011. Chitosan—A versatile semi-synthetic polymer in biomedical applications. *Progress in polymer science*, 36, 981-1014.
- DAVID, L. N. & MICHAEL, M. C. 2013. Principles of biochemistry. Sixth edition. New York: *Susan Winslow*.
- DE CAMPOS, A. M., DIEBOLD, Y., CARVALHO, E. L., SÁNCHEZ, A. & ALONSO, M. J. 2004. Chitosan nanoparticles as new ocular drug delivery systems: *in vitro* stability, *in vivo* fate, and cellular toxicity. *Pharmaceutical research*, 21, 803-810.
- DE LA ESCOSURA-MUÑIZ, A., SÁNCHEZ-ESPINEL, C., DÍAZ-FREITAS, B. N., GONZÁLEZ-FERNÁNDEZ, A. F., MALTEZ-DA COSTA, M. & MERKOÇI, A. 2009. Rapid identification and quantification of tumor cells using an electrocatalytic method based on gold nanoparticles. *Analytical chemistry*, 81, 10268-10274.
- DE LA HUNTY, M., MORET, S., CHADWICK, S., LENNARD, C., SPINDLER, X. & ROUX, C. 2015. Understanding physical developer (PD): part II—is PD targeting eccrine constituents? *Forensic science international*, 257, 488-495.
- DE LA HUNTY, M., SPINDLER, X., CHADWICK, S., LENNARD, C. & ROUX, C. 2014. Synthesis and application of an aqueous Nile red microemulsion for the development of fingermarks on porous surfaces. *Forensic science international*, 244, e48-e55.
- DE PINHO NEVES, A. L., MILIOLI, C. C., MÜLLER, L., RIELLA, H. G., KUHNEN, N. C. & STULZER, H. K. 2014. Factorial design as tool in chitosan nanoparticles development by ionic gelation technique. *Colloids and Surfaces A: Physicochemical and Engineering Aspects*, 445, 34-39.
- DEACON, M., DAVIS, S., WHITE, R., NORDMAN, H., CARLSTEDT, I., ERRINGTON, N., ROWE, A. & HARDING, S. 1999. Are chitosan–mucin interactions specific to different regions of the stomach? Velocity ultracentrifugation offers a clue. *Carbohydrate Polymers*, 38, 235-238.
- DEGLAIRE, A. & MOUGHAN, P. J. 2012. Animal models for determining amino acid digestibility in humans—a review. *British Journal of Nutrition*, 108, S273-S281.

- DENG, Q.-Y., ZHOU, C.-R. & LUO, B.-H. 2006. Preparation and characterization of chitosan nanoparticles containing lysozyme. *Pharmaceutical biology*, 44, 336-342.
- DEPAN, D., KUMAR, A. P. & SINGH, R. P. 2009. Cell proliferation and controlled drug release studies of nanohybrids based on chitosan-g-lactic acid and montmorillonite. *Acta Biomaterialia*, 5, 93-100.
- DESAI, M. P., LABHASETWAR, V., AMIDON, G. L. & LEVY, R. J. 1996. Gastrointestinal uptake of biodegradable microparticles: effect of particle size. *Pharmaceutical research*, 13, 1838-1845.
- DESAI, M. P., LABHASETWAR, V., WALTER, E., LEVY, R. J. & AMIDON, G. L. 1997. The mechanism of uptake of biodegradable microparticles in Caco-2 cells is size dependent. *Pharmaceutical research*, 14, 1568-1573.
- DHALL, J. K. & KAPOOR, A. 2016. Development of latent prints exposed to destructive crime scene conditions using wet powder suspensions. *Egyptian Journal of Forensic Sciences*, 6, 396-404.
- DILAG, J., KOBUS, H. & ELLIS, A. V. 2009. Cadmium sulfide quantum dot/chitosan nanocomposites for latent fingerprint detection. *Forensic science international*, 187, 97-102.
- DILAG, J., KOBUS, H. & ELLIS, A. V. 2013. CdS/polymer nanocomposites synthesized via surface initiated RAFT polymerization for the fluorescent detection of latent fingerprints. *Forensic science international*, 228, 105-114.
- DOMINGOS, R. F., BAALOUSHA, M. A., JU-NAM, Y., REID, M. M., TUFENKJI, N., LEAD, J. R., LEPPARD, G. G. & WILKINSON, K. J. 2009. Characterizing manufactured nanoparticles in the environment: multimethod determination of particle sizes. *Environmental science & technology*, 43, 7277-7284.
- DOUGLAS, K. L. & TABRIZIAN, M. 2005. Effect of experimental parameters on the formation of alginate-chitosan nanoparticles and evaluation of their potential application as DNA carrier. *Journal of Biomaterials Science, Polymer Edition*, 16, 43-56.
- DOUGLAS, W. R. 1972. Of pigs and men and research. *Space life sciences*, 3, 226-234.
- DOWNING, D. T. & STRAUSS, J. S. 1974. Synthesis and composition of surface lipids of human skin. *Journal of Investigative Dermatology*, 62, 228-244.
- DRUCE, J. F. & BRISTOW, L. C. 2010. Latent mark development and analysis within a modern policing environment. *Surface and Interface Analysis*, 42, 343-346.
- DUDHANI, A. R. & KOSARAJU, S. L. 2010. Bioadhesive chitosan nanoparticles: Preparation and characterization. *Carbohydrate polymers*, 81, 243-251.
- DUNG, T. H., LEE, S.-R., HAN, S.-D., KIM, S.-J., JU, Y.-M., KIM, M.-S. & YOO, H. 2007. Chitosan-TPP nanoparticle as a release system of antisense oligonucleotide in the oral environment. *Journal of nanoscience and nanotechnology*, 7, 3695-3699.
- DYER, A., HINCHCLIFFE, M., WATTS, P., CASTILE, J., JABBAL-GILL, I., NANKERVIS, R., SMITH, A. & ILLUM, L. 2002. Nasal delivery of insulin using novel chitosan based formulations: a comparative study in two animal models between simple chitosan formulations and chitosan nanoparticles. *Pharmaceutical research*, 19, 998-1008.

- EVETT, I. W. & WILLIAMS, R. L. 2015. A review of the sixteen points fingerprint standard in England and Wales. *Journal of Forensic Identification*, 65, 557-580.
- FAIRLEY, C., BLEAY, S., SEARS, V. & NICDAEID, N. 2012. A comparison of multi-metal deposition processes utilising gold nanoparticles and an evaluation of their application to 'low yield' surfaces for finger mark development. *Forensic science international*, 217, 5-18.
- FAN, W., YAN, W., XU, Z. & NI, H. 2012. Formation mechanism of monodisperse, low molecular weight chitosan nanoparticles by ionic gelation technique. *Colloids and Surfaces B: Biointerfaces*, 90, 21-27.
- FAROKHZAD, O. C. & LANGER, R. 2009. Impact of nanotechnology on drug delivery. *ACS nano*, 3, 16-20.
- FARUKI, M. Z., RAZZAQUE, E. & BHUIYAN, M. A. 2013. Improvement of Solubility of badly water soluble drug (Ibuprofen) by using Surfactants and Carriers. *International Journal of Pharmaceutical Sciences and Research*, 4, 1569-1574.
- FAULDS, H. 1880. On the skin-furrows of the hand. *Nature*, 22, 605.
- FEFELOVA, N. A., NURKEEVA, Z. S., MUN, G. A. & KHUTORYANSKIY, V. V. 2007. Mucoadhesive interactions of amphiphilic cationic copolymers based on [2-(methacryloyloxy) ethyl] trimethylammonium chloride. *International journal of pharmaceutics*, 339, 25-32.
- FIEBRIG, I., HARDING, S. E., ROWE, A. J., HYMAN, S. C. & DAVIS, S. S. 1995. Transmission electron microscopy studies on pig gastric mucin and its interactions with chitosan. *Carbohydrate polymers*, 28, 239-244.
- FRITZ, P., FRICK, A., VAN BRONSWIJK, W., LEWIS, S., BEAUDOIN, A., BLEAY, S. & LENNARD, C. 2015. Variability and subjectivity in the grading process for evaluating the performance of latent fingerprint detection techniques. *Journal of Forensic Identification*, 65, 851-867.
- GALTON, F. 1892. Finger Prints. *Macmillan and Co.* London, New yourk.
- GAN, Q. & WANG, T. 2007. Chitosan nanoparticle as protein delivery carrier—systematic examination of fabrication conditions for efficient loading and release. *Colloids and Surfaces B: Biointerfaces*, 59, 24-34.
- GAN, Q., WANG, T., COCHRANE, C. & MCCARRON, P. 2005. Modulation of surface charge, particle size and morphological properties of chitosan-TPP nanoparticles intended for gene delivery. *Colloids and Surfaces B: Biointerfaces*, 44, 65-73.
- GANESH, M. & LEE, S. G. 2013. Synthesis, characterization and drug release capability of new cost effective mesoporous silica nano particles for ibuprofen drug delivery. *Int J Cont Auto*, 6, 207-16.
- GAO, D., LI, F., SONG, J., XU, X., ZHANG, Q. & NIU, L. 2009. One step to detect the latent fingerprints with gold nanoparticles. *Talanta*, 80, 479-483.
- GARG, R. K., KUMARI, H. & KAUR, R. 2011. A new technique for visualization of latent fingerprints on various surfaces using powder from turmeric: a rhizomatous herbaceous plant (*Curcuma longa*). *Egyptian Journal of Forensic Sciences*, 1, 53-57.
- GARLEA, A., POPA, M., POHOAȚĂ, V. & MELNIG, V. 2007. Ibuprofen/ketoprofen entrapment in chitosan based vesicle carrier. *Rom. J. Biophys*, 17, 157-168.

- GASPAR, V., SOUSA, F., QUEIROZ, J. & CORREIA, I. 2011. Formulation of chitosan–TPP–pDNA nanocapsules for gene therapy applications. *Nanotechnology*, 22, 1-12.
- GAVINI, E., HEGGE, A. B., RASSU, G., SANNA, V., TESTA, C., PIRISINO, G., KARLSEN, J. & GIUNCHEDI, P. 2006. Nasal administration of carbamazepine using chitosan microspheres: *in vitro/in vivo* studies. *International journal of pharmaceutics*, 307, 9-15.
- GIERSZEWSKA-DRUŻYŃSKA, M. & OSTROWSKA-CZUBENKO, J. 2010. The effect of ionic crosslinking on thermal properties of hydrogel chitosan membranes. *Progress on Chemistry and Application of Chitin and its Derivatives, Polish Chitin Society, Łódź, XV*, 25-32.
- GIRI, T., KUMAR, THAKUR, A., ALEXANDER, A., BADWAIK, H. & TRIPATHI, D. K. 2012. Modified chitosan hydrogels as drug delivery and tissue engineering systems: present status and applications. *Acta Pharmaceutica Sinica B*, 2, 439-449.
- GIROD, A., RAMOTOWSKI, R. & WEYERMANN, C. 2012. Composition of fingerprint residue: A qualitative and quantitative review. *Forensic science international*, 223, 10-24.
- GIROD, A. & WEYERMANN, C. 2014. Lipid composition of fingerprint residue and donor classification using GC/MS. *Forensic science international*, 238, 68-82.
- GOKCE, Y., CENGIZ, B., YILDIZ, N., CALIMLI, A. & AKTAS, Z. 2014. Ultrasonication of chitosan nanoparticle suspension: Influence on particle size. *Colloids and Surfaces A: Physicochemical and Engineering Aspects*, 462, 75-81.
- GOLDSTEIN, J. & HARVEY, Y. 1975. Practical scanning electron microscopy. (ed.) New York: Plenum Press.
- GOMATHI, T., SUDHA, P., FLORENCE, J. A. K., VENKATESAN, J. & ANIL, S. 2017. Fabrication of letrozole formulation using chitosan nanoparticles through ionic gelation method. *International journal of biological macromolecules*, 104, 1820-1832.
- GONZALEZ, L. M., MOESER, A. J. & BLIKSLAGER, A. T. 2015. Porcine models of digestive disease: the future of large animal translational research. *Translational Research*, 166, 12-27.
- GOYCOOLEA, F., MORRIS, E. & GIDLEY, M. 1995. Screening for synergistic interactions in dilute polysaccharide solutions. *Carbohydrate polymers*, 28, 351-358.
- GRAHAM, D. 1969. Some technical aspects of the demonstration and visualization of fingerprints on human skin. *Journal of forensic sciences*, 14, 1-12.
- GRIEBINGER, J., DÜNNHAUPT, S., CATTOZ, B., GRIFFITHS, P., OH, S., I GÓMEZ, S. B., WILCOX, M., PEARSON, J., GUMBLETON, M. & ABDULKARIM, M. 2015. Methods to determine the interactions of micro- and nanoparticles with mucus. *European Journal of Pharmaceutics and Biopharmaceutics*, 96, 464-476.
- GUPTA, K. & JABRAIL, F. H. 2006. Effects of degree of deacetylation and cross-linking on physical characteristics, swelling and release behavior of chitosan microspheres. *Carbohydrate Polymers*, 66, 43-54.
- HADGRAFT, J. & VALENTA, C. 2000. pH, pKa and dermal delivery. *International journal of pharmaceutics*, 200, 243-247.

- HAMDINE, M., HEUZEY, M.-C. & BÉGIN, A. 2005. Effect of organic and inorganic acids on concentrated chitosan solutions and gels. *International journal of biological macromolecules*, 37, 134-142.
- HANSEN, D. B. & JOULLIÉ, M. M. 2005. The development of novel ninhydrin analogues. *Chemical Society Reviews*, 34, 408-417.
- HAQUE, F., WESTLAND, A. D., MILLIGAN, J. & KERR, F. M. 1989. A small particle (iron oxide) suspension for detection of latent fingerprints on smooth surfaces. *Forensic Science International*, 41, 73-82.
- HARDING, S. E. 1997. The intrinsic viscosity of biological macromolecules. Progress in measurement, interpretation and application to structure in dilute solution. *Progress in biophysics and molecular biology*, 68, 207-262.
- HARDING, S. E., DAVIS, S. B., DEACON, M. P. & FIEBRIG, I. 1999. Biopolymer mucoadhesives. *Biotechnology and genetic engineering reviews*, 16, 41-86.
- HASHAD, R. A., ISHAK, R. A., FAHMY, S., MANSOUR, S. & GENEIDI, A. S. 2016. Chitosan-tripolyphosphate nanoparticles: Optimization of formulation parameters for improving process yield at a novel pH using artificial neural networks. *International journal of biological macromolecules*, 86, 50-58.
- HASSANI, S., LAOUINI, A., FESSI, H. & CHARCOSSET, C. 2015. Preparation of chitosan-TPP nanoparticles using microengineered membranes-Effect of parameters and encapsulation of tacrine. *Colloids and Surfaces A: Physicochemical and Engineering Aspects*, 482, 34-43.
- HAUZE, D. B., PETROVSKAIA, O., TAYLOR, B., JOULLIÉ, M. M., RAMOTOWSKI, R. & CANTU, A. 1998. 1, 2-Indanediones: new reagents for visualizing the amino acid components of latent prints. *Journal of Forensic Science*, 43, 744-747.
- HAWTHORNE, M. R. 2008. Fingerprints: analysis and understanding. (ed.) *CRC Press*.
- HE, P., DAVIS, S. S. & ILLUM, L. 1998. *In vitro* evaluation of the mucoadhesive properties of chitosan microspheres. *International Journal of Pharmaceutics*, 166, 75-88.
- HE, Y. & PARK, K. 2016. Effects of the microparticle shape on cellular uptake. *Molecular pharmaceutics*, 13, 2164-2171.
- HEDLEY, C. L. 2001. Carbohydrates in grain legume seeds: improving nutritional quality and agronomic characteristics. *Wallingford: CAB International*.
- HEINRITZ, S. N., MOSENTHIN, R. & WEISS, E. 2013. Use of pigs as a potential model for research into dietary modulation of the human gut microbiota. *Nutrition research reviews*, 26, 191-209.
- HEJAJI, E. M., SMITH, A. M. & MORRIS, G. A. 2017. Designing chitosan-tripolyphosphate microparticles with desired size for specific pharmaceutical or forensic applications. *International journal of biological macromolecules*, 95, 564-573.
- HELMUS, M. N., GIBBONS, D. F. & CEBON, D. 2008. Biocompatibility: meeting a key functional requirement of next-generation medical devices. *Toxicologic pathology*, 36, 70-80.
- HENRY, E. R. 1905. Classification and uses of finger prints. *HM Stationery Office*.
- HERSCHEL, W. J. 1916. The origin of finger-printing, *H. Milford, Oxford University Press*.
- HOANG, V., WILLIAMS, M. & SIMPSON, H. 2010. Monosaccharide composition of fundic and duodenal mucins in sheep infected with *Haemonchus contortus* or *Teladorsagia circumcincta*. *Veterinary parasitology*, 170, 253-261.

- HOSSEINI, S. F., ZANDI, M., REZAEI, M. & FARAHMANDGHAHI, F. 2013. Two-step method for encapsulation of oregano essential oil in chitosan nanoparticles: Preparation, characterization and *in vitro* release study. *Carbohydrate Polymers*, 95, 50-56.
- HOU, D., GUI, R., HU, S., HUANG, Y., FENG, Z. & PING, Q. 2015. Preparation and Characterization of Novel Drug-Inserted-Montmorillonite Chitosan Carriers for Ocular Drug Delivery. *Advances in Nanoparticles*, 4, 70-84.
- HU, B., PAN, C., SUN, Y., HOU, Z., YE, H. & ZENG, X. 2008. Optimization of fabrication parameters to produce chitosan– tripolyphosphate nanoparticles for delivery of tea catechins. *Journal of agricultural and food chemistry*, 56, 7451-7458.
- HU, X., ZHANG, Y., ZHOU, H. & WAN, H. 2015. PEGylated chitosan microspheres as mucoadhesive drug-delivery carriers for puerarin. *Journal of Applied Polymer Science*, 132, 1-9.
- HUANG, K.-S., SHEU, Y.-R. & CHAO, I.-C. 2009. Preparation and properties of nanochitosan. *Polymer-Plastics Technology and Engineering*, 48, 1239-1243.
- HUANG, M., KHOR, E. & LIM, L.-Y. 2004. Uptake and cytotoxicity of chitosan molecules and nanoparticles: effects of molecular weight and degree of deacetylation. *Pharmaceutical research*, 21, 344-353.
- HUMPHRAY, S. J., SCOTT, C. E., CLARK, R., MARRON, B., BENDER, C., CAMM, N., DAVIS, J., JENKS, A., NOON, A. & PATEL, M. 2007. A high utility integrated map of the pig genome. *Genome biology*, 8, R139.1-139.11
- HUMPHREYS, J. D., PORTER, G. & BELL, M. 2008. The quantification of fingerprint quality using a relative contrast index. *Forensic science international*, 178, 46-53.
- HUNTER, R. J. 1981. Zeta potential in colloid science: principles and applications. (ed.) London: *Academic Press*.
- HUNTER, R. J. 1993. Introduction to modern colloid science. (ed.) *Oxford University Press*.
- HURD, C. D. 1970. The acidities of ascorbic and sialic acids. *Journal of chemical education*, 47, 481-482.
- IL DUEIK, I. M. A. & MORRIS, G. A. 2013. Latent Fingerprint Enhancement Using Tripolyphosphate-Chitosan Microparticles. *International Journal of Carbohydrate Chemistry*, 2013, 1-4.
- ILLUM, L., FARRAJ, N. F. & DAVIS, S. S. 1994. Chitosan as a novel nasal delivery system for peptide drugs. *Pharmaceutical research*, 11, 1186-1189.
- IRVINE, J., AFROSE, A. & ISLAM, N. 2018. Formulation and delivery strategies of ibuprofen: challenges and opportunities. *Drug development and industrial pharmacy*, 44, 173-183.
- ISLAM, N. & FERRO, V. 2016. Recent advances in chitosan-based nanoparticulate pulmonary drug delivery. *Nanoscale*, 8, 14341-14358.
- ISLAM, N. U., AHMED, K. F., SUGUNAN, A. & DUTTA, J. 2007. Forensic fingerprint enhancement using bioadhesive chitosan and gold nanoparticles. *2nd IEEE International Conference on Nano/Micro Engineered and Molecular Systems. IEEE*, 411-415.
- JABER, N., LESNIEWSKI, A., GABIZON, H., SHENAWI, S., MANDLER, D. & ALMOG, J. 2012. Visualization of latent fingermarks by nanotechnology: Reversed development on paper—A remedy to the variation in sweat composition. *Angewandte Chemie*, 124, 12390-12393.

- JAIN, A., THAKUR, K., SHARMA, G., KUSH, P. & JAIN, U. K. 2016. Fabrication, characterization and cytotoxicity studies of ionically cross-linked docetaxel loaded chitosan nanoparticles. *Carbohydrate Polymers*, 137, 65-74.
- JAIN, A. K., CHEN, Y. & DEMIRKUS, M. 2007. Pores and ridges: High-resolution fingerprint matching using level 3 features. *IEEE transactions on pattern analysis and machine intelligence*, 29, 15-27.
- JAIN, A. K. & FENG, J. 2011. Latent fingerprint matching. *IEEE Transactions on pattern analysis and machine intelligence*, 33, 88-100.
- JAIN, A. K., PRABHAKAR, S. & PANKANTI, S. 2002. On the similarity of identical twin fingerprints. *Pattern Recognition*, 35, 2653-2663.
- JAIN, D. & BANERJEE, R. 2008. Comparison of ciprofloxacin hydrochloride-loaded protein, lipid, and chitosan nanoparticles for drug delivery. *Journal of Biomedical Materials Research Part B: Applied Biomaterials*, 86, 105-112.
- JAIN, J. L., SUNJAN, J. & NITIN, J. 2005. Fundamentals of Biochemistry. Sixth edition. India. S. Chand & Company LTD.
- JAMES, J., POUNDS, C. & WILSHIRE, B. 1991a. Obliteration of latent fingerprints. *J Forensic Sci*, 36, 1376-86.
- JAMES, J. D., POUNDS, C. A. & WILSHIRE, B. 1991b. Flake metal powders for revealing latent fingerprints. *Journal of Forensic Science*, 36, 1368-1375.
- JAMES, J. D., POUNDS, C. A. & WILSHIRE, B. 1993. Magnetic flake powders for fingerprint development. *Journal of Forensic Science*, 38, 391-401.
- JAMES, S. H. & NORDBY, J. J. 2003. Forensic Science An Introduction to Scientific and Investigative Techniques. (ed.) London, New York, Washington. CRC Press: Boca Raton
- JANES, K. & ALONSO, M. 2003. Depolymerized chitosan nanoparticles for protein delivery: preparation and characterization. *Journal of applied polymer science*, 88, 2769-2776.
- JANES, K., CALVO, P. & ALONSO, M. 2001. Polysaccharide colloidal particles as delivery systems for macromolecules. *Advanced drug delivery reviews*, 47, 83-97.
- JARDIM, K. V., JOANITTI, G. A., AZEVEDO, R. B. & PARIZE, A. L. 2015. Physico-chemical characterization and cytotoxicity evaluation of curcumin loaded in chitosan/chondroitin sulfate nanoparticles. *Materials Science and Engineering: C*, 56, 294-304.
- JARUDILOKKUL, S., TONGTHAMMACHAT, A. & BOONAMNUAYVITTAYA, V. 2011. Preparation of chitosan nanoparticles for encapsulation and release of protein. *Korean Journal of Chemical Engineering*, 28, 1247-1251.
- JASUJA, O. P., TOOFANY, M., SINGH, G. & SODHI, G. 2009. Dynamics of latent fingerprints: The effect of physical factors on quality of ninhydrin developed prints—A preliminary study. *Science & Justice*, 49, 8-11.
- JAYAKUMAR, R., PRABAHARAN, M., NAIR, S. & TAMURA, H. 2010. Novel chitin and chitosan nanofibers in biomedical applications. *Biotechnology advances*, 28, 142-150.
- JELVEHGARI, M., HASSANZADEH, D., KIAFAR, F., LOVEYM, B. D. & AMIRI, S. 2011. Preparation and determination of drug-polymer interaction and *in-vitro* release of mefenamic acid microspheres made of celluloseacetate phthalate and/or ethylcellulose polymers. *Iranian journal of pharmaceutical research: IJPR*, 10, 457-467.

- JI, J., HAO, S., LIU, W., ZHANG, J., WU, D. & XU, Y. 2011. Preparation and evaluation of O-carboxymethyl chitosan/cyclodextrin nanoparticles as hydrophobic drug delivery carriers. *Polymer bulletin*, 67, 1201-1213.
- JIA, H. & KERR, L. L. 2013. Sustained ibuprofen release using composite poly (lactic-co-glycolic acid)/titanium dioxide nanotubes from Ti implant surface. *Journal of pharmaceutical sciences*, 102, 2341-2348.
- JIN-GOU, J., JING-FEN, Z., SHI-LEI, H., DAN-JUN, W., LI, L. & YI, X. 2012. Preparation, Characterization of Hydrophobic Drug in Combine Loaded Chitosan/Cyclodextrin/Trisodium Citrate Nanoparticles and *in vitro* Release Study. *Chemical Research In Chinese Universities*, 28, 166-170.
- JIN, Y.-J., LUO, Y.-J., LI, G.-P., LI, J., WANG, Y.-F., YANG, R.-Q. & LU, W.-T. 2008. Application of photoluminescent CdS/PAMAM nanocomposites in fingerprint detection. *Forensic Science International*, 179, 34-38.
- JINGOU, J., SHILEI, H., WEIQI, L., DANJUN, W., TENGFEL, W. & YI, X. 2011. Preparation, characterization of hydrophilic and hydrophobic drug in combine loaded chitosan/cyclodextrin nanoparticles and *in vitro* release study. *Colloids and Surfaces B: Biointerfaces*, 83, 103-107.
- JONASSEN, H., KJØNIKSEN, A.-L. & HIORTH, M. 2012. Effects of ionic strength on the size and compactness of chitosan nanoparticles. *Colloid and Polymer Science*, 290, 919-929.
- JONES, B., REYNOLDS, A., RICHARDSON, M. & SEARS, V. 2010a. Nano-scale composition of commercial white powders for development of latent fingerprints on adhesives. *Science and Justice*, 50, 150-155.
- JONES, B. J., DOWNHAM, R. & SEARS, V. 2010b. Effect of substrate surface topography on forensic development of latent fingerprints with iron oxide powder suspension. *Surface and Interface Analysis*, 42, 438-442.
- JONES, B. J., DOWNHAM, R. & SEARS, V. G. 2012. Nanoscale Analysis of the Interaction Between Cyanoacrylate and Vacuum Metal Deposition in the Development of Latent Fingermarks on Low-Density Polyethylene. *Journal of forensic sciences*, 57, 196-200.
- JUNQUEIRA, L. C. & CARNEIRO, J. 2003. Basic histology: text & atlas. Tenth edition. London, New York: *Lange Medical Books/McGraw Hill*.
- KABKLANG, P., RIENGROJPITAK, S. & SUWANSAMRITH, W. 2009. Latent fingerprint detection by various formulae of SPR on wet non-porous surfaces. *J Sci Res Chula Univ*, 34, 59-64.
- KAFSHGARI, M. H., KHORRAM, M., KHODADOOST, M. & KHAVARI, S. 2011. Reinforcement of chitosan nanoparticles obtained by an ionic cross-linking process. *Iran Polym J*, 20, 445-456.
- KAMARI, Y. & GHIACI, M. 2016. Preparation and characterization of ibuprofen/modified chitosan/TiO₂ hybrid composite as a controlled drug-delivery system. *Microporous and Mesoporous Materials*, 234, 361-369.
- KANG, B.-S., LEE, S.-E., NG, C. L., KIM, J.-K. & PARK, J.-S. 2015. Exploring the Preparation of Albendazole-Loaded Chitosan-Tripolyphosphate Nanoparticles. *Materials*, 8, 486-498.
- KAPOOR, S., SODHI, G. S. & KUMAR, S. 2015. Visualization of latent fingermarks using Rhodamine B: a new method. *Int J Forensic Sci Pathol*, 3, 199-201.
- KARARLI, T. T. 1995. Comparison of the gastrointestinal anatomy, physiology, and biochemistry of humans and commonly used laboratory animals. *Biopharmaceutics & drug disposition*, 16, 351-380.

- KARLINSZKY, L. & HARKAI, G. 1990. Detection of Latent Fingerprints: Application of Cyanoacrylate for the inside of Cars. *Forensic Science International*, 46, 29-30.
- KAS, H. S. 1997. Chitosan: properties, preparations and application to microparticulate systems. *Journal of Microencapsulation*, 14, 689-711.
- KASAAI, M. R., ARUL, J. & CHARLET, G. 2000. Intrinsic viscosity–molecular weight relationship for chitosan. *Journal of Polymer Science Part B: Polymer Physics*, 38, 2591-2598.
- KATAKAM, P., PHALGUNA, Y. & HARINARAYANA, D. 2015. Formulation, characterization and *in vitro* evaluation of Capecitabine loaded Polycaprolactone-chitosan Nanospheres. *Bangladesh Pharmaceutical Journal*, 17, 18-24.
- KATAS, H. & ALPAR, H. O. 2006. Development and characterisation of chitosan nanoparticles for siRNA delivery. *Journal of controlled release*, 115, 216-225.
- KAWADKAR, J. & CHAUHAN, M. K. 2012. Intra-articular delivery of genipin cross-linked chitosan microspheres of flurbiprofen: preparation, characterization, *in vitro* and *in vivo* studies. *European journal of Pharmaceutics and Biopharmaceutics*, 81, 563-572.
- KAWASHIMA, Y., HANDA, T., KASAI, A., TAKENAKA, H., LIN, S. & ANDO, Y. 1985a. Novel method for the preparation of controlled-release theophylline granules coated with a polyelectrolyte complex of sodium polyphosphate–chitosan. *Journal of pharmaceutical sciences*, 74, 264-268.
- KAWASHIMA, Y., HANDA, T., KASAI, A., TAKENAKA, H. & LIN, S. Y. 1985b. The effects of thickness and hardness of the coating film on the drug release rate of theophylline granules coated with chitosan-sodium tripolyphosphate complex. *Chemical and pharmaceutical bulletin*, 33, 2469-2474.
- KEAN, T. & THANOU, M. 2010. Biodegradation, biodistribution and toxicity of chitosan. *Advanced drug delivery reviews*, 62, 3-11.
- KENDALL, F. & REHN, B. 1983. Rapid method of super glue® fuming application for the development of latent fingerprints. *Journal of Forensic Science*, 28, 777-780.
- KENT, T., THOMAS, G., REYNOLDSON, T. & EAST, H. 1976. A vacuum coating technique for the development of latent fingerprints on polythene. *Science and Justice*, 16, 93-101.
- KHAN, I. A., ANJUM, K., ALI, M. S. & DIN, K.-U. 2011. A comparative study of interaction of ibuprofen with biocompatible polymers. *Colloids and surfaces B: biointerfaces*, 88, 72-77.
- KIM, K., KIM, K., RYU, J. H. & LEE, H. 2015. Chitosan-catechol: A polymer with long-lasting mucoadhesive properties. *Biomaterials*, 52, 161-170.
- KIM, K. M., SON, J. H., KIM, S. K., WELLER, C. L. & HANNA, M. A. 2006. Properties of chitosan films as a function of pH and solvent type. *Journal of food science*, 71, E119-E124.
- KLEINE-BRUEGGENEY, H., ZORZI, G., FECKER, T., EL GUEDDARI, N., MOERSCHBACHER, B. & GOYCOOLEA, F. 2015. A rational approach towards the design of chitosan-based nanoparticles obtained by ionotropic gelation. *Colloids and Surfaces B: Biointerfaces*, 135, 99-108.
- KNOWLES, A. 1978. Aspects of physicochemical methods for the detection of latent fingerprints. *Journal of Physics E: Scientific Instruments*, 11, 713-721.

- KO, J., PARK, H., HWANG, S., PARK, J. & LEE, J. 2002. Preparation and characterization of chitosan microparticles intended for controlled drug delivery. *International journal of pharmaceuticals*, 249, 165-174.
- KOLIANDRIS, A., LEE, A., FERRY, A.-L., HILL, S. & MITCHELL, J. 2008. Relationship between structure of hydrocolloid gels and solutions and flavour release. *Food Hydrocolloids*, 22, 623-630.
- KOMALAM, A., MURALEEGHARAN, L. G., SUBBURAJ, S., SUSEELA, S., BABU, A. & GEORGE, S. 2012. Designed plasmonic nanocatalysts for the reduction of eosin Y: absorption and fluorescence study. *International Nano Letters*, 2, 1-9.
- KOMARINSKI, P. 2005. Automated fingerprint identification systems (AFIS). (ed.) USA, UK. *Academic Press: Elsevier*
- KONG, A., ZHANG, D. & LU, G. 2005. A Study of identical twins' palmprints for personal authentication. *Advances in Biometrics: Springer*.
- KONG, A. W.-K., ZHANG, D. & LU, G. 2006. A study of identical twins' palmprints for personal verification. *Pattern Recognition*, 39, 2149-2156.
- KOO, H., HUH, M. S., SUN, I.-C., YUK, S. H., CHOI, K., KIM, K. & KWON, I. C. 2011. In vivo targeted delivery of nanoparticles for theranosis. *Accounts of chemical research*, 44, 1018-1028.
- KOTADIYA, R., PATEL, V., PATEL, H. & KORADIYA, H. 2009. Effect of cross-linking on physicochemical properties of chitosan mucoadhesive microspheres: A factorial approach. *International Journal of Green Pharmacy (IJGP)*, 3, 85-62.
- KOTZE, A., LUESSEN, H., DE BOER, A., VERHOEF, J. & JUNGINGER, H. 1999. Chitosan for enhanced intestinal permeability: prospects for derivatives soluble in neutral and basic environments. *European journal of pharmaceutical sciences*, 7, 145-151.
- KRASNICI, S., WERNER, A., EICHHORN, M. E., SCHMITT-SODY, M., PAHERNIK, S. A., SAUER, B., SCHULZE, B., TEIFEL, M., MICHAELIS, U. & NAUJOKS, K. 2003. Effect of the surface charge of liposomes on their uptake by angiogenic tumor vessels. *International journal of cancer*, 105, 561-567.
- KROGSTAD, E. A., RATHBONE, M. J. & WOODROW, K. A. 2014. Vaginal drug delivery. Focal Controlled Drug Delivery. (ed.) *Domb A., Khan W. Boston: Springer*
- KULKARNI, P. V., KESHAVAYYA, J. & KULKARNI, V. H. 2007. Effect of method of preparation and process variables on controlled release of insoluble drug from chitosan microspheres. *Polymers for Advanced Technologies*, 18, 814-821.
- KUMAR, M. R., MUZZARELLI, R. A., MUZZARELLI, C., SASHIWA, H. & DOMB, A. 2004. Chitosan chemistry and pharmaceutical perspectives. *Chemical reviews*, 104, 6017-6084.
- KUMAR, R. & KAR, A. 2014. 'Microencapsulation of Nutraceuticals Using Spray Freeze Drying Method: A Brief Review. *Indo Global Journal of Pharmaceutical Sciences*, 4, 47-51.
- KUNJACHAN, S. & JOSE, S. 2010. Understanding the mechanism of ionic gelation for synthesis of chitosan nanoparticles using qualitative techniques. *Asian journal of pharmaceuticals*, 4, 148-153.
- KURITA, K. 1998. Chemistry and application of chitin and chitosan. *Polymer Degradation and stability*, 59, 117-120.

- KWANG-HEE, K. P. 1983. Acid-base equilibria and related properties of chitosan. *Bulletin of the Korean Chemical Society*, 4, 68-72.
- LABIB, S., ERB, A., KRAUS, M., WICKERT, T. & RICHLING, E. 2004. The pig caecum model: a suitable tool to study the intestinal metabolism of flavonoids. *Molecular nutrition & food research*, 48, 326-332.
- LAD, M., TODD, T., MORRIS, G., MACNAUGHTAN, W., SWORN, G. & FOSTER, T. 2013. On the origin of sharp peaks in the X-ray diffraction patterns of xanthan powders. *Food chemistry*, 139, 1146-1151.
- LAI, S. K., WANG, Y.-Y., WIRTZ, D. & HANES, J. 2009. Micro-and macrorheology of mucus. *Advanced drug delivery reviews*, 61, 86-100.
- LAYNE, E. 1957. [73] Spectrophotometric and turbidimetric methods for measuring proteins. *Methods in enzymology*, 3, 447-454.
- LEE, J. W., PARK, J. H. & ROBINSON, J. R. 2000. Bioadhesive-based dosage forms: The next generation. *Journal of Pharmaceutical Sciences*, 89, 850-866.
- LEE, K. Y., HA, W. S. & PARK, W. H. 1995. Blood compatibility and biodegradability of partially N-acylated chitosan derivatives. *Biomaterials*, 16, 1211-1216.
- LEHR, C.-M., BOUWSTRA, J. A., SCHACHT, E. H. & JUNGINGER, H. E. 1992. *In vitro* evaluation of mucoadhesive properties of chitosan and some other natural polymers. *International journal of Pharmaceutics*, 78, 43-48.
- LENG, Y. 2009. Materials characterization: introduction to microscopic and spectroscopic methods. (ed.) Hong Kong: *John Wiley & Sons*.
- LEVIS, K. A., LANE, M. E. & CORRIGAN, O. I. 2003. Effect of buffer media composition on the solubility and effective permeability coefficient of ibuprofen. *International journal of pharmaceutics*, 253, 49-59.
- LEWIS, L. A., SMITHWICK, R., DEVAULT, G. L., BOLINGER, B. & LEWIS, S. 2001. Processes involved in the development of latent fingerprints using the cyanoacrylate fuming method. *Journal of Forensic Science*, 46, 241-246.
- LEWIS, M. J. 1990. Physical properties of foods and food processing systems. (ed.) Cambridge England. *Woodhead limited: Elsevier*.
- LI, J. & HUANG, Q. 2012. Rheological properties of chitosan–tripolyphosphate complexes: From suspensions to microgels. *Carbohydrate Polymers*, 87, 1670-1677.
- LIANG, Y., CUI, Z., ZHU, S. & YANG, X. 2011. Characterization of self-organized TiO₂ nanotubes on Ti–4Zr–22Nb–2Sn alloys and the application in drug delivery system. *Journal of Materials Science: Materials in Medicine*, 22, 461-467.
- LIESE, A. & HILTERHAUS, L. 2013. Evaluation of immobilized enzymes for industrial applications. *Chemical Society Reviews*, 42, 6236-6249.
- LIGHT, D. B. & COOLEY, D. A. 2004. Cells, Tissues, and Skin. (ed.) USA: *Chelsea House*.
- LIN, W.-C., YU, D.-G. & YANG, M.-C. 2005. pH-sensitive polyelectrolyte complex gel microspheres composed of chitosan/sodium tripolyphosphate/dextran sulfate: swelling kinetics and drug delivery properties. *Colloids and surfaces B: Biointerfaces*, 44, 143-151.
- LINDEN, S., SUTTON, P., KARLSSON, N., KOROLIK, V. & MCGUCKIN, M. 2008. Mucins in the mucosal barrier to infection. *Mucosal immunology*, 1, 183-197.
- LIU, H. & GAO, C. 2009. Preparation and properties of ionically cross-linked chitosan nanoparticles. *Polymers for Advanced Technologies*, 20, 613-619.

- LIU, H., ZHAO, Y., CHENG, S., HUANG, N. & LENG, Y. 2012. Syntheses of novel chitosan derivative with excellent solubility, anticoagulation, and antibacterial property by chemical modification. *Journal of applied polymer science*, 124, 2641-2648.
- LIU, J., SHI, Z., YU, Y., YANG, R. & ZUO, S. 2010. Water-soluble multicolored fluorescent CdTe quantum dots: Synthesis and application for fingerprint developing. *Journal of colloid and interface science*, 342, 278-282.
- LIU, L.-S., LIU, S.-Q., NG, S. Y., FROIX, M., OHNO, T. & HELLER, J. 1997. Controlled release of interleukin-2 for tumour immunotherapy using alginate/chitosan porous microspheres. *Journal of Controlled Release*, 43, 65-74.
- LIU, L., GILL, S. K., GAO, Y., HOPE-WEEKS, L. J. & CHENG, K. H. 2008a. Exploration of the use of novel SiO₂ nanocomposites doped with fluorescent Eu³⁺/sensitizer complex for latent fingerprint detection. *Forensic science international*, 176, 163-172.
- LIU, Y., YAN, K., JIANG, G., XIONG, Y., DU, Y. & SHI, X. 2014. Electrical Signal Guided Ibuprofen Release from Electrodeposited Chitosan Hydrogel. *International Journal of Polymer Science*, 2014, 1-8.
- LIU, Z., JIAO, Y., WANG, Y., ZHOU, C. & ZHANG, Z. 2008b. Polysaccharides-based nanoparticles as drug delivery systems. *Advanced drug delivery reviews*, 60, 1650-1662.
- LÓPEZ-LEÓN, T., CARVALHO, E., SEIJO, B., ORTEGA-VINUESA, J. & BASTOS-GONZÁLEZ, D. 2005. Physicochemical characterization of chitosan nanoparticles: electrokinetic and stability behavior. *Journal of Colloid and Interface Science*, 283, 344-351.
- LU, Z., STEENEKAMP, J. H. & HAMMAN, J. H. 2005. Cross-linked cationic polymer microparticles: effect of N-trimethyl chitosan chloride on the release and permeation of ibuprofen. *Drug development and industrial pharmacy*, 31, 311-317.
- LUEBEN, H., RENTEL, C.-O., KOTZÉ, A., LEHR, C.-M., DE BOER, A., VERHOEF, J. & JUNGINGER, H. 1997. Mucoadhesive polymers in peroral peptide drug delivery. IV. Polycarbophil and chitosan are potent enhancers of peptide transport across intestinal mucosae *in vitro*. *Journal of controlled release*, 45, 15-23.
- LUO, Y. & WANG, Q. 2014. Recent development of chitosan-based polyelectrolyte complexes with natural polysaccharides for drug delivery. *International journal of biological macromolecules*, 64, 353-367.
- MA, R., BULLOCK, E., MAYNARD, P., REEDY, B., SHIMMON, R., LENNARD, C., ROUX, C. & MCDONAGH, A. 2011. Fingerprint detection on non-porous and semi-porous surfaces using NaYF₄: Er, Yb up-converter particles. *Forensic science international*, 207, 145-149.
- MACKIE, A. R., GOYCOOLEA, F. M., MENCHICCHI, B., CARAMELLA, C. M., SAPORITO, F., LEE, S., STEPHANSEN, K., CHRONAKIS, I. S., HIORTH, M. & ADAMCZAK, M. 2017. Innovative methods and applications in mucoadhesion research. *Macromolecular bioscience*, 17, 1-32.
- MADSEN, F., EBERTH, K. & SMART, J. D. 1998. A rheological assessment of the nature of interactions between mucoadhesive polymers and a homogenised mucus gel. *Biomaterials*, 19, 1083-1092.
- MALTONI, D., MAIO, D., JAIN, A. K. & PRABHAKAR, S. 2009. Handbook of fingerprint recognition. Second edition. USA: Springer.

- MANDLIK, S. K. & RANPISE, N. S. 2017. Implementation of experimental design methodology in preparation and characterization of zolmitriptan loaded chitosan nanoparticles. *International Current Pharmaceutical Journal*, 6, 16-22.
- MANTLE, M. & ALLEN, A. 1978. A colorimetric assay for glycoproteins based on the periodic acid/Schiff stain. *Biochemical Society Transactions*, 6, 607-609.
- MARTINS, A. F., DE OLIVEIRA, D. M., PEREIRA, A. G., RUBIRA, A. F. & MUNIZ, E. C. 2012. Chitosan/TPP microparticles obtained by microemulsion method applied in controlled release of heparin. *International journal of biological macromolecules*, 51, 1127-1133.
- MASARUDIN, M. J., CUTTS, S. M., EVISON, B. J., PHILLIPS, D. R. & PIGRAM, P. J. 2015. Factors determining the stability, size distribution, and cellular accumulation of small, monodisperse chitosan nanoparticles as candidate vectors for anticancer drug delivery: application to the passive encapsulation of [14C]-doxorubicin. *Nanotechnology, science and applications*, 8, 67-80.
- MATET, M., HEUZEY, M.-C., POLLET, E., AJJI, A. & AVÉROUS, L. 2013. Innovative thermoplastic chitosan obtained by thermo-mechanical mixing with polyol plasticizers. *Carbohydrate polymers*, 95, 241-251.
- MATHUR, N. K. & NARANG, C. K. 1990. Chitin and chitosan, versatile polysaccharides from marine animals. *Journal Of Chemical Education*, 67, 938-942.
- MATLACK, A. 2010. Introduction to green chemistry. Second edition. London, New York. *CRC Press: Boca Raton*.
- MATSUNO, K. & SUZUKI, S. 2008. Simple fluorimetric method for quantification of sialic acids in glycoproteins. *Analytical biochemistry*, 375, 53-59.
- MCCLEAN, S., PROSSER, E., MEEHAN, E., O'MALLEY, D., CLARKE, N., RAMTOOLA, Z. & BRAYDEN, D. 1998. Binding and uptake of biodegradable poly-DL-lactide micro-and nanoparticles in intestinal epithelia. *European Journal of Pharmaceutical Sciences*, 6, 153-163.
- MENCHICCHI, B., FUENZALIDA, J. P., BOBBILI, K. B., HENSEL, A., SWAMY, M. J. & GOYCOOLEA, F. M. 2014. Structure of chitosan determines its interactions with mucin. *Biomacromolecules*, 15, 3550-3558.
- MENG-LUND, E., MUFF-WESTERGAARD, C., SANDER, C., MADELUNG, P. & JACOBSEN, J. 2014. A mechanistic based approach for enhancing buccal mucoadhesion of chitosan. *International journal of pharmaceutics*, 461, 280-285.
- MENZEL, E. 1979. Laser detection of latent fingerprints—treatment with phosphorescers. *Journal of Forensic Science*, 24, 582-585.
- MENZEL, E. & DUFF, J. 1979. Laser detection of latent fingerprints—treatment with fluorescers. *Journal of Forensic Science*, 24, 96-100.
- MENZEL, E. & FOX, K. 1980. Laser detection of latent fingerprints: preparation of fluorescent dusting powders and the feasibility of a portable system. *journal of forensic science*, 25, 150-153.
- MENZEL, E., TAKATSU, M., MURDOCK, R., BOULDIN, K. & CHENG, K. 2000. Photoluminescent CdS/dendrimer nanocomposites for fingerprint detection. *Journal of Forensic Science*, 45, 770-773.
- MENZEL, E. R., BURT, J. A., SINOR, T. W., TUBACH-LEY, W. & JORDAN, K. 1983. Laser detection of latent fingerprints: treatment with glue containing cyanoacrylate ester. *Journal of Forensic Science*, 28, 307-317.

- MESHALI, M. & GABR, K. 1993. Effect of interpolymer complex formation of chitosan with pectin or acacia on the release behaviour of chlorpromazine HCl. *International Journal of Pharmaceutics*, 89, 177-181.
- MEYERS, S. N., ROGATCHEVA, M. B., LARKIN, D. M., YERLE, M., MILAN, D., HAWKEN, R. J., SCHOOK, L. B. & BEEVER, J. E. 2005. Piggy-BACing the human genome: II. A high-resolution, physically anchored, comparative map of the porcine autosomes. *Genomics*, 86, 739-752.
- MEZGER, T. G. 2006. The rheology handbook: for users of rotational and oscillatory rheometers. Second edition. Germany: *Vincentz Network GmbH & Co KG*.
- MI, F.-L., SHYU, S.-S., CHEN, C.-T. & SCHOUNG, J.-Y. 1999. Porous chitosan microsphere for controlling the antigen release of Newcastle disease vaccine: preparation of antigen-adsorbed microsphere and *in vitro* release. *Biomaterials*, 20, 1603-1612.
- MI, F. L., SUNG, H. W. & SHYU, S. S. 2001. Release of indomethacin from a novel chitosan microsphere prepared by a naturally occurring crosslinker: examination of crosslinking and polycation–anionic drug interaction. *Journal of Applied Polymer Science*, 81, 1700-1711.
- MILADI, K., SFAR, S., FESSI, H. & ELAISSARI, A. 2015. Enhancement of alendronate encapsulation in chitosan nanoparticles. *Journal of Drug Delivery Science and Technology*, 30, 391-396.
- MIRI, T. 2011. Viscosity and oscillatory rheology. *Practical food rheology: An interpretive approach*.(ed.) Oxford: *Wiley-Blackwell*, 7-28.
- MITRA, S., GAUR, U., GHOSH, P. & MAITRA, A. 2001. Tumour targeted delivery of encapsulated dextran–doxorubicin conjugate using chitosan nanoparticles as carrier. *Journal of Controlled Release*, 74, 317-323.
- MOHAMED, A. A. 2011. Gold is going forensic. *Gold Bulletin*, 44, 71-77.
- MOHAMMADPOUR DOUNIGHI, N., ESKANDARI, R., AVADI, M., ZOLFAGHARIAN, H., MIR MOHAMMAD SADEGHI, A. & REZAYAT, M. 2012. Preparation and *in vitro* characterization of chitosan nanoparticles containing Mesobuthus eupeus scorpion venom as an antigen delivery system. *Journal of Venomous Animals and Toxins Including Tropical Diseases*, 18, 44-52.
- MOHAMMADPOURDOUNIGHI, N., BEHFAR, A., EZABADI, A., ZOLFAGHARIAN, H. & HEYDARI, M. 2010. Preparation of chitosan nanoparticles containing Naja naja oxiana snake venom. *Nanomedicine: Nanotechnology, Biology and Medicine*, 6, 137-143.
- MOHARRAM, M., REICHA, F., KINAWY, N. & EL HOTABY, W. 2012. Factors Controlling The Adsorption Capacity Of Crosslinked Chitosan Beads And Natural Montmorillonite Powder: Comparative Study. *Journal of Applied Sciences Research*, 8, 5425-5435.
- MONSKY, W. L., FUKUMURA, D., GOHONGI, T., ANCIKIEWCZ, M., WEICH, H. A., TORCHILIN, V. P., YUAN, F. & JAIN, R. K. 1999. Augmentation of transvascular transport of macromolecules and nanoparticles in tumors using vascular endothelial growth factor. *Cancer Research*, 59, 4129-4135.
- MONTALTO, N. A., OJEDA, J. J. & JONES, B. J. 2013. Determining the order of deposition of natural latent fingerprints and laser printed ink using chemical mapping with secondary ion mass spectrometry. *Science & Justice*, 53, 2-7.
- MONTGOMERY, D. C. 2017. Design and analysis of experiments. Ninth edition. USA: *John wiley & sons, Inc*.

- MORELLY, S., TANG, M. & ALVAREZ, N. 2017. The Impotence of Non-Brownian Particles on the Gel Transition of Colloidal Suspensions. *Polymers*, 9, 1-13.
- MORENO-BAUTISTA, G. & TAM, K. C. 2011. Evaluation of dialysis membrane process for quantifying the *in vitro* drug-release from colloidal drug carriers. *Colloids and Surfaces A: Physicochemical and Engineering Aspects*, 389, 299-303.
- MORET, S., SPINDLER, X., LENNARD, C. & ROUX, C. 2015. Microscopic examination of fingermark residues: Opportunities for fundamental studies. *Forensic science international*, 255, 28-37.
- MORRIS, G. A., CASTILE, J., SMITH, A., ADAMS, G. G. & HARDING, S. E. 2009. Macromolecular conformation of chitosan in dilute solution: A new global hydrodynamic approach. *Carbohydrate Polymers*, 76, 616-621.
- MORRIS, G. A., CASTILE, J., SMITH, A., ADAMS, G. G. & HARDING, S. E. 2011. The effect of prolonged storage at different temperatures on the particle size distribution of tripolyphosphate (TPP)-chitosan nanoparticles. *Carbohydrate Polymers*, 84, 1430-1434.
- MORRIS, G. A., KÖK, S. M., HARDING, S. E. & ADAMS, G. G. 2010. Polysaccharide drug delivery systems based on pectin and chitosan. *Biotechnology and Genetic Engineering Reviews*, 27, 257-284.
- MOSHARRAF, M. & NYSTRÖM, C. 1995. The effect of particle size and shape on the surface specific dissolution rate of micro-sized practically insoluble drugs. *International Journal of Pharmaceutics*, 122, 35-47.
- MOTWANI, S. K., CHOPRA, S., TALEGAONKAR, S., KOHLI, K., AHMAD, F. J. & KHAR, R. K. 2008. Chitosan-sodium alginate nanoparticles as submicroscopic reservoirs for ocular delivery: Formulation, optimisation and *in vitro* characterisation. *European Journal of Pharmaceutics and Biopharmaceutics*, 68, 513-525.
- MÜLLER, R., JACOBS, C. & KAYSER, O. 2001. Nanosuspensions as particulate drug formulations in therapy: rationale for development and what we can expect for the future. *Advanced drug delivery reviews*, 47, 3-19.
- MURPHY, W. J., LARKIN, D. M., EVERTS-VAN DER WIND, A., BOURQUE, G., TESLER, G., AUVIL, L., BEEVER, J. E., CHOWDHARY, B. P., GALIBERT, F. & GATZKE, L. 2005. Dynamics of mammalian chromosome evolution inferred from multispecies comparative maps. *Science*, 309, 613-617.
- MUZZARELLI, R. A. 1996. Chitosan-based dietary foods. *Carbohydrate Polymers*, 29, 309-316.
- NAJAFABADI, A. H., ABDOUSS, M. & FAGHIHI, S. 2014. Synthesis and evaluation of PEG-O-chitosan nanoparticles for delivery of poor water soluble drugs: Ibuprofen. *Materials Science and Engineering: C*, 41, 91-99.
- NANDA, R. K., PATIL, S. S. & NAVATHAR, D. A. 2012. Chitosan nanoparticles loaded with thiocolchicoside. *Der Pharma Chemica*, 4, 1619-25.
- NASTI, A., ZAKI, N. M., DE LEONARDIS, P., UNGPHAIBOON, S., SANSONGSAK, P., RIMOLI, M. G. & TIRELLI, N. 2009. Chitosan/TPP and chitosan/TPP-hyaluronic acid nanoparticles: systematic optimisation of the preparative process and preliminary biological evaluation. *Pharmaceutical research*, 26, 1918-1930.
- NICOLAIDES, N. 1974. Skin lipids: their biochemical uniqueness. *Science*, 186, 19-26.

- NIV, Y. & BOLTIN, D. 2012. Secreted and membrane-bound mucins and idiopathic peptic ulcer disease. *Digestion*, 86, 258-263.
- NO, H. K. & MEYERS, S. P. 1989. Crawfish chitosan as a coagulant in recovery of organic compounds from seafood processing streams. *Journal of Agricultural and Food Chemistry*, 37, 580-583.
- NOKHODCHI, A., AMIRE, O. & JELVEHGARI, M. 2010. Physico-mechanical and dissolution behaviours of ibuprofen crystals crystallized in the presence of various additives. *Daru: journal of Faculty of Pharmacy, Tehran University of Medical Sciences*, 18, 74-83.
- NOKHODCHI, A., HOMAYOUNI, A., ARAYA, R., KAIALY, W., OBEIDAT, W. & ASARE-ADDO, K. 2015. Crystal engineering of ibuprofen using starch derivatives in crystallization medium to produce promising ibuprofen with improved pharmaceutical performance. *RSC Advances*, 5, 46119-46131.
- NYSTRÖM, B., KJØNIKSEN, A.-L. & IVERSEN, C. 1999. Characterization of association phenomena in aqueous systems of chitosan of different hydrophobicity¹. *Advances in Colloid and Interface Science*, 79, 81-103.
- O'NEILL, M. E. 1937. The Development of Latent Fingerprints on Paper. *Journal of Criminal Law and Criminology (1931-1951)*, 28, 432-441.
- ODÉN, S. & VON HOFSTEN, B. 1954. Detection of fingerprints by the ninhydrin reaction. *Nature*, 173, 449-450.
- ODUOR-ODETO, P., STRUSZEZYK, M. & PETER, M. G. 2005. Characterisation of Chitosan from Blowfly Larvae and Some Crustacean Species from Kenyan Marine Waters Prepared Under Different Conditions. *Western Indian Ocean Journal of Marine Science*, 4, 99-108.
- OH, S., SHIN, W. S. & KIM, H. T. 2016. Effects of pH, dissolved organic matter, and salinity on ibuprofen sorption on sediment. *Environmental Science and Pollution Research*, 23, 22882-22889.
- PANKANTI, S., PRABHAKAR, S. & JAIN, A. K. 2002. On the individuality of fingerprints. *IEEE Transactions on pattern analysis and machine intelligence*, 24, 1010-1025.
- PANYAM, J., SAHOO, S. K., PRABHA, S., BARGAR, T. & LABHASETWAR, V. 2003. Fluorescence and electron microscopy probes for cellular and tissue uptake of poly (D, L-lactide-co-glycolide) nanoparticles. *International journal of pharmaceutics*, 262, 1-11.
- PAPADIMITRIOU, S., BIKIARIS, D., AVGOUSTAKIS, K., KARAVAS, E. & GEORGARAKIS, M. 2008. Chitosan nanoparticles loaded with dorzolamide and pramipexole. *Carbohydrate Polymers*, 73, 44-54.
- PARIDA, U. K., ROUT, N. & BINDHANI, B. K. 2013. *In vitro* properties of chitosan nanoparticles induce apoptosis in human lymphoma SUDHL-4 cell line. *Advances in Bioscience and Biotechnology*, 2013, 1118-1127.
- PARK, S. W., LEE, D., CHOI, Y. S., JEON, H. B., LEE, C.-H., MOON, J.-H. & KWON, I. K. 2014. Mesoporous TiO₂ implants for loading high dosage of antibacterial agent. *Applied Surface Science*, 303, 140-146.
- PARTAL, P. & FRANCO, J. M. 2010. Non-Newtonian fluids. *Rheology: encyclopaedia of life support systems (EOLSS)*, UNESCO. *Eolss, Oxford*, 96-119.
- PARVEEN, S. M. S., MISRA, R. M. S. & SAHOO, S. K. P. 2012. Nanoparticles: a boon to drug delivery, therapeutics, diagnostics and imaging. *Nanomedicine: Nanotechnology, Biology, and Medicine*, 8, 147-166.

- PATEL JAYVADAN, K., PATEL NIRAV, V. & SHAH SHREERAJ, H. 2009. Formulation and *in-vitro* evaluation of mesalamine matrix tablets using chitosan for colonic drug delivery. *Journal of Pharmacy Research Vol, 2*, 1319-1323.
- PATEL, K. S. & PATEL, M. B. 2014. Preparation and evaluation of chitosan microspheres containing nicorandil. *International journal of pharmaceutical investigation*, 4, 32-37.
- PATI, F., ADHIKARI, B. & DHARA, S. 2011. Development of chitosan–tripolyphosphate fibers through pH dependent ionotropic gelation. *Carbohydrate research*, 346, 2582-2588.
- PATIL, J., KAMALAPUR, M., MARAPUR, S. & KADAM, D. 2010. Ionotropic gelation and polyelectrolyte complexation: the novel techniques to design hydrogel particulate sustained, modulated drug delivery system: a review. *Digest Journal of Nanomaterials and Biostructures*, 5, 241-248.
- PATTERSON, J. K., LEI, X. G. & MILLER, D. D. 2008. The pig as an experimental model for elucidating the mechanisms governing dietary influence on mineral absorption. *Experimental Biology and Medicine*, 233, 651-664.
- PAVIA, D. L., LAMPMAN, G. M., KRIZ, G. S. & VYVYAN, J. A. 2008. Introduction to spectroscopy. Fourth edition. USA: *Cengage Learning*.
- PERINELLI, D. R., CAMPANA, R., SKOURAS, A., BONACUCINA, G., CESPI, M., MASTROTTO, F., BAFFONE, W. & CASETTARI, L. 2018. Chitosan Loaded into a Hydrogel Delivery System as a Strategy to Treat Vaginal Co-Infection. *Pharmaceutics*, 10, 1-15.
- PEZZINI, B. R., ISSA, M. G., DUQUE, M. D. & FERRAZ, H. G. 2015. Applications of USP apparatus 3 in assessing the *in vitro* release of solid oral dosage forms. *Brazilian Journal of Pharmaceutical Sciences*, 51, 265-272.
- PHILLIPS, C. E., COLE, D. O. & JONES, G. W. 1990. Physical developer: a practical and productive latent print developer. *Journal of Forensic Identification*, 40, 135-147.
- PICOUT, D. R. & ROSS-MURPHY, S. B. 2003. Rheology of biopolymer solutions and gels. *The Scientific World Journal*, 3, 105-121.
- PIEROG, M., GIERSZEWSKA-DRUŻYŃSKA, M. & OSTROWSKA-CZUBENKO, J. 2009. Effect of ionic crosslinking agents on swelling behavior of chitosan hydrogel membranes. *Progress on Chemistry and Application of Chitin and Its Derivatives*, 14, 75-82.
- PIGMAN, W. W. & GOEPP, R. M. 1945. Chemistry of the Carbohydrates. (ed.) New York. *Academic puess inc: Elsevier*.
- PIGMENTS, H. 2008. The Way Forward For Titanium Dioxide. *Plastics, Additives and Compounding*, 10, 36-37.
- PILLAI, C., PAUL, W. & SHARMA, C. P. 2009. Chitin and chitosan polymers: Chemistry, solubility and fiber formation. *Progress in polymer science*, 34, 641-678.
- PILLAY, V. & FASSIHI, R. 1998. Evaluation and comparison of dissolution data derived from different modified release dosage forms: an alternative method. *Journal of Controlled Release*, 55, 45-55.
- POLAKOWSKI, C., SOCHAN, A., BIEGANOWSKI, A., RYZAK, M., FÖLDÉNYI, R. & TÓTH, J. 2014. Influence of the sand particle shape on particle size distribution measured by laser diffraction method. *International Agrophysics*, 28, 195-200.

- POLLI, J. E., LAWRENCE, X. Y., COOK, J. A., AMIDON, G. L., BORCHARDT, R. T., BURNSIDE, B. A., BURTON, P. S., CHEN, M. L., CONNER, D. P. & FAUSTINO, P. J. 2004. Summary workshop report: biopharmaceutics classification system—implementation challenges and extension opportunities. *Journal of pharmaceutical sciences*, 93, 1375-1381.
- POLSON, C. J. 1950. Finger prints and finger printing: an historical study. *J. Crim. L. & Criminology*, 41, 495 - 517.
- PONNURAJ, R., JANAKIRAMAN, K., GOPALAKRISHNAN, S., SENTHILNATHAN, K., MEGANATHAN, V. & SARAVANAN, P. 2015. Formulation And Characterization of Epigallocatechin Gallate Nanoparticles. *Indo American Journal of Pharm Research*, 5, 387-399.
- POPA, D. E., LUPULIASA, D., STANESCU, A.-A., BARCA, M., DRAGOMIROIU, G. T. A. B., MIRON, D. S. & RADULESCU, F. S. 2014. Simulation of the in vivo exposure to ibuprofen based on *in vitro* dissolution profiles from solid dosage forms. *FARMACIA*, 62, 475-485.
- POPAT, A., LIU, J., LU, G. Q. M. & QIAO, S. Z. 2012. A pH-responsive drug delivery system based on chitosan coated mesoporous silica nanoparticles. *Journal of Materials Chemistry*, 22, 11173-11178.
- POUNDS, A., GRIGG, R. & MONGKOLAUSSAVARATANA, T. 1990. The use of 1, 8-diazafluoren-9-one (DFO) for the fluorescent detection of latent fingerprints on paper. A preliminary evaluation. *Journal of Forensic Science*, 35, 169-175.
- PULSIFER, D. P., MUHLBERGER, S. A., WILLIAMS, S. F., SHALER, R. C. & LAKHTAKIA, A. 2013. An objective fingerprint quality-grading system. *Forensic science international*, 231, 204-207.
- PUVVADA, Y. S., VANKAYALAPATI, S. & SUKHAVASI, S. 2012. Extraction of chitin from chitosan from exoskeleton of shrimp for application in the pharmaceutical industry. *International Current Pharmaceutical Journal*, 1, 258-263.
- QANDIL, A. M., OBADAT, A. A., ALI, M. A. M., AL-TAANI, B. M., TASHTOUSH, B. M., AL-JBOUR, N. D., AL REMAWI, M. M., AL-SOU'OD, K. A. & BADWAN, A. A. 2009. Investigation of the interactions in complexes of low molecular weight chitosan with ibuprofen. *Journal of solution chemistry*, 38, 695-712.
- QAQISH, R. & AMIJI, M. 1999. Synthesis of a fluorescent chitosan derivative and its application for the study of chitosan–mucin interactions. *Carbohydrate Polymers*, 38, 99-107.
- QI, L. & XU, Z. 2004. Lead sorption from aqueous solutions on chitosan nanoparticles. *Colloids and Surfaces A: Physicochemical and Engineering Aspects*, 251, 183-190.
- QIU, X., LEPORATTI, S., DONATH, E. & MÖHWALD, H. 2001. Studies on the drug release properties of polysaccharide multilayers encapsulated ibuprofen microparticles. *Langmuir*, 17, 5375-5380.
- QUINCHE, N. & MARGOT, P. 2010. Coulier, Paul-Jean (1824-1890): a precursor in the history of fingerprint detection and their potential use for identifying their source (1863). *Journal of forensic identification*, 60 (2), 129-134.
- QUN, G. & AJUN, W. 2006. Effects of molecular weight, degree of acetylation and ionic strength on surface tension of chitosan in dilute solution. *Carbohydrate Polymers*, 64, 29-36.

- QUONG, D. & NEUFELD, R. 1998. DNA protection from extracapsular nucleases, within chitosan-or poly-L-lysine-coated alginate beads. *Biotechnology and bioengineering*, 60, 124-134.
- RAMASASTRY, P., DOWNING, D. T., POCHI, P. E. & STRAUSS, J. S. 1970. Chemical composition of human skin surface lipids from birth to puberty. *Journal of Investigative Dermatology*, 54, 139-144.
- RAMPINO, A., BORGOGNA, M., BLASI, P., BELLICH, B. & CESARO, A. 2013. Chitosan nanoparticles: Preparation, size evolution and stability. *International journal of pharmaceuticals*, 455, 219-228.
- RAO, K. & BALCK, K. 1980. Type classification of fingerprints: A syntactic approach. *IEEE Transactions on Pattern Analysis and Machine Intelligence*, 2, 223-231.
- RAO, M. A. 2010. Rheology of fluid and semisolid foods: principles and applications. Second edition. USA: *Springer*.
- REMUÑÁN-LÓPEZ, C., PORTERO, A., VILA-JATO, J. L. & ALONSO, M. J. 1998. Design and evaluation of chitosan/ethylcellulose mucoadhesive bilayered devices for buccal drug delivery. *Journal of controlled release*, 55, 143-152.
- REYNOLDS, A., JONES, B., SEARS, V. & BOWMAN, V. Nano-scale analysis of titanium dioxide fingerprint-development powders. *Journal of Physics: Conference Series*, 2008. IOP Publishing, 126/ 012069, 1-4
- RHIM, J.-W., HONG, S.-I., PARK, H.-M. & NG, P. K. 2006. Preparation and characterization of chitosan-based nanocomposite films with antimicrobial activity. *Journal of agricultural and food chemistry*, 54, 5814-5822.
- RILEY, R. G., SMART, J. D., TSIBOUKLIS, J., DETTMAR, P. W., HAMPSON, F., DAVIS, J. A., KELLY, G. & WILBER, W. R. 2001. An investigation of mucus/polymer rheological synergism using synthesised and characterised poly (acrylic acid) s. *International journal of pharmaceuticals*, 217, 87-100.
- RINAUDC, M., PAVLOV, G. & DESBRIERES, J. 1999. Solubilization of chitosan in strong acid medium. *International Journal of Polymer Analysis and Characterization*, 5, 267-276.
- RINAUDO, M. 2006. Chitin and chitosan: properties and applications. *Progress in polymer science*, 31, 603-632.
- ROBERTS, G. A. 1992. Chitin chemistry. First edition. London: *Macmillan Press LTD*.
- ROHATGI, R. & KAPOOR, A. 2016. Development of latent fingerprints on wet non-porous surfaces with SPR based on basic fuchsin dye. *Egyptian Journal of Forensic Sciences*, 6, 179-184.
- ROSE, M. C. & VOYNOW, J. A. 2006. Respiratory tract mucin genes and mucin glycoproteins in health and disease. *Physiological reviews*, 86, 245-278.
- ROSSI, S., BONFERONI, M. C., LIPPOLI, G., BERTONI, M., FERRARI, F., CARAMELLA, C. & CONTE, U. 1995. Influence of mucin type on polymer-mucin rheological interactions. *Biomaterials*, 16, 1073-1079.
- ROSSI, S., FERRARI, F., BONFERONI, M. C. & CARAMELLA, C. 2001. Characterization of chitosan hydrochloride–mucin rheological interaction: influence of polymer concentration and polymer: mucin weight ratio. *European journal of pharmaceutical sciences*, 12, 479-485.
- ROUX, C., JONES, N., LENNARD, C. & STOILOVIC, M. 2000. Evaluation of 1, 2-indanedione and 5, 6-dimethoxy-1, 2-indanedione for the detection of latent fingerprints on porous surfaces. *Journal of Forensic Science*, 45, 761-769.

- ROWELL, F., HUDSON, K. & SEVIOUR, J. 2009. Detection of drugs and their metabolites in dusted latent fingermarks by mass spectrometry. *Analyst*, 134, 701-707.
- RUHEMANN, S. 1910. CXXXII.—Cyclic di- and tri-ketones. *Journal of the Chemical Society, Transactions*, 97, 1438-1449.
- SAFERSTEIN, R. 2004. Criminalistics: an introduction to forensic science. Eighth edition. USA: *Upper Saddle River. Prentice Hall*.
- SAHOO, S., PARVEEN, S. & PANDA, J. 2007. The present and future of nanotechnology in human health care. *Nanomedicine: Nanotechnology, Biology and Medicine*, 3, 20-31.
- SAILAJA, A. K., AMARESHWAR, P. & CHAKRAVARTY, P. 2010. Chitosan nanoparticles as a drug delivery system. *Res. J. Pharm. Biol. Chem. Sci*, 1, 474-484.
- SAITO, Y., PUTAUX, J., OKANO, T., GAILL, F. & CHANZY, H. 1997. Structural aspects of the swelling of β chitin in HCl and its conversion into α chitin. *Macromolecules*, 30, 3867-3873.
- SAM, N. M., REMA, P. & NAIR, V. B. 2015. Study of fingerprint patterns in South Indian population. *Journal of Indian Academy of Forensic Medicine*, 37, 369-373.
- SAMETBAND, M., SHWEKY, I., BANIN, U., MANDLER, D. & ALMOG, J. 2007. Application of nanoparticles for the enhancement of latent fingerprints. *Chemical Communications*, (11), 1142-1144.
- SARMENTO, B., RIBEIRO, A., VEIGA, F., FERREIRA, D. & NEUFELD, R. 2007a. Insulin-loaded nanoparticles are prepared by alginate ionotropic pre-gelation followed by chitosan polyelectrolyte complexation. *Journal of nanoscience and nanotechnology*, 7, 2833-2841.
- SARMENTO, B., RIBEIRO, A., VEIGA, F., SAMPAIO, P., NEUFELD, R. & FERREIRA, D. 2007b. Alginate/chitosan nanoparticles are effective for oral insulin delivery. *Pharmaceutical research*, 24, 2198-2206.
- SATYANARAYANA, U. & CHAKRAPANI, U. 2013. *Biochemistry (with Clinical Concepts & Case Studies)*. Forth edition. India: *Elsevier*.
- SAUZIER, G., FRICK, A. & LEWIS, S. 2013. Investigation into the performance of physical developer formulations for visualizing latent fingerprints on paper. *Journal of Forensic Identification*, 63, 70-89.
- SCHNETZ, B. & MARGOT, P. 2001. Technical note: latent fingermarks, colloidal gold and multimetal deposition (MMD): Optimisation of the method. *Forensic Science International*, 118, 21-28.
- SCRIVENER, K. L. 2004. Backscattered electron imaging of cementitious microstructures: understanding and quantification. *Cement and Concrete Composites*, 26, 935-945.
- SCRUTON, B., ROBINS, B. & BLOTT, B. 1975. The deposition of fingerprint films. *Journal of Physics D: Applied Physics*, 8, 714-723.
- SEARS, V., BLEAY, S., BANDEY, H. & BOWMAN, V. 2012. A methodology for finger mark research. *Science & Justice*, 52, 145-160.
- SEVERINO, P., DA SILVA, C. F., DA SILVA, M. A., SANTANA, M. H. & SOUTO, E. B. 2016. Chitosan Cross-Linked Pentasodium Tripolyphosphate Micro/Nanoparticles Produced by Ionotropic Gelation. *Sugar Tech*, 18, 49-54.
- SEZER, A. & AKBUĞA, J. 1995. Controlled release of piroxicam from chitosan beads. *International journal of pharmaceuticals*, 121, 113-116.

- SHAH, B. R., LI, Y., JIN, W., AN, Y., HE, L., LI, Z., XU, W. & LI, B. 2016. Preparation and optimization of Pickering emulsion stabilized by chitosan-tripolyphosphate nanoparticles for curcumin encapsulation. *Food Hydrocolloids*, 52, 369-377.
- SHAH, D. & LONDHE, V. 2011. Optimization and characterization of levamisole-loaded chitosan nanoparticles by ionic gelation method using 23 factorial design by Minitab® 15. *Therapeutic delivery*, 2, 171-179.
- SHAH, S., PAL, A., KAUSHIK, V. & DEVI, S. 2009. Preparation and characterization of venlafaxine hydrochloride-loaded chitosan nanoparticles and *in vitro* release of drug. *Journal of applied polymer science*, 112, 2876-2887.
- SHEN, J., SUN, L.-D. & YAN, C.-H. 2008. Luminescent rare earth nanomaterials for bioprobe applications. *Dalton Transactions*, 42, 5687-5697.
- SHI, X.-Y. & TAN, T.-W. 2002. Preparation of chitosan/ethylcellulose complex microcapsule and its application in controlled release of Vitamin D 2. *Biomaterials*, 23, 4469-4473.
- SHU, Q., QU, F. & GILL, H. S. 2001. Probiotic treatment using Bifidobacterium lactis HN019 reduces weanling diarrhea associated with rotavirus and Escherichia coli infection in a piglet model. *Journal of pediatric gastroenterology and nutrition*, 33, 171-177.
- SHU, X. & ZHU, K. 2000. A novel approach to prepare tripolyphosphate/chitosan complex beads for controlled release drug delivery. *International journal of pharmaceuticals*, 201, 51-58.
- SHWETA, A. & SONIA, P. 2013. Pharmaceutical relevance of crosslinked chitosan in microparticulate drug delivery. *Int. Res. J. Pharm*, 4, 45-51.
- SIAFAKA, P. I., TITOPOULOU, A., KOUKARAS, E. N., KOSTOGLU, M., KOUTRIS, E., KARAVAS, E. & BIKIARIS, D. N. 2015. Chitosan derivatives as effective nanocarriers for ocular release of timolol drug. *International journal of pharmaceuticals*, 495, 249-264.
- SIEGEL, R. A. & RATHBONE, M. J. 2012. Overview of controlled release mechanisms. *Fundamentals and Applications of Controlled Release Drug Delivery* (ed.). 19-43. Springer.
- SIGNORETTO, M., GHEDINI, E., NICHELE, V., PINNA, F., CROCELLÀ, V. & CERRATO, G. 2011. Effect of textural properties on the drug delivery behaviour of nanoporous TiO₂ matrices. *Microporous and mesoporous Materials*, 139, 189-196.
- SILVA, M. M., CALADO, R., MARTO, J., BETTENCOURT, A., ALMEIDA, A. J. & GONÇALVES, L. M. D. 2017. Chitosan Nanoparticles as a Mucoadhesive Drug Delivery System for Ocular Administration. *Marine drugs*, 15, 1-16.
- SINGH, B. & AGARWAL, R. 2002. Design, development and optimization of controlled release microcapsules of diltiazem hydrochloride. *Indian journal of pharmaceutical sciences*, 64, 378-385.
- SINHA, V., SINGLA, A., WADHAWAN, S., KAUSHIK, R., KUMRIA, R., BANSAL, K. & DHAWAN, S. 2004. Chitosan microspheres as a potential carrier for drugs. *International journal of pharmaceuticals*, 274, 1-33.
- SINKORA, M., STEPANOVA, K., BUTLER, J. E., FRANCIS, D., SANTIAGO-MATEO, K., POTOCKOVA, H., KAROVA, K. & SINKOROVA, J. 2011. Ileal Peyer's patches are not necessary for systemic B cell development and maintenance and do not contribute significantly to the overall B cell pool in swine. *The Journal of Immunology*, 201, 1-12.

- SKOOG, D. A., WEST, D. M., HOLLER, F. J. & CROUCH, S. 2013. Fundamentals of analytical chemistry. Ninth edition. USA: *Brooks/Cole, Cengage Learning*.
- SMART, J. D. 2005. The basics and underlying mechanisms of mucoadhesion. *Advanced drug delivery reviews*, 57, 1556-1568.
- SMIDSRØD, O. & HAUG, A. 1971. Estimation of the relative stiffness of the molecular chain in polyelectrolytes from measurements of viscosity at different ionic strengths. *Biopolymers*, 10, 1213-1227.
- SODHI, G. & KAUR, J. 1999. A novel, cost effective organic fingerprint powder based on fluorescent eosin yellow dye. *Indian J Criminol*, 27, 73-74.
- SODHI, G. & KAUR, J. 2000. Organic Fingerprint Powders Based on Fluorescent Phloxine B Dye. *Defence Science Journal*, 50, 213-215.
- SODHI, G. & KAUR, J. 2004. Fingerprint Powder Formulation based on Azure II Dye. *Defence Science Journal*, 54, 179-182.
- SODHI, G. & KAUR, J. 2006. Nanoparticle size fingerprint dusting composition based on fluorescent eosin Y dye. *Fingerprint Whorld*, 32, 146-147.
- SODHI, G. S. & KAUR, J. 2001. Powder method for detecting latent fingerprints: a review. *Forensic science international*, 120, 172-176.
- SOGIAS, I. A., WILLIAMS, A. C. & KHUTORYANSKIY, V. V. 2008. Why is chitosan mucoadhesive? *Biomacromolecules*, 9, 1837-1842.
- SOGIAS, I. A., WILLIAMS, A. C. & KHUTORYANSKIY, V. V. 2012. Chitosan-based mucoadhesive tablets for oral delivery of ibuprofen. *International journal of pharmaceuticals*, 436, 602-610.
- SOLOMON, O. & CIUTĂ, I. 1962. Détermination de la viscosité intrinsèque de solutions de polymères par une simple détermination de la viscosité. *Journal of Applied Polymer Science*, 6, 683-686.
- SOSNIK, A., DAS NEVES, J. & SARMENTO, B. 2014. Mucoadhesive polymers in the design of nano-drug delivery systems for administration by non-parenteral routes: a review. *Progress in Polymer Science*, 39, 2030-2075.
- STAUFFER, E., BECUE, A., SINGH, K. V., THAMPI, K. R., CHAMPOD, C. & MARGOT, P. 2007. Single-metal deposition (SMD) as a latent fingerprint enhancement technique: an alternative to multimetal deposition (MMD). *Forensic Science International*, 168, e5-e9.
- STOILOVIC, M. 1993. Improved method for DFO development of latent fingerprints. *Forensic science international*, 60, 141-153.
- STOJANOVIC, Z. & MARKOVIC, S. 2012. Determination of Particle Size Distributions by Laser Diffraction. *Institute of technical sciences of SASA, Belgrade*, 11 - 20.
- STOKES, D. 2008. Principles and Practice of Variable Pressure/Environmental Scanning Electron Microscopy (VPA-ESEM). (ed.) UK: *John Wiley & Sons*.
- STOSZ, J. D. & ALYEA, L. A. Automated system for fingerprint authentication using pores and ridge structure. Automatic systems for the identification and inspection of humans, 1994. *International Society for Optics and Photonics*, 2277, 210-223.
- SUDHA, P. N. 2017. Industrial Applications of Marine Biopolymers. (ed.) London, New York. *CRC Press: Boca Raton*.
- SULLIVAN, D. J., CRUZ-ROMERO, M., COLLINS, T., CUMMINS, E., KERRY, J. P. & MORRIS, M. A. 2018. Synthesis of monodisperse chitosan nanoparticles. *Food Hydrocolloids*, 83, 355-364.

- SUN, Z., PAULINO, A. A., FENG, J., CHAI, Z., TAN, T. & JAIN, A. K. A study of multibiometric traits of identical twins. *SPIE Defense, Security, and Sensing*, 2010. *International Society for Optics and Photonics*, 7667, 1-12.
- TAKEUCHI, H., THONGBORISUTE, J., MATSUI, Y., SUGIHARA, H., YAMAMOTO, H. & KAWASHIMA, Y. 2005. Novel mucoadhesion tests for polymers and polymer-coated particles to design optimal mucoadhesive drug delivery systems. *Advanced drug delivery reviews*, 57, 1583-1594.
- TANG, C., GUAN, Y.-X., YAO, S.-J. & ZHU, Z.-Q. 2014. Preparation of ibuprofen-loaded chitosan films for oral mucosal drug delivery using supercritical solution impregnation. *International journal of pharmaceutics*, 473, 434-441.
- TANG, D.-W., YU, S.-H., HO, Y.-C., HUANG, B.-Q., TSAI, G.-J., HSIEH, H.-Y., SUNG, H.-W. & MI, F.-L. 2013. Characterization of tea catechins-loaded nanoparticles prepared from chitosan and an edible polypeptide. *Food Hydrocolloids*, 30, 33-41.
- TANG, E., HUANG, M. & LIM, L. 2003. Ultrasonication of chitosan and chitosan nanoparticles. *International Journal of Pharmaceutics*, 265, 103-114.
- THAKUR, K., AHUJA, M. & KUMAR, A. 2013. Carboxymethyl functionalization of amylopectin and its evaluation as a nanometric drug carrier. *International journal of biological macromolecules*, 62, 25-29.
- THEAKER, B. J., HUDSON, K. E. & ROWELL, F. J. 2008. Doped hydrophobic silica nano- and micro-particles as novel agents for developing latent fingerprints. *Forensic Science International*, 174, 26-34.
- THEYS, P., TURGIS, Y., LEPAREUX, A., CHEVET, G. & CECCALDI, P. 1968. New technique for bringing out latent fingerprints on paper: vacuum metallisation. *Int. Criminal Police Rev*, 217, 106-109.
- THOMAS, G. 1978. The physics of fingerprints and their detection. *Journal of Physics E: Scientific Instruments*, 11, 722-731.
- THOMAS, G. & REYNOLDS, T. 1975. Some observations on fingerprint deposits. *Journal of Physics D: Applied Physics*, 8, 724-729.
- THOMAS, J., TOUCHMAN, J., BLAKESLEY, R., BOUFFARD, G., BECKSTROM-STERNBERG, S., MARGULIES, E., BLANCHETTE, M., SIEPEL, A., THOMAS, P. & MCDOWELL, J. 2003. Comparative analyses of multi-species sequences from targeted genomic regions. *Nature*, 424, 788-793.
- THORNTON, D. J. & SHEEHAN, J. K. 2004. From mucins to mucus: toward a more coherent understanding of this essential barrier. *Proceedings of the American Thoracic Society*, 1, 54-61.
- TISSIER, P., DIDIERJEAN, J., PRUD'HOMME, C., PICHARD, J. & CRISPINO, F. 1999. A'cyanoacrylate case'for developing fingerprints in cars. *Science & justice: journal of the Forensic Science Society*, 39, 163-166.
- TIYABOONCHAI, W. 2003. Chitosan nanoparticles: a promising system for drug delivery. *Naresuan University Journal*, 11, 51-66.
- TOKUMITSU, H., ICHIKAWA, H. & FUKUMORI, Y. 1999. Chitosan-gadopentetic acid complex nanoparticles for gadolinium neutron-capture therapy of cancer: preparation by novel emulsion-droplet coalescence technique and characterization. *Pharmaceutical research*, 16, 1830-1835.
- TORCHILIN, V. P. 2000. Drug targeting. *European Journal of Pharmaceutical Sciences*, 11, S81-S91.
- TROWELL, F. 1975. A method for fixing latent fingerprints developed with iodine. *Journal of the Forensic Science Society*, 15, 189-195.

- TSAI, M. L., BAI, S. W. & CHEN, R. H. 2008. Cavitation effects versus stretch effects resulted in different size and polydispersity of ionotropic gelation chitosan–sodium tripolyphosphate nanoparticle. *Carbohydrate Polymers*, 71, 448-457.
- USKOKOVIC, V., LEE, K., LEE, P. P., FISCHER, K. E. & DESAI, T. A. 2012. Shape effect in the design of nanowire-coated microparticles as transepithelial drug delivery devices. *ACS nano*, 6, 7832-7841.
- VAN EERDENBRUGH, B., VERMANT, J., MARTENS, J. A., FROYEN, L., HUMBEECK, J. V., VAN DEN MOOTER, G. & AUGUSTIJNS, P. 2010. Solubility increases associated with crystalline drug nanoparticles: methodologies and significance. *Molecular pharmaceuticals*, 7, 1858-1870.
- VANDERKOLK, J. R. 2001. Levels of quality and quantity in detail. *Journal of Forensic Identification*, 51, 461-468.
- VARGA, N., BENKÓ, M., SEBÓK, D. & DÉKÁNY, I. 2014. BSA/polyelectrolyte core–shell nanoparticles for controlled release of encapsulated ibuprofen. *Colloids and Surfaces B: Biointerfaces*, 123, 616-622.
- VASIR, J. K., TAMBWEKAR, K. & GARG, S. 2003. Bioadhesive microspheres as a controlled drug delivery system. *International Journal of Pharmaceutics*, 255, 13-32.
- VIEIRA, A. P., BADSHAH, S. & AIROLDI, C. 2013. Ibuprofen-loaded chitosan and chemically modified chitosans—Release features from tablet and film forms. *International journal of biological macromolecules*, 52, 107-115.
- VLLASALIU, D., EXPOSITO-HARRIS, R., HERAS, A., CASETTARI, L., GARNETT, M., ILLUM, L. & STOLNIK, S. 2010. Tight junction modulation by chitosan nanoparticles: comparison with chitosan solution. *International journal of pharmaceutics*, 400, 183-193.
- WALLACE-KUNKEL, C., LENNARD, C., STOILOVIC, M. & ROUX, C. 2007. Optimisation and evaluation of 1, 2-indanedione for use as a fingerprint reagent and its application to real samples. *Forensic science international*, 168, 14-26.
- WAN, Y., CREBER, K. A., PEPPLEY, B. & BUI, V. T. 2003. Synthesis, characterization and ionic conductive properties of phosphorylated chitosan membranes. *Macromolecular Chemistry and Physics*, 204, 850-858.
- WANG, J. J., ZENG, Z. W., XIAO, R. Z., XIE, T., ZHOU, G. L., ZHAN, X. R. & WANG, S. L. 2011. Recent advances of chitosan nanoparticles as drug carriers. *Int J Nanomedicine*, 6, 765-774.
- WANG, K. & LIU, Q. 2014. Chemical structure analyses of phosphorylated chitosan. *Carbohydrate research*, 386, 48-56.
- WANG, M., LI, M., YANG, M., ZHANG, X., YU, A., ZHU, Y., QIU, P. & MAO, C. 2015a. NIR-induced highly sensitive detection of latent fingerprints by NaYF₄: Yb, Er upconversion nanoparticles in a dry powder state. *Nano research*, 8, 1800-1810.
- WANG, M., ZHU, Y. & MAO, C. 2015b. Synthesis of NIR-responsive NaYF₄: Yb, Er upconversion fluorescent nanoparticles using an optimized solvothermal method and their applications in enhanced development of latent fingerprints on various smooth substrates. *Langmuir*, 31, 7084-7090.
- WANG, P. & GRANADOS, R. R. 1997. An intestinal mucin is the target substrate for a baculovirus enhancer. *Proceedings of the National Academy of Sciences*, 94, 6977-6982.

- WANG, X.-Q. & ZHANG, Q. 2012. pH-sensitive polymeric nanoparticles to improve oral bioavailability of peptide/protein drugs and poorly water-soluble drugs. *European Journal of Pharmaceutics and Biopharmaceutics*, 82, 219-229.
- WANG, X., CHI, N. & TANG, X. 2008a. Preparation of estradiol chitosan nanoparticles for improving nasal absorption and brain targeting. *European Journal of Pharmaceutics and Biopharmaceutics*, 70, 735-740.
- WANG, Y., WANG, Y., YANG, R. & JIN, Y. 2008b. Study on amidation reaction between CdS/PAMAM and amino acid and its application to latent fingerprint development. *Guang pu xue yu guang pu fen xi= Guang pu*, 28, 2843-2846.
- WANG, Y. F., YANG, R. Q., WANG, Y. J., SHI, Z. X. & LIU, J. J. 2009. Application of CdSe nanoparticle suspension for developing latent fingerprints on the sticky side of adhesives. *Forensic science international*, 185, 96-99.
- WARGACKI, S. P., LEWIS, L. A. & DADMUN, M. D. 2007. Understanding the chemistry of the development of latent fingerprints by superglue fuming. *Journal of forensic sciences*, 52, 1057-1062.
- WEI, Q., LI, X., DU, X., ZHANG, X. & ZHANG, M. 2017. Universal and one-step visualization of latent fingerprints on various surfaces using hydrophilic cellulose membrane and dye aqueous solution. *Science China Chemistry*, 60, 1250-1257.
- WEYERMANN, C., ROUX, C. & CHAMPOD, C. 2011. Initial results on the composition of fingerprints and its evolution as a function of time by GC/MS analysis. *Journal of forensic sciences*, 56, 102-108.
- WHITE, P. C. 2010. Crime scene to court: The Essentials of forensic science. Third edition. Cambridge: *RSC Publishing*.
- WILSHIRE, B. 1996. Advances in fingerprint detection. *Endeavour*, 20, 12-15.
- WIN, P. P., SHIN-YA, Y., HONG, K. J. & KAJIUCHI, T. 2005. Effect of proteolytic enzymes in gastrointestinal fluids on drug release from polyelectrolyte complex microspheres based on partially phosphorylated chitosan. *Polymer international*, 54, 533-536.
- WINSTANLEY, P., CONSTABLE, S. & WALLEY, T. 2007. *Medical Pharmacology: A Clinical Core Text for Integrated Curricula with Self-assessment*. (ed.) UK: *Elsevier Health Sciences*.
- WOOD, L. 1991. The discovery of superglue fuming. *Finger Print World*, 16, 117-8.
- WU, L., ZHANG, J. & WATANABE, W. 2011. Physical and chemical stability of drug nanoparticles. *Advanced drug delivery reviews*, 63, 456-469.
- WU, Y., YANG, W., WANG, C., HU, J. & FU, S. 2005. Chitosan nanoparticles as a novel delivery system for ammonium glycyrrhizinate. *International journal of pharmaceutics*, 295, 235-245.
- WYDRO, P., KRAJEWSKA, B. & HĄC-WYDRO, K. 2007. Chitosan as a lipid binder: A Langmuir monolayer study of chitosan– lipid interactions. *Biomacromolecules*, 8, 2611-2617.
- XIANG-XIN, Z. & CHUN-GE, L. 1988. The historical application of hand prints in Chinese litigation. *Journal of Forensic Identification*, 38, 277-284.
- XU, Q., ENSIGN, L. M., BOYLAN, N. J., SCHÖN, A., GONG, X., YANG, J.-C., LAMB, N. W., CAI, S., YU, T. & FREIRE, E. 2015. Impact of surface polyethylene glycol (PEG) density on biodegradable nanoparticle transport in mucus *ex vivo* and distribution *in vivo*. *ACS nano*, 9, 9217-9227.

- XU, Y. & DU, Y. 2003. Effect of molecular structure of chitosan on protein delivery properties of chitosan nanoparticles. *International Journal of Pharmaceutics*, 250, 215-226.
- YALPANI, M. & HALL, L. D. 1984. Some chemical and analytical aspects of polysaccharide modifications. III. Formation of branched-chain, soluble chitosan derivatives. *Macromolecules*, 17, 272-281.
- YAMAMOTO, H. & AMAIKE, M. 1997. Biodegradation of cross-linked chitosan gels by a microorganism. *Macromolecules*, 30, 3936-3937.
- YAMASHITA, B. & FRENCH, M. 2011. The fingerprint sourcebook. Latent print developmentus. (ed.) Department of Justice, Washington: NIJ. 7-67.
- YAN, N. & CHEN, X. 2015. Don't waste seafood waste: Turning cast-off shells into nitrogen-rich chemicals would benefit economies and the environment. *Nature*, 524, 155-158.
- YANG, H.-C. & HON, M.-H. 2009. The effect of the molecular weight of chitosan nanoparticles and its application on drug delivery. *Microchemical Journal*, 92, 87-91.
- YANG, H., ZHU, S. & PAN, N. 2004. Studying the mechanisms of titanium dioxide as ultraviolet-blocking additive for films and fabrics by an improved scheme. *Journal of Applied Polymer Science*, 92, 3201-3210.
- YANG, X., FORIER, K., STEUKERS, L., VAN VLIERBERGHE, S., DUBRUEL, P., BRAECKMANS, K., GLORIEUX, S. & NAUWYNCK, H. J. 2012. Immobilization of Pseudorabies Virus in Porcine Tracheal Respiratory Mucus Revealed by Single Particle Tracking. *PLoS ONE*, 7, 1-9.
- YANG, Y., HU, W., WANG, X. & GU, X. 2007. The controlling biodegradation of chitosan fibers by N-acetylation *in vitro* and *in vivo*. *Journal of Materials Science: Materials in Medicine*, 18, 2117-2121.
- YIEN, L., ZIN, N. M., SARWAR, A. & KATAS, H. 2012. Antifungal activity of chitosan nanoparticles and correlation with their physical properties. *International journal of biomaterials*, 2012, 1-9.
- YIH, T. & AL-FANDI, M. 2006. Engineered nanoparticles as precise drug delivery systems. *Journal of cellular biochemistry*, 97, 1184-1190.
- YOKSAN, R., JIRAWUTTHIWONGCHAI, J. & ARPO, K. 2010. Encapsulation of ascorbyl palmitate in chitosan nanoparticles by oil-in-water emulsion and ionic gelation processes. *Colloids and Surfaces B: Biointerfaces*, 76, 292-297.
- ZHANG, H. & NEAU, S. H. 2001. *In vitro* degradation of chitosan by a commercial enzyme preparation: effect of molecular weight and degree of deacetylation. *Biomaterials*, 22, 1653-1658.
- ZHANG, H., OH, M., ALLEN, C. & KUMACHEVA, E. 2004. Monodisperse chitosan nanoparticles for mucosal drug delivery. *Biomacromolecules*, 5, 2461-2468.
- ZHANG, L. & KOSARAJU, S. L. 2007. Biopolymeric delivery system for controlled release of polyphenolic antioxidants. *European Polymer Journal*, 43, 2956-2966.
- ZHANG, Q., WU, Q., LIN, D. & YAO, S. 2013. Effect and mechanism of sodium chloride on the formation of chitosan–cellulose sulfate–tripolyphosphate crosslinked beads. *Soft Matter*, 9, 10354-10363.
- ZHAO, J. & WU, J. 2006. Preparation and characterization of the fluorescent chitosan nanoparticle probe. *Chinese Journal of Analytical Chemistry*, 34, 1555-1559.
- ZHAO, P., LIU, H., DENG, H., XIAO, L., QIN, C., DU, Y. & SHI, X. 2014. A study of chitosan hydrogel with embedded mesoporous silica nanoparticles loaded

by ibuprofen as a dual stimuli-responsive drug release system for surface coating of titanium implants. *Colloids and Surfaces B: Biointerfaces*, 123, 657-663.

ZUR MÜHLEN, A., SCHWARZ, C. & MEHNERT, W. 1998. Solid lipid nanoparticles (SLN) for controlled drug delivery—drug release and release mechanism. *European journal of pharmaceutics and biopharmaceutics*, 45, 149-155.

Chapter 9

Appendices

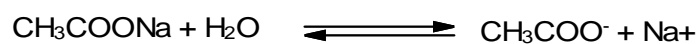
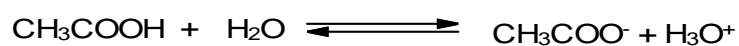
9 Appendices

9.1 Appendix A:

Acetate buffer calculations:

Molecular weight of glacial acetic acid (CH_3COOH) = 60 g/mol

Molecular weight for sodium acetate trihydrate ($\text{CH}_3\text{COONa} \cdot 3\text{H}_2\text{O}$) = 134.08 g/mol



Equation for weak acid and its salt is:

$$\text{pH}_{(\text{buffer})} = \text{pK}_a + \log [\text{salt}_{(\text{aq})} / \text{acid}_{(\text{aq})}]$$

The same approach was used for all acetate buffers, summarised as follows:

Table A.1: Shows the weights of glacial acetic acid and sodium acetate trihydrate used to make 13 acetate buffers

Acetate buffer	pH	Ionic strength	Acetic acid (g) in 1 L	Sodium acetate trihydrate (g) in 1 L
AB-1	3.3	0.1 M	5.799	0.466
AB-2	3.3	0.3 M	17.376	1.397
AB-3	3.3	0.5 M	28.996	2.331
AB-4	4.3	0.1 M	4.41	3.55
AB-5	4.3	0.3 M	13.2	10.7
AB-6	4.3	0.5 M	22.044	17.746
AB-7	5.3	0.1 M	1.32	10.616
AB-8	5.3	0.3 M	3.888	31.54
AB-9	5.3	0.5 M	6.602	53.08
AB-10	3.8	0.2 M	10.798	2.746
AB-11	3.8	0.4 M	21.597	5.491
AB-12	4.8	0.2 M	5.66	14.39
AB-13	4.8	0.4 M	11.319	28.781

9.2 Appendix B:

Table B.1: Shows the volumes of chitosan solutions and TPP solutions to make five ratios of CS: TPP nanoparticles

CS:TPP ratios	CS (mL)	TPP (mL)
3:1	40	39.5
4:1	40	30
5:1	50	30
6:1	50	24
7:1	50	21

9.3 Appendix C:

Table C.1: Shows the volumes of chitosan solutions and TPP solutions to effects of formation CS: TPP nanoparticles ratios loaded ibuprofen

CS:TPP ratios	CS (mL)	TPP (mL)	Ibuprofen (1.5 mg/mL) (mL)
3:1	40	39.5	10.0
4:1	40	30	8.8
5:1	50	30	10.1
6:1	50	24	9.3
7:1	50	21	8.9

9.4 Appendix D:

Particles size distribution curves of chitosan nanoparticles (CS: TPP) (blank) and ibuprofen loaded chitosan nanoparticles (CS-IBU-TPP)

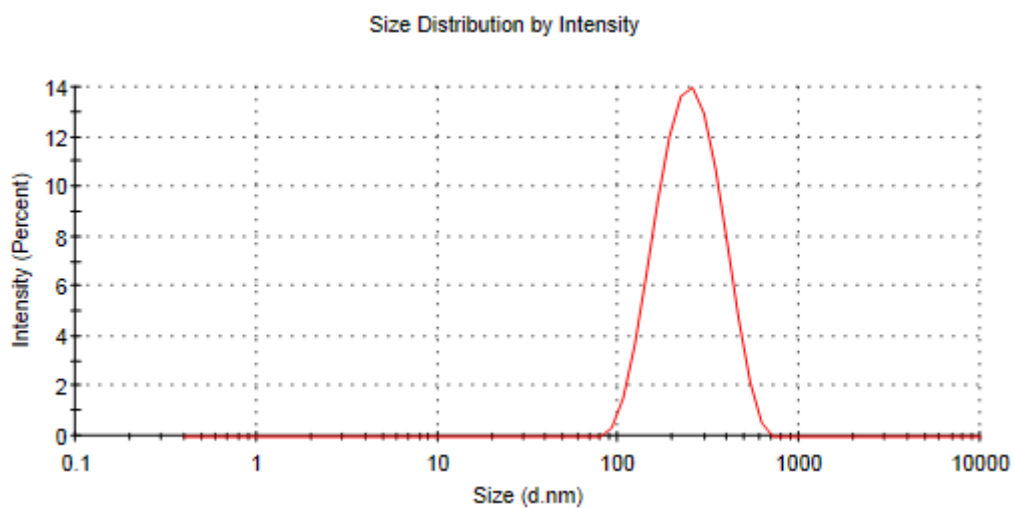


Figure D.1: Blank chitosan nanoparticle at CS: TPP (3:1) ratio

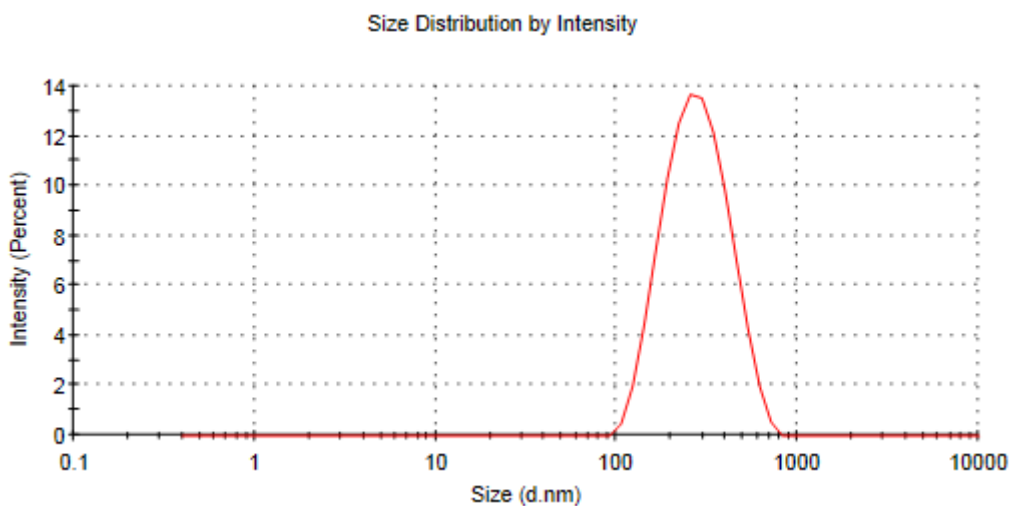


Figure D.2: Blank chitosan nanoparticle at CS-TPP (4:1) ratio

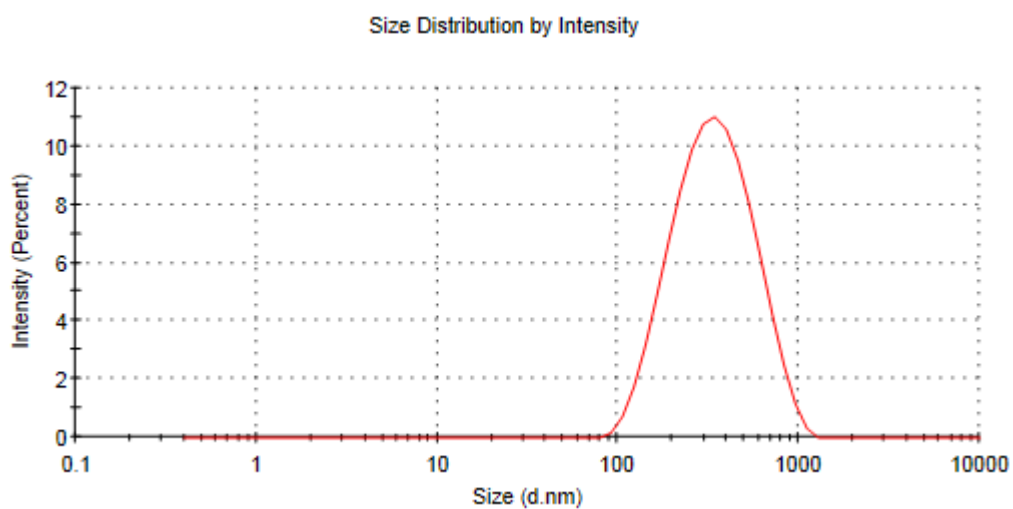


Figure D.3: Blank chitosan nanoparticle at CS: TPP (5:1) ratio

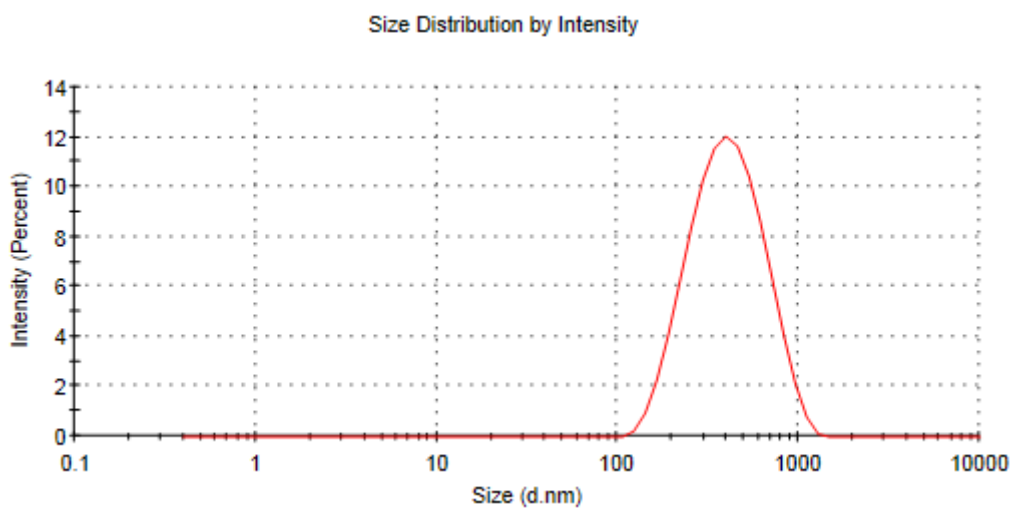


Figure D.4: Blank chitosan nanoparticle at CS: TPP (6:1) ratio

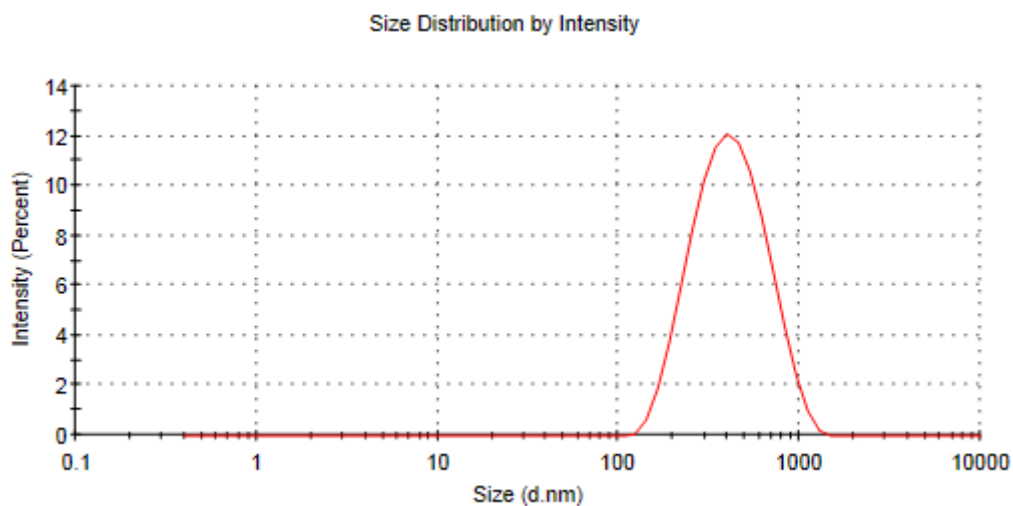


Figure D.5: Blank chitosan nanoparticle at CS-TPP (7:1) ratio

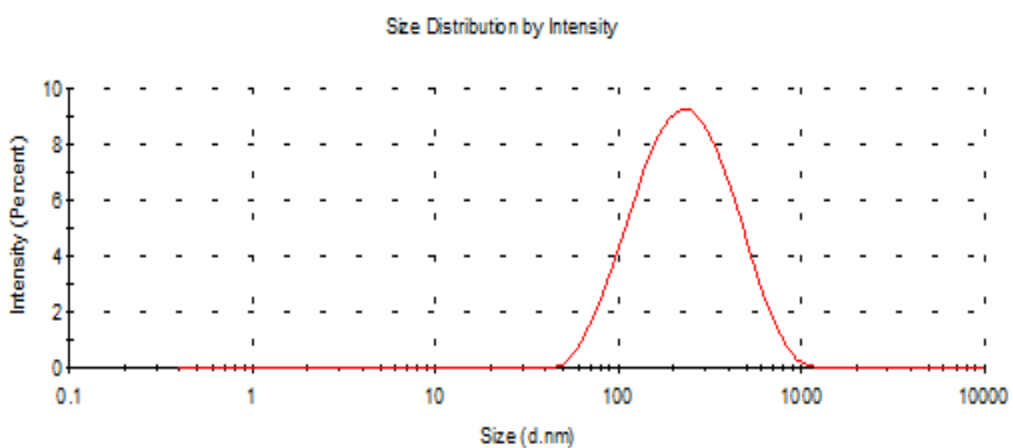


Figure D.6: Ibuprofen loaded chitosan nanoparticle (CS-IBU- TPP) at 3:1 ratio

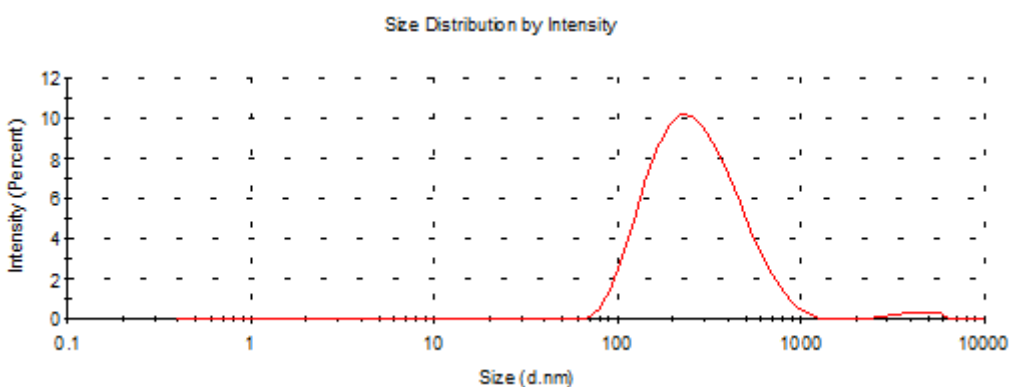


Figure D.7: Ibuprofen loaded chitosan nanoparticle (CS-IBU- TPP) at 4:1 ratio

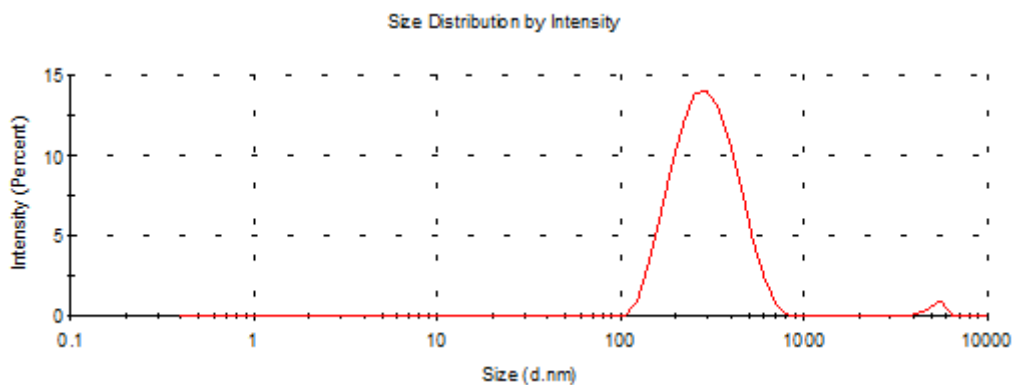


Figure D.8: Ibuprofen loaded chitosan nanoparticle (CS-IBU- TPP) at 5:1 ratio

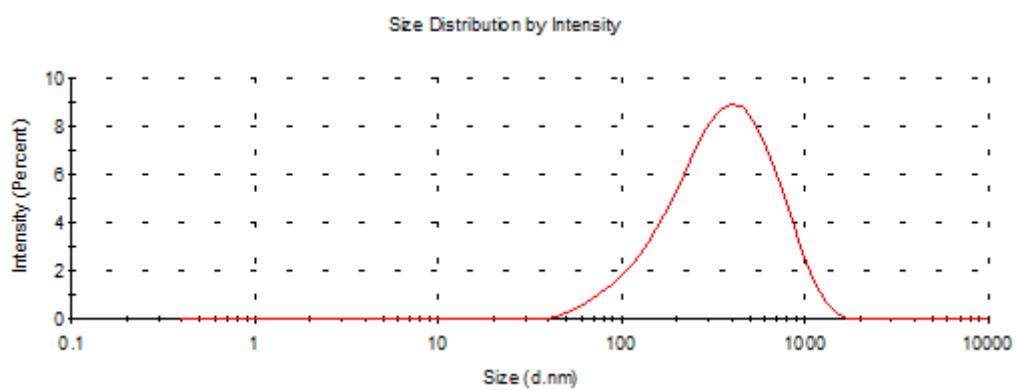


Figure D.9: Ibuprofen loaded chitosan nanoparticle (CS-IBU- TPP) at 6:1 ratio

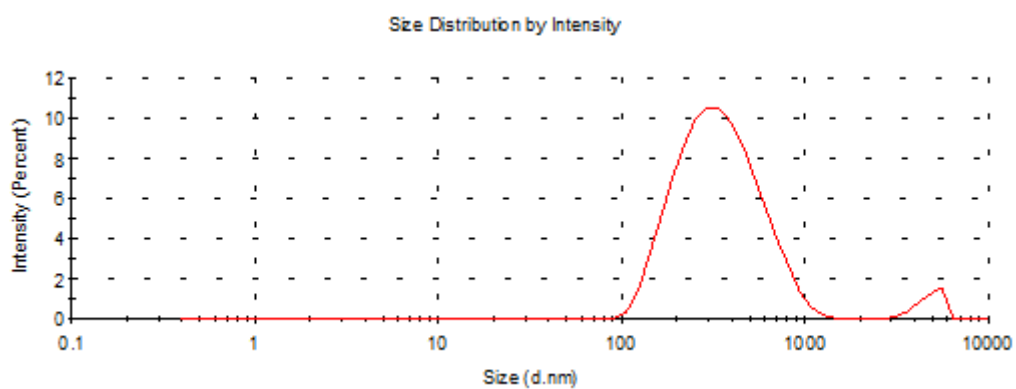


Figure D.10: Ibuprofen loaded chitosan nanoparticle (CS-IBU- TPP) at 7:1 ratio

9.5 Appendix E:

Particles size distribution curves of chitosan nanoparticles (CS-IBU-TPP) at 5:1 (CS: TPP) fixed ratio and different concentration of ibuprofen

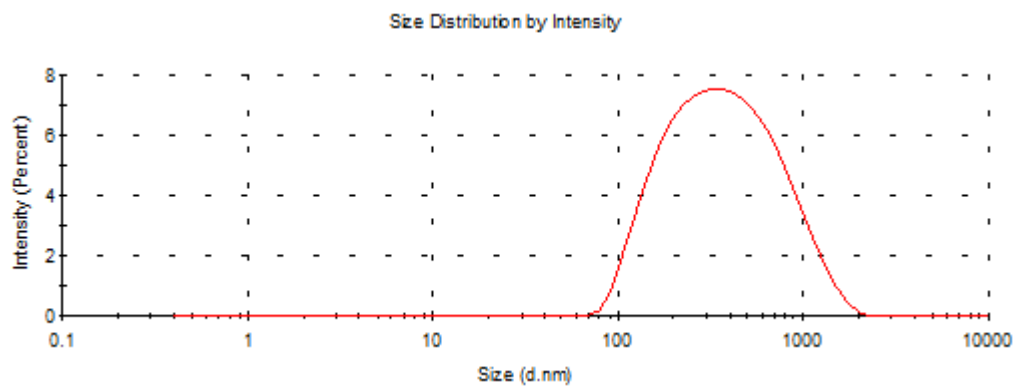


Figure E.1: Ibuprofen (0.5 mg/mL) loaded chitosan nanoparticle (CS-IBU- TPP)

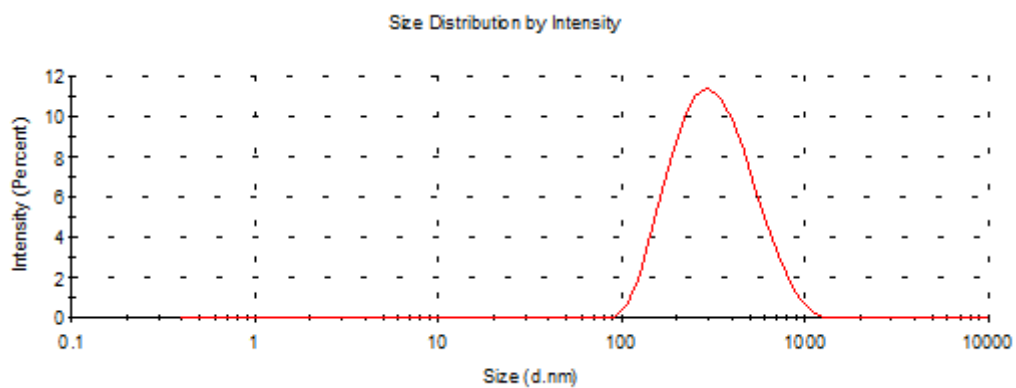


Figure E.2: Ibuprofen (1.0 mg/mL) loaded chitosan nanoparticle (CS-IBU- TPP)

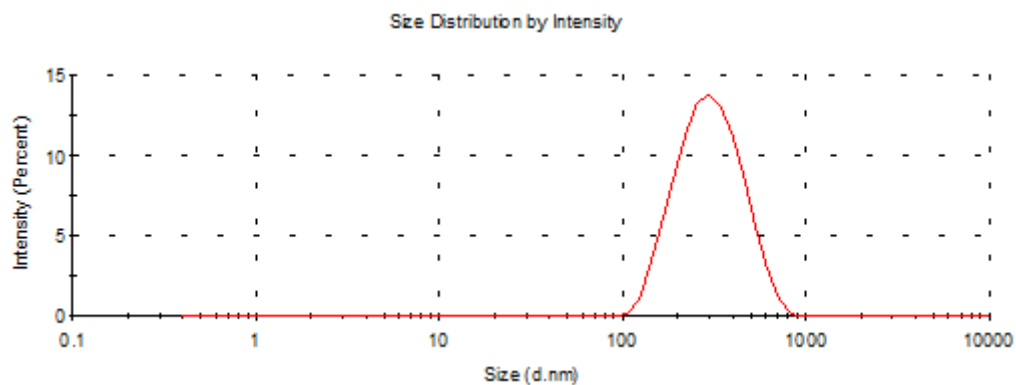


Figure E.3: Ibuprofen (1.5 mg/mL) loaded chitosan nanoparticle (CS-IBU- TPP)

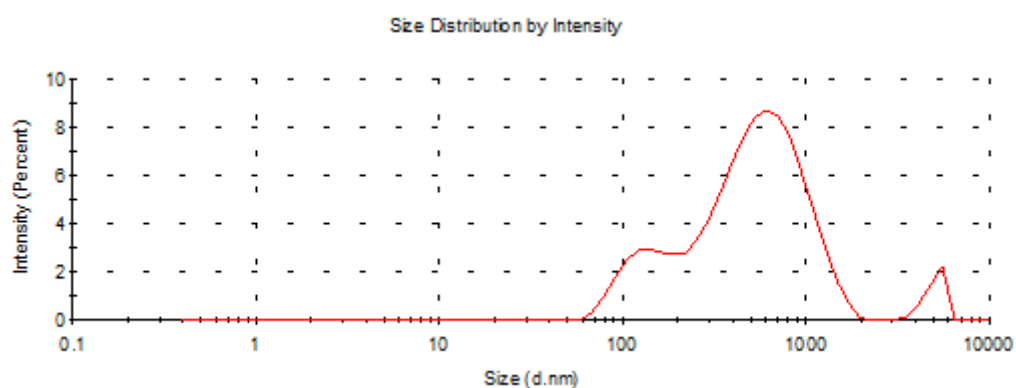


Figure E.4: Ibuprofen (2.0 mg/mL) loaded chitosan nanoparticle (CS-IBU- TPP)

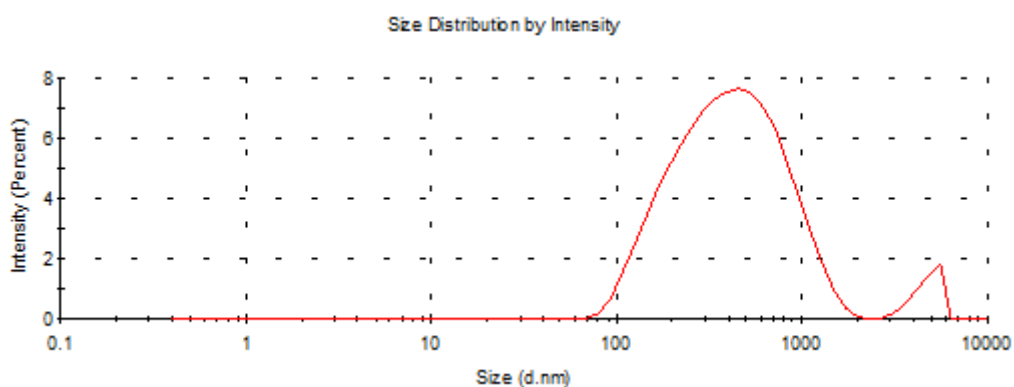


Figure E.5: Ibuprofen (2.5 mg/mL) loaded chitosan nanoparticle (CS-IBU- TPP)

9.6 Appendix F:

Particles size distribution curves of chitosan nanoparticles-mucin mixture

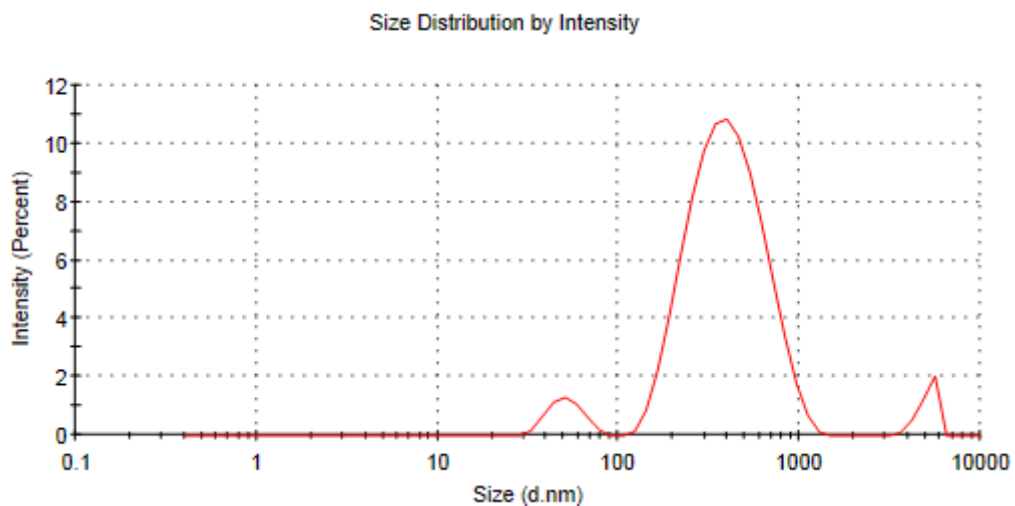


Figure F.1: Chitosan nanoparticles-mucin mixture at 3:1 ratio

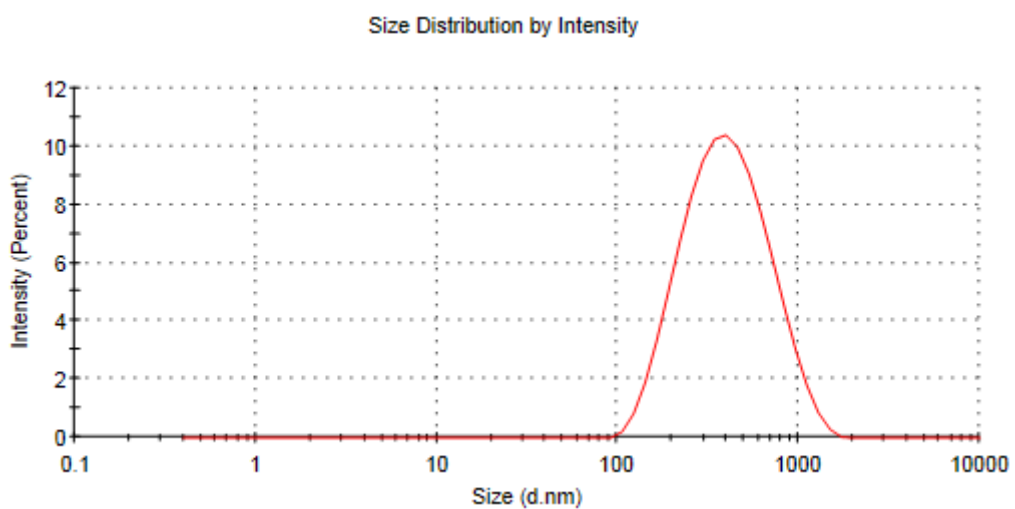


Figure F.2: Chitosan nanoparticles-mucin mixture at 4:1 ratio

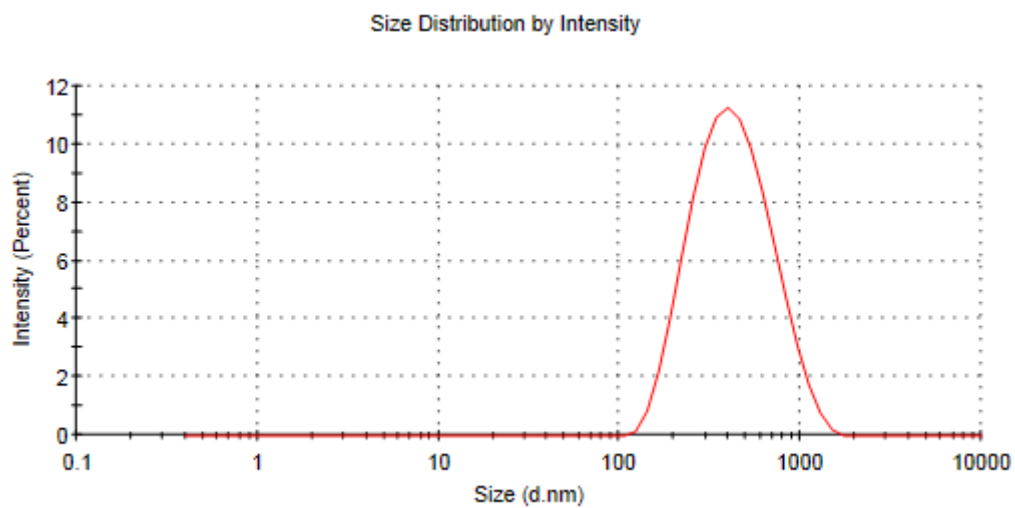


Figure F.3: Chitosan nanoparticles-mucin mixture at 5:1 ratio

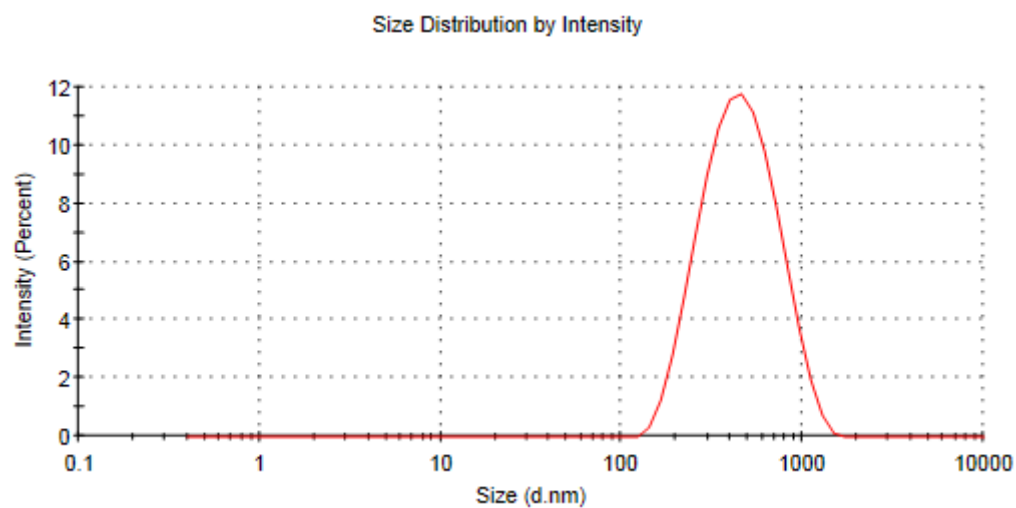


Figure F.6: Chitosan nanoparticles-mucin mixture at 6:1 ratio

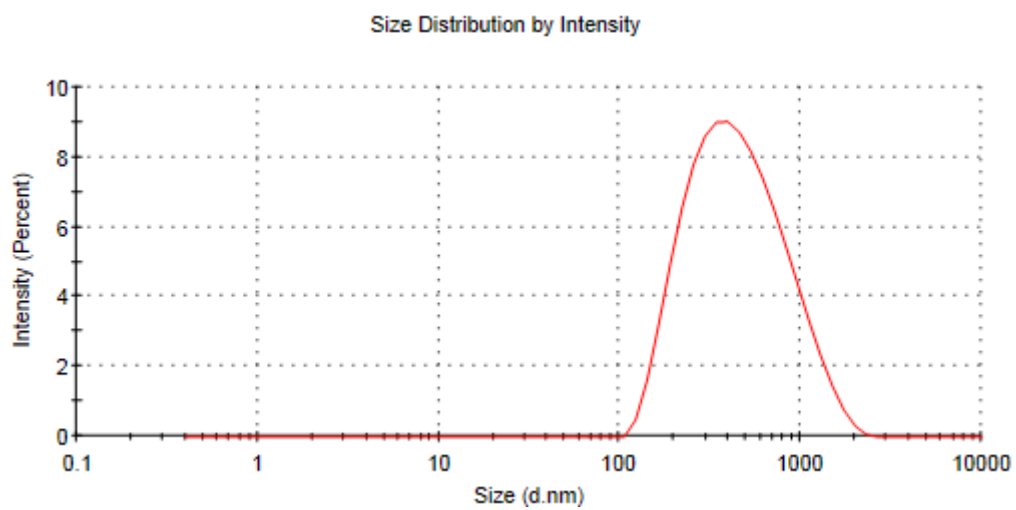


Figure F.7: Chitosan nanoparticles-mucin mixture at 7:1 ratio

9.7 Appendix G:

THE UNIVERSITY OF HUDDERSFIELD
School of Applied Sciences

Form 2: Ethical Review Application

SECTION A: TO BE COMPLETED BY THE APPLICANT

Before completing this section please refer to the School Research Ethics web pages which can be found at <https://www.hud.ac.uk/sas/research/researchgovernanceandethics/>
Applicants should consult the appropriate ethical guidelines.

Please ensure that the statements in Section C are completed by the applicant (and project supervisors for PGR, PGT, and UG students) prior to submission.

Project Title	Evaluation of Chitosan: TPP nanoparticles for latent finger print visualisation
Applicant	Ezzeddin Hejjaji
Supervisor (where applicable)	Prof Gordon Morris
Project start date	June 2018
Project end date	July 2018
Department	Applied Sciences/ Chemistry

SECTION B: PROJECT OUTLINE (TO BE COMPLETED IN FULL BY THE APPLICANT)

Issue	Please provide sufficient detail to allow appropriate consideration of any ethical issues. Forms with insufficient detail will need to be resubmitted.
Aims and objectives of the study. Please state the aims and objectives of the study.	To determine whether different formulations of chitosan tripolyphosphate (TPP) nanoparticles can be used to visualise latent finger prints. Chitosan TPP nanoparticles should interact with finger marks and this interaction should depend on, for example, the nanoparticle charge. In this project different nanoparticle formulations are being tested. In order to do this we need approximately 4 or 5 volunteers to leave their finger marks for visualisation. <i>NB</i> finger marks are what is made by a person, after visualisation they are finger prints.
Brief overview of experimental design	Adult volunteer participants will be asked to

The experimental design only needs to be explained in sufficient detail to explain the research methods that will be used during the study.	produce finger marks for visualisation using chitosan TPP nanoparticles.
Does your study require any permissions for study such as NHS Research Ethics Committee and R&D approval? If so, please give details of current status of any applications made or permissions granted	N/A
Participants Please outline who will participate in your research. Might any of the participants be considered 'vulnerable' (e.g. children)	Participants will be research students at the University of Huddersfield (up to 5 required).
Access to participants Please give details about how participants will be identified and contacted.	Participants will be contacted through personal contacts of the researcher.
How will your data be recorded and stored?	All data will be stored on local university computers
Informed consent. Please outline how you will obtain informed consent.	Participants will be shown a summary of how the information they provide will be recorded and processed. Participants will then be asked to sign a statement at the start of the session, demonstrating their understanding of how the information will be used. Participants will also be told that they can withdraw from the study at any point and that if they do so they will be allowed to request that the information they gave until the point of withdrawal be deleted.
Confidentiality Please outline the level of confidentiality you will offer respondents and how this will be respected. You should also state who will have access to the data and how it will be stored (this information should be included on your information sheet).	Participants will be told that they will not be required to provide any of their personal information, including their names or other identification methods.
Anonymity If you offer your participants anonymity, please indicate how this will be achieved.	Participants will be referred to as Participant 1, Participant 2 <i>etc.</i>
Harm Please outline your assessment of the extent to which your research might induce psychological stress, anxiety, cause harm or negative consequences for the participants	No element physical or psychological harm should be present, and if participants feel uncomfortable they will be allowed to leave.

<p>(beyond the risks encountered in normal life). If more than minimal risk, you should outline what support there will be for participants. If you believe that there is minimal likely harm, please articulate why you believe this to be so.</p>	
<p>Does the project involve the use of any human tissue? If so, please provide detail on the nature of the samples and any actions you are taking to ensure compliance with the Human Tissue Act.</p>	N/A
<p>Does the project involve the use of Genetically Modified Organisms (GMOs)? Please provide details explain how you are minimising any ethical issues associated with researching and producing GMOs (NB this committee does not consider H&S matters pertaining to the generation and use of GMOs).</p>	N/A
<p>Does the project include any security sensitive information? Please explain how processing of all security sensitive information will be in full compliance with the “Oversight of security sensitive research material in UK universities: guidance (October 2012)” (Universities UK, recommended by the Association of Chief Police Officers)</p> <p>Security sensitive materials are confirmed as research:</p> <ul style="list-style-type: none"> • Commissioned by the military • Commissioned under an EU security call • Involves the acquisition of security clearance • Concerns terrorist or extreme groups 	N/A

Retrospective applications. If your application for Ethics approval is retrospective, please explain why this has arisen.

SECTION C – SUMMARY OF ETHICAL ISSUES (TO BE COMPLETED BY THE APPLICANT)

Please give a summary of the ethical issues arising from your research and any action that will be taken to address the issue(s).

SECTION D – ADDITIONAL DOCUMENTS CHECKLIST (TO BE COMPLETED BY THE APPLICANT)

Please supply copies of all relevant supporting documentation electronically. If this is not available electronically, please provide explanation and supply hard copy.

I have included the following documents

Information sheet	Yes	<input checked="" type="checkbox"/>	Not applicable	<input type="checkbox"/>
Consent form (for interviews)	Yes	<input checked="" type="checkbox"/>	Not applicable	<input type="checkbox"/>
Letters	Yes	<input type="checkbox"/>	Not applicable	<input type="checkbox"/>
Questionnaire	Yes	<input type="checkbox"/>	Not applicable	<input checked="" type="checkbox"/>
Interview schedule	Yes	<input type="checkbox"/>	Not applicable	<input checked="" type="checkbox"/>

SECTION E – STATEMENT BY APPLICANT

I confirm that the information I have given in this form on ethical issues is correct.

Applicant name/signature: Gordon Morris



Date: 25/06/2018

Affirmation by Supervisor (where applicable)

I can confirm that, to the best of my understanding, the information presented by the applicant is correct and appropriate to allow an informed judgement on whether further ethical approval is required

Supervisor name/signature:

Date:

If you have any queries relating to the completion or consideration of this form, please do not hesitate to contact r.m.phillips@hud.ac.uk

9.8 Appendix H:

Participant Information sheet



What is the purpose of the study?

The aim of this study is to find chitosan-tripolyphosphate (CS: TPP) nanoparticles can be used in the potential development of latent finger prints.

Do I have to take part?

No, participation is completely voluntary. You can opt out at any point during the study.

What are the benefits of taking part?

You will be participating in ongoing doctoral research project in the development of novel finger print development techniques. This will add to the body of literature in this area and may in the future be of interest to law enforcement agencies. We cannot guarantee the study will help you personally but the information we obtain from your contribution to the study will help to increase the understanding of how different chitosan nanoparticle formulations interact with finger marks.

What will happen during this study?

Your finger marks will be taken by making finger marks on glass slides using 3 different fingers in a depletion series. This is to enable the research team to determine whether novel formulations can interact with finger marks with different levels of fatty acids for example. In a depletion series the participant will make a finger mark on a glass slide and then after an appropriate time period on another glass slide and so on. When the participant has made their finger marks they are free to leave and the researcher will develop their latent finger marks using different chitosan nanoparticle formulations.

What will happen to the results of this study?

The results will form part of research project on the potential of chitosan nanoparticles as visualisation tools for latent finger marks. Your information will be completely confidential. No identifying factors will be published, and only the researcher and their supervisors will have access to the original data. Once analysed the results will be written up into a student thesis which will be freely available via the University's repository. It is also expected that some or all of the results of the study will be published in the scientific literature at a future date.

Who is organizing this study?

The study is organised by the University of Huddersfield.

Researcher: Ezzeddin Hejjaji,

Email: Ezzeddin.Hejjaji@hud.ac.uk

Research Supervisor: Prof. G. Morris

School of Applied Sciences

University of Huddersfield

Email: g.morris@hud.ac.uk

9.9 Appendix I:

Informed Consent Form

Please initial to
show
acceptance

1. I have read the participant information sheet. _____
2. I have had the opportunity to ask any questions and to discuss the research study. _____
3. All my questions (if any) have received satisfactory answers. _____
4. I understand what the purpose of this study is and how I will be involved. _____
5. I do not require any further information but am free to request it at any time. _____
6. I have had enough time to decide to join the study. _____
7. I understand that my participation is entirely voluntary, and that I can withdraw at any time without giving a reason. _____
8. I agree to take part in this research study. _____

Name (PRINT)

Date

Signature

Researcher (PRINT)

Date

Signature

Further information

If you would like further information or you have any questions, please contact my project supervisor Prof. Gordon Morris g.morris@hud.ac.uk